

Existence and Stability Analysis of Ferroresonance Using the Generalized State-Space Averaging Technique

by

Jama A Mohamed

B.S., University of North Carolina at Charlotte (1992)
M.S.E.E., University of North Carolina at Charlotte (1994)

Submitted to the Department of Electrical Engineering and Computer Science
in partial fulfillment of the requirements for the degree of

Doctor of Science in Electrical Engineering

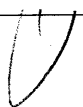
at the

MASSACHUSETTS INSTITUTE OF TECHNOLOGY


February, 2000

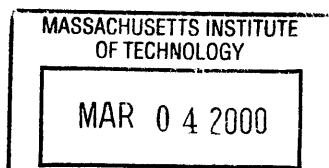
© Jama A Mohamed, MM. All rights reserved.

The author hereby grants to MIT permission to reproduce and distribute publicly paper and electronic copies of this thesis document in whole or in part, and to grant others the right to do so.

Author  _____
Department of Electrical Engineering and Computer Science
January 27, 2000

Certified by _____
Bernard C. Lesieutre
Associate Professor of Electrical Engineering
Thesis Supervisor

Accepted by  _____
Arthur C. Smith
Chairman, Departmental Committee on Graduate Students



ENG

Existence and Stability Analysis of Ferroresonance Using the Generalized State-Space Averaging Technique

by

Jama A Mohamed

Submitted to the Department of Electrical Engineering and Computer Science
on January 27, 2000, in partial fulfillment of the
requirements for the degree of
Doctor of Science in Electrical Engineering

Abstract

Ferroresonance can induce an undesired over-voltage often accompanied with a phase reversal which can damage power distribution transformers and motors and cause injury to the system operators. Similarly, under some conditions, power distribution transformers can excite subharmonic frequencies which in turn can damage the transformer winding and loads connected to the grid lines. While present analysis tools are based on analytical or experimental investigations, no rigorous systematic way exists to analyze ferroresonance and subharmonic problems in power distribution transformers.

The purpose of this thesis is to develop a systematic methodology to study ferroresonance and subharmonic problems in power distribution transformers, particularly, their existence, stability, and bifurcations. The methodology proposed for studying the ferroresonance problem is the generalized state-space averaging technique. Both single-phase and three-phase ferroresonance are considered. Appropriate models are developed for the single-phase and three-phase power distribution transformers which are suitable for the study of the ferroresonance problem, i.e, low frequency models.

The theory of the incremental-input describing function is revisited and a subtle flaw in the formulation of the theory is modified to address the stability of general systems, particularly at synchronous frequency. A generalized Nyquist criterion is presented to assess the stability of the periodic solutions. The modified incremental-input describing function theory is applied to single-phase ferroresonance systems.

Thesis Supervisor: Bernard C. Lesieutre

Title: Associate Professor of Electrical Engineering

Dedication

To

my parents

and

my wife

Acknowledgements

I owe much to many people who have contributed considerably to this thesis directly and indirectly. I would like to take this moment to thank these individuals for their assistance and encouragement in reaching this point.

First, I must thank profusely my advisor, Bernard Lesieutre; his breath of knowledge, his willingness to explain issues in details, and his high standards have not only guided my work to success but also have helped me to grow as a scientist. His interest in and direction of my thesis have been invaluable throughout this effort.

I have been most fortunate to have the opportunity to work closely with Professor George Verghese during my graduate work at MIT. He suggested many ideas for mitigating the problems that arose in my research. I appreciate his constant drilling and motivation to force me to understand and grasp of the necessary theory. I also thank George for being a member of my thesis and area exam committees. I would also like to thank the other members of my thesis committee Professor James Kirtley and Professor Aleksandar Stanković for taking the time to review and evaluate my work.

It has been a privilege to have an academic advisor, Professor Munther Dahleh, who constantly guided me through my academic development at MIT in the last five years. I am very grateful for his advice and direction.

I would like to thank James Hockenberry who was always willing to spend some time to proofread my thesis. His patience with my writing was indefatigable.

I am particularly appreciative of my friends and family Thuraya and Ahmed Abdi, Vahe Caliskan, Ali Farah, Kafi Hassan, James Hockenberry, Abdirahman Ibrahim, Ray Jalilvand, Kathy Millis, Vivian Mizuno, and Philip Yoon, who provided me with constant support and encouragement through the years at MIT.

I would like to thank the people and agents who supported me financially the last five years at MIT: GEM Ph.D. Engineering fellowship, MIT EECS Graduate Alumni Fellowship Fund, Vinto Hayes, GSO Fellowship, EECS Academic & Research Support, and the Harold E Edgerton Fund. I gratefully acknowledge Peggy Carney for her boundless effort in administrating my fellowship funds.

Finally, this thesis is dedicated to my wife, my best friend, Suad Mohamed. Without her constant support and motivation, I could never have achieved all that I have. To her I owe more than I can ever express.

Acknowledgements

Contents

| | | |
|----------|---|-----------|
| 1 | Introduction | 23 |
| 1.1 | Previous Work on Ferroresonance | 25 |
| 1.1.1 | Experimental Investigation of Ferroresonance | 26 |
| 1.1.2 | Theoretical Investigation of Ferroresonance | 28 |
| 1.1.2.1 | Time Domain Approach | 28 |
| 1.1.2.2 | Frequency Domain Approach | 33 |
| 1.2 | Modeling Ferroresonance | 34 |
| 1.2.1 | Single-Phase Ferroresonance Model | 35 |
| 1.2.2 | Three-Phase Ferroresonance Model | 35 |
| 1.3 | Contribution of the Thesis | 35 |
| 1.4 | Organization of the Thesis | 36 |
| 2 | Modeling Ferroresonance in Power Distribution Networks | 39 |
| 2.1 | Single-Phase Ferroresonance Model | 39 |
| 2.2 | Three-phase Ferroresonance Models | 41 |
| 2.2.1 | Balanced Power System Network | 41 |
| 2.2.2 | One Switch Opened Ferroresonance Model | 44 |
| 2.2.3 | Two Switches Opened Ferroresonance Model | 47 |
| 3 | Synchronous Incremental-input Describing Function | 51 |
| 3.1 | Dual-Input Describing Function | 51 |
| 3.1.1 | Condition For Instability | 53 |
| 3.1.2 | Existence of Multiple Steady-State Solutions | 55 |
| 3.1.3 | Incremental-Input Describing Function Applications | 57 |
| 3.2 | Modified Dual-Input Describing Function Analysis | 62 |

| | | |
|----------|--|-----------|
| 3.2.1 | Nyquist Stability Analysis Criterion | 62 |
| 3.2.2 | Describing Function Analysis | 66 |
| 3.2.3 | Dual-input Describing Function Analysis | 70 |
| 3.2.4 | Stability Analysis Using Incremental-input Describing Function | 72 |
| 4 | Generalized State-Space Averaging Methodology | 81 |
| 4.1 | Harmonic Periodic Solutions | 81 |
| 4.1.1 | Existence of Harmonic Periodic Solutions | 82 |
| 4.1.2 | Stability of Harmonic Periodic Solutions | 87 |
| 4.2 | Subharmonic Periodic Solutions | 91 |
| 4.2.1 | Sub-Synchronous Responses | 92 |
| 4.2.2 | Synchronous Responses | 93 |
| 4.2.3 | Existence of Subharmonic Periodic Solutions | 96 |
| 4.2.4 | Stability of Subharmonic Periodic Solutions | 97 |
| 5 | Analysis Tools: Poincaré Map, Floquet Theory, and GSSA Method | 99 |
| 5.1 | Model Formulation for Duffing Oscillator | 99 |
| 5.2 | Time Simulations for the Duffing Oscillator | 100 |
| 5.3 | Generalized State-Space Averaging Method | 101 |
| 5.3.1 | Harmonic Solutions for Duffing Oscillator | 101 |
| 5.3.2 | Subharmonic Solutions for Duffing Oscillator | 108 |
| 5.4 | Floquet Theory | 117 |
| 5.4.1 | Application of Floquet Theory to Duffing Oscillator | 119 |
| 5.4.1.1 | Harmonic Solutions of Duffing Oscillator | 120 |
| 5.4.1.2 | Subharmonic Solutions of Duffing Oscillator | 124 |
| 5.5 | Poincaré Maps | 126 |
| 5.5.1 | Application of the Poincaré Map to the Duffing Oscillator | 129 |

| | | |
|----------|--|------------|
| 5.6 | Connections Between Poincaré Map, Floquet Theory, and GSSA | 130 |
| 6 | Applications | 133 |
| 6.1 | Single-phase Ferroresonance | 133 |
| 6.1.1 | Harmonic Periodic Solutions | 134 |
| 6.1.1.1 | Line Inductance Variations | 134 |
| 6.1.1.2 | Input Voltage Magnitude Variations | 134 |
| 6.1.2 | Stability of Harmonic Periodic Solutions | 135 |
| 6.1.3 | Robustness analysis for the steady-state solutions | 140 |
| 6.2 | Three-phase Ferroresonance: All Switches Closed | 142 |
| 6.2.1 | Harmonic Periodic Solutions | 144 |
| 6.2.2 | Stability of Harmonic Periodic Solutions | 146 |
| 6.3 | Three-phase Ferroresonance: One Switch Opened | 151 |
| 6.3.1 | Harmonic Periodic Solutions | 153 |
| 6.3.2 | Stability of Harmonic Periodic Solutions | 155 |
| 6.4 | Three-phase Ferroresonance: Two Switches Opened | 160 |
| 6.4.1 | Harmonic Periodic Solutions | 161 |
| 6.4.2 | Stability of Harmonic Periodic Solutions | 162 |
| 6.5 | Switching Simulations | 167 |
| 7 | Concluding Remarks | 177 |
| 7.1 | Summary | 177 |
| 7.2 | Suggestions for Future Work | 179 |
| 7.2.1 | Other Models for the Transformer Core | 179 |
| 7.2.2 | Simplification of the System Model (DAE) | 179 |
| 7.2.3 | MIMO Synchronous Incremental-Input Describing Function | 180 |
| 7.2.4 | Methods to Approximate Matrix A | 180 |

| | | |
|----------|--|------------|
| 7.2.5 | Investigations of Subharmonic Steady-state Solutions | 181 |
| 7.2.6 | Improvement of Numerical Computations | 181 |
| A | Appendices | 183 |
| A.1 | Three-Phase Ferroresonance: Opened One Conductor | 183 |
| A.2 | Three-Phase Ferroresonance: Opened Two conductors | 186 |
| A.3 | Synchronous Incremental-Input Describing Function | 188 |
| | Bibliography | 195 |

List of Figures

| | | |
|------|---|----|
| 1.1 | 1300-MVA Power transformer (Westinghouse Electric Corporation) | 24 |
| 1.2 | Ferroresonance: Discontinuous jump amplitude | 25 |
| 1.3 | Ferroresonance: Subharmonic responses | 26 |
| 1.4 | Ferroresonance: Amplitude-modulated oscillations | 27 |
| 1.5 | Series nonlinear circuit | 29 |
| 1.6 | Graphical solution of ferroresonance circuit [1] | 30 |
| 1.7 | Nonlinear Feedback System | 33 |
| | | |
| 2.1 | Parallel high voltage transmission lines | 39 |
| 2.2 | Single-phase ferroresonance circuit model: I | 40 |
| 2.3 | Single-phase ferroresonance circuit model: II | 40 |
| 2.4 | Three-phase balanced power system network: All switches closed | 42 |
| 2.5 | Three-phase power system network: One switch opened | 45 |
| 2.6 | Three-phase power system network: Two switches opened | 47 |
| | | |
| 3.1 | Nonlinear interconnected feedback system | 52 |
| 3.2 | Complex Plane | 54 |
| 3.3 | Single-phase ferroresonance circuit model | 57 |
| 3.4 | $G(j\omega)$ and $-N^{-1}(\mathcal{A}, \phi)$ for $R = 0.002$ pu, $C = 50$ pu, and $L = 0.021$ pu . . . | 60 |
| 3.5 | Time simulation for $R = 0.002$ pu, $C = 50$ pu, and $L = 0.021$ pu | 60 |
| 3.6 | $G(j\omega)$ and $-N^{-1}(\mathcal{A}, \phi)$ for $R = 0.002$ pu, $C = 50$ pu, and $L = 0.023$ pu . . . | 61 |
| 3.7 | Time simulation for $R = 0.002$ pu, $C = 50$ pu, and $L = 0.025$ pu | 61 |
| 3.8 | Frequency response of system one | 64 |
| 3.9 | Frequency response of system two | 64 |
| 3.10 | Frequency response of system three | 65 |

| | | |
|------|---|-----|
| 3.11 | Frequency response of system four | 65 |
| 3.12 | Nonlinear Element | 67 |
| 3.13 | Frequency response of $G(j\omega)$ | 76 |
| 3.14 | Loci of $G(j\omega)$ and $\frac{-1}{N(\mathcal{A},\phi)}$ at Φ_1 | 78 |
| 3.15 | System time simulations at operating point Φ_1 | 78 |
| 3.16 | Loci of $G(j\omega)$ and $\frac{-1}{N(\mathcal{A},\phi)}$ at Φ_2 | 79 |
| 3.17 | System time simulations at operating point Φ_2 | 79 |
| 3.18 | Loci of $G(j\omega)$ and $\frac{-1}{N(\mathcal{A},\phi)}$ at Φ_3 | 80 |
| 3.19 | System time simulations at operating point Φ_3 | 80 |
| 4.1 | Series linear LC circuit | 84 |
| 4.2 | Series nonlinear circuit | 91 |
| 4.3 | Harmonic solutions | 95 |
| 4.4 | Subharmonic Solutions | 96 |
| 5.1 | Nonlinear interconnected system [2] | 99 |
| 5.2 | Duffing oscillator: Harmonic steady-state response | 101 |
| 5.3 | Duffing oscillator: Subharmonic steady-state response | 102 |
| 5.4 | Approximated harmonic solutions: $k = \pm 7$ and $\delta = 0.15$ | 103 |
| 5.5 | Eigenvalues of the approximated harmonic system: $k = \pm 7$ and $\delta = 0.15$ | 104 |
| 5.6 | Approximated harmonic solutions: $k = \pm 11$ and $\delta = 0.15$ | 104 |
| 5.7 | Eigenvalues of the approximated harmonic system: $k = \pm 11$ and $\delta = 0.15$ | 105 |
| 5.8 | Approximated harmonic solutions: $k = \pm 17$ and $\delta = 0.15$ | 106 |
| 5.9 | Eigenvalues of the approximated harmonic system: $k = \pm 17$ and $\delta = 0.15$ | 106 |
| 5.10 | Approximated harmonic solutions: $k = \pm 25$ and $\delta = 0.15$ | 107 |
| 5.11 | Eigenvalues of the approximated harmonic system: $k = \pm 25$ and $\delta = 0.15$ | 107 |
| 5.12 | Approximated harmonic solutions: $k = \pm 7$ and $\delta = 0.22$ | 108 |

| | | |
|------|---|-----|
| 5.13 | Eigenvalues of the approximated harmonic system: $k = \pm 7$ and $\delta = 0.22$. . . | 109 |
| 5.14 | Approximated harmonic solutions: $k = \pm 11$ and $\delta = 0.22$ | 110 |
| 5.15 | Eigenvalues of the approximated harmonic system: $k = \pm 11$ $\delta = 0.22$ | 110 |
| 5.16 | Approximated harmonic solutions: $k = \pm 17$ and $\delta = 0.22$ | 111 |
| 5.17 | Eigenvalues of the approximated harmonic system: $k = \pm 17$ $\delta = 0.22$ | 111 |
| 5.18 | Approximated harmonic solutions: $k = \pm 25$ and $\delta = 0.22$ | 112 |
| 5.19 | Eigenvalues of the approximated harmonic system: $k = \pm 25$ $\delta = 0.22$ | 112 |
| 5.20 | Approximated Subharmonic solutions: $k = \pm 7$ and $\delta = 0.22$ | 113 |
| 5.21 | Eigenvalues of the approximated subharmonic system: $k = \pm 7$ | 113 |
| 5.22 | Approximated Subharmonic solutions: $k = \pm 11$ and $\delta = 0.22$ | 114 |
| 5.23 | Eigenvalues of the approximated subharmonic system: $k = \pm 11$ | 114 |
| 5.24 | Approximated Subharmonic solutions: $k = \pm 17$ and $\delta = 0.22$ | 115 |
| 5.25 | Eigenvalues of the approximated subharmonic system: $k = \pm 17$ | 115 |
| 5.26 | Approximated Subharmonic solutions: $k = \pm 25$ and $\delta = 0.22$ | 116 |
| 5.27 | Eigenvalues of the approximated subharmonic system: $k = \pm 25$ | 116 |
| 5.28 | Variational system simulations for $\tilde{x}_0 = [1 \ 0]$ | 122 |
| 5.29 | Variational system simulations for $\tilde{x}_0 = [0 \ 1]$ | 122 |
| 5.30 | Variational system simulations for $\tilde{x}_0 = [1 \ 0]$ | 125 |
| 5.31 | Variational system simulations for $\tilde{x}_0 = [0 \ 1]$ | 126 |
| 6.1 | Steady-state solutions for $M = 0.25$ pu: Single-phase | 135 |
| 6.2 | Steady-state solutions for $L = 0.025$ pu: Single-phase | 136 |
| 6.3 | Eigenvalues for curve \mathcal{C}_1 : Single-phase | 137 |
| 6.4 | Eigenvalues for curve \mathcal{C}_2 : Single-phase | 137 |
| 6.5 | Eigenvalues for curve \mathcal{C}_3 : Single-phase | 138 |
| 6.6 | Eigenvalues for point P_1 : Single-phase | 138 |

| | | |
|------|---|-----|
| 6.7 | Eigenvalues for point P_2 : Single-phase | 139 |
| 6.8 | Time simulations for $\lambda(t)$ case one: Single-phase | 139 |
| 6.9 | Time simulations for $\lambda(t)$ case two: Single-phase | 140 |
| 6.10 | Steady-state solutions for $M = 1.0$ pu: All switches closed | 145 |
| 6.11 | Steady-state solutions for 40, 60, and 120 mile transmission line lengths | 145 |
| 6.12 | Eigenvalues of the linearized system: All switches closed | 149 |
| 6.13 | Simulink block diagram for the system: All switches closed | 149 |
| 6.14 | Time simulations for $\lambda_1(t)$: All switches closed | 150 |
| 6.15 | Time simulations for $\lambda_2(t)$: All switches closed | 150 |
| 6.16 | Time simulations for $\lambda_3(t)$: All switches closed | 151 |
| 6.17 | Steady-state solutions for $M = 1.0$ pu: One switch opened | 153 |
| 6.18 | Steady-state solutions for 60 mile transmission line length: One switch opened | 154 |
| 6.19 | Steady-state solutions for 60 mile transmission line length: One switch opened | 154 |
| 6.20 | Eigenvalues for curve \mathcal{C}_1 : One switch opened | 155 |
| 6.21 | Eigenvalues for curve \mathcal{C}_4 : One switch opened | 156 |
| 6.22 | Eigenvalues for curve \mathcal{C}_5 : One switch opened | 156 |
| 6.23 | Eigenvalues for curve \mathcal{C}_2 : One switch opened | 157 |
| 6.24 | Eigenvalues for curve \mathcal{C}_3 : One switch opened | 157 |
| 6.25 | Simulink block diagram for the system: One switch opened | 158 |
| 6.26 | Time simulations for $\lambda_1(t)$: One switch opened | 158 |
| 6.27 | Time simulations for $\lambda_2(t)$: One switch opened | 159 |
| 6.28 | Time simulations for $\lambda_3(t)$: One switch opened | 159 |
| 6.29 | Steady-state harmonic solutions for $M = 1.0$ pu: Two switches opened | 162 |
| 6.30 | Steady-state solutions for 60 mile transmission line length: Two switches opened | 163 |
| 6.31 | Eigenvalues for curve \mathcal{C}_1 : Two switches opened | 164 |

| | | |
|------|--|-----|
| 6.32 | Eigenvalues for curve \mathcal{C}_2 : Two switches opened | 164 |
| 6.33 | Eigenvalues for curve \mathcal{C}_3 : Two switches opened | 165 |
| 6.34 | System time simulations: Two switches opened | 165 |
| 6.35 | Time simulations for $\lambda_1(t)$: Two switches opened | 166 |
| 6.36 | Time simulations for $\lambda_2(t)$: Two switches opened | 166 |
| 6.37 | Time simulations for $\lambda_3(t)$: Two switches opened | 167 |
| 6.38 | Simulink block diagram for the system: Switching simulations | 168 |
| 6.39 | Time simulations for $\lambda_1(t)$: S_1 opened solution one | 169 |
| 6.40 | Time simulations for $\lambda_2(t)$: S_1 opened solution one | 169 |
| 6.41 | Time simulations for $\lambda_3(t)$: S_1 opened solution one | 170 |
| 6.42 | Time simulations for $\lambda_1(t)$: S_1 opened solution Two | 170 |
| 6.43 | Time simulations for $\lambda_2(t)$: S_1 opened solution Two | 171 |
| 6.44 | Time simulations for $\lambda_3(t)$: S_1 opened solution Two | 171 |
| 6.45 | Time simulations for $\lambda_1(t)$: S_1 opened solution Three | 172 |
| 6.46 | Time simulations for $\lambda_2(t)$: S_1 opened solution Three | 172 |
| 6.47 | Time simulations for $\lambda_3(t)$: S_1 opened solution three | 173 |
| 6.48 | Time simulations for $\lambda_1(t)$: S_1 and S_2 opened solution case one | 173 |
| 6.49 | Time simulations for $\lambda_2(t)$: S_1 and S_2 opened solution case one | 174 |
| 6.50 | Time simulations for $\lambda_3(t)$: S_1 and S_2 solution case one | 174 |
| 6.51 | Time simulations for $\lambda_1(t)$: S_1 and S_2 opened solution case two | 175 |
| 6.52 | Time simulations for $\lambda_2(t)$: S_1 and S_2 opened solution case two | 175 |
| 6.53 | Time simulations for $\lambda_3(t)$: S_1 and S_2 opened solution case two | 176 |
| 7.1 | Eigenvalues of approximated system: $k = \pm 35$ | 180 |
| A.1 | Open-loop frequency response of the system: $\omega \geq 0$ | 190 |
| A.2 | Open-loop frequency response of the system: $-\infty \leq \omega \leq \infty$ | 191 |

| | |
|--|-----|
| A.3 $G(j\omega)$ and $-\frac{1}{N(\mathcal{A},\phi)}$ loci | 193 |
|--|-----|

List of Tables

| | | |
|-----|---|-----|
| 5.1 | Approximated harmonic Solutions: $\delta = 0.15$ | 123 |
| 5.2 | Approximated harmonic Solutions: $\delta = 0.22$ | 124 |
| 5.3 | Approximated subharmonic Solutions: $\delta = 0.22$ | 126 |
| 5.4 | Harmonic Solutions: $\delta = 0.15$ | 130 |
| 5.5 | Harmonic solutions: $\delta = 0.22$ | 131 |
| 5.6 | Subharmonic Solutions: $\delta = 0.22$ | 131 |

List of Tables

List of Symbols

Roman letters

- A Jacobian matrix of slowly varying system, see equation (4.27)
- B Incremental-input for the nonlinear element, see equation (3.5)
- C Linear Capacitance of transmission lines, see equation (2.2)
- $f(x)$ Nonlinear vector field, see equation (4.1)
- $F_k(X_k)$ Slowly varying vector field, see equation (4.8)
- $G(s)$ Linear transfer function, see equation (3.12)
- H_k Slowly varying nonlinear vector field, see equation (6.3)
- $i_L(t)$ Nonlinear inductive current, see equation (2.1)
- K_1 Linear constant coefficient term for the transformer core model, see equation (2.1)
- K_5 Nonlinear constant coefficient term for the transformer core model, see equation (2.1)
- L Linear inductance of transmission lines, see equation (2.2)
- $L(s)$ System loop-gain, see equation (3.9)
- M Magnitude of the sinusoidal input, $v(t)$
- $N(\mathcal{A})$ Describing function gain, see equation (3.7)
- $N(\mathcal{A}, \phi)$ Synchronous incremental-input describing function gain, see equation (3.8)
- $P(\tau)$ Poincaré map, see equation (5.39)
- Q_{k-n} Jacobian matrix of $F_k(X_k)$, see equation (4.27)
- R Linear resistance of transmission lines, see equation (2.2)
- $r(t)$ Reference input, see equation (3.4)
- $v(t)$ Sinusoidal input voltage, see equation (2.2)
- X_k Complex amplitude, see equation (4.3)
- $X_k(t)$ Slowly varying complex amplitude, see equation (4.4)
- \mathcal{A} Input magnitude for the nonlinear element, see equation (3.3)
- \mathcal{C} Solution curve, page 135

\mathcal{X} Real part of $G(j\omega)$, see equation (3.12)

\mathcal{Y} Imaginary part of $G(j\omega)$, see equation (3.12)

Greek letters

γ Input incremental magnitude, see equation (3.4)

$\lambda(t)$ Flux linkage across the nonlinear core, see equation (2.1)

μ Eigenvalue, see equation (4.17)

ϕ Phase angle for the input of the nonlinear element, see equation (3.8)

$\Phi(t)$ Fundamental solution matrix, see equation (5.10)

Ψ Monodromy matrix

ρ Floquet exponent, see equation (5.22)

σ Damping factor, see equation (3.63)

θ Input phase angle, see equation (3.2)

Chapter 1

Introduction

The dynamics of physical systems, such as, electrical systems, electromechanical systems, mechanical systems, and systems from other engineering disciplines, can be modeled with nonlinear differential-algebraic equations or nonlinear differential equations. By studying the dynamics of these models, we can probe the behavior of these physical systems which in turn allows us to design or control these systems to perform specific operations.

Some phenomena are essentially nonlinear and can only occur in the presence of a nonlinearity in the system. These phenomena cannot be described or predicted by linear dynamical systems. Hence the analysis of nonlinear dynamical systems is more complicated than that for linear systems. Some of the characteristics of nonlinear systems that cannot be predicted by linear systems are: finite escape time responses, multiple equilibria, limit cycle phenomenon, periodic or almost periodic responses, chaos, and multiple modes of behavior.

One specific example of a nonlinear dynamical system is the power system transmission and distribution network. These systems comprise generators, transmission lines, power transformers, and loads. In this research, we focus on the nonlinear characteristics of the power transformers.

The nonlinear characteristics of iron-core power system transformers (example shown in Fig. 1.1) have been investigated for many years. These devices can induce a high voltage due to ferroresonance phenomenon. *Ferroresonance* is a nonlinear phenomenon which can induce discontinuous jump amplitude responses, subharmonic responses, or amplitude-modulated almost-periodic oscillations. The main components that initiate ferroresonance are a voltage source, a lightly damped system, and a closed-path between the compensator capacitance or transmission line capacitance and the nonlinear inductance of the transformer core.

Lightly loaded power transformers are susceptible to overvoltage due to ferroresonance problem. The existence of an overvoltage at the primary terminals of the transformer can increase the potential difference between the transformer windings and cause corona phenomena. This phenomenon may lead to the failure of the transformer which can injure system operators. It might also damage other equipment connected to the system such as,

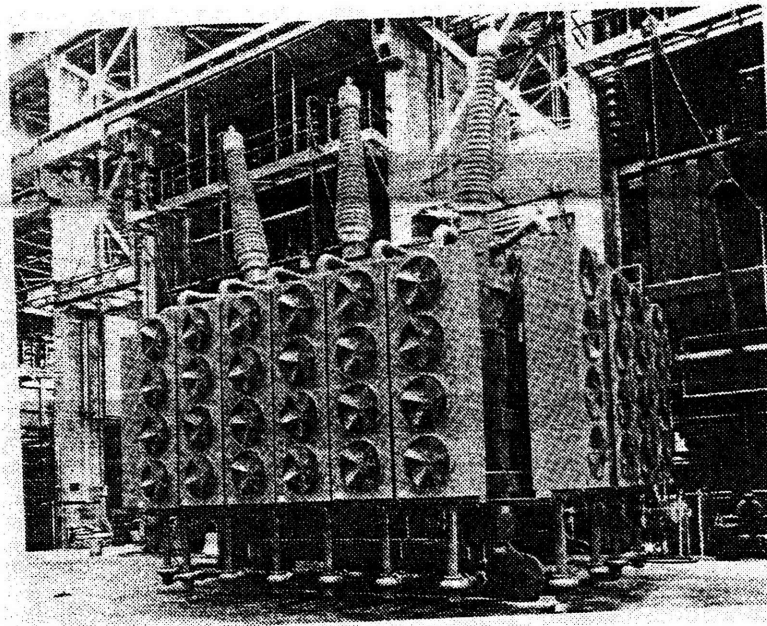


Figure 1.1: 1300-MVA Power transformer (Westinghouse Electric Corporation)

lighting arresters, fuses, circuit breakers, and motors. For example, reversal of direction of rotation of motors under ferroresonance is reported in [3]. Figure 1.2 shows a jump voltage during a ferroresonance. The amplitude of the response $\lambda(t)$ jumped from 0.514 pu to 1.197 pu which is an increase of more than 2.3 times.

Besides the overvoltage problem, the responses of submultiple frequencies, known as subharmonic frequencies, at the transformer terminal can damage the transformer and equipment connected to the power distribution network. They can also interfere with communication lines close to the network grid. Some examples of subharmonic frequencies are $\frac{1}{3}f_0$, $\frac{1}{5}f_0$, $\frac{1}{7}f_0$, where f_0 is the frequency of the driving signal. These odd-order subharmonics may be increased or quenched by changes in the initial conditions of the state variables. They can appear in either stable oscillations or transient oscillations. In Fig. 1.3, $\lambda(t)$ is the response of the transformer while $v_i(t)$ is input of the transformer. In this case, the frequency of the flux $\lambda(t)$ is $\frac{1}{3}$ of the input frequency.

The third behavior of ferroresonance is responses with almost-periodic oscillations with amplitude-modulation. The frequency of this amplitude-modulation is close to the frequency of the driving signal. The domain in which these amplitude-modulated oscillations lie is much smaller than the domain of the harmonic and subharmonic responses. Kumar

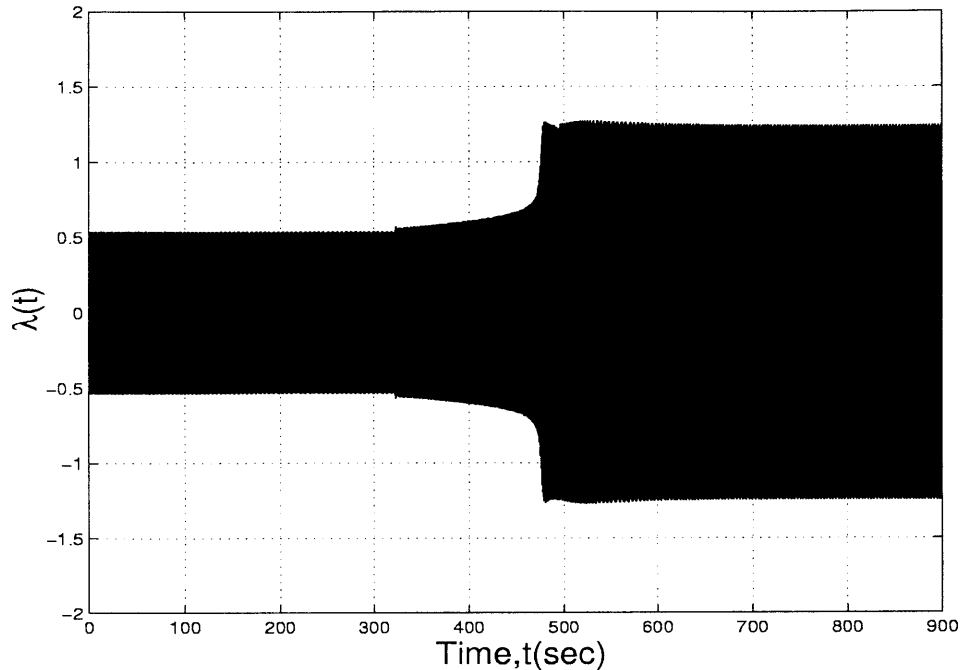


Figure 1.2: Ferroresonance: Discontinuous jump amplitude

and Ertem verified these peculiar oscillations with experimental simulations [4]. Figure 1.4 depicts amplitude-modulated responses under ferroresonance condition.

To unfold the chronological history of ferroresonance, we will review the research activities on the ferroresonance phenomenon in the last 80 years.

1.1 Previous Work on Ferroresonance

The word ferroresonance was introduced in 1920 by Boucherot [5]. Due to practical interest, this phenomenon was investigated heavily in the 1930s when it was discovered that a series line capacitor and the nonlinear inductance of a transformer core can trigger ferroresonance under some conditions.

Research on the ferroresonance problem has been carried out using two different approaches. The first one uses experimental investigations, while the second concentrates on developing models and analytical tools to investigate the behavior of the ferroresonance phenomenon.

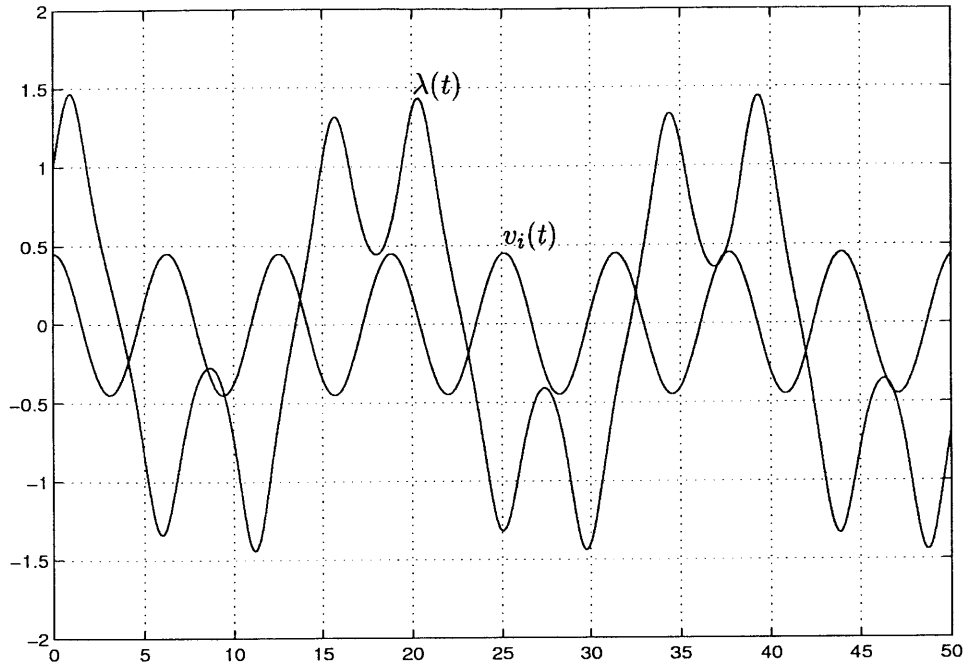


Figure 1.3: Ferroresonance: Subharmonic responses

1.1.1 Experimental Investigation of Ferroresonance

In 1931, Weller noticed that opening a line conductor can result in an abnormal voltage in a lightly loaded power transformer bank [6]. Clarke conducted an experiment with a transformer bank made up of three single-phase transformers, a transmission circuit, fuses, and a three-phase power generator [3]. Similarly, three-phase core type and shell type transformers were investigated. Clarke noticed for the three-phase transformers if the power generator is grounded and the transformer is lightly loaded and grounded, there is no overvoltage across the transformer terminals. On the other hand, if the power generator is ungrounded and one or two conductors are opened, a high sustained voltage results which can damage the transformer bank. Furthermore, if the system is loaded, the ferroresonance overvoltage will be mitigated or eliminated totally.

A rural 14.4/24.9KV distribution system was investigated in [7]. This experiment investigated six 75KVA transformer banks with switching locations varying from 1500 feet to 9 miles with no load on the open phases or the banks. The findings of this experiment are as follows: de-energizing one or two of the phases can excite a sustained overvoltage; and loading the secondary of the open phase reduced the magnitude of the voltage across

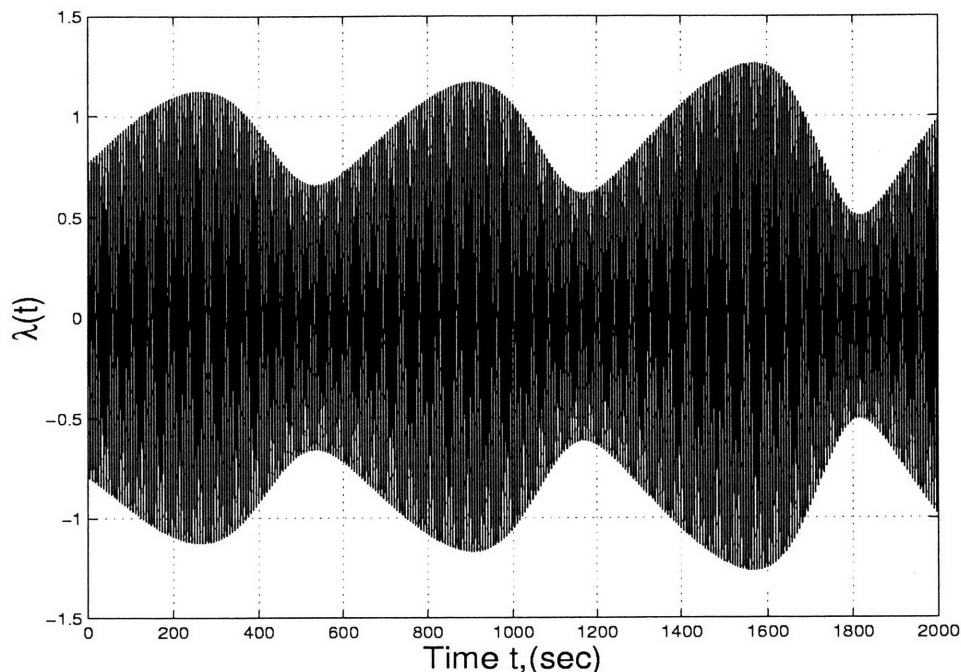


Figure 1.4: Ferroresonance: Amplitude-modulated oscillations

the primary terminals.

Auer and Schultz used a Transient Network Analyzer (TNA) to investigate the ferroresonance overvoltage and subharmonic responses of 14.4/24.9KV grounded-Wye distribution system [8]. Investigating the ferroresonance behavior in a three-phase Wye/Delta transformer bank using a TNA, Auer and Schultz concluded the following: during switching of one or two lines, this system induces an overvoltage which can damage lighting arresters, automatic circuit reclosers, power transformers, cutouts and meters. Furthermore, grounding the primary of the transformer or loading the secondary of the transformer will reduce the magnitude of the ferroresonance overvoltage. Similar results were found in [9]. Hopkinson also found this phenomenon in three-phase Delta/Wye and Wye/Delta configurations of three-phase transformer banks using a transient network analyzer [10,11]. Smith and Swanson showed that remotely grounded-Wye/grounded-Wye power transformers energized from remote locations with single-pole switches result in an overvoltage [12].

Mairs, Stuehm, and Mork [13] implemented experimental investigations on five-legged core transformers on rural electric power systems. This research uncovered that the five-legged core type transformers can induce an overvoltage on unexcited phases. This

ferroresonance is caused by switching of one or two phases during a system fault. To minimize or prevent the ferroresonance problem in this type of transformer, the authors gave the following recommendations: for five-legged transformers, circuit breakers and switches must be simultaneous three-phase interrupt devices;

Most recently, Mork and Stuehm [14] demonstrated chaotic behavior by varying the magnitude of the input voltage, the lengths of transmission lines and the transformer core characteristics. They investigated grounded-Wye to grounded-Wye 75KVA five-legged wound-core power transformer with voltage rating 12470/7200GY-480/277GY. This experiment showed for different parameters the response of the system is periodic while in other cases it is chaotic.

1.1.2 Theoretical Investigation of Ferroresonance

The general characteristics of ferroresonance in power system transformers have been known for some time. However, in order to determine specifically the behavior of such a phenomenon, an analytical treatment is necessary. With such an analysis it is possible to gain insight helpful for investigating the conditions under which the ferroresonance can occur and methods to remedy the problem. In the past 82 years, two approaches for analytical treatments for ferroresonance problem were explored; the time domain and the frequency domain approaches.

1.1.2.1 Time Domain Approach

Odessey and Weber proposed the first analytical work for this problem in 1938 [1]. This analysis used a graphical method. Odessey and Weber studied a series circuit consisting of a sinusoidal input voltage, a capacitor, a resistor, and a saturable-core reactor as shown in Fig 1.5. The steady-state voltage of the circuit can be denoted as

$$E = \sqrt{(IR)^2 + \left(E_L - \frac{I}{\omega C}\right)^2} \quad (1.1)$$

where I is current of the series circuit, $E_L = f(I)$ is the voltage across the nonlinear inductor which is a function of the current, and ω is the angular frequency of the input voltage. Hence, E_L is the volt-ampere characteristic of the nonlinear reactor. Under sinusoidal conditions

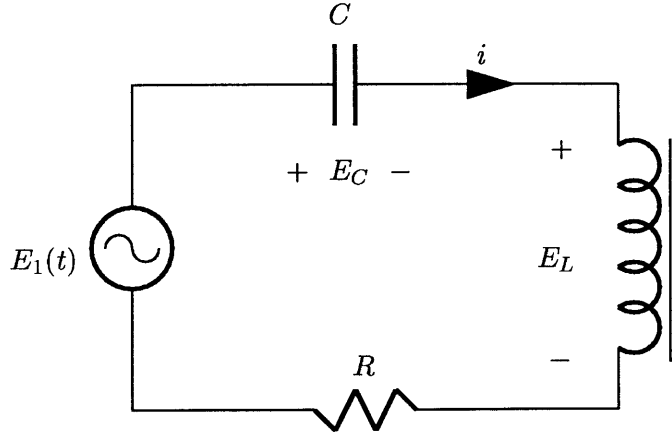


Figure 1.5: Series nonlinear circuit

the following equation holds

$$E_L = \pm \sqrt{E^2 - (IR)^2} + \frac{I}{\omega C} \quad (1.2)$$

Odessey and Weber found the solution of the above equation by plotting the left and the right side of the equation. It is clear that the right side of (1.2) has two terms in I : the first term is an ellipse and the second term is a straight line. Therefore, for particular values of E , R , and C the circuit will have either three solutions or one solution, as depicted in Fig 1.6. In the figure, curve B is the voltage across the linear capacitor, curve C is the voltage across the nonlinear inductor, curve D is $\pm \sqrt{E^2 - (IR)^2}$, and curve A is the voltage defined in equation (1.2). Furthermore, for given input magnitude E , C and R the circuit can have three solutions as shown in the figure at the intersections between curves A and C at the locations 1, 2, and 3. Using physical insight, Odessey and Weber found that there are two stable solutions at locations 1 and 2 and one unstable solutions at the location 2. In a similar circuit topology, Thomson and Rüdenberg proposed a generalized method using a graphical approach in 1939 [15,16]. Both authors considered series and parallel single-phase circuits. For the series circuit, Thomson [17] generalized this graphical analysis to include the core parameters, such as, magnetic flux strength H , magnetic flux density B , the cross sectional area of the core A , and the number of turns of the winding n . If the critical stability conditions for one reactor are know this method enables one to determine the critical stability conditions for any other core which has the same grade of iron.

In 1953 this graphical approach was extended to three-phase circuits [9], such as,

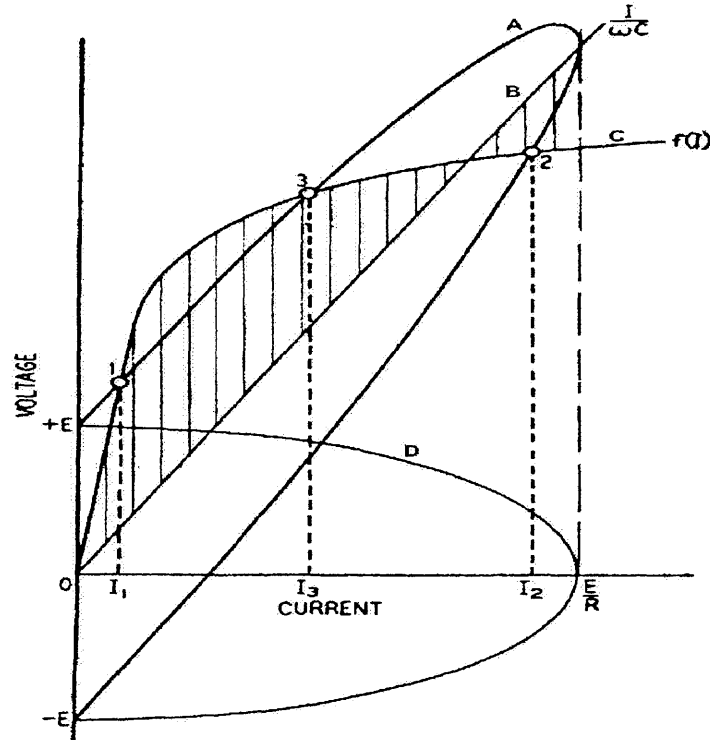


Figure 1.6: Graphical solution of ferroresonance circuit [1]

three-phase power transformers. These authors investigated the existence of ferroresonance when one or two lines of the network were opened. They deduced from their analysis that, if one or two lines are opened, the system will experience a high transient voltage and reversal of phase rotation. Increasing the load or the power factor of the load will increase the ratio of the capacitor KVA to transformer KVA at which multivalued voltages can occur.

Hayashi proposed a more detailed analysis in the 1950s [18]. In his approach, Hayashi approximated the nonlinearity of the saturable core by polynomials. He used two types of polynomials, symmetric and non-symmetric. After the approximation the core, Hayashi assumed the solution of the differential equation to have the following form in steady-state

$$i(t) = x \sin(\omega t) + y \cos(\omega t) \quad (1.3)$$

where ω is the frequency of the input signal. After approximating the steady-state solution, he formulated the variational system. This variational system has similar form to Hill's equation. The stability of this equation was investigated using Hill's approach [19] which

uses Floquet exponents to assess the stability of the time-varying variational system.

More recently, Kieny [20] used the series circuit as shown in Fig. 1.2 and applied the theory of bifurcations. The steady-state solutions of the system were computed using Newton's method. From these steady-state solutions, the bifurcations diagrams were formulated. For different values of input voltage, the system exhibited both Hopf and pitch fork bifurcations. The system also exhibited a $\frac{1}{3}$ subharmonic response.

The critical input voltages at the bifurcation points were computed. To ascertain the stability of the steady-state branches, the Poincaré map and its Jacobian were computed. Then, the stability of the system was assessed by examining the magnitude of the eigenvalues of the Jacobian matrix of the map. This research extended the understanding of the ferroresonance problem, particularly for the single-phase series circuits.

A 25MVA 110/44/4KV power auto-transformer was investigated in [21,22]. These authors designated the nonlinear core with an odd polynomial of the following form

$$i(t) = a\phi + b\phi^n, \quad \text{where } n = 11 \quad (1.4)$$

The first term represents the inverse of the linear inductance of the core while the higher-order term approximates the saturation of the core. In their research the series circuit was modified. A damping resistor was connected in parallel with the iron core to simulate the core loss of the transformer. To simplify the computation of the steady-state solutions of the nonlinear system, the authors approximated the solution up to the first harmonic and utilized a similar nonlinear core model as in equation (1.3). The steady-state solution of the system was computed using the harmonic balance approach. The critical values of the magnitude input voltage and the capacitance of the capacitor were computed. The authors pointed out that for some combinations of circuit parameters, ferroresonance can occur even for an input voltage of very small magnitudes. Plots in flux-capacitance and flux-input magnitude spaces show jumps of the flux for some critical values of the system parameters.

Kieny, Le Roy and Sbai [23] computed the steady-state solutions of a series ferroresonance circuit using the Galerkin method. For periodic systems, harmonic balancing and the Galerkin method are equivalent. Since the Galerkin method imposes difficulty in convergence during initialization if the initial condition is not well chosen, the authors used the pseudo-arclength continuation method. The continuation method finds the solution of the system at a point in a branch and then approximates a second point in the branch using

the previous solution as an initial guess. In this research the nonlinear core was represented as in (1.4) with $n = 9$. The authors concluded with similar results as previous methods. However, a higher degree of accuracy was claimed for this method. One drawback of this method is that it is not applicable to computations of non-periodic steady-state responses, such as, pseudo-periodic or chaotic steady-state responses which can occur in ferroresonance systems. Another drawback of this paper is that the investigators never checked the stability of the steady-state solutions or even in that matter, the characteristic stability of the turning points of the bifurcation diagrams.

So far we have only considered a power system with grounded generation. In [24] the stability domains of three-phase ferroresonance in an isolated neutral network with grounded-neutral voltage transformer were investigated. This type of topology can occur in distribution networks in factories and public distribution networks which are temporarily isolated. The nonlinearity of the iron core was denoted as in equation (1.4) with $n = 5$. These authors employed Clarke transformations and decoupled the o component from the α and β components since the three-phase model cannot be reduced into a single-phase representation. The method of harmonic balance was employed to compute the steady-state solution of the system. The stability of these steady-state solutions was assessed by examining the sign of the Jacobian matrix of the harmonic equations. In this research, the authors computed steady-state solutions with the same frequency as the frequency of the input f_0 . Other solutions were computed with frequencies: $3f_0$, $\frac{1}{2}f_0$ and $2f_0$.

In [25] a series circuit which contained a voltage source, capacitor, resistor and nonlinear iron-core was investigated using the Newton-Raphson scheme. The authors first discretised the nonlinear differential equation using the trapezoidal rule. To compute the transient response, the authors solved the nonlinear algebraic equations at n successive time-steps to obtain the transient response from $t = 0$ to $t = T$, where T is the period of the input signal. Similarly, to compute the steady-state solution, they assumed that there exists an initial condition such that the transient response is identical to the steady-state response of the system. Hence, they formulated the Newton-Raphson scheme to find that initial condition. The authors also compared their results with the results of using the Hybrid Technique [26]. Around bifurcation points, the authors used the continuation method, since the Jacobian matrix is singular at the turning points.

Ferroresonance of three-phase oscillations in ungrounded power system networks was investigated in [27]. These authors used a similar approach and a similar core model as those in [24]; however, they computed the steady-state response as a boundary value problem. The system was converted into an autonomous representation by adding two more states

to the original system. The AUTO software package was used to compute the steady-state solutions of the system. From these steady-state solutions, the bifurcation diagrams were generated. The bifurcation parameters used in this system were the magnitude of the input voltage and the capacitance of the transmission lines, i.e. the zero-sequence capacitance.

1.1.2.2 Frequency Domain Approach

In the frequency domain, the system is formulated in a feedback setting by quasi-linearizing the nonlinear elements in the system. This linearization depends on steady-state solutions of the system. Then, using this linearized model, we employ frequency domain techniques to analyze the stability of the steady-state solutions. In this section, we consider the nonlinear feedback system shown in Fig 1.7. The series ferroresonance circuit which comprises a

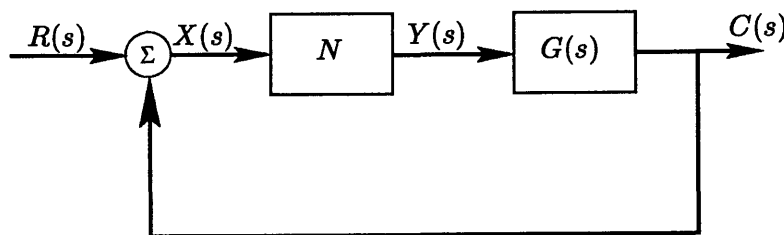


Figure 1.7: Nonlinear Feedback System

resistor, capacitor, and nonlinear inductor can be formulated in a feedback setting as in Fig. 1.7. X is the flux of the core, R is the input voltage of the transformer, $G(s)$ is the frequency domain representation of the linear part of the system, N is the representation of the nonlinearity, Y is the output of the nonlinear element and C is the output of $G(s)$. The objective of this scheme is to approximate N using the steady-state value of the magnitude and the phase of the error signal, and then use the frequency domain techniques such as the Nyquist criterion [28–31] to assess the stability of the feedback system.

In this approach the steady-state solution of the system is computed using the the describing function method [32–35]. The method used to analyze the stability of the steady-state solution is based on the theory developed by West, Douce, and Livesley in [36]. This theory is known as the *Incremental-Input Describing Function Analysis*. This method assesses the stability of the feedback system by adding the input signal to an incremental input with the same frequency but different phase and checks the stability of the incremental system using the Nyquist criterion.

Swift [37] applied this theory to a single-phase transformer in 1969. He found by fixing the line capacitance and resistance of the transmission lines and varying the magnitude of the input voltage and the line inductance of the system, the system can have different solutions. Some of these solutions are stable while others are unstable. Further application to this theory, Kumar and Ertem investigated capacitor voltage transformer for existence of ferroresonance [4] in 1991. In this study, they found harmonic and subharmonic of the system solutions and also they investigated the corresponding stability of these steady-state solutions.

In Chapter 3, we will give a detailed explanations in this theory.

1.2 Modeling Ferroresonance

Analyzing ferroresonance requires a model to which we can apply analytical tools in order to isolate the regions in which ferroresonance can occur for a given system. In general ferroresonance models can be classified into two categories: single-phase and three-phase representations. Transformer models, particularly those which can handle low frequency simulations, are well developed and can be found in [38–42].

Generally, there are three model representations for the nonlinearity of the transformer inductance: two-term nonlinear polynomial, pseudo-nonlinear with hysteresis, and true-nonlinear with hysteresis.

In this research, we employ the two-term polynomial core models given by equation (1.4), where n can take the values $\{3, 5, 7, \dots\}$. This model simplifies the complexity of the system dynamics and it gives results which agree with experimental results for well behaved systems. Two popular ways to compute the coefficient of the polynomial are given by [43,44]. The first one uses the least-square curve fitting method while the other one chooses specific points of the root-mean-square values of the voltage and the current of the nonlinear core using some optimal rule. In benchmark tests, the second method was more robust than the least-square method.

Before stating the criterion of the two models of ferroresonance systems, we give some definitions from [45], written here for easy accessibility. Single-phase ferroresonance is said to occur if the system can be reduced using Thévenin transformations in the linear part and then the nonlinear inductance of the transformer is connected in series or if a three-phase system can be resolved into separate single-phase representations in which ferroresonance

occurs in the same way as when they are connected in the three-phase system. Furthermore, the three-phase ferroresonance is said to occur if the three-phases are strongly coupled, i.e., if the internal dynamics of the decoupled system differ from the internal dynamics of the full system.

1.2.1 Single-Phase Ferroresonance Model

There are three possible scenarios for which single-phase ferroresonance can occur [45]:

- A voltage transformer connected to a high-voltage line, which is disconnected but running alongside another energized line.
- A voltage transformer and the capacitance between hv/mv.
- A voltage transformer and the capacitance constituted by an open circuit breaker.

1.2.2 Three-Phase Ferroresonance Model

In the three-phase ferroresonance, there are two types:

- Voltage transformers connected to a system with an insulated neutral and very low zero-sequence capacitance.
- An unloaded power transformer, supplied accidentally on one or two phases.

1.3 Contribution of the Thesis

The objective of this research is to develop a systematic tool to analyze ferroresonance in nonlinear dynamical systems. The single-phase overvoltage or jump phenomenon problem will be formulated in a control setting with a modified Nyquist criterion. This theory was introduced by West, Douce, and Livesley, however, there is a subtle error in the theory. In this research, the theory will be corrected and some examples are presented to prove the modifications of the theory.

The generalized state-space averaging method is applied to the ferroresonance problem for the first time to examine the existence and stability of harmonic and subharmonic

periodic steady-state solutions. Both single-phase and three-phase ferroresonance are considered. Additionally, harmonic and subharmonic periodic solutions are examined in terms of their bifurcations, and the limits of the system parameters are computed to gain an in-depth insight into the characteristics of ferroresonance phenomenon.

The first published work in this thesis was presented at the 31st North American Power Symposium October, 1999 in San Luis Obispo CA. This paper addresses the single-phase ferroresonance problem in power transformers [46].

1.4 Organization of the Thesis

The remainder of this thesis is divided into six chapters. Chapter 2 develops the ferroresonance models. In this research we are considering two power system topologies that are prime candidates for the ferroresonance phenomenon. The first scenario is a single-phase representation of a power system network. The second case is a power system network topology with a lightly loaded or insufficient damped three-phase power distribution network with single-pole switching. In this type of switching, three-phase transformers are vulnerable to excessive line-to-line or line-to-ground overvoltages. In the three-phase transformer models, three separate models are considered: all switches closed, one switch opened, and two switches opened. In all of the models we will formulate a system of nonlinear differential equations that govern the internal dynamics of the nonlinear dynamical system.

In chapter 3, the Nyquist stability criterion is reviewed and the notion of the describing function is introduced. Along with this, the theory of the synchronous incremental-input describing function which was introduced by West, Douce, and Livesley [36] is reviewed. A sufficient condition for the stability of a nonlinear feedback system with a third-order memoryless nonlinearity was derived by West, Douce, and Livesley; however, it fails to address the stability of general systems, particularly at synchronous frequency. Incorrect mapping regions were chosen to determine the poles that lie in the right-half s -plane of the closed-loop system. In this research, the theory will be corrected to assess the stability of nonlinear systems which have odd monomial memoryless nonlinearities. The modified incremental-input describing function will follow. For further illustrations, we take a single-phase ferroresonance example and compute the steady-state solution and the stability of the periodic solutions to see subtle differences between the original incremental-input describing function and modified one.

Chapter 4 lays the groundwork for the generalized state-space averaging methodol-

ogy. This method has been shown in [47–51] to be an effective tool to analyze pulse-width modulated (PWM) switching power converters and oscillations in nonlinear systems. However, Averaging theory dates to the days of van der Pol and Duffing era [52,19,18,53–55]. The generalized state-space averaging method is a way of representing a periodic signal as linear combinations of the basis functions $e^{jk\omega t}$. The coordinates of this space are slowly-varying functions of time. If the signal is periodic, then the coordinates are constant; otherwise they are slowly varying functions compared to the variations of the frequency of the signal. Hence, this method gives robust results for systems that have responses such as harmonics, subharmonics, superharmonics, and chaotic behavior.

Poincaré and Floquet theory will be introduced in Chapter 5. A forced Duffing oscillator is analyzed as a benchmark test for Poincaré, Floquet, and the generalized state-space averaging method, particularly assessing the stability of the periodic solutions of the oscillator.

Next, in Chapter 6, the generalized state-space methodology is applied to single-phase and three-phase power transformers to study the existence and stability of harmonic and subharmonic periodic steady-state responses. The bifurcations of these steady-state solutions will be investigated to find the limits of the parameters of the system at the bifurcation points.

Finally, Chapter 7 concludes the thesis with a summary and suggestions for future work.

1.4 Organization of the Thesis

Chapter 2

Modeling Ferroresonance in Power Distribution Networks

2.1 Single-Phase Ferroresonance Model

Single-phase ferroresonance can arise in three scenarios as defined in Section 1.2.1. The first case occurs two high voltage transmission lines run in parallel with different operating voltages, say 150KV and 75KV, as shown in Figure 2.1. Since line 2 is open at both ends,

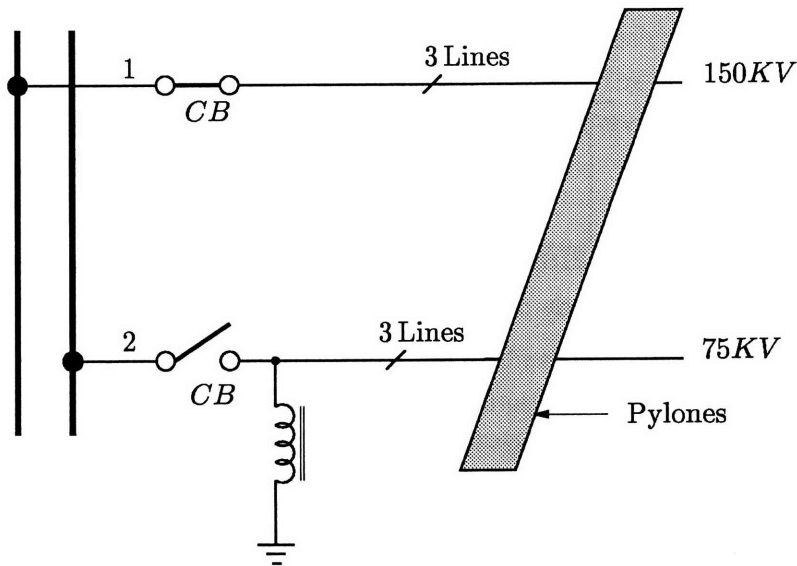


Figure 2.1: Parallel high voltage transmission lines

the capacitance between the two lines induces a voltage across the transformer connected to line 2. An equivalent circuit is shown in Fig. 2.2 where C_t is the resultant lumped capacitance between line 1 and 2, $v(t)$ is the resultant voltage across the capacitance between the lines, C_1 is the combination of line capacitance C_2 and the compensating capacitance of the transformer, and L , R and C_2 are a π model representation of the transmission line. For single-phase power distribution networks, Fig. 2.3 represents a ferroresonance model where C_1 , L and R are the transmission line parameters. All the transformer losses are assumed

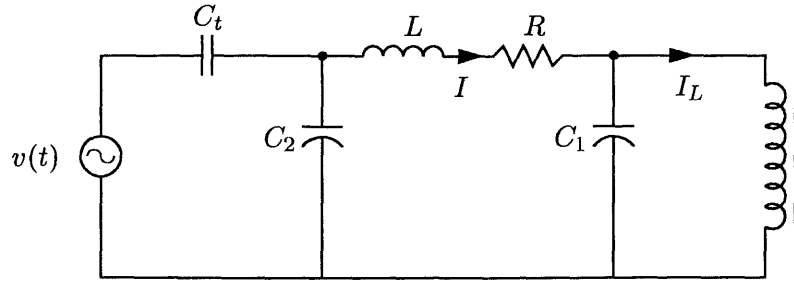


Figure 2.2: Single-phase ferroresonance circuit model: I

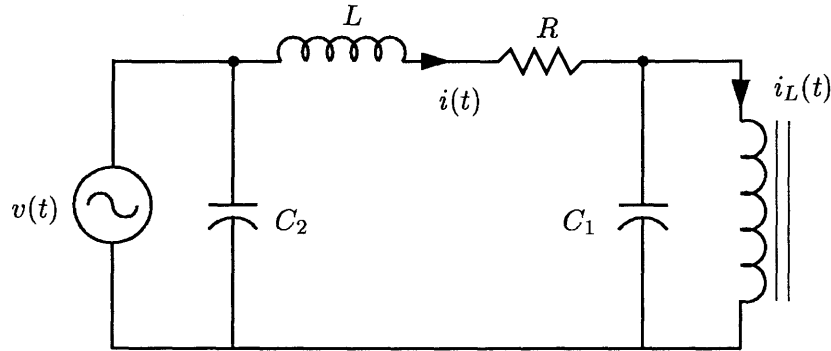


Figure 2.3: Single-phase ferroresonance circuit model: II

to be negligible in this model. The secondary of the transformer is unloaded and we also neglect the leakage reactance.

The relation between the current $i_L(t)$ and the flux $\lambda(t)$ shown in Fig. 2.3 can be modeled as

$$i_L(t) = K_1\lambda + K_5\lambda^5 \quad (2.1)$$

The first term of this equation represents the linear region of the magnetization characteristic curve and its coefficient is related to the linear inductance of the transformer while the nonlinear term approximates the saturation effect of the core. In this formulation, all the measured quantities are normalized utilizing the following bases: linear transformer reactance, rated angular frequency, and the rated voltage of the transformer.

The dynamics of System Fig. 2.3 is governing by the following nonlinear differential

equation:

$$L \frac{di(t)}{dt} + Ri(t) + \frac{d\lambda(t)}{dt} = v(t) \quad \text{where} \quad v(t) = M \cos(t) \quad (2.2)$$

$$i(t) = C \frac{d^2\lambda(t)}{dt^2} + i_L(t)$$

Further simplification of (2.1) and (2.2) yields

$$\frac{d^3\lambda}{dt^3} + a_1 \frac{d^2\lambda}{dt^2} + a_2 \frac{d\lambda}{dt} + a_3\lambda + a_4\lambda^4 \frac{d\lambda}{dt} + a_5\lambda^5 = a_6 M \cos(t) \quad (2.3)$$

where,

$$a_1 = \frac{R}{L}, \quad a_2 = \frac{1+L}{LC}, \quad a_3 = \frac{R}{LC}, \quad a_4 = \frac{20}{C}, \quad a_5 = \frac{4R}{LC}, \quad \text{and} \quad a_6 = \frac{1}{LC} \quad (2.4)$$

In this model we have four parameters R , L , C and M . The values of the first three parameters depend on the weather and the length of the transmission lines while M depends on the amplitude of the input voltage. Since the secondary of the transformer is unloaded, we eliminated the model of the secondary winding from the network diagram.

2.2 Three-phase Ferroresonance Models

For three-phase ferroresonance representations, we outlined two situations in Section 1.2.2. We consider a lightly loaded three-phase power distribution transformer, a line modeled as a π model representation, a balanced positive-sequence generator, and a circuit breaker. The critical element in this topology is the circuit breaker. We are interested in two cases: one of the legs of the circuit breaker is opened while the other two are closed; two legs of the circuit breaker are opened while the third leg is closed.

To gain some insight, first we consider a topology where all the switches are closed. Then, we will extend our analysis for the other two circumstances.

2.2.1 Balanced Power System Network

Consider the three-phase power system network shown in Fig. 2.4. In this topology, the system is operating under normal conditions. All the legs of the circuit breaker S_1 , S_2 , and S_3 are closed.

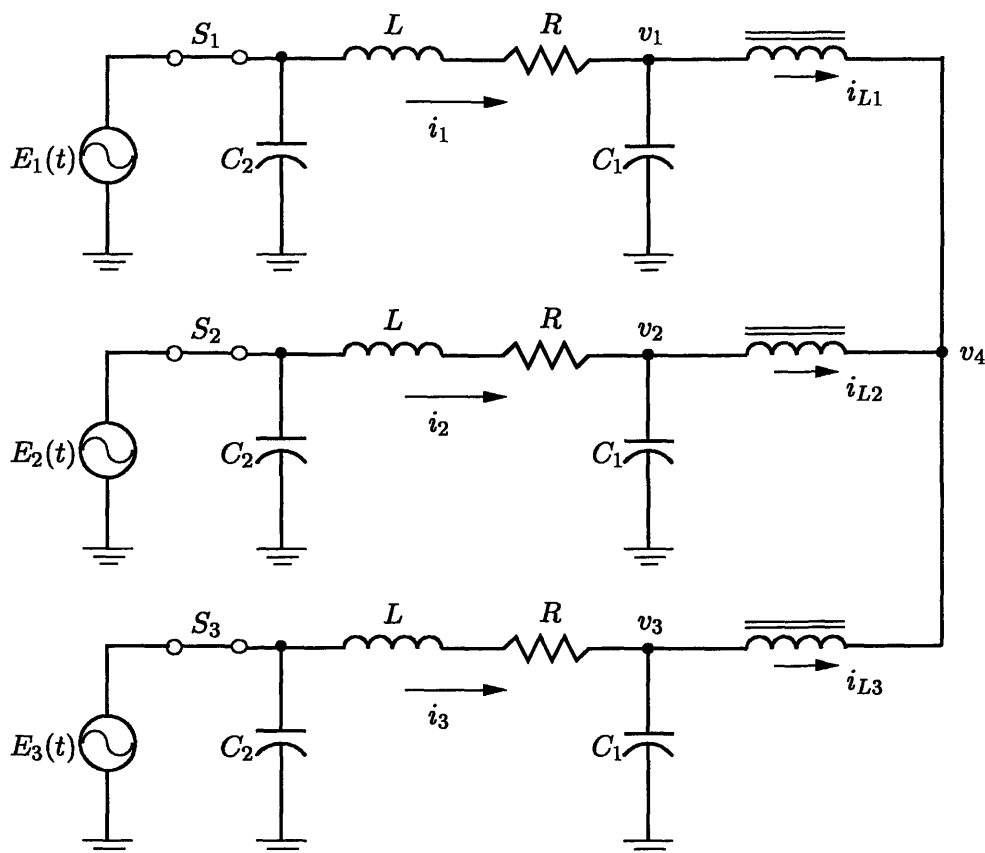


Figure 2.4: Three-phase balanced power system network: All switches closed

The π model branch C_2 , L , and R represent the transmission line impedance of the network, while C_1 is the equivalent capacitance of C_2 and the capacitance of a compensator across the primary side of the transformer to support the voltage level at the transformer terminals. All the lines are assumed to have the same line parameters. Furthermore, varying the length of the transmission will change the line impedance. The three voltages $E_1(t)$, $E_2(t)$, and $E_3(t)$ represent a grounded-Wye connected balanced positive-sequence three-phase generator. The three nonlinear inductances represent the primary of the ungrounded-Wye connected three-phase power distribution transformer. All the leakage resistance and reactance of the transformer are ignored since they are much smaller than the transmission line reactance and resistance. The secondary side of the transformer is unloaded. Similarly, the capacitance between the windings of the transformer are disregarded since they are very small.

To formulate a differential equation that governs the dynamics of this nonlinear

system, we need to apply Kirchoff's voltage and current laws. From nodes labeled with v_1 , v_2 , and v_3 , the current constraints of the connection are given by

$$C_1 \frac{dv_1}{dt} + i_{L1} = i_1 \quad (2.5a)$$

$$C_1 \frac{dv_2}{dt} + i_{L2} = i_2 \quad (2.5b)$$

$$C_1 \frac{dv_3}{dt} + i_{L3} = i_3 \quad (2.5c)$$

Similarly, computing the voltage drop across E_1 and v_1 , E_2 and v_2 , and E_3 and v_3 we have the following

$$L \frac{di_1}{dt} + Ri_1 + v_1 = E_1 \quad (2.6a)$$

$$L \frac{di_2}{dt} + Ri_2 + v_2 = E_2 \quad (2.6b)$$

$$L \frac{di_3}{dt} + Ri_3 + v_3 = E_3 \quad (2.6c)$$

Furthermore, calculating the voltage drop across v_1 and v_2 , v_1 and v_3 , and the current constraint at node 4 yields the following differential equation

$$\frac{d\lambda_1}{dt} - \frac{d\lambda_3}{dt} - v_1 + v_3 = 0 \quad (2.7a)$$

$$\frac{d\lambda_2}{dt} - \frac{d\lambda_3}{dt} - v_2 + v_3 = 0 \quad (2.7b)$$

$$i_{L1} + i_{L2} + i_{L3} = 0 \quad (2.7c)$$

The relation between the current and the flux linkages of the nonlinear elements takes the following form:

$$i_{Li} = K_1 \lambda_i + K_n \lambda_i^n \quad \text{where } i = 1, 2, 3 \quad n = 3, 5, 7, \dots \quad \text{and } K_1, K_n \in \mathbb{R} \quad (2.8)$$

For further simplifications, the system defined in Fig. 2.4 can be denoted as

$$\frac{dv_1}{dt} + a_1\lambda_1 + a_2\lambda_1^n - a_3i_1 = 0 \quad (2.9a)$$

$$\frac{dv_2}{dt} + a_1\lambda_2 + a_2\lambda_2^n - a_3i_2 = 0 \quad (2.9b)$$

$$\frac{dv_3}{dt} + a_1\lambda_3 + a_2\lambda_3^n - a_3i_3 = 0 \quad (2.9c)$$

$$\frac{di_1}{dt} + a_5i_1 + a_4v_1 = a_4E_1 \quad (2.9d)$$

$$\frac{di_2}{dt} + a_5i_2 + a_4v_2 = a_4E_2 \quad (2.9e)$$

$$\frac{di_3}{dt} + a_5i_3 + a_4v_3 = a_4E_3 \quad (2.9f)$$

$$\frac{d\lambda_1}{dt} - \frac{d\lambda_3}{dt} - v_1 + v_3 = 0 \quad (2.9g)$$

$$\frac{d\lambda_2}{dt} - \frac{d\lambda_3}{dt} - v_2 + v_3 = 0 \quad (2.9h)$$

$$K_1(\lambda_1 + \lambda_2 + \lambda_3) + K_n(\lambda_1^n + \lambda_2^n + \lambda_3^n) = 0 \quad (2.9i)$$

where

$$a_1 = \frac{K_1}{C_1} \quad a_2 = \frac{K_n}{C_1} \quad a_3 = \frac{1}{C_1} \quad a_4 = \frac{1}{L} \quad \text{and} \quad a_5 = \frac{R}{L} \quad (2.10)$$

this is a set of nonlinear differential-algebraic equations (DAE). Hence, we have 9 state variables where each of the state variable is related to the other states by an algebraic equation.

2.2.2 One Switch Opened Ferroresonance Model

For the second case, consider the following unbalanced power system network depicted in Fig. 2.5. In this topology, the system is operating under unbalanced conditions. Switch S_1 is open while S_2 and S_3 are closed.

The relations between the currents and the flux linkages of the nonlinear elements take the following form:

$$i_{Li} = K_1\lambda_i + K_n\lambda_i^n \quad \text{where} \quad i = 1, 2, 3 \quad \text{and} \quad n = 3, 5, 7, \dots \quad (2.11)$$

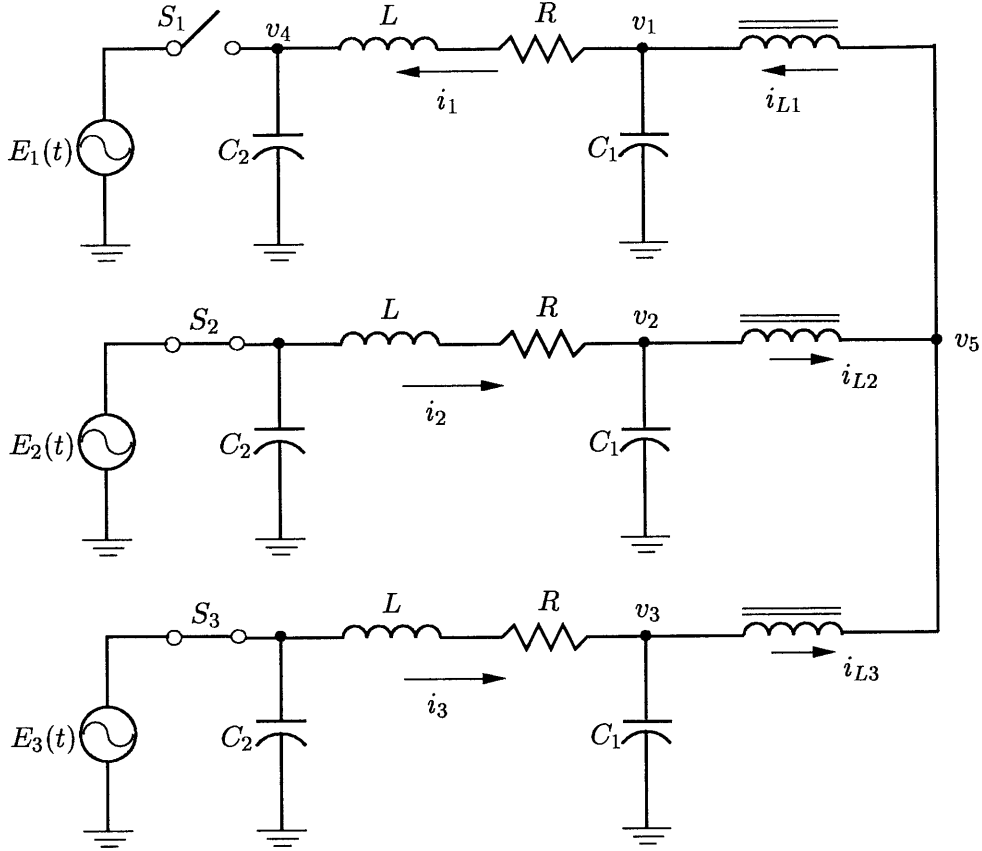


Figure 2.5: Three-phase power system network: One switch opened

To formulate the differential equation that governs the dynamics of this unbalanced power system network, we need to apply Kirchhoff's voltage and current laws. At nodes labeled with $v_1, v_2, v_3,$ and v_4 , the current constraints of the junctions are given by

$$C_1 \frac{dv_1}{dt} - i_{L1} + i_1 = 0 \quad (2.12a)$$

$$C_1 \frac{dv_2}{dt} + i_{L2} - i_2 = 0 \quad (2.12b)$$

$$C_1 \frac{dv_3}{dt} + i_{L3} - i_3 = 0 \quad (2.12c)$$

$$C_2 \frac{dv_4}{dt} - i_1 = 0 \quad (2.12d)$$

Likewise, computing the voltage drop across v_1 and v_4 , E_2 and v_2 , and E_3 and v_3 we

have the following

$$L \frac{di_1}{dt} + Ri_1 + v_4 - v_1 = 0 \quad (2.13a)$$

$$L \frac{di_2}{dt} + Ri_2 + v_2 = E_2 \quad (2.13b)$$

$$L \frac{di_3}{dt} + Ri_3 + v_3 = E_3 \quad (2.13c)$$

In addition, the voltage drop across v_1 and v_2 , v_1 and v_3 , and the current constraint at node 5 yield the following differential equations

$$\frac{d\lambda_2}{dt} + \frac{d\lambda_1}{dt} + v_1 - v_2 = 0 \quad (2.14a)$$

$$\frac{d\lambda_3}{dt} + \frac{d\lambda_1}{dt} + v_1 - v_3 = 0 \quad (2.14b)$$

$$i_{L1} - i_{L2} - i_{L3} = 0 \quad (2.14c)$$

For further simplifications, the system defined in Fig. 2.5 can be denoted as

$$\frac{dv_1}{dt} - a_1\lambda_1 - a_2\lambda_1^n + a_3i_1 = 0 \quad (2.15a)$$

$$\frac{dv_2}{dt} + a_1\lambda_2 + a_2\lambda_2^n - a_3i_2 = 0 \quad (2.15b)$$

$$\frac{dv_3}{dt} + a_1\lambda_3 + a_2\lambda_3^n - a_3i_3 = 0 \quad (2.15c)$$

$$\frac{dv_4}{dt} - a_6i_1 = 0 \quad (2.15d)$$

$$\frac{di_1}{dt} + a_5i_1 + a_4v_4 - a_4v_1 = 0 \quad (2.15e)$$

$$\frac{di_2}{dt} + a_5i_2 + a_4v_2 = a_4E_2 \quad (2.15f)$$

$$\frac{di_3}{dt} + a_5i_3 + a_4v_3 = a_4E_3 \quad (2.15g)$$

$$\frac{d\lambda_2}{dt} + \frac{d\lambda_1}{dt} + v_1 - v_2 = 0 \quad (2.15h)$$

$$\frac{d\lambda_3}{dt} + \frac{d\lambda_1}{dt} + v_1 - v_3 = 0 \quad (2.15i)$$

$$K_1(\lambda_1 - \lambda_2 - \lambda_3) + K_n(\lambda_1^n - \lambda_2^n - \lambda_3^n) = 0 \quad (2.15j)$$

where

$$a_1 = \frac{K_1}{C_1} \quad a_2 = \frac{K_n}{C_1} \quad a_3 = \frac{1}{C_1} \quad a_4 = \frac{1}{L} \quad a_5 = \frac{R}{L} \quad \text{and} \quad a_6 = \frac{1}{C_2} \quad (2.16)$$

Similarly, these are nonlinear differential-algebraic equations (DAE). Hence, we have 10 state variables where each of the state variables is associated to the other states by an algebraic equation.

2.2.3 Two Switches Opened Ferroresonance Model

Finally, in the third situation, consider the following unbalanced power system network depicted in Fig. 2.6. In this topology, the system is operating under unbalanced conditions. Switches S_1 and S_2 are opened while S_3 is closed.

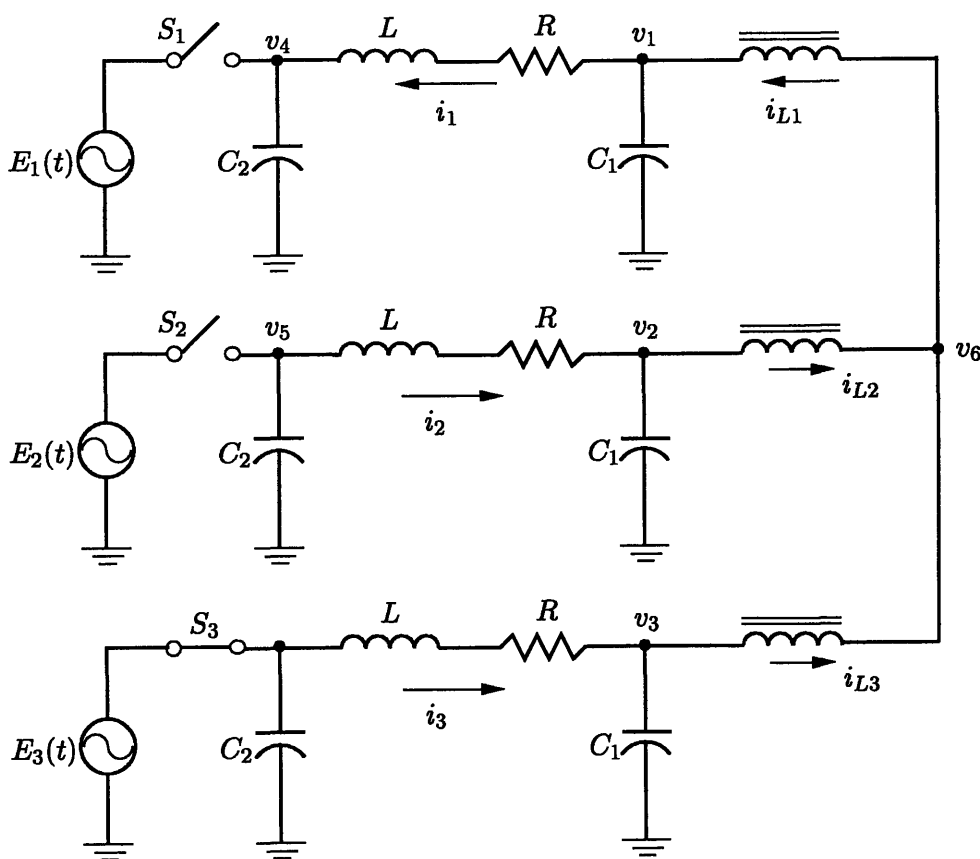


Figure 2.6: Three-phase power system network: Two switches opened

To model the system, we need to formulate the differential equations that govern the internal dynamics of this unbalanced power system network. Application of Kirchhoff's voltage and current laws is required. From the nodes labeled with v_1 , v_2 , v_3 , v_4 , and v_5 , the current constraints of the junctions are given by

$$C_1 \frac{dv_1}{dt} - i_{L1} + i_1 = 0 \quad (2.17a)$$

$$C_1 \frac{dv_2}{dt} - i_{L2} + i_2 = 0 \quad (2.17b)$$

$$C_1 \frac{dv_3}{dt} + i_{L3} - i_3 = 0 \quad (2.17c)$$

$$C_2 \frac{dv_4}{dt} - i_1 = 0 \quad (2.17d)$$

$$C_2 \frac{dv_5}{dt} - i_2 = 0 \quad (2.17e)$$

Analogously, computing the voltage drop across v_1 and v_4 , v_2 and v_5 , and E_3 and v_3 we have the following differential equations

$$L \frac{di_1}{dt} + Ri_1 - v_1 + v_4 = 0 \quad (2.18a)$$

$$L \frac{di_2}{dt} + Ri_2 - v_2 + v_5 = 0 \quad (2.18b)$$

$$L \frac{di_3}{dt} + Ri_3 + v_3 = E_3 \quad (2.18c)$$

Furthermore, the voltage drop across v_1 and v_3 , v_2 and v_3 , and the current constraint at node 6 yield the following differential equations

$$\frac{d\lambda_1}{dt} + \frac{d\lambda_3}{dt} + v_1 - v_3 = 0 \quad (2.19a)$$

$$\frac{d\lambda_2}{dt} + \frac{d\lambda_3}{dt} + v_2 - v_3 = 0 \quad (2.19b)$$

$$i_{L3} - i_{L1} - i_{L2} = 0 \quad (2.19c)$$

For further simplifications, the system defined in Fig. 2.6 can be denoted as

$$\frac{d v_1}{d t} - a_1 \lambda_1 - a_2 \lambda_1^n + a_3 i_1 = 0 \quad (2.20a)$$

$$\frac{d v_2}{d t} - a_1 \lambda_2 - a_2 \lambda_2^n + a_3 i_2 = 0 \quad (2.20b)$$

$$\frac{d v_3}{d t} + a_1 \lambda_3 + a_2 \lambda_3^n - a_3 i_3 = 0 \quad (2.20c)$$

$$\frac{d v_4}{d t} - a_6 i_1 = 0 \quad (2.20d)$$

$$\frac{d v_5}{d t} - a_6 i_2 = 0 \quad (2.20e)$$

$$\frac{d i_1}{d t} + a_5 i_1 - a_4 v_1 + a_4 v_4 = 0 \quad (2.20f)$$

$$\frac{d i_2}{d t} + a_5 i_2 - a_4 v_2 + a_4 v_5 = 0 \quad (2.20g)$$

$$\frac{d i_3}{d t} + a_5 i_3 + a_4 v_3 = a_4 E_3 \quad (2.20h)$$

$$\frac{d \lambda_1}{d t} + \frac{d \lambda_3}{d t} + v_1 - v_3 = 0 \quad (2.20i)$$

$$\frac{d \lambda_2}{d t} + \frac{d \lambda_3}{d t} + v_2 - v_3 = 0 \quad (2.20j)$$

$$K_1(\lambda_1 + \lambda_2 - \lambda_3) + K_n(\lambda_1^n + \lambda_2^n - \lambda_3^n) = 0 \quad (2.20k)$$

This model is a nonlinear differential-algebraic equation (DAE). Hence, we have 11 state variables where each of the state variable is associated to the other states by an algebraic equation.

These four models (2.3), (2.9), (2.15), and (2.20) will be analyzed using the generalized state-space averaging method in Chapter 6. Particularly, we will investigate the equilibrium states of the systems and their stability. Furthermore, we will examine bifurcation diagrams of these steady-state solutions.

2.2 Three-phase Ferroresonance Models

Chapter 3

Synchronous Incremental-input Describing Function

One approach to simplifying the analysis of a nonlinear system is the optimal quasi-linearization method which is based on *sinusoidal-input describing function analysis*. In this method the nonlinear element is linearized based on a few parameters such as the magnitude and the frequency of the gain of the nonlinear element. The elegance of the sinusoidal-input describing function analysis is apparent in a nonautonomous system. The error of this approximation is a function of the inherent nonlinearity of the system.

For power system distribution networks under ferroresonance conditions, there are multiple solutions and sub-harmonic oscillations for a given input amplitude, frequency, and initial state. The input is assumed to be a sinusoidal signal. An intuitive approach to analyzing the stability of a steady-state solution is to perturb the steady-state solution and then probe the stability of the incremental system. Such a method is called the *synchronous incremental-input describing function methodology*.

The purpose of this section is to show how the ferroresonance problem, particularly, single-phase ferroresonance problem can be solved using a synchronous incremental-input describing function. Also in this section we will point out and fix a flaw in the previously developed theory of the synchronous incremental-input describing function.

3.1 Dual-Input Describing Function

To describe the incremental-input describing function method and to point out a flaw in the theory, we apply the theory to an example which West, Douce, and Livesley used to demonstrate their results [36].

Consider the following nonlinear system shown in Fig. 3.1 where $G(s)$ is a strictly proper rational linear transfer function and $N(x)$ is given by

$$N(x) = x^3. \tag{3.1}$$

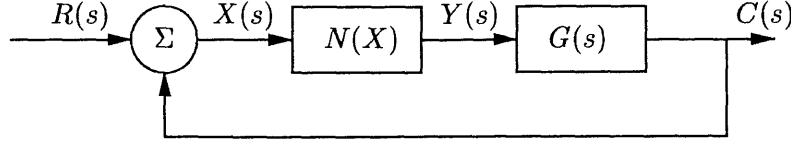


Figure 3.1: Nonlinear interconnected feedback system

Assume the input to the system $r(t)$ is a sinusoidal function of the form

$$r(t) = M \cos(\omega t + \theta) \quad (3.2)$$

and the steady-state error signal $x(t)$ has the following form

$$x(t) = \mathcal{A} \cos(\omega t + \phi). \quad (3.3)$$

To examine the stability of this steady-state solution, suppose an incremental-input is applied to the system. With the incremental signal, the input of the system will take the following form

$$r(t) = M \cos(\omega t + \theta) + \gamma \cos(n\omega t) \quad \text{where } \gamma \ll M. \quad (3.4)$$

Due to the incremental-input, the error signal takes the form

$$x(t) = \mathcal{A} \cos(\omega t + \phi) + B \cos(n\omega t) \quad \text{where } B \ll \mathcal{A} \quad (3.5)$$

The output of the synchronous component of the nonlinear element due to this error signal is given by

$$\begin{aligned} y(t) &= x^3 \\ &= (\mathcal{A} \cos(\omega t + \phi) + B \cos(n\omega t))^3 \\ &= \frac{3\mathcal{A}}{4} (\mathcal{A}^2 + 2B^2) \cos(\omega t + \phi) + \frac{3B}{4} (2\mathcal{A}^2 + B^2) \cos(n\omega t) + \frac{\mathcal{A}^3}{4} \cos(3\omega t + 3\phi) + \\ &\quad \frac{B^3}{4} \cos(3n\omega t) + \frac{3\mathcal{A}^2 B}{4} \{\cos[3\omega t + 2\phi] + \cos[\omega t + 2\phi]\} + \\ &\quad \frac{3\mathcal{A} B^2}{4} \{\cos[3\omega t + \phi] + \cos[\omega t - \phi]\}. \end{aligned} \quad (3.6)$$

Since $G(s)$ is a low-pass filter only small band of frequencies will pass particularly, the fundamental frequency of the driving signal. Suppose $G(s)$ only passes the fundamental

frequency, ω component. Hence, the gain of the nonlinear element due to the primary signal $\mathcal{A} \cos(\omega t + \phi)$ without the incremental-input signal is given by

$$\begin{aligned} N(\mathcal{A}) &= \frac{Y}{X} \quad \text{where } B = 0 \\ &= \frac{3}{4} \mathcal{A}^2 \end{aligned} \quad (3.7)$$

where X and Y are the input-output complex amplitudes of the nonlinear element. In the nomenclature $N(\mathcal{A})$ is defined as the *describing function gain*. Similarly, the gain due to the first order *synchronous incremental-input describing function* is given by

$$\begin{aligned} N(\mathcal{A}, \phi) &= \frac{Y}{X} \\ &= \frac{\frac{3}{2} \mathcal{A}^2 B + \frac{3}{4} \mathcal{A}^2 B e^{j2\phi}}{B} \\ &= \frac{3}{4} \mathcal{A}^2 (2 + e^{j2\phi}). \end{aligned} \quad (3.8)$$

Note that $N(\mathcal{A})$ depends solely upon the amplitude of the input to the nonlinear device while $N(\mathcal{A}, \phi)$ is a function of the input amplitude and a phase angle ϕ which can take on values in $(0, 2\pi)$.

To study the stability of this steady-state solution, we will investigate the dynamics of the incremental system. If the incremental system is stable, then we will conclude that the steady-state solution is stable since it is robust to incremental disturbance. In the frequency domain, the Nyquist criterion is an obvious choice to employ for assessing the stability of the incremental system.

3.1.1 Condition For Instability

To investigate the stability of the steady-state solution of the system shown in Fig. 3.1, the incremental-input was set to zero and the loop-gain of the system was computed as

$$L(j\omega) = \frac{3\mathcal{A}^2}{4} G(j\omega) \quad (3.9)$$

under the assumption that the linear system attenuates the higher order harmonics. Consider a Nyquist plot of the loop-gain. If we hypothesize that the loop-gain never crosses the negative real axis, then increasing or decreasing the magnitude of the input signal M will cause the loop-gain locus to shift closer or further away from the origin without a phase

shift. Based on the Nyquist criterion, this system is stable in the closed-loop for all values of \mathcal{A} since there are no encirclements of $(-1, 0)$ point. Thus the system is stable for all non-synchronous incremental inputs.

Suppose a synchronous incremental-input as given in equation (3.3) is applied to the system where B can be represented by

$$B = B_0 e^{\sigma t}. \quad (3.10)$$

where B_0 is the smallest measurable signal. Then, the loop-gain of the incremental system can be represented at

$$L(j\omega) = \left[\frac{3}{2} \mathcal{A}^2 + \frac{3}{4} \mathcal{A}^2 e^{j2\phi} \right] G(j\omega). \quad (3.11)$$

This loop-gain is independent of the parameter σ . Hence, the stability depends on whether the incremental loop-gain encloses the $(-1, 0)$ point. With the incremental input magnitude γ and the angular frequency ω_s , $G(j\omega_s)$ can be written as

$$G(j\omega_s) = \mathcal{X} + j\mathcal{Y}, \quad \text{where } \mathcal{X} = \text{Re}\{G(j\omega_s)\}, \quad \mathcal{Y} = \text{Im}\{G(j\omega_s)\}. \quad (3.12)$$

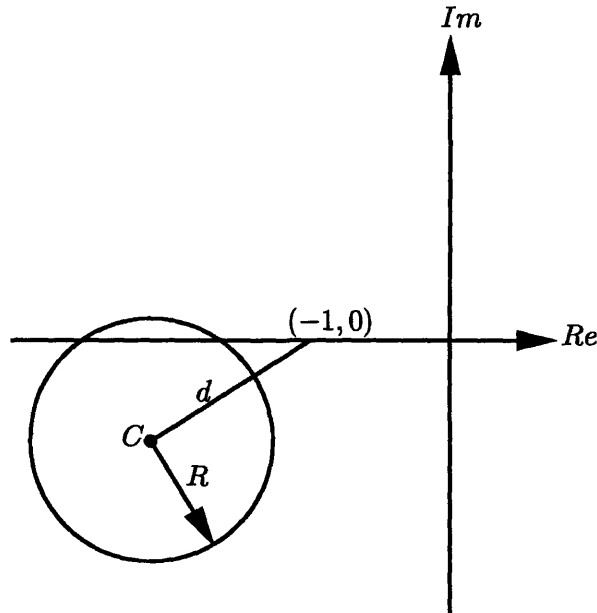


Figure 3.2: Complex Plane

For this frequency, ω_s , the incremental loop-gain locus form a circle with a center at $\frac{3\mathcal{A}^2}{2}(\mathcal{X} + j\mathcal{Y})$ and a radius $\frac{3\mathcal{A}^2}{4}(\mathcal{X}^2 + \mathcal{Y}^2)^{\frac{1}{2}}$. Hence, for the circle to enclose the $(-1, 0)$ point, the distance d between the center of the circle and the $(-1, 0)$ point must be greater than the radius of the circle R as depicted in Fig. 3.2. For the critical condition, where d equals to R , This constraint can be written as

$$\mathcal{A}^4 - \frac{16\mathcal{X}}{9(\mathcal{X}^2 + \mathcal{Y}^2)}\mathcal{A}^2 + \frac{16}{27(\mathcal{X}^2 + \mathcal{Y}^2)} = 0 \quad (3.13)$$

Then,

$$\mathcal{A}^2 = \frac{4}{9(\mathcal{X}^2 + \mathcal{Y}^2)}[2\mathcal{X} \pm \sqrt{\mathcal{X}^2 - 3\mathcal{Y}^2}] \quad (3.14)$$

Thus, the condition for instability is given by

$$\frac{\mathcal{Y}}{\mathcal{X}} \leq \frac{1}{\sqrt{3}}. \quad (3.15)$$

This constraint says that if the ratio of the imaginary and the real parts of $G(j\omega_s)$ is greater than $\frac{1}{\sqrt{3}}$, the steady-state solution at which the system is operating, is a stable operating point. Hence, our task is to examine the magnitude of $G(j\omega_s)$ to assess the stability of the system. This approach is simpler than linearizing the system around the steady-state solution and then using Floquet theory to compute the eigenvalues of the system since the variational system is a time-variant system.

3.1.2 Existence of Multiple Steady-State Solutions

A steady-state solution of a system can be computed using the describing function method. Suppose the input to the system depicted in Fig. 3.1 has the form

$$r(t) = M \cos(\omega_s t + \theta) \quad (3.16)$$

and the input to the nonlinear element is given by

$$x(t) = \mathcal{A} \cos(\omega t + \phi) \quad (3.17)$$

assuming that all the higher harmonics are attenuated by the linear system $G(j\omega)$. The describing function gain of the system is given by

$$N(\mathcal{A}) = \frac{3}{4}\mathcal{A}^2. \quad (3.18)$$

The de-sensitivity function of the system can be represented as

$$[1 + N(\mathcal{A})(\mathcal{X} + j\mathcal{Y})]\mathcal{A} = Me^{-j\phi}. \quad (3.19)$$

Separating the above equation into real and imaginary parts yields

$$[1 + \mathcal{X}N(\mathcal{A})]\mathcal{A} = M \cos(\phi) \quad (3.20a)$$

$$\mathcal{Y}N(\mathcal{A})\mathcal{A} = -M \sin(\phi). \quad (3.20b)$$

Solving for ϕ in (3.20b), we have

$$\phi = -\arcsin \left[\frac{\mathcal{Y}N(\mathcal{A})\mathcal{A}}{M} \right] \quad (3.21)$$

and substituting ϕ into (3.20a) results in

$$[(\mathcal{X}^2 + \mathcal{Y}^2)N^2(\mathcal{A}) + 2\mathcal{X}N(\mathcal{A}) + 1]\mathcal{A}^2 = M^2. \quad (3.22)$$

Eliminating $N(\mathcal{A})$ and simplifying further yields

$$\mathcal{A}^6 + \frac{8\mathcal{X}}{3(\mathcal{X}^2 + \mathcal{Y}^2)}\mathcal{A}^4 + \frac{16}{9(\mathcal{X}^2 + \mathcal{Y}^2)}\mathcal{A}^2 - \frac{16M^2}{9(\mathcal{X}^2 + \mathcal{Y}^2)} = 0. \quad (3.23)$$

The equation is cubic in \mathcal{A}^2 , and depending upon the sign of \mathcal{X} can have three positive real solutions or one positive real solution [56]. Applying Sturm's Theorem [57] to (3.23), the condition to have three positive real roots is given by

$$\frac{\mathcal{Y}}{\mathcal{X}} < \frac{1}{\sqrt{3}}. \quad (3.24)$$

Hence, if the condition in (3.24) is satisfied the system depicted in Fig. 3.1 will have three solutions. One can show that for the three solutions case, two are stable and one is unstable. On the other hand, if equation (3.24) is not satisfied the system will have only one stable steady-state solution.

Based on the aforementioned analyses, West, Douce, and Livesley concluded that if the locus of $G(j\omega)$ does not cross the negative real axis in the $L(j\omega)$ plane and the condition

shown in equation (3.24) is not satisfied, the steady-state solution of the system is stable.

3.1.3 Incremental-Input Describing Function Applications

Swift [37] applied this theory to study the single-phase ferroresonance problem. He examined the stability of the steady-state solutions and the existence of jump resonance conditions. The circuit model that he used for his study is shown in Fig. 3.3. In this model the core-loss, leakage resistance, and reactance of the transformer were assumed to be negligible. The relationship between the current and the flux linkage in the nonlinear core used

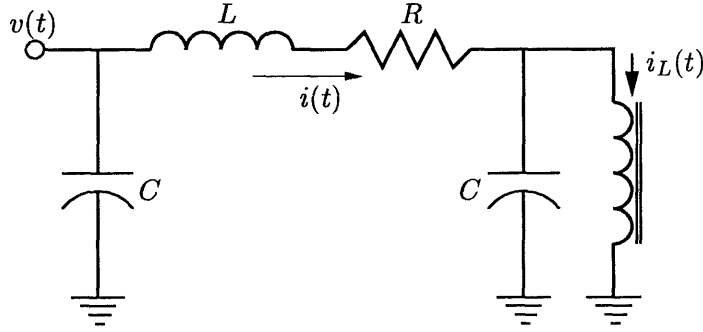


Figure 3.3: Single-phase ferroresonance circuit model

in this study is given by

$$i_L(t) = K_1\lambda + K_5\lambda^5. \quad (3.25)$$

The differential equation that relates the input voltage and the flux linkage of the transformer can be written

$$\frac{d\lambda}{dt} + L\frac{di}{dt} + Ri = v(t). \quad (3.26)$$

The above equation can be mapped into the frequency domain as

$$\Lambda = G_0(s)V - G(s)I_L, \quad \text{where} \quad (3.27)$$

$$G(s) = \frac{R + Ls}{s(Lcs^2 + RCs + 1)}, \quad G_0(s) = \frac{1}{s(Lcs^2 + RCs + 1)}.$$

The characteristic equation of the system can be written as

$$N(\mathcal{A}, \phi)G(j\omega) = -1 \quad \text{where} \quad N(\mathcal{A}, \phi) = U_1 + U_2 e^{j2\phi} \quad (3.28)$$

where,

$$U_1 = 1 + \frac{15}{2}\mathcal{A}^4 \quad U_2 = 5\mathcal{A}^4 \quad (3.29)$$

and \mathcal{A} is the amplitude of the flux.

To ascertain the stability of the steady-state solution of the system defined in equation (3.27), the inverse synchronous incremental gain and the linear system $G(j\omega)$ are plotted in the complex plane. If there exists an intersection between these two loci at the synchronous frequency ω_s , then the steady-state solution is unstable; otherwise, the steady state solution is stable. Note that the intersection of these points at the specified frequency is equivalent to an encirclement of the point $(-1, 0)$ using the Nyquist criterion. The following example uses the two sets of parameters that Swift used for his study.

EXAMPLE 3.1

Consider the system defined in equation (3.27). Suppose the following parameters are given,

$$\begin{aligned} (i) \quad R &= 0.002 \text{ pu}, \quad C = 50.0 \text{ pu}, \quad L = 0.021 \text{ pu}, \quad \text{and} \quad \omega_s = 1.0 \text{ pu} \\ (ii) \quad R &= 0.002 \text{ pu}, \quad C = 50.0 \text{ pu}, \quad L = 0.025 \text{ pu}, \quad \text{and} \quad \omega_s = 1.0 \text{ pu} \end{aligned} \quad (3.30)$$

and suppose the nonlinear element has the terminal relationship defined in equation (3.25).

For the first set of data, the magnitude of the input of the system was 0.167 pu. The magnitude of the steady-state solution of the error signal \mathcal{A} that corresponds to this input was 1.25 pu. To study the stability of this steady-state solution, the incremental system was formulated and the Nyquist criterion was applied to it. Figure 3.4 depicts the negative of the inverse incremental gain $\frac{1}{N(\mathcal{A}, \theta)}$ and the linear system $G(j\omega)$ locus. For the given parameters, there is no intersection between the two loci at the operating frequency $\omega_s = 1.0$ pu which implies that there exists one stable steady-state solution for these parameters.

To examine the validity of this result, time simulations were performed using the dynamic system simulator Simulink [58]. Figure 3.5 shows the time simulation of the system for M equal to 0.167 pu. To examine the stability of this solution, a synchronous incremental-input signal was applied to the system at $t = 8000$ sec with an amplitude of

0.022 pu. When the incremental-input was removed at $t = 10,000$ sec, the steady state solution attained its original value which confirms the robust stability of this steady-state solution.

Similarly, for the second set of data, the input magnitude was 0.167 pu and the corresponding steady-state error magnitude was 0.9 pu. Figure 3.6 shows the plot of the two loci, the negative inverse of the incremental gain and the linear system locus. In this plot there exists an intersection between the linear system $G(j\omega)$ and the negative inverse of the synchronous incremental-input gain at the operating frequency $\omega_s = 1.0$ pu. This indicates that three steady-state solutions exist, one unstable and two stable solutions.

Similarly, time simulations were performed to examine the validity of the results. Since it is not possible to capture an unstable solution in a physical system or even a system simulator, we can only hope to see the two stable solutions. The third solution, the unstable one, can only be observed in the analytical solution. Figure 3.7 depicts the time simulation of the system. After 8000 sec, an incremental signal with an amplitude of 0.022 pu was applied to the system. The magnitude of the error signal \mathcal{A} jumped from 0.9 pu to 1.5 pu. The incremental signal was removed from the system at $t = 10000$ sec. However, the amplitude of the $\lambda(t)$ stayed at 1.5 pu. Clearly, this behavior shows the steady-state solution moved from one stable solution to another stable solution. This result agrees with the incremental-input describing function analysis.

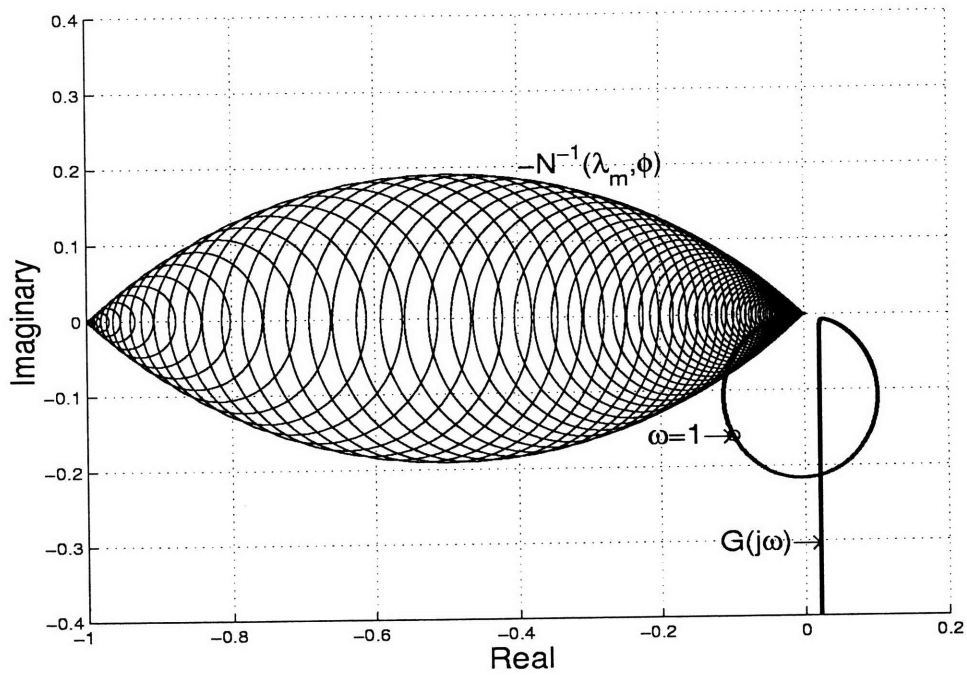


Figure 3.4: $G(j\omega)$ and $-N^{-1}(\mathcal{A}, \phi)$ for $R = 0.002$ pu, $C = 50$ pu, and $L = 0.021$ pu

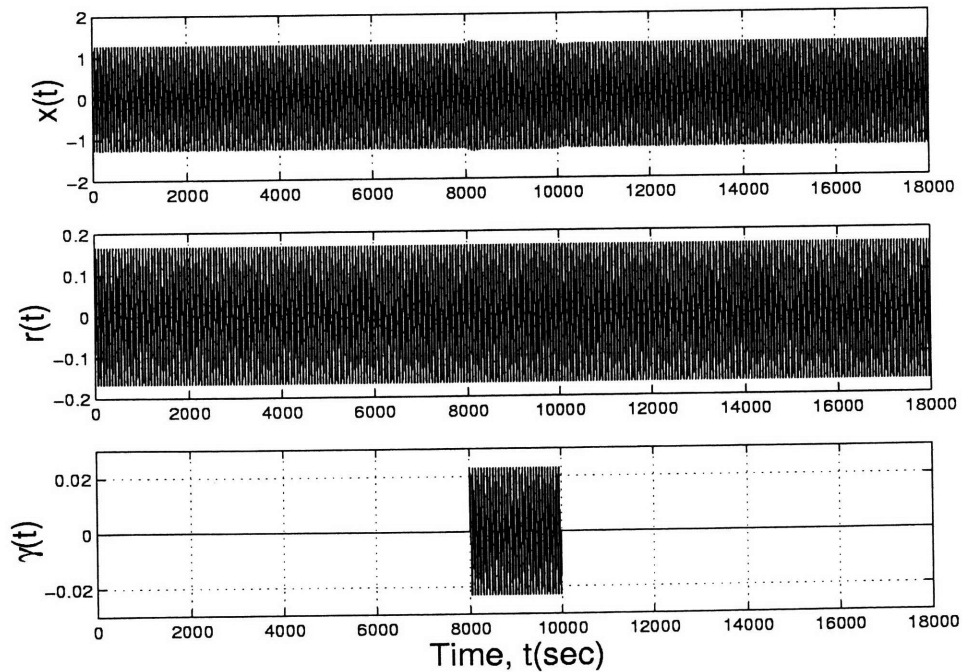


Figure 3.5: Time simulation for $R = 0.002$ pu, $C = 50$ pu, and $L = 0.021$ pu

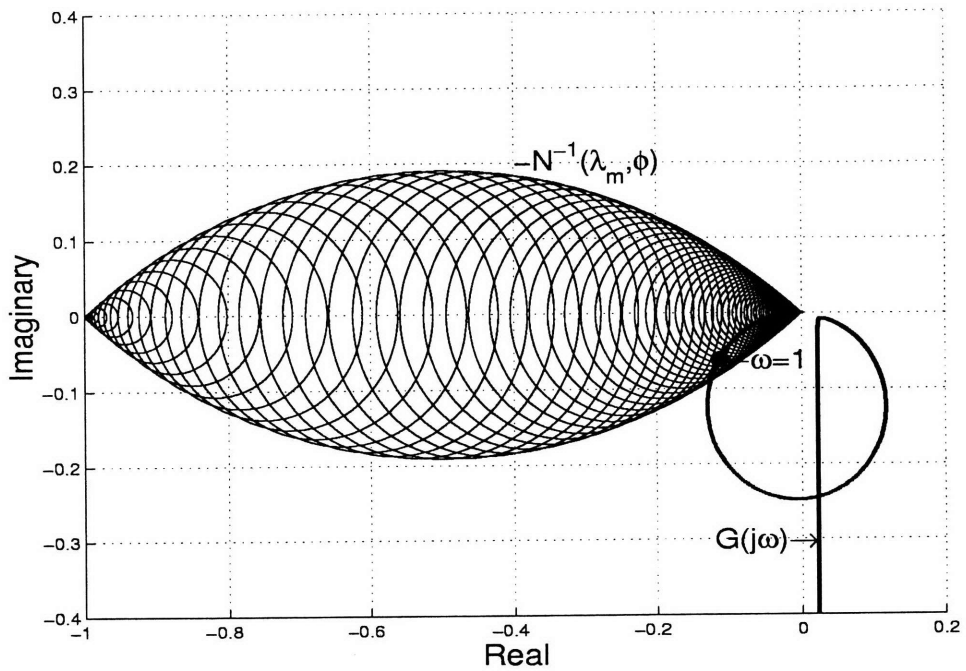


Figure 3.6: $G(j\omega)$ and $-N^{-1}(\mathcal{A}, \phi)$ for $R = 0.002$ pu, $C = 50$ pu, and $L = 0.023$ pu

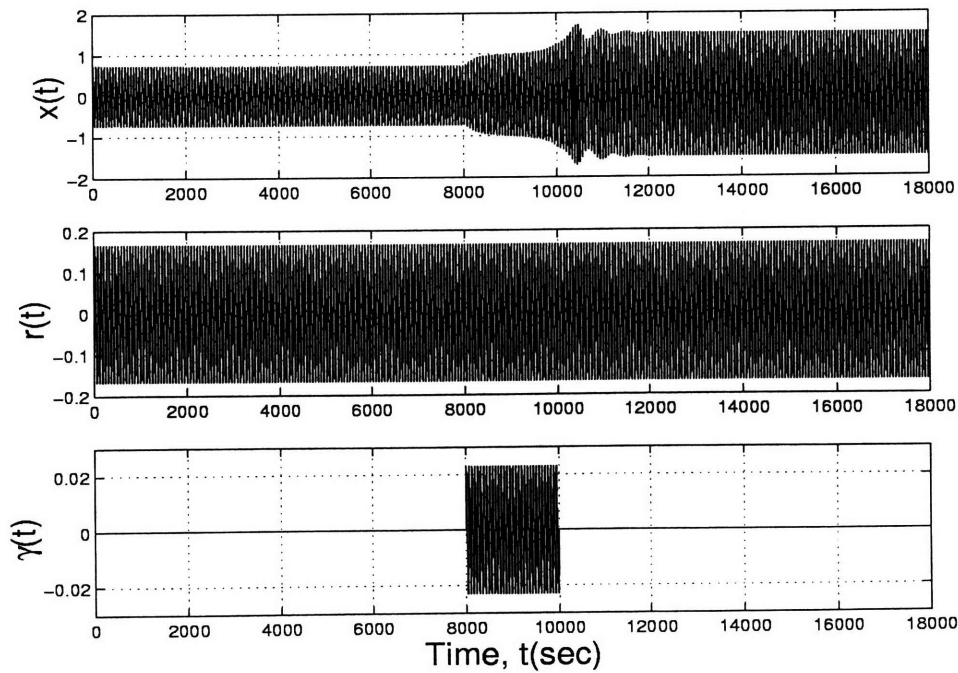


Figure 3.7: Time simulation for $R = 0.002$ pu, $C = 50$ pu, and $L = 0.025$ pu

3.2 Modified Dual-Input Describing Function Analysis

In this section we demonstrate that there is a flaw in the theory of incremental-input describing function. Since it is used in industry and research institutions [59,32,4,37], eliminating the flaw in the theory, particularly at the synchronous frequency, is necessary. First the extended Nyquist theory is presented, then the proposed incremental-input describing function analysis is formulated.

3.2.1 Nyquist Stability Analysis Criterion

In this section, a general overview of the basis for the Nyquist stability criterion for feedback systems is given. There are different ways to approach guaranteeing the stability of a feedback system. For a single loop SISO system, the system can be analyzed using the classical control approach which includes Root Locus, Routh and Hurwitz criterion, Bode plot, Nichols charts, and Nyquist criterion [28,29,60]. The Nyquist criterion is suitable for a large class of control systems. Without analytical computation of the input-output map of the system, the Nyquist criterion determines the relative stability of the closed-loop system. This criterion is based on Cauchy's Principle of the Argument in complex variables. Before stating this theorem some preliminary definitions will be stated.

DEFINITION 3.2

If $L(s)$ possesses a derivative at point $s = s_0$ and at every point in some neighborhood of s_0 , then $L(s)$ is said to be analytic at s_0 and s_0 is called a holomorphic point.

DEFINITION 3.3

If $L(s)$ is not analytic at point s_0 , but every neighborhood of s_0 contains points at which $L(s)$ is analytic, then s_0 is called a singular point of $L(s)$, and s_0 is called a meromorphic point.

Now, let's state Cauchy's Principle of the Argument without a proof, since the proof of the theorem can be found in [61] and other complex analysis references.

THEOREM 3.4

Suppose $L(s)$ is a meromorphic function within and on a closed curve \mathcal{D} and $L(s)$ has neither poles nor zeros on \mathcal{D} , then

$$\frac{1}{2\pi i} \int_{\mathcal{D}} \ln\{L(s)\} ds = Z - P \quad (3.31)$$

where Z and P are the number of zeros and poles respectively, of $L(s)$ contained in the region bounded by \mathcal{D} , each counted as many times as its multiplicity.

Rather than solving the integral equation in (3.31) to find the zeros and poles in the closed contour \mathcal{D} , the mapping theorem can be utilized. If the closed contour \mathcal{D} in the s -plane is mapped into the $L(s)$ plane, the number of encirclements N of the locus $L(s)$ around $(0, 0)$ is the difference between the numbers of zeros and poles in the closed contour \mathcal{D} .

Thus, to ascertain the stability of the system defined by the open-loop transfer function $L(s)$, $L(j\omega)$ is plotted in the complex plane and the number of encirclements N of the $(0, 0)$ point is equal to $Z - P$. If the number of encirclements of the point $(-1, 0)$ is zero and assuming that there are no unstable open-loop poles of $L(s)$, then the system defined by $L(s)$ is stable in the closed-loop. On the other hand, if $|N|$ is not equal to zero, given that there are no unstable open-loop poles of $L(s)$, then the closed-loop of the system defined by the open-loop function $L(s)$ is unstable. For MIMO systems (multi-input multi-output), the determinant of the loop-gain can be computed, and the Nyquist stability criterion can be applied [29].

For instance, suppose the characteristic equation of the system is given by

$$1 + KG(s) = 0 \quad (3.32)$$

where $G(s)$ is a stable minimum-phase transfer function and K is a positive constant. To examine the stability of the system in closed-loop, we determine if a complex number s exists such that (3.32) is satisfied. We note that $s = \sigma + j\omega$, where σ and ω are real numbers, and σ is the damping factor of the response while ω is the angular frequency of the response. Let's consider four cases for $G(s)$. Suppose the frequency response of $G(s)$ has the form shown in Fig. (3.8)

By examining the loop-gain of the system shown in Fig. 3.8, the closed-loop system is stable since the loop-gain locus does not intersect the $(-1, 0)$ point for $\sigma = 0$. Similarly, if we fix ω at some frequency, say ω_1 , and vary σ from zero to $+\infty$, all the loci go to the right of the point $KG(j\omega_1)$ locus and approach zero since $G(j\omega)$ is a non-minimum-phase proper rational transfer function [62]. However, if we vary σ from zero to $-\infty$, we will find all the

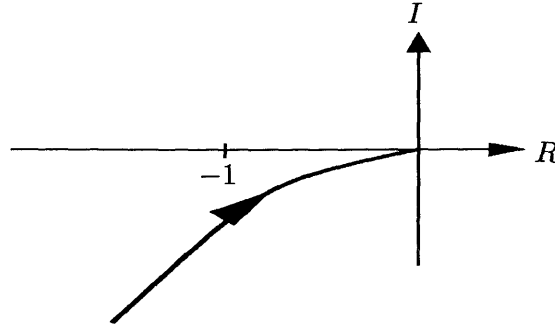


Figure 3.8: Frequency response of system one

loci starting from the point $KG(j\omega_1)$ go to the left of that point. Hence, it's possible that some locus will cross the point $(-1, 0)$. Since the damping factor is negative, the system is stable in closed-loop.

Next, suppose the loop-gain of the system has the frequency response shown in Fig. 3.9. This loop-gain cuts the $(-1, 0)$ point for $\sigma = 0$. Hence, the response of the system in closed-loop will have oscillatory terms since at least one of the damping factors is zero. Therefore, the system is marginally stable.

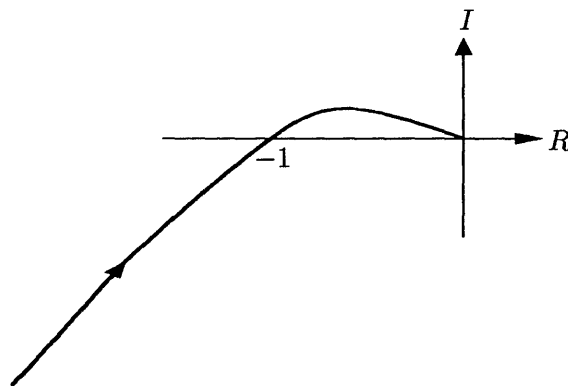


Figure 3.9: Frequency response of system two

For the third case, suppose the frequency response of the loop-gain of the system is the one depicted in Fig. (3.10). This loop-gain encloses the $(-1, 0)$ point for $\sigma = 0$, hence, there exists a positive σ and ω such that (3.32) is satisfied. Hence, this system is unstable

in closed-loop.

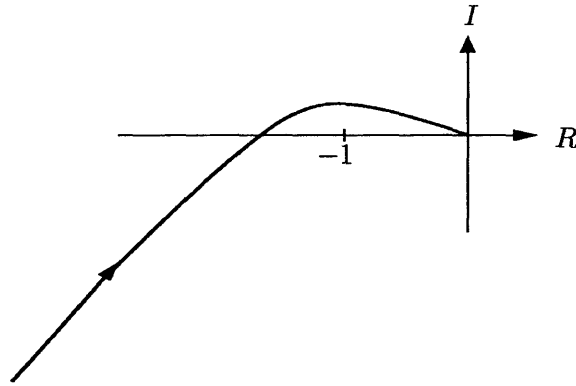


Figure 3.10: Frequency response of system three

Finally, suppose the frequency response of the loop-gain is the one shown in Fig. 3.11. At $\omega = 1$, the frequency response is a circle, hence varying σ from zero to ∞ will move the circle to the origin. Therefore, it is possible for some positive σ the circle may intersect the $(-1, 0)$ point which in turn destabilizes the closed-loop system, particularly the inputs with the frequency ω_1 .

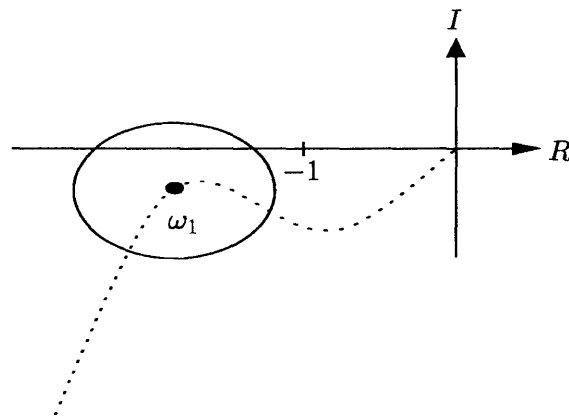


Figure 3.11: Frequency response of system four

The authors of [36] fail to examine variations of σ . As shown in Section 3.1, the loop-gain of the system is a circle for some given angular frequency. Hence, fixing ω and varying σ from 0 to ∞ will move the circle to the origin which in turn can cause an intersection with the $(-1, 0)$ point.

Therefore, the necessary and sufficient condition for the stability of a loop-gain in a closed-loop is the loci of the loop-gain does not intersect the $(-1, 0)$ point for all values of ω and for all non-negative values of σ .

The synchronous incremental-input describing function can also be applied to systems with an unstable nonminimum-phase open-loop transfer function. In Appendix A.3, we give a procedure that the theory can be applied in a large class of systems.

In the following subsections, we will apply the theory of synchronous incremental-input describing functions to a system to understand this modification. First we will revisit the describing function analysis in a general setting. Then, presentations of the synchronous incremental-input describing function analysis and an example will follow.

3.2.2 Describing Function Analysis

To use linear control tools for a limit cycle stability analysis of our system, approximation of the nonlinear element is required. Under the describing function technique, the input of the nonlinear element is assumed to be dominated by the fundamental frequency, and the nonlinearity is approximated by the complex gain of the fundamental frequency. If other harmonics have a strong influence on the output signal of the nonlinear element, the nonlinearity can be approximated using a describing function matrix [63,35]. The notion of describing function will allow us to compute approximate steady-state solutions of the system. Hence, let us first review the sinusoidal-input describing function theory.

Consider the nonlinear interconnected feedback system shown in Fig. 3.1 where $G(s)$ is a strictly proper rational transfer function and $N(x)$ is a memoryless nonlinear odd monomial.

$$N(x) = kx^n, \text{ for } n \text{ can take the values } 3, 5, 7, 9, \dots \quad (3.33)$$

Assume the input to the system $r(t)$ is a sinusoidal function of the form:

$$r(t) = M \sin(\omega t). \quad (3.34)$$

Furthermore, assume the linear system is low-pass and time-invariant; since the linear system will attenuate the higher harmonics that the nonlinear device produces [64–66], the error signal will have a sinusoidal behavior which is synchronous with the driving signal but with a phase discrepancy. This phase difference depends on the characteristic behavior

of the linear system; the faster the system response, the smaller the phase delay between the input-output map. The describing function theory can be used to linearize a nonlinear element. This type of linearization is called a sinusoidal-input describing function or optimal quasi-linearization. Before deriving the input-output map and the harmonic linearization of the nonlinear element, the sinusoidal-input describing function will be defined.

Definition 1

The sinusoidal-input describing function is the ratio of the complex amplitude of the interested harmonic of the output map of the nonlinear element to the complex amplitude of the corresponding input.

To derive the quasi-linearized gain of the nonlinear element, let us consider the following nonlinear element. The input to this nonlinear device is defined as

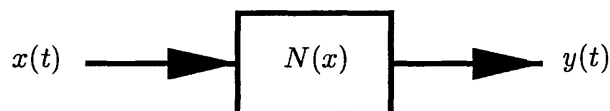


Figure 3.12: Nonlinear Element

$$x(t) = \mathcal{A} \sin(\omega t + \theta) \quad (3.35)$$

where \mathcal{A} is the steady-state magnitude of the error signal. The output of the nonlinear element is then

$$\begin{aligned} y(t) &= kx(t)^n, \quad \text{for } n \text{ can take the values } 3, 5, 7, 9, \dots \\ &= k(\mathcal{A} \sin(\omega t + \theta))^n \\ &= k\mathcal{A}^n \sin(\omega t + \theta) \left(\frac{1 - \cos(2\omega t + 2\theta)}{2} \right)^{\frac{n-1}{2}} \\ &= k\mathcal{A}^n \left(\frac{1}{2} \right)^{\frac{n-1}{2}} \sin(\omega t + \theta) \sum_{\alpha=0}^{\frac{n-1}{2}} \binom{\frac{n-1}{2}}{\alpha} (-1)^\alpha \cos^\alpha(2\omega t + 2\theta). \end{aligned} \quad (3.36)$$

The output of the nonlinear element in Fig. 3.12 due to the first harmonic is given by

$$y(t) = \mathcal{K} \mathcal{A}^n \sin(\omega t + \theta) \quad \text{where } \mathcal{K} = k \left(\frac{1}{2} \right)^{\frac{n-1}{2}} \left(\beta_1 + \frac{1}{2} \beta_2 \right) \quad (3.37)$$

where

$$\begin{aligned}\beta_1 &= \frac{1}{2\pi} \sum_{\alpha, \text{even}}^{\frac{n-1}{2}} \int_0^{2\pi} \left(\frac{n-1}{\alpha}\right) \left(\frac{1}{2}\right)^{\frac{\alpha}{2}} (1 + \cos(4\omega t + 4\theta))^{\frac{\alpha}{2}} dt \\ \beta_2 &= \frac{1}{2\pi} \sum_{\alpha, \text{odd}}^{\frac{n-1}{2}} \int_0^{2\pi} \left(\frac{n-1}{\alpha}\right) \left(\frac{1}{2}\right)^{\frac{\alpha-1}{2}} (1 + \cos(4\omega t + 4\theta))^{\frac{\alpha-1}{2}} dt.\end{aligned}\tag{3.38}$$

The quasi-linearization of the nonlinear element yields

$$N(A) = \mathcal{K}A^{n-1}.\tag{3.39}$$

From equation (3.39), the gain $N(A)$ is a function of the amplitude of the error signal. Therefore, for a given input magnitude M and frequency ω_s of the system shown in Fig. 3.1 with the nonlinearity defined in equation (3.33), the steady-state error magnitude can be computed by finding the de-sensitivity transfer function of the system in Fig. 3.1. Then, this yields

$$\mathcal{A}e^{j(\omega t + \theta)} = \frac{1}{1 + N(\mathcal{A})G(j\omega)} M e^{j\omega t}\tag{3.40}$$

For further simplifications, we have

$$\mathcal{A}e^{j\theta} = \frac{1}{1 + N(\mathcal{A})G(j\omega)} M.\tag{3.41}$$

Using Euler's formula, then eliminating θ in the above equation and solving for A , yields

$$\mathcal{A}^{2n} + \frac{2\mathcal{X}}{\mathcal{K}(\mathcal{X}^2 + \mathcal{Y}^2)} \mathcal{A}^{n+1} + \frac{1}{\mathcal{K}^2(\mathcal{X}^2 + \mathcal{Y}^2)} \mathcal{A}^2 - \frac{M^2}{\mathcal{K}^2(\mathcal{X}^2 + \mathcal{Y}^2)} = 0\tag{3.42}$$

Hence, the roots of the above equation give the solutions of the steady-state magnitude of the error signal. Depending on the characteristics of the linear system $G(j\omega)$ and type of the nonlinearity, either one real positive solution or three real positive solutions of \mathcal{A} exist. The following theorem proves this statement:

THEOREM 3.5

Suppose $G(j\omega)$ is a strictly proper rational transfer function. Define

$$f_1(\mathcal{A}) = \mathcal{K}^2(\mathcal{X}^2 + \mathcal{Y}^2)\mathcal{A}^{2n} + 2\mathcal{K}\mathcal{X}\mathcal{A}^{n+1} + \mathcal{A}^2 - M^2\tag{3.43}$$

where,

$$\mathcal{X} = \text{Re}[G(j\omega)], \quad \mathcal{Y} = \text{Im}[G(j\omega)], \quad (3.44)$$

and if the following conditions

$$\begin{aligned} (i) \quad & \mathcal{X} < 0 \\ (ii) \quad & \frac{\mathcal{Y}}{\mathcal{X}} < \frac{n-1}{2\sqrt{n}} \end{aligned} \quad (3.45)$$

are satisfied for some ω and $f_1(\mathcal{A}_1)$ and $f_1(\mathcal{A}_2)$ have different signs for a given M , where \mathcal{A}_1 and \mathcal{A}_2 are the positive real roots of

$$f_2(\mathcal{A}) = n\mathcal{K}^2(\mathcal{X}^2 + \mathcal{Y}^2)\mathcal{A}^{2(n-1)} + (n+1)\mathcal{K}\mathcal{X}\mathcal{A}^n + 1 \quad \text{where } \mathcal{A}_2 > \mathcal{A}_1 > \mathcal{A}_0 \quad (3.46)$$

then, there exist three positive real roots of equation (3.43).

Proof From Descartes' theorem [57], the number of positive real roots of $f_1(\mathcal{A})$ cannot exceed the number of sign changes of the coefficients of $f_1(\mathcal{A})$. If the following inequality

$$2\mathcal{K}\mathcal{X} < 0 \implies \mathcal{X} < 0 \quad \text{for } \mathcal{K} = \{k > 0 : k \in \mathbb{R}^1\} \quad (3.47)$$

is satisfied, then the number of sign changes of $f_1(\mathcal{A})$ and $f_1(-\mathcal{A})$ is equal to 3. First, to show that one of the real roots is positive, we examine the limits of $f_1(\mathcal{A})$. If \mathcal{A} goes to infinity, then $f_1(\mathcal{A})$ is a positive number. On the other hand if \mathcal{A} goes to zero from the left, then the sign of $f_1(\mathcal{A})$ is negative for some input magnitude M . Since $f_1(\mathcal{A})$ changes sign between zero and infinity, there exists one positive real root of $f_1(\mathcal{A})$. Call this positive real root \mathcal{A}_0 . Similarly, for $f_1(\mathcal{A})$ to have two more distinct positive real roots, there must exist at least one maximum and one minimum peak of $f_1(\mathcal{A})$ where \mathcal{A} is greater than \mathcal{A}_0 . If the maximum and the minimum values of $f_1(\mathcal{A})$ have different signs then clearly equation (3.43) has three positive real roots. To find these peak values, the derivative of $f_1(\mathcal{A})$ is computed

$$f_2(\mathcal{A}) = 2n\mathcal{K}^2(\mathcal{X}^2 + \mathcal{Y}^2)\mathcal{A}^{2n-1} + 2(n+1)\mathcal{K}\mathcal{X}\mathcal{A}^n + 2\mathcal{A} \quad (3.48)$$

Setting zero to $f_2(\mathcal{A})$ yields

$$n\mathcal{K}^2(\mathcal{X}^2 + \mathcal{Y}^2)\mathcal{A}^{2(n-1)} + (n+1)\mathcal{K}\mathcal{X}\mathcal{A}^{n-1} + 1 = 0 \quad (3.49)$$

Using the quadratic formula, the roots of (3.49) are

$$\begin{aligned} \mathcal{A}_1 &= \left[\frac{1}{4n\mathcal{K}^2(\mathcal{X}^2 + \mathcal{Y}^2)} \left(-2(n+1)\mathcal{K}\mathcal{X} - P \right) \right]^{\frac{1}{n-1}} \\ \mathcal{A}_2 &= \left[\frac{1}{4n\mathcal{K}^2(\mathcal{X}^2 + \mathcal{Y}^2)} \left(-2(n+1)\mathcal{K}\mathcal{X} + P \right) \right]^{\frac{1}{n-1}} \\ \text{where } P &= \sqrt{4(n+1)^2\mathcal{K}^2\mathcal{X}^2 - 16n\mathcal{K}^2(\mathcal{X}^2 + \mathcal{Y}^2)} \end{aligned} \quad (3.50)$$

\mathcal{A}_1 and \mathcal{A}_2 can be guaranteed to have positive real values if the following conditions are satisfied

$$\begin{aligned} (i) \quad & \frac{\mathcal{Y}}{\mathcal{X}} < \frac{n-1}{2\sqrt{n}} \\ (ii) \quad & \mathcal{X} < 0. \end{aligned} \quad (3.51)$$

\mathcal{A}_1 and \mathcal{A}_2 are the points that lie in the domain of $f_1(\mathcal{A})$ where the function takes on maximum and minimum values. Hence, if $f_1(\mathcal{A}_1)$ and $f_1(\mathcal{A}_2)$ have different signs, then equation (3.43) will have three positive real roots. On the other hand, if the two roots of $f_2(\mathcal{A})$ coincide then $f_1(\mathcal{A})$ will have an inflection point. In this case $f_1(\mathcal{A})$ will have two positive real roots and one negative real root. This proves the theorem ■

To find the stability of these steady-state solutions, particularly for lightly damped systems which exhibit the ferroresonance phenomenon for small perturbation around the steady-state operating point, the synchronous incremental-input describing function can be employed.

3.2.3 Dual-input Describing Function Analysis

The stability of the perturbed system can be investigated simply by examining the stability of the synchronous incremental loop gain of the system. Hence, we need to compute the incremental gain of the system. The synchronous incremental output of the nonlinear device shown in Fig. 3.1 is

$$\begin{aligned} y(t) &= (\mathcal{A} \sin(\omega t + \theta) + B \sin(\omega t))^n \\ &= \sum_{\alpha=0}^n \binom{n}{\alpha} (\mathcal{A} \sin(\omega t + \theta))^{n-\alpha} (B \sin(\omega t))^\alpha \quad \text{where } B \ll \mathcal{A}. \end{aligned} \quad (3.52)$$

The terms of the output nonlinear element due to the first power of B are given by

$$\begin{aligned} y(t) &= \mathcal{K} \mathcal{A}^{n-1} B \binom{n}{1} \sin(\omega t) \sin^{n-1}(\omega t + \theta) \\ &= \mathcal{K} n \left(\frac{1}{2}\right)^{n-1} B \mathcal{A}^{n-1} \left(\beta_1 \sin(\omega t) + \frac{1}{2} \beta_2 \sin(\omega t + 2\theta) \right) \end{aligned} \quad (3.53)$$

where β_1 and β_2 are defined in equation (3.38). Then, by the definition of the synchronous incremental-input describing function, we have the following

$$N(\mathcal{A}, \theta) = W_1 \mathcal{A}^{n-1} + \frac{1}{2} W_2 \mathcal{A}^{n-1} e^{j2\theta} \quad (3.54)$$

where

$$W_1 = \mathcal{K} n \left(\frac{1}{2}\right)^{n-1} \beta_1, \quad W_2 = \mathcal{K} n \beta_2 \left(\frac{1}{2}\right)^{n-1}. \quad (3.55)$$

For a given value of \mathcal{A} , $N(\mathcal{A}, \theta)$ is a circle with a center at $W_1 \mathcal{A}^{n-1}$ and a radius of $\frac{1}{2} W_2 \mathcal{A}^{n-1}$. Also the negative of the inverse of $N(\mathcal{A}, \theta)$ is a circle with a center of $\frac{W_1}{W_2^2 - W_1^2}$ and a radius at $\frac{W_2}{W_2^2 - W_1^2}$. The following lemma proves this claim.

LEMMA 3.6

$$\text{If } -\frac{1}{N(\mathcal{A}, \theta)} = -\frac{1}{W_1 + W_2 e^{j2\theta}} \quad (3.56)$$

where W_1 and W_2 are defined in equation (3.55), and θ is a random variable that can take on values from 0 to 2π , then for a fixed value of the error magnitude \mathcal{A} , $-\frac{1}{W_1 + W_2 e^{j2\theta}}$ is a circle which has a center at $(\frac{W_1}{W_2^2 - W_1^2}, 0)$ and radius of $\frac{W_2}{W_2^2 - W_1^2}$.

Proof: Writing $e^{j2\theta}$ as $\sin(\theta)$ and $\cos(\theta)$ using Euler's formula, we have

$$\begin{aligned} -\frac{1}{W_1 + W_2 e^{j2\theta}} &= -\frac{1}{W_1 + W_2 \cos(2\theta) + jW_2 \sin(2\theta)} \\ &= -\frac{W_1 + W_2 \cos(2\theta) - jW_2 \sin(2\theta)}{W_1^2 + 2W_1 W_2 \cos(2\theta) + W_2^2}. \end{aligned} \quad (3.57)$$

The real and imaginary parts of equation (3.57), are

$$\begin{aligned} \mathcal{U} &= -\frac{W_1 + W_2 \cos(2\theta)}{W_1^2 + 2W_1W_2 \cos(2\theta) + W_2^2} \\ \mathcal{V} &= \frac{W_2 \sin(2\theta)}{W_1^2 + 2W_1W_2 \cos(2\theta) + W_2^2}. \end{aligned} \quad (3.58)$$

Solving for $\cos(2\theta)$ and $\sin(2\theta)$ from equation (3.58), yields

$$\begin{aligned} \cos(2\theta) &= -\frac{W_1 + (W_1^2 + W_2^2)\mathcal{U}}{W_2 + 2W_1W_2\mathcal{U}} \\ \sin(2\theta) &= \frac{(W_1^2 + 2W_1W_2 \cos(2\theta) + W_2^2)\mathcal{V}}{W_2}. \end{aligned} \quad (3.59)$$

Using the identity

$$\sin^2(2\theta) + \cos^2(2\theta) = 1 \quad (3.60)$$

the following expression is yielded

$$\begin{aligned} W_1^2\mathcal{U}^2 + W_1^2\mathcal{V}^2 + 2W_1\mathcal{U} - W_2^2\mathcal{U}^2 - W_2^2\mathcal{V}^2 &= -1 \\ (W_1^2 - W_2^2)\mathcal{U}^2 + 2W_1\mathcal{U} + (W_1^2 - W_2^2)\mathcal{V}^2 &= -1 \\ \mathcal{U}^2 + \frac{2W_1}{W_1^2 - W_2^2}\mathcal{U} + \mathcal{V}^2 &= \frac{-1}{W_1^2 - W_2^2}. \end{aligned} \quad (3.61)$$

Completing the square yields

$$\left(\mathcal{U} + \frac{W_1}{W_1^2 - W_2^2}\right)^2 + \mathcal{V}^2 = \left(\frac{W_2}{W_1^2 - W_2^2}\right)^2 \quad (3.62)$$

which is a circle with a center at $(\frac{W_1}{W_1^2 - W_2^2}, 0)$ and a radius of $\frac{W_2}{W_1^2 - W_2^2}$ which proves the lemma. ■

3.2.4 Stability Analysis Using Incremental-input Describing Function

To ascertain the stability of the steady-state solution of the system, the incremental-input describing function is used by examining the characteristic equation of the incremental system. For completeness, the characteristic equation of the incremental system is given by

$$1 + (W_1 + W_2 e^{j\phi}) \mathcal{A}^{n-1} G(\sigma + j\omega_s) = 0 \quad \text{for } \omega = \omega_s \quad (3.63)$$

where, ω_s is the frequency of the driving signal. To check the stability of this characteristic equation, the Nyquist criterion can be applied.

For a given σ and ω_s , $G(\sigma + \omega_s)$ can be written as

$$G(\sigma + \omega_s) = \mathcal{X} + j\mathcal{Y}. \quad (3.64)$$

Upon substitution we have the following,

$$1 + \left(W_1 + \frac{1}{2} W_2 e^{j2\theta} \right) \mathcal{A}^{n-1} (\mathcal{X} + j\mathcal{Y}) = 0. \quad (3.65)$$

The real and imaginary parts of equation (3.65) are given respectively by

$$\begin{aligned} 1 + \left(W_1 \mathcal{A}^{n-1} + \frac{1}{2} W_2 \mathcal{A}^{n-1} \cos(2\theta) \right) \mathcal{X} - \frac{1}{2} W_2 \mathcal{A}^{n-1} \mathcal{Y} \sin(2\theta) &= 0 \\ \left(W_1 \mathcal{A}^{n-1} + \frac{1}{2} W_2 \mathcal{A}^{n-1} \cos(2\theta) \right) \mathcal{Y} + \frac{1}{2} W_2 \mathcal{A}^{n-1} \mathcal{X} \sin(2\theta) &= 0 \end{aligned} \quad (3.66)$$

From the imaginary part of equation (3.66), the value of 2θ can be obtained as follows:

$$2\theta = -\arcsin\left(\frac{2W_1\mathcal{Y}}{W_2(\mathcal{X}^2 + \mathcal{Y}^2)}\right) - \arctan\left(\frac{\mathcal{Y}}{\mathcal{X}}\right) \quad (3.67)$$

If equation (3.67) is substituted into the real part of equation (3.66), the following can be obtained

$$q^2 + \frac{8W_1\mathcal{X}}{(4W_1^2 - W_2^2)(\mathcal{X}^2 + \mathcal{Y}^2)} q + \frac{4}{(4W_1^2 - W_2^2)(\mathcal{X}^2 + \mathcal{Y}^2)} = 0 \quad (3.68)$$

where

$$q = \mathcal{A}^{n-1}, \quad (n-1) \text{ is a real even number.} \quad (3.69)$$

The solution of equation (3.68) yields

$$q = \frac{2}{(4W_1^2 - W_2^2)(\mathcal{X}^2 + \mathcal{Y}^2)} \left(-2W_1\mathcal{X} \pm W_2 \sqrt{\mathcal{X}^2 + \left(1 - \frac{4W_1^2}{W_2^2}\right) \mathcal{Y}^2} \right). \quad (3.70)$$

The necessary and sufficient conditions for equation (3.68) to have two positive real roots are

$$\begin{aligned} (i) \quad & \mathcal{X} < 0 \\ (ii) \quad & \left| \frac{\mathcal{Y}}{\mathcal{X}} \right| < \frac{1}{\sqrt{\frac{4W_1^2}{W_2^2} - 1}}. \end{aligned} \quad (3.71)$$

If the above conditions are satisfied, the critical values for the error signal magnitude A are

$$A = \left(\frac{2}{(4W_1^2 - W_2^2)(\mathcal{X}^2 + \mathcal{Y}^2)} \left(-2W_1\mathcal{X} \pm W_2\sqrt{\mathcal{X}^2 + \left(1 - \frac{4W_1^2}{W_2^2}\right)\mathcal{Y}^2} \right) \right)^{\frac{1}{n-1}}. \quad (3.72)$$

Therefore, if the conditions defined in equation (3.71) are satisfied for a given M and ω_s , for σ equal to zero, then there exist three steady-state solutions of which two are stable; however, if equation (3.71) is only satisfied for some σ greater than zero, then there exists one unstable steady-state solution; on the other hand, if it is not satisfied for any non-negative value of σ , there exists one stable steady-state solution.

To apply this theory to a problem, the following systematic approach can be followed: first, compute the incremental-input describing function $N(\mathcal{A}, \theta)$ using equation (3.54). Then, the stability of $G(j\omega)$ can be verified by employing the Nyquist criterion. Finally, the locus of $G(\sigma + j\omega_s)$ and the negative of the inverse of the incremental gain $N(\mathcal{A}, \theta)$ are examined. For each given \mathcal{A} and ω_s , it is obvious from equation (3.71) that the upper and the lower bounds of the nonlinearity envelope of $\frac{-1}{N(\mathcal{A}, \theta)}$ are defined by

$$e(v) = \pm \frac{v}{\sqrt{\frac{4W_1^2}{W_2^2} - 1}} \quad \text{where } v \in [0, \infty]. \quad (3.73)$$

Let us apply this theory to an example in order to see how the machinery of the theory can be applied to physical systems, such as, single-phase and three-phase ferroresonance and nonlinear lightly damped systems.

EXAMPLE 3.7

Consider the following system transfer function

$$G(s) = \frac{P(s)}{Q(s)}, \quad \text{where}$$

$$P(s) = 584(s^4 + 7.28s^3 + 725.17s^2 + 2886.98s + 1.3 \times 10^5)$$

$$Q(s) = s^6 + 21.5s^5 + 793.4s^4 + 1.173 \times 10^4 s^3 + 1.6 \times 10^5 s^2 + 1.246 \times 10^6 s + 1.5 \times 10^8. \quad (3.74)$$

Suppose the input signal and the nonlinearity for the system shown in figure 2.2 are defined by

$$r(t) = 0.39 \sin(10t), \quad N(x) = x^3. \quad (3.75)$$

To investigate the stability of the system for various input amplitudes M , the steps outlined earlier can be carried out. First, the error magnitude is computed using equation (3.42). For this input, one solution of the error signal exists, $\mathcal{A} = 0.5411$. Since the error magnitude is known, the incremental-input describing function can be computed using equation (3.54). Hence,

$$N(\mathcal{A}, \theta) = \frac{3}{4} \mathcal{A}^2 \left(1 + \frac{1}{2} e^{j2\theta} \right) \quad \text{where } W_1 = W_2 = 1. \quad (3.76)$$

Next, the stability of $G(\omega)$ is examined using the Nyquist criterion.

Figure 3.13 depicts the frequency response of this open-loop transfer function. It is clear from this frequency response, that this open-loop system is stable in closed-loop because there is no encirclement around the critical point $(-1, 0)$.

As shown in the figure, we will consider three different operating points Φ_1 , Φ_2 , and Φ_3 . By using frequency scaling we will force the system frequency to be 10 at each operating point. For the first case, suppose the system is operating at Φ_1 . To check the stability of this operating point for small synchronous perturbations, the incremental system must be examined at that operating frequency. This can be done as shown earlier, namely by plotting the nonlinearity envelope $-\frac{1}{N(\mathcal{A}, \theta)}$, the point $G(j10)$, and the locus $G(\sigma + j10)$. Hence, if there is an intersection between the nonlinearity envelope $-\frac{1}{N(\mathcal{A}, \theta)}$ and the point $G(j10)$ or the envelope $-\frac{1}{N(\mathcal{A}, \theta)}$ and the locus $G_1(\sigma + j10)$, the steady-state solution is an unstable operating point.

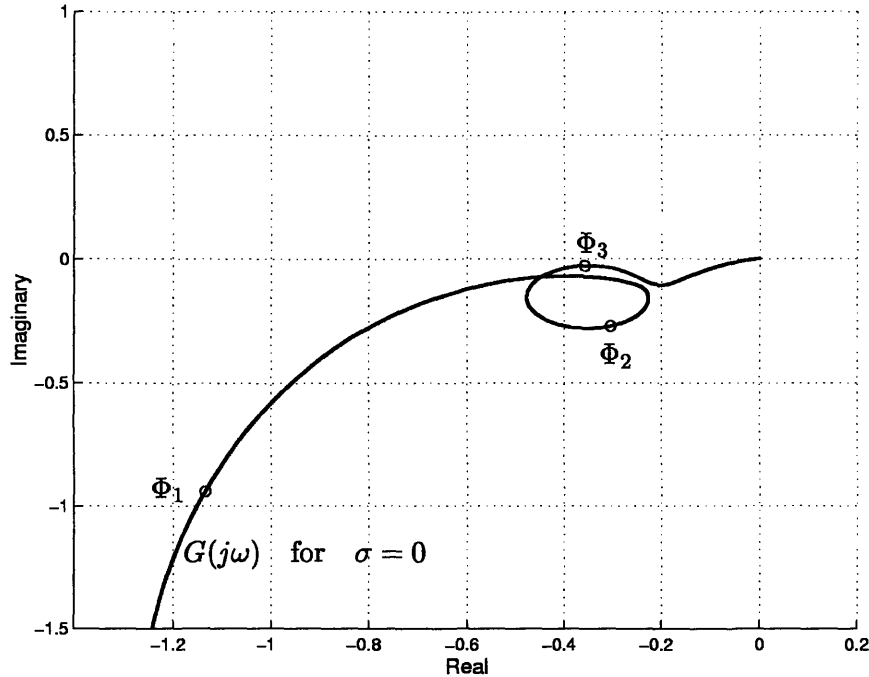
Figure 3.13: Frequency response of $G(j\omega)$

Figure 3.14 shows these loci. It is clear from the figure that no intersection exists between these loci for nonnegative values of σ . Therefore, we can conclude that this operating point is stable for small synchronous perturbations. For further verification of this result, system simulations were performed. Figure 3.15 depicts the time simulation of the system at this operating point using Matlab. After 100 sec, a perturbation signal $\gamma = 0.002$ was applied to the system and then turned off after 20 sec. From the time response, it is clear that this operating point is stable for small synchronous disturbances, which agrees with our analysis.

For the second case at Φ_2 , the magnitude of the input signal is chosen to be $M = 0.80$, and the corresponding error signal magnitude is $\mathcal{A} = 1.039$. As shown in Fig. 3.16, there is no intersection between the nonlinearity envelope $-\frac{1}{N(\mathcal{A}, \theta)}$ and the point $G_1(j10)$. However there is an intersection between the nonlinearity envelope $-\frac{1}{N(\mathcal{A}, \theta)}$ and the locus $G(\sigma + j10)$ which implies that some positive values of σ exist which satisfy equation (3.63). Hence, this steady-state solution is unstable which implies that Φ_2 is an unstable operating point.

For further verification, the time simulations of the system were performed. Figure 3.17 shows the time simulation of the system, and it agrees with our analysis. At this

operating point one unstable solution exists since the inequality (3.71) is not satisfied. At this operating point, the method in [36] fails to detect the instability of the operating point Φ_2 .

At the third operating point, Φ_3 , the magnitude of the input signal is $M = 0.39$, and the corresponding error magnitudes are $\mathcal{A} = 0.514$, $\mathcal{A} = 0.691$ and $\mathcal{A} = 1.197$. For this input, there is an intersection between the nonlinearity envelope and the point $G(j10)$ as depicted in Fig. 3.18. This implies that the condition defined in (3.71) is satisfied which implies that three steady-state solutions exist.

To capture the three steady-state solutions and their stability, time simulations were performed. For the input magnitude $M = 0.39$, the system responded with a steady-state solution $\mathcal{A} = 0.514$. At $t = 2000$ sec, a synchronous incremental-input with an amplitude of 0.0095 was applied to the system in such a way that the system response to be $\mathcal{A} = 0.691$. However, the response jumped to $\mathcal{A} = 1.197$. After the incremental signal was turned off at $t = 2500$ sec, the amplitude of the response persisted at $\mathcal{A} = 1.197$. Figure 3.19 shows the time simulation of the system. This agrees with our analysis for predicting jump solutions for small perturbations.

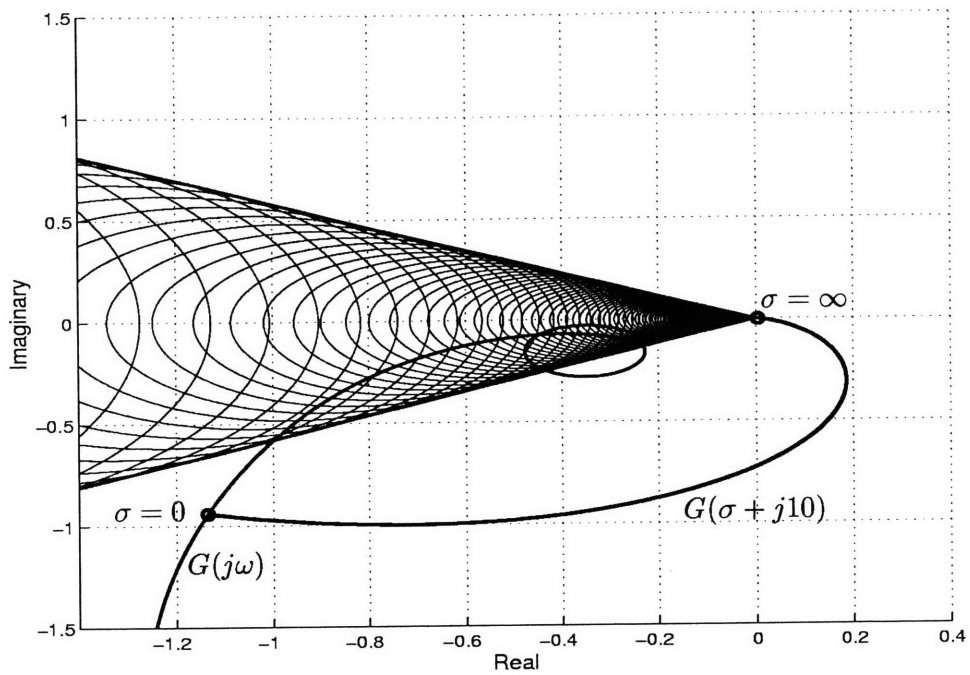


Figure 3.14: Loci of $G(j\omega)$ and $\frac{-1}{N(\mathcal{A},\phi)}$ at Φ_1

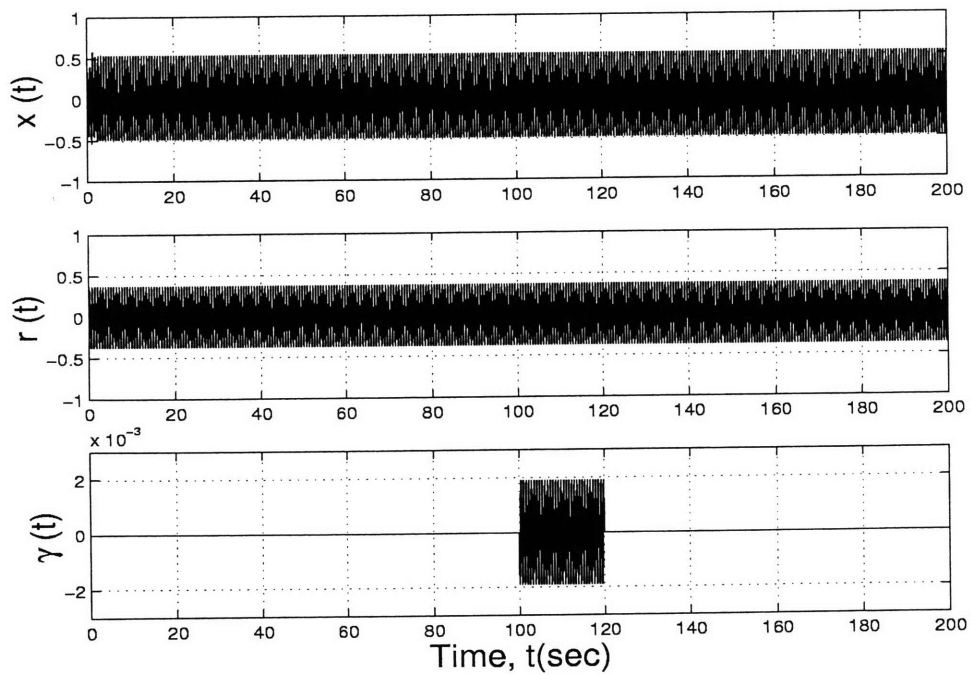


Figure 3.15: System time simulations at operating point Φ_1

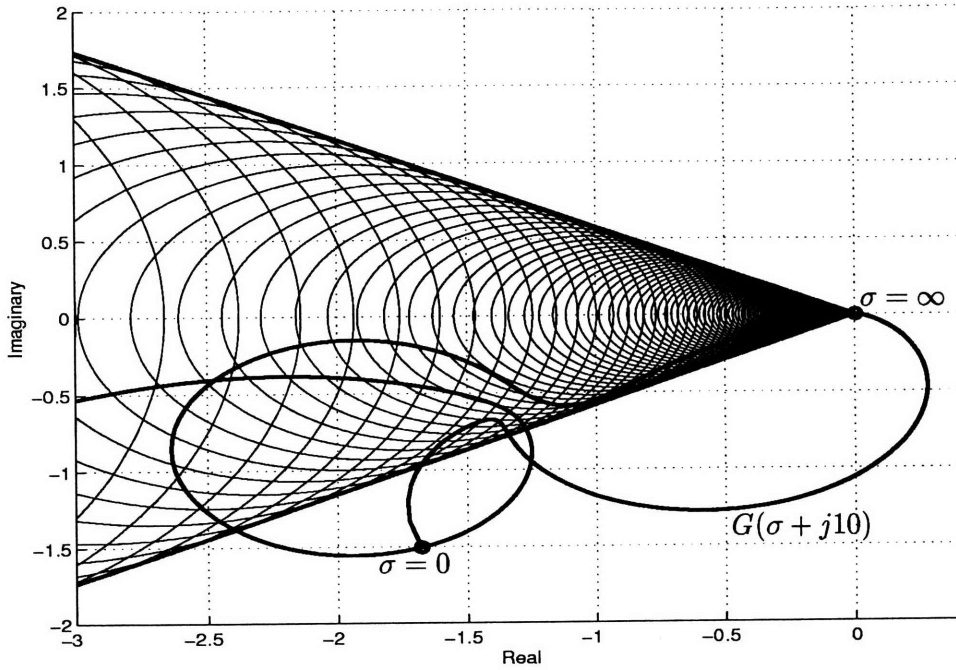


Figure 3.16: Loci of $G(j\omega)$ and $\frac{-1}{N(A,\phi)}$ at Φ_2

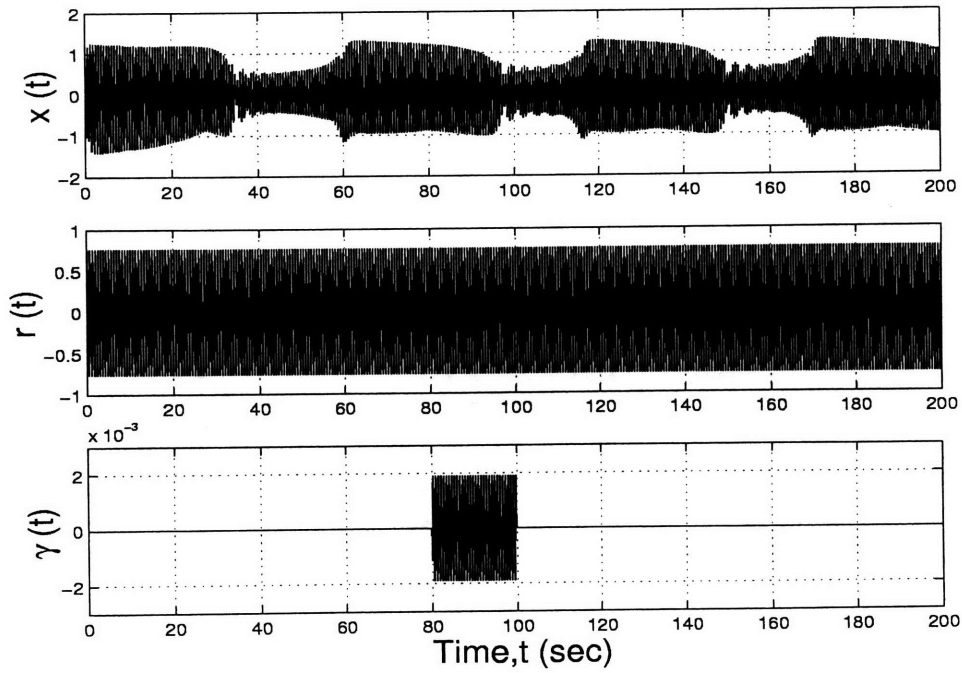


Figure 3.17: System time simulations at operating point Φ_2

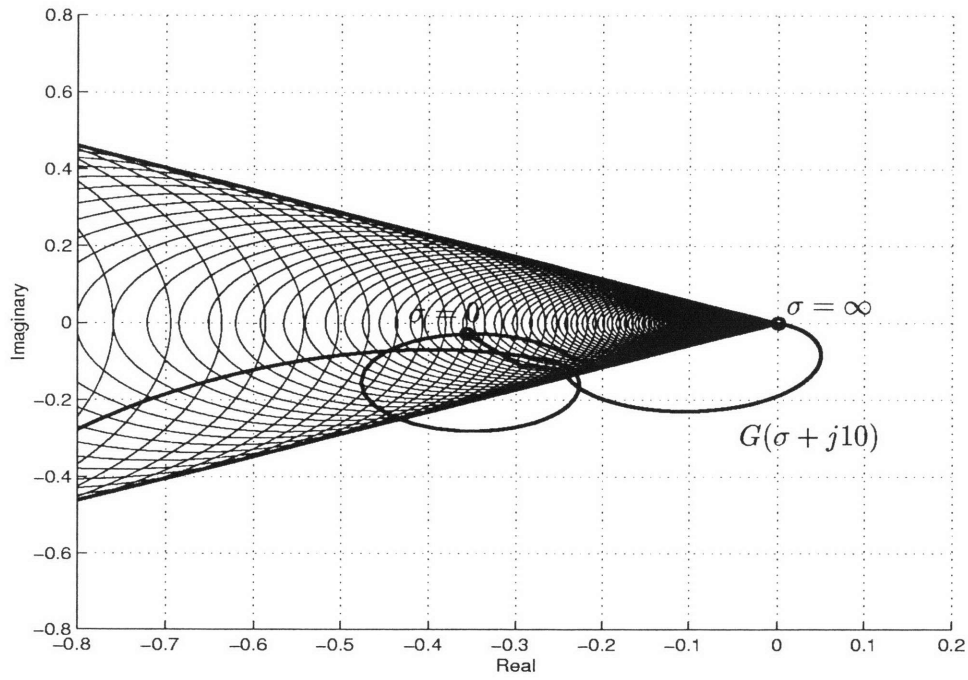


Figure 3.18: Loci of $G(j\omega)$ and $\frac{-1}{N(A,\phi)}$ at Φ_3

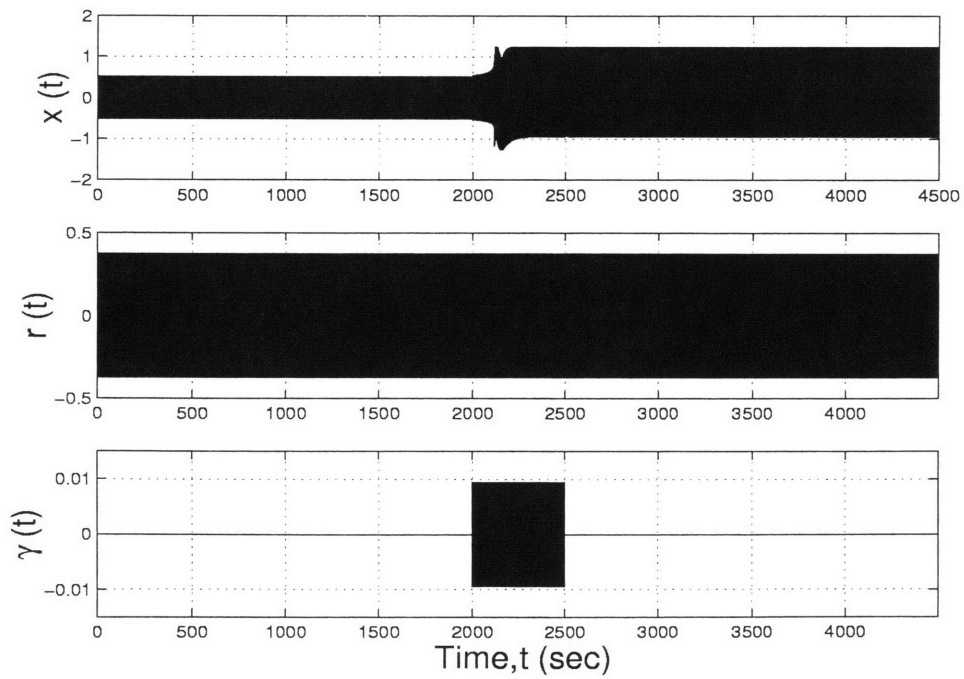


Figure 3.19: System time simulations at operating point Φ_3

Chapter 4

Generalized State-Space Averaging Methodology

Our analysis in this thesis involves the study of periodic steady-state solutions, their stability characteristics, and how they vary as a function of a parameter. To facilitate this analysis we perform a variable transformation, motivated by Fourier Analysis, in which the state variables may be interpreted as slowly-varying Fourier coefficients. In steady-state they correspond to the Fourier series coefficients of periodic steady-state solutions. This approach is called the “Generalized State-Space Averaging Method” in the power electronics literature [47–51].

The generalized state-space averaging method can be employed to investigate harmonic and subharmonic steady-state periodic solutions and their stability. In the following sections, we will formulate the generalized state-space averaging methodology as a tool to compute the harmonic and subharmonic periodic steady-state responses for nonlinear systems.

4.1 Harmonic Periodic Solutions

The general form of the nonlinear system we consider in this thesis is given by

$$\dot{x} = f(x) + g(t) \tag{4.1}$$

where $x \in \mathbb{R}^{n \times 1}$ is a state vector, $f(x)$ is a nonlinear function of the state variable and $g(t)$ is a periodic forcing function with period T . Furthermore, the nonlinear vector field $f(x)$ has a polynomial representation as shown below

$$f(x_i) = K_1 x_i + K_2 x_i^m \quad i = 1, 2, \dots, n \quad \text{and} \quad K_1, K_2 \in \mathbb{R} \tag{4.2}$$

where m is an odd number which can take the values of 3, 5, and so on depending on the model of the transformer core.

Experience with the ferroresonance problem suggests that the steady-state solutions

of (4.1) will include periodic solutions with insignificant higher harmonic components and sometimes subharmonic components. These periodic steady-state solutions have a Fourier series representation

$$x(t) = \sum_{k=-\infty}^{k=\infty} X_k e^{jk\omega t} \quad (4.3)$$

where ω is the frequency of the driving signal (or subharmonic if present) and X_k is the complex Fourier coefficients.

Equation (4.3) satisfies the system equation (4.1) only in periodic steady-state. For further analysis of the system, and in particular, stability analysis of the periodic solutions, it is useful to employ the following variable transformation that is motivated by (4.3)

$$x(t) = \sum_{k=-\infty}^{k=\infty} X_k(t) e^{jk\omega t}. \quad (4.4)$$

$X_k(t)$ in (4.4) may be considered to be slowly varying Fourier coefficients which can be defined as follows

$$X_k(t) = \frac{1}{T} \int_{t-T}^t x(\tau) e^{-jk\omega\tau} d\tau. \quad (4.5)$$

The time derivative of (4.4) is

$$\frac{d}{dt}x(t) = \sum_{k=-\infty}^{k=\infty} \left[\frac{d}{dt}X_k(t) + jk\omega X_k(t) \right] e^{jk\omega t}. \quad (4.6)$$

4.1.1 Existence of Harmonic Periodic Solutions

For systems which exhibit periodic steady-state solutions, (4.1) may be written in terms of the time-varying harmonic coefficients as

$$\begin{aligned} \sum_{k=-\infty}^{k=\infty} \left[\frac{d}{dt}X_k(t) + jk\omega X_k(t) \right] e^{jk\omega t} &= f\left(\sum_{k=-\infty}^{k=\infty} X_k(t) e^{jk\omega t} \right) + \sum_{k=-\infty}^{k=\infty} G_k e^{jk\omega t} \\ &= \sum_{k=-\infty}^{k=\infty} F_k(X_k(t)) e^{jk\omega t} + \sum_{k=-\infty}^{k=\infty} G_k e^{jk\omega t} \end{aligned} \quad (4.7)$$

where F_k and G_k take the following form

$$F_k(X_k) = \sum_{m_1} \sum_{m_2} \cdots \sum_{m_{\eta-1}} X_{m_1} X_{m_2} X_{m_3} \cdots X_{k-m_1-m_2-\cdots-m_{\eta-1}}$$

$$G_k = \begin{cases} \frac{M_i}{2} & \text{for } k = \pm \eta_i \\ 0 & \text{for } k \neq \pm \eta_i \end{cases} \quad (4.8)$$

where M_i are the amplitudes of the harmonics of the input and η_i are the angular frequencies of the input signal. For instance, if the input is $2 \cos(t) + 5 \cos(2t)$, then $M_1 = 2$, $M_2 = 5$, $\eta_1 = 1$, and $\eta_2 = 2$.

Factoring out $e^{jk\omega t}$, (4.7) may be expressed as an infinite dimensional system of nonlinear differential equations

$$\frac{d}{dt} X_k(t) = -jk\omega X_k(t) + F_k(X_k(t)) + G_k \quad -\infty < k < \infty. \quad (4.9)$$

Of course in practice we must truncate the number of terms considered in the analysis, and care must be taken specifically with the initial conditions of (4.9) so that they satisfy the initial conditions of (4.1) and allow the coefficients to be truly slowly varying. One way to measure the truncation level is to examine the average power \mathbb{P}_k of the truncated solution. One can increase the level of truncation until the difference of \mathbb{P}_k and \mathbb{P}_{k-1} is acceptable, where \mathbb{P}_k is defined as

$$\mathbb{P}_k(t) = \sum_{k=0}^{k=q} |X_k(t)|^2. \quad (4.10)$$

To illustrate the importance of choosing an appropriate initial condition, we consider the following undriven linear LC circuit with initial conditions $i(0)$ and $v(0)$. The differential equation the governs the circuit is given by

$$L \frac{di}{dt} + v = 0 \quad (4.11a)$$

$$C \frac{dv}{dt} - i = 0 \quad (4.11b)$$

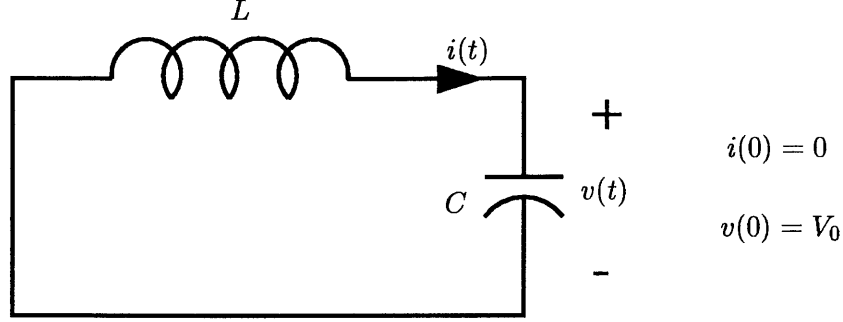


Figure 4.1: Series linear LC circuit

The solution of this system takes the form

$$i(t) = \sum_k I_k(t) e^{jk\omega t}, \quad -\infty \leq k \leq \infty \quad \text{and} \quad \omega = \frac{1}{\sqrt{LC}} \quad (4.12a)$$

$$v(t) = \sum_k V_k(t) e^{jk\omega t} \quad (4.12b)$$

where $I_k(t)$ and $V_k(t)$ are the time-varying amplitudes of the current and voltage of the circuit. Then, the time derivatives of (4.12) are given by

$$\frac{d}{dt} i(t) = \sum_k \left[\frac{d}{dt} I_k(t) + jk\omega I_k(t) \right] e^{jk\omega t}, \quad -\infty \leq k \leq \infty \quad \text{and} \quad \omega = \frac{1}{\sqrt{LC}} \quad (4.13a)$$

$$\frac{d}{dt} v(t) = \sum_k \left[\frac{d}{dt} V_k(t) + jk\omega V_k(t) \right] e^{jk\omega t}. \quad (4.13b)$$

Substituting (4.12) and (4.13) into (4.11) yields the following differential equations

$$L \sum_k \left[\frac{d}{dt} I_k(t) + jk\omega I_k(t) \right] e^{jk\omega t} + \sum_k V_k(t) e^{jk\omega t} = 0 \quad (4.14a)$$

$$C \sum_k \left[\frac{d}{dt} V_k(t) + jk\omega V_k(t) \right] e^{jk\omega t} - \sum_k I_k(t) e^{jk\omega t} = 0 \quad (4.14b)$$

with the initial conditions

$$\sum_k I_k(0) = 0 \quad (4.15a)$$

$$\sum_k V_k(0) = V_0. \quad (4.15b)$$

Factoring by the $\{e^{jk\omega t}\}$ terms, we have the following set of infinite differential equations

$$\frac{d}{dt}I_k(t) = -jk\omega I_k(t) - \frac{1}{L}V_k(t) \quad (4.16a)$$

$$\frac{d}{dt}V_k(t) = -jk\omega V_k(t) + \frac{1}{C}I_k(t) \quad (4.16b)$$

with the initial conditions defined in (4.15). The characteristic equation of the system is given by

$$\mu_k^2 + j2k\omega\mu_k + (1 - k^2)\omega^2 = 0. \quad (4.17)$$

The eigenvalues of the system are

$$\mu_{1,k} = j(1 - k)\omega \quad \text{and} \quad \mu_{2,k} = -j(1 + k)\omega, \quad \text{for} \quad -\infty \leq k \leq \infty. \quad (4.18)$$

Hence, the solution of the system defined in (4.16) is given by

$$V_k(t) = \eta_{1,k}e^{j(1-k)\omega t} + \eta_{2,k}e^{-j(1+k)\omega t} \quad \text{where} \quad \eta_{1,k}, \eta_{2,k} \in \mathbb{C} \quad (4.19a)$$

$$I_k(t) = j(1 - k)\eta_{1,k}\omega C e^{j(1-k)\omega t} - j(1 + k)\eta_{2,k}\omega C e^{-j(1+k)\omega t}. \quad (4.19b)$$

It is clear from (4.19) that for some linear combinations of $\eta_{1,k}$ and $\eta_{2,k}$, the amplitudes of the voltage and the current, $V_k(t)$ and $I_k(t)$, contain pure oscillatory terms. Hence, this amplitude are not constant or slowly varying amplitudes. One way to force amplitude to be constant or slowly varying is to choose $\eta_{1,k}$ and $\eta_{2,k}$ such that

$$\sum_k \eta_{1,k} + \eta_{2,k} = V_0 \quad (4.20a)$$

$$\sum_k (1 - k)\eta_{1,k} - (1 + k)\eta_{2,k} = 0 \quad (4.20b)$$

are satisfied. We have two equations and we would like to solve for an infinite number of variables. Therefore, such equations have an infinite number of solutions. Constraining $\eta_{1,k}$ and $\eta_{2,k}$ by the following equations, we can force the amplitudes to be slowly varying variables.

$$\begin{cases} \text{for } k = \pm 1 & \eta_{2,-1} = \eta_{1,1} \quad \text{and} \quad \eta_{2,1} = -\eta_{1,-1} \\ \text{otherwise} & \eta_{2,\pm k} = -\eta_{1,\mp k}. \end{cases} \quad (4.21)$$

In this scheme, we have $\eta_{2,-1} = \eta_{1,1} = \frac{1}{2}V_0$. Hence, by choosing the right initial condition,

we forced the amplitudes to be slowly varying variables relative to the frequency of the carrier. In this case, the amplitudes are constant, and the solution of the circuit is given by

$$\begin{aligned}
 v(t) &= \frac{1}{2}Ae^{j\omega t} + \frac{1}{2}Ae^{-j\omega t} \\
 &= V_0 \cos(\omega t) \\
 i(t) &= -C\omega V_0 \frac{1}{j2}e^{j\omega t} + C\omega V_0 \frac{1}{j2}e^{-j\omega t} \\
 &= -V_0 \sqrt{\frac{C}{L}} \sin(\omega t).
 \end{aligned} \tag{4.22}$$

Since the differential equation defined in (4.11) is linear, we can also compute the solution of the system as follows. We assume the voltage across the capacitor takes the form

$$v(t) = K \cos(\omega t + \phi). \tag{4.23}$$

This equation has two unknowns, K and ϕ . Under the given initial conditions, we can compute K and ϕ easily. Hence the voltage across the capacitor and the current through the inductor take the form

$$\begin{aligned}
 v(t) &= V_0 \cos(\omega t) \\
 i(t) &= -V_0 \sqrt{\frac{C}{L}} \sin(\omega t).
 \end{aligned} \tag{4.24}$$

This solution agrees with the solution computed earlier in (4.22).

To compute the steady-state solutions of the system defined in (4.9), the time derivatives are set to zero as given here

$$-jk\omega X_k(t) + F_k(X_k(t)) + G_k = 0 \quad -\infty < k < \infty. \tag{4.25}$$

Hence, the existence of nontrivial solutions of these equations implies the existence of a harmonic steady-state periodic solution of the system defined in (4.1).

If we apply the generalized state-space averaging method to finite dimensional non-linear system, for example, a third order system, we end up with an infinite dimensional system like (4.25). In this approach, one may ask if the problem was needlessly complicated rather than simplified. We use this complicated model to analyze the system dynamics for the following reasons. First, the generalized state-space averaged model is much faster to

simulate than the full system, particularly for lightly damped systems, because the averaged variables do not change much within a small time interval; therefore, we can use a large step size to integrate the system dynamics. Another reason to employ this method is to assess the stability of the periodic steady-state solution, which is hard to assess for the full system, since the steady-state solution is periodic. If we linearize the system around the periodic solution, the Jacobian matrix of the system is not constant; it is time dependent. Furthermore, the generalized state-space averaging model is an autonomous system while the full system is a non-autonomous system.

4.1.2 Stability of Harmonic Periodic Solutions

Assessing the stability of the periodic solutions of the system defined in (4.1) requires a close examination of the evolution of the slowly varying system. One way to ascertain the stability of the slowly varying amplitudes is to linearize the system and then perform an eigenvalue analysis. The following theorem will give us conditions for the stability of the envelope dynamics.

THEOREM 4.1

Suppose the following system

$$\dot{X}_k(t) = -jk\omega X_k(t) + F_k(X_k(t)) + G_k \quad \text{where} \quad -\infty \leq k \leq \infty \quad (4.26)$$

has a steady-state solution \bar{X}_k . Then, the steady-state solution \bar{X}_k is stable if the eigenvalues of A have negative real parts, where

$$A = -jk\omega\delta_{k,n} + Q_{k-n}, \quad \text{where} \quad -\infty \leq k \leq \infty \quad \text{and} \quad -\infty \leq n \leq \infty \quad (4.27)$$

and Q_{k-n} is the Jacobian matrix of the vector field $F_K(X_k(t))$. Furthermore, if μ is an eigenvalue of A , then $\mu \pm jk\omega$ is also an eigenvalue of A .

Proof To prove the theorem, first let us construct the matrix Q_{k-n} , the Jacobian matrix of the nonlinear function $F_k(X_k(t))$.

To gain insight in the form of the Jacobian matrix, suppose the nonlinear function $f(x)$ defined in (4.1) takes the form

$$f(x) = x^2. \quad (4.28)$$

Then, the function F_k defined in (4.25) becomes

$$F_k = \sum_m X_m X_{k-m}. \quad (4.29)$$

The Jacobian matrix of the function F_k yields

$$\begin{aligned} Q_{k-n} &= \frac{\partial F_k}{\partial X_n} = \frac{\partial}{\partial X_n} \left[\sum_m X_m X_{k-m} \right] \\ &= \sum_m \frac{\partial}{\partial X_n} [X_m X_{k-m}] \\ &= 2X_{\{k-n\}} \quad \text{where } -\infty < n < \infty \quad \text{and} \quad -\infty < k < \infty. \end{aligned} \quad (4.30)$$

To see the pattern, let assume further that $f(x)$ takes the form

$$f(x) = x^3 \quad (4.31)$$

then, F_k yields

$$F_k = \sum_{m_1} \sum_{m_2} X_{m_1} X_{m_2} X_{k-m_1-m_2}. \quad (4.32)$$

In the general monomial case, the Jacobian of $F_k(X_k(t))$ is given by

$$\begin{aligned} Q_{k-n} &= \frac{\partial F_k}{\partial X_n} = \frac{\partial}{\partial X_n} \sum_{m_1} \sum_{m_2} X_{m_1} X_{m_2} X_{k-m_1-m_2} \\ &= \sum_m \sum_n \frac{\partial}{\partial X_n} \{X_{m_1} X_{m_2} X_{k-m_1-m_2}\} \\ &= \sum_{m_1} \sum_{m_2} X_{m_1} X_{m_2} \frac{\partial}{\partial X_n} \{X_{k-m_1-m_2}\} + X_{m_1} X_{k-m_1-m_2} \frac{\partial}{\partial X_n} \{X_{m_2}\} + \\ &\quad X_{m_2} X_{k-m_1-m_2} \frac{\partial}{\partial X_n} \{X_{m_1}\}. \end{aligned} \quad (4.33)$$

The partials are non-zero only when $j = k - m_1 - m_2$, $j = m_2$ or $j = m_1$, otherwise the partials are zero. For the case where the partials are non-zero, we have

$$Q_{k-n} = \frac{\partial F_k}{\partial X_n} = \sum_{m_1} X_{m_1} X_{k-m_1-n} + \sum_{m_1} X_{m_1} X_{k-n-m_1} + \sum_{m_2} X_{m_2} X_{k-n-m_2}. \quad (4.34)$$

Since the indexes are dummy variables, changing the index from m_1 to m_2 , we have

$$Q_{k-n} = 3 \sum_m X_m X_{\{k-n\}-m}, \quad \text{where } -\infty < n < \infty \quad \text{and} \quad -\infty < k < \infty. \quad (4.35)$$

Hence, for the general case where $f(x) = x + x^\nu$, $Q_{\{k-n\}}$ takes the form

$$Q_{k-n} = \nu \sum_{m_1} \sum_{m_2} \cdots \sum_{m_{\nu-2}} X_{m_1} X_{m_2} \cdots X_{m_{\nu-2}} X_{\{k-n\}-m_1-m_2-\cdots-m_{\nu-2}} \quad (4.36)$$

where $-\infty < n < \infty$ and $-\infty < k < \infty$.

It is clear that Q is an infinite dimensional matrix. In matrix form, Q has the following structure

$$Q_{k-n} = \begin{bmatrix} \vdots & & & & & & \vdots & & \\ \cdots & Q_0 & Q_{-1} & Q_{-2} & Q_{-3} & Q_{-4} & Q_{-5} & Q_{-6} & \cdots \\ & Q_1 & Q_0 & Q_{-1} & Q_{-2} & Q_{-3} & Q_{-4} & Q_{-5} & \\ & Q_2 & Q_1 & Q_0 & Q_{-1} & Q_{-2} & Q_{-3} & Q_{-4} & \\ & Q_3 & Q_2 & Q_1 & Q_0 & Q_{-1} & Q_{-2} & Q_{-3} & \\ & Q_4 & Q_3 & Q_2 & Q_1 & Q_0 & Q_{-1} & Q_{-2} & \\ & Q_5 & Q_4 & Q_3 & Q_2 & Q_1 & Q_0 & Q_{-1} & \\ \cdots & Q_6 & Q_5 & Q_4 & Q_3 & Q_2 & Q_1 & Q_0 & \cdots \\ & \vdots & & & & & & \vdots & \end{bmatrix} \quad (4.37)$$

Hence, Q is a Toeplitz matrix. Since $X_k = X_{-k}$ for real systems, Q is also Hermitian [67].

Then, the matrix A takes the following form

$$A = \begin{bmatrix} \vdots & & & & & & \vdots & & \\ \cdots & Q_0 + j2\omega & Q_{-1} & Q_{-2} & Q_{-3} & Q_{-4} & \cdots & & \\ & Q_1 & Q_0 + j\omega & Q_{-1} & Q_{-2} & Q_{-3} & & & \\ & Q_2 & Q_1 & Q_0 & Q_{-1} & Q_{-2} & & & \\ & Q_3 & Q_2 & Q_1 & Q_0 - j\omega & Q_{-1} & & & \\ \cdots & Q_4 & Q_3 & Q_2 & Q_1 & Q_0 - j2\omega & \cdots & & \\ & \vdots & & & & & & \vdots & \end{bmatrix} \quad (4.38)$$

Similarly, A is a Toeplitz matrix.

Suppose μ is an eigenvalue of A , then

$$\begin{bmatrix} \vdots & & & & & & \\ \cdots & Q_0 + j2\omega & Q_{-1} & Q_{-2} & Q_{-3} & Q_{-4} & \cdots \\ & Q_1 & Q_0 + j\omega & Q_{-1} & Q_{-2} & Q_{-3} & \\ & Q_2 & Q_1 & Q_0 & Q_{-1} & Q_{-2} & \\ & Q_3 & Q_2 & Q_1 & Q_0 - j\omega & Q_{-1} & \\ \cdots & Q_4 & Q_3 & Q_2 & Q_1 & Q_0 - j2\omega & \cdots \\ & \vdots & & & & & \end{bmatrix} \begin{bmatrix} \vdots \\ v_{-2} \\ v_{-1} \\ v_0 \\ v_1 \\ v_2 \\ \vdots \end{bmatrix} = \mu \begin{bmatrix} \vdots \\ v_{-2} \\ v_{-1} \\ v_0 \\ v_1 \\ v_2 \\ \vdots \end{bmatrix} \quad (4.39)$$

holds, where $[\cdots, v_{-2}, v_{-1}, v_0, v_1, v_2, \cdots]^T$ is a right eigenvector that corresponds to μ . These eigenvectors are infinite since A is an infinite matrix. Define the matrix

$$A' = A \pm j\omega I \quad (4.40)$$

where I is an identity matrix. The eigenvalues of A' are the eigenvalues of A plus $\pm j\omega$, which equal $\mu \pm j\omega$. If we closely examine A' , we can see that A' is equal to A shifted up or down by one. However, since A is an infinite-dimensional matrix, there is no difference between A' and A ; actually $A' = A$. This proves that if A has an eigenvalue of μ then $\mu \pm jk\omega$ is also an eigenvalue of A .

If we set $k = 0$, the eigenvalues that correspond to the truncated matrix are μ_0 , where μ_0 is a vector. The dimension of μ_0 depends on the dimension of the system defined in (4.1). Therefore, the stability of the system can be assessed by examining the eigenvalues of A when $k = 0$, since the other eigenvalues differ by $\pm jk\omega$. We call μ_0 the *fundamental eigenvalues*, since these eigenvalues are the bases for the eigenvalues of A . Graphically, the eigenvalues appear on either the $j\omega$ -axis or lines parallel to the $j\omega$ -axis in the complex plane.

If the system defined in (4.1) is linear, there is no coupling among the harmonics of matrix A ; however, if the system is nonlinear there may be coupling among the harmonics of A . Therefore, setting $k = 0$ will not give us μ_0 , there will be errors in the sums. To decrease these errors, we choose some $k = q$ such that the difference between the average power of the solution and the truncated solution in one cycle is negligible. For the truncated system, the eigenvalues will also appear to lie on lines parallel to the $j\omega$ -axis with some dispersion at the ends. These dispersions are due to the truncation of A . ■

The *fundamental eigenvalues* are related to the Floquet exponents as shown in [68,69]. Hence, one can compute the eigenvalues of the system using a time domain approach using Floquet theory or in the frequency domain invoking the generalized state-space averaging method. We will elaborate on this subject in Chapter 5.

4.2 Subharmonic Periodic Solutions

An interesting phenomenon in dynamical systems is the possibility of generating a steady-state periodic solution whose fundamental frequency is a submultiple of the frequency of the forcing term. For the linear case, if the frequency of the free oscillation is $\frac{\omega}{n}$, then a periodic external input of frequency ω can excite the free oscillation in addition to the driving frequency. But, in general, linear dynamical systems have damping; hence, the free oscillations will damp out depending upon the time constant of the system. On the other hand, even if a nonlinear system has some damping it is still possible that an external force of a given frequency might be able to excite and sustain a subharmonic of lower frequency.

The subharmonic phenomenon occurs in power system networks, particularly, if the system contains a lightly loaded distribution transformer. The mechanism that induces or quenches the subharmonic phenomenon depends on the initial state of the system or system internal parameters. Changing system parameters modifies the system dynamics which in turn can drive the system into a subharmonic region. Hence, it is possible for the system to have periodic solutions which oscillate at frequencies which are submultiple of the frequency of the input signal.

To understand the subharmonic phenomenon, let's take a simple example which we can solve analytically. Consider the following nonlinear series circuit

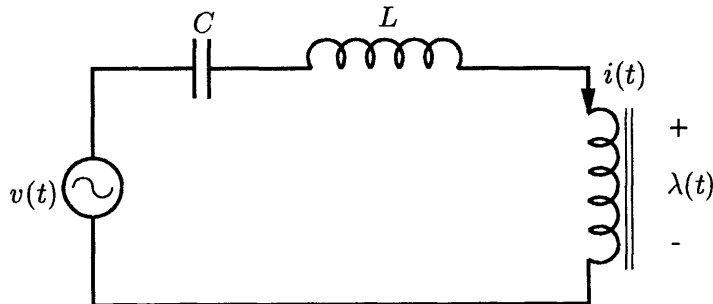


Figure 4.2: Series nonlinear circuit

where $v(t)$ and $i(t)$ are defined as

$$v(t) = \frac{1}{3} \cos(3t + 3\theta) \quad \text{and} \quad i(t) = K\lambda(t)^3. \quad (4.41)$$

The differential equation that describes the circuit dynamics is given by

$$L \frac{di(t)}{dt} + \frac{1}{C} \int i dt + \frac{d\lambda(t)}{dt} = \frac{1}{3} \cos(3t + 3\theta). \quad (4.42)$$

Taking the time derivative of equation (4.42), we have the following

$$L \frac{d^2 i(t)}{dt^2} + \frac{i}{C} + \frac{d^2 \lambda(t)}{dt^2} = -\sin(3t + 3\theta). \quad (4.43)$$

In order to investigate the sensitivity of the solutions of equation (4.43) to variations of initial conditions and system parameters, we compute two independent steady-state solutions. One of these steady-state solutions has the same frequency as the driving signal while the other solution is $\frac{1}{3}$ of the frequency of the input function. Then we choose some initial conditions and parameters to steer the system responses to those aforementioned steady-state solutions.

Let's first investigate the sensitivity of the system response to initial conditions.

4.2.1 Sub-Synchronous Responses

Suppose the steady-state solution of the flux $\lambda(t)$ has this form

$$\lambda(t) = \mathcal{A}_1 \sin(t + \theta). \quad (4.44)$$

Then, the current takes the form

$$i(t) = \frac{3}{4} K \mathcal{A}_1^3 \sin(t + \theta) - \frac{1}{4} K \mathcal{A}_1^3 \sin(3t + 3\theta). \quad (4.45)$$

Substituting equations (4.44) and (4.45) into (4.43), we have the following

$$\frac{9}{4} LCK \mathcal{A}_1^3 \sin(3t + 3\theta) - \frac{3}{4} LCK \mathcal{A}_1^3 \sin(t + \theta) - \frac{1}{4} K \mathcal{A}_1^3 \sin(3t + 3\theta) + \quad (4.46a)$$

$$\frac{3}{4} K \mathcal{A}_1^3 \sin(t + \theta) - C \mathcal{A}_1 \sin(t + \theta) + C \sin(3t + 3\theta) = 0. \quad (4.46b)$$

Equating the sub-synchronous and synchronous components of (4.46a) and (4.46b) yields

$$-\frac{3}{4}LCK\mathcal{A}_1^3 + \frac{3}{4}K\mathcal{A}_1^3 - C\mathcal{A}_1 = 0 \quad (4.47a)$$

$$\frac{9}{4}LCK\mathcal{A}_1^3 - \frac{1}{4}K\mathcal{A}_1^3 + C = 0. \quad (4.47b)$$

Factoring \mathcal{A}_1 out in equation (4.47a) and then adding (4.47a) and (4.47b), we have

$$\mathcal{A}_1 = \frac{3(1 - LC)}{(1 - 9LC)} \quad (4.48)$$

Suppose we are given the following system parameters: $C = \frac{1}{27}$, $L = \frac{1}{3}$, and $K = \frac{9}{2000}$, then \mathcal{A}_1 is equal to $\frac{10}{3}$ which simultaneously satisfy both (4.47a) and (4.47b). Hence, the steady-state response of the flux and the current yield

$$\begin{aligned} \lambda(t) &= \frac{10}{3} \sin(t + \theta) \\ i(t) &= \frac{1}{8} \sin(t + \theta) - \frac{1}{24} \sin(3t + 3\theta) \end{aligned} \quad (4.49)$$

with the initial conditions $\lambda(0) = 0$ and $\frac{d\lambda(0)}{dt} = \frac{10}{3}$. In this case, we choose θ to be multiple of π .

4.2.2 Synchronous Responses

Now, suppose the steady-state solution of the flux $\lambda(t)$ has this form

$$\lambda = \mathcal{A}_2 \sin(3t + 3\theta). \quad (4.50)$$

Then, the current has the steady-state solution

$$i(t) = \frac{3}{4}K\mathcal{A}_2^3 \sin(3t + 3\theta) - \frac{1}{4}K\mathcal{A}_2^3 \sin(9t + 9\theta). \quad (4.51)$$

Substituting equations (4.50) and (4.51) into (4.43), we have the following

$$\frac{81}{4}LCK\mathcal{A}_2^3 \sin(9t + 9\theta) - \frac{27}{4}LCK\mathcal{A}_2^3 \sin(3t + 3\theta) - \frac{1}{4}K\mathcal{A}_2^3 \sin(9t + 9\theta) + \quad (4.52a)$$

$$\frac{3}{4}K\mathcal{A}_2^3 \sin(3t + 3\theta) - 9C\mathcal{A}_2 \sin(3t + 3\theta) + C \sin(3t + 3\theta) = 0. \quad (4.52b)$$

By harmonic balancing for the synchronous components of equation (4.46), we have

$$-\frac{27}{4}LCK\mathcal{A}_2^3 + \frac{3}{4}K\mathcal{A}_2^3 - 9C\mathcal{A}_2 + C = 0 \quad (4.53a)$$

$$\frac{81}{4}LCK\mathcal{A}_2^3 - \frac{1}{4}K\mathcal{A}_2^3 = 0. \quad (4.53b)$$

Solving for B in (4.53a), we have $\mathcal{A}_2 = \frac{1000}{8999}$ which approximately equal to $\mathcal{A}_2 \approx \frac{1}{9}$ where $C = \frac{1}{27}$, $L = \frac{1}{3}$, and $K = \frac{9}{2000}$. This value of \mathcal{A}_2 satisfies both both equations in (4.53).

The flux and the current take the following expressions

$$\lambda(t) = \frac{1}{9} \sin(3t + 3\theta) \quad (4.54a)$$

$$i(t) = \frac{1}{216000} \sin(3t + 3\theta) - \frac{1}{648000} \sin(9t + 9\theta) \quad (4.54b)$$

with the initial conditions $\lambda(0) = 0$ and $\frac{d\lambda(0)}{dt} = \frac{1}{3}$. In this case the fundamental frequency of the response is synchronous to the frequency of the input signal. Hence, we call this solution a synchronous response.

It is clear from this example, that for a given initial condition the steady-state solution of the flux can have frequencies which are subharmonics or harmonics of the frequency of the input signal. To verify these conclusions, the system defined in (4.43) was simulated using Simulink [58]. Under the initial condition $\{\lambda(0) = 0, \frac{d\lambda(0)}{dt} = \frac{10}{3}\}$, the steady-state solution of the flux of the core agrees with the values computed earlier as shown in Fig. 4.3. Since the magnitude of the flux is small in this case, we plotted $3\lambda(t)$ to capture the correlation of the frequencies of the signals. Similarly, for the initial condition $\{\lambda(0) = 0, \frac{d\lambda(0)}{dt} = \frac{1}{3}\}$ the simulation outcome agrees with the results found earlier as depicted in Fig. 4.4. It is clear now that if we choose an initial condition and vary system parameters, such as C , L , or K , the system can respond with signals which are harmonics or subharmonics of the driving signal.

For large complex nonlinear power systems, some of the methods which can be used to compute subharmonic periodic steady-state solutions are: perturbation procedures [70], time transformation methods [71], harmonic balance methods [72], iteration methods [19], and averaging methods [19]. In this thesis, we use the generalized state-space averaging method to investigate the steady-state subharmonic periodic solutions and their stability.

To capture the steady-state subharmonic periodic solution with an $\frac{\omega}{n}$ th order subhar-

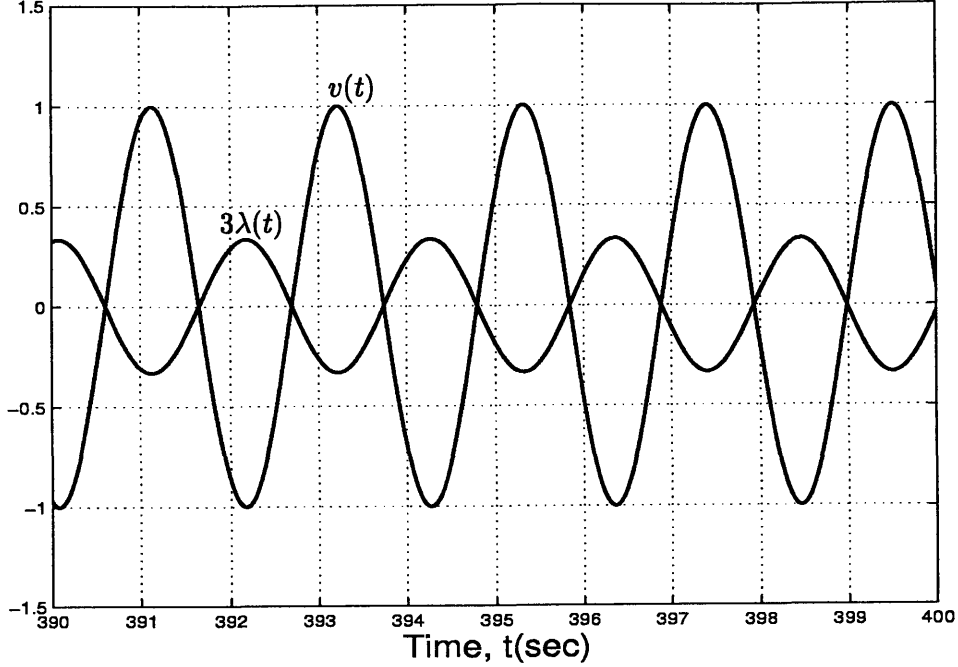


Figure 4.3: Harmonic solutions

monic, the response of the system can be formulated using a Fourier series representation

$$x_{\frac{\omega}{n}}(t) = \sum_{k=-\infty}^{\infty} X_{k\frac{\omega}{n}}(t) e^{jk\frac{\omega}{n}t}, \quad n \in \mathbb{N} \quad (4.55)$$

where $\frac{\omega}{n}$ is the angular frequency of the response $x(t)$ and ω is the frequency of the input signal. $X_{k\frac{\omega}{n}}(t)$ is the projection of $x(t)$ defined as

$$X_{k\frac{\omega}{n}}(t) = \frac{1}{T} \int_{t-T}^t x(\tau) e^{-jk\frac{\omega}{n}\tau} d\tau. \quad (4.56)$$

Furthermore, the time derivatives of (4.55) are given by

$$\frac{d}{dt} x_{\frac{\omega}{n}}(t) = \sum_{k=-\infty}^{\infty} \left[\frac{d}{dt} X_{k\frac{\omega}{n}}(t) + jk\frac{\omega}{n} X_{k\frac{\omega}{n}}(t) \right] e^{jk\frac{\omega}{n}t}. \quad (4.57)$$

Equations (4.55) and (4.57) allow us to separate the carrier from the amplitude of the responses of nonlinear systems which in turn allow us to study the steady-state amplitudes and their stability. In the following two sections, we investigate the steady-state subharmonic periodic solutions and their stability respectively.

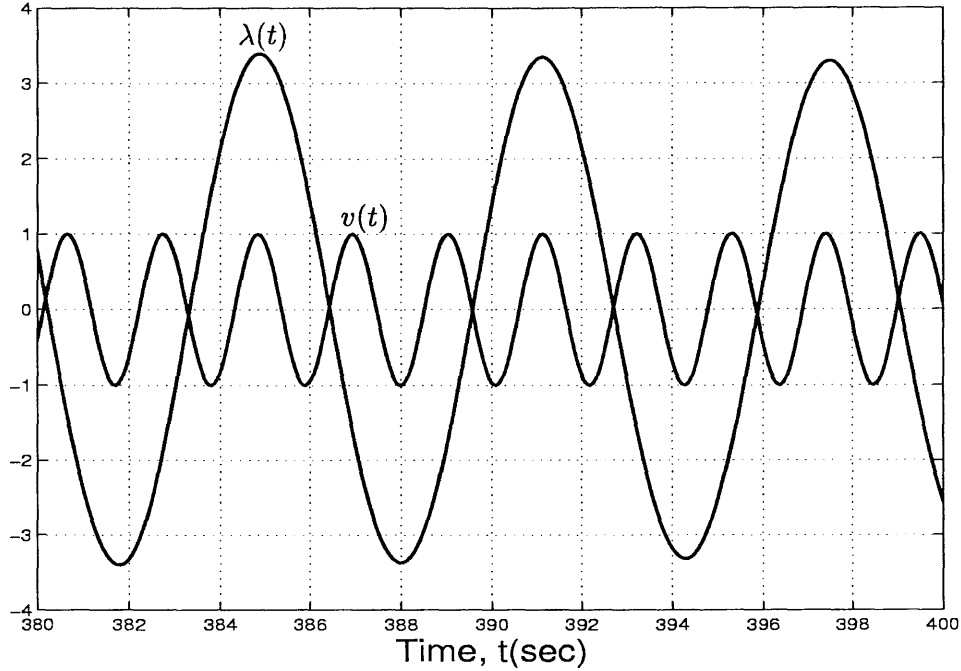


Figure 4.4: Subharmonic Solutions

4.2.3 Existence of Subharmonic Periodic Solutions

Consider the following nonlinear differential equation

$$\dot{x} = f(x) + g(t) \quad (4.58)$$

where $f(x)$ is a nonlinear function of the state variable and $g(t)$ is a forcing function which is periodic in time with period T , where $T = \frac{2\pi}{\omega}$. Furthermore, the nonlinear vector field $f(x)$ has a polynomial representation as shown below

$$f(x_i) = K_1 x_i + K_2 x_i^m \quad \text{and} \quad K_1, K_2 \in \mathbb{R} \quad (4.59)$$

Applying (4.55) and (4.57) to (4.58), we have the following system of nonlinear algebraic equations whose solutions give the steady-state amplitude of (4.58)

$$-jk \frac{\omega}{n} X_{k \frac{\omega}{n}}(t) + F_{k \frac{\omega}{n}}(X_{k \frac{\omega}{n}}(t)) + G_{k \frac{\omega}{n}} = 0 \quad \text{where} \quad -\infty \leq k \leq \infty \quad (4.60)$$

where $F_{k\frac{\omega}{n}}(X_{k\frac{\omega}{n}}(t))$ and G_k take the following form

$$F_{k\frac{\omega}{n}}(X_{k\frac{\omega}{n}}) = \sum_{m_1} \sum_{m_2} \cdots \sum_{m_{\alpha-1}} X_{m_1\frac{\omega}{n}} X_{m_2\frac{\omega}{n}} X_{m_3\frac{\omega}{n}} \cdots X_{m_{\alpha-1}\frac{\omega}{n}} X_{k\frac{\omega}{n} - m_1\frac{\omega}{n} - m_2\frac{\omega}{n} - \cdots - m_{\alpha-1}\frac{\omega}{n}}$$

$$G_k = \begin{cases} \frac{M_i}{2} & \text{for } k = \pm \alpha_i \\ 0 & \text{for } k \neq \pm \alpha_i. \end{cases} \quad (4.61)$$

Hence, existence of nontrivial solutions of these equations implies existence of subharmonic steady-state periodic solutions of the system defined in (4.58).

4.2.4 Stability of Subharmonic Periodic Solutions

The following theorem gives the conditions of the stability of the steady-state subharmonic periodic solutions of the system defined in (4.58).

THEOREM 4.2

Suppose the following nonlinear differential equation

$$\frac{d}{dt} X_{k\frac{\omega}{n}}(t) = -jk\frac{\omega}{n} X_{k\frac{\omega}{n}}(t) + F_{k\frac{\omega}{n}}(X_{k\frac{\omega}{n}}(t)) + G_{k\frac{\omega}{n}}, \quad \text{where } -\infty \leq k \leq \infty \quad (4.62)$$

has a steady-state solution $\bar{X}_{k\frac{\omega}{n}}$. Then, the steady-state solution $\bar{X}_{k\frac{\omega}{n}}$ is stable if the eigenvalues of A have negative real parts, where

$$A = -jk\frac{\omega}{n} + Q_{\{k-j\}\frac{\omega}{n}}, \quad \text{where } -\infty \leq k \leq \infty \quad \text{and} \quad -\infty \leq j \leq \infty. \quad (4.63)$$

Furthermore, if A has an eigenvalue of μ , then $\mu \pm jk\frac{\omega}{n}$ is also an eigenvalue of A .

We omit the proof of this theorem since it follows similar reasoning as Theorem 4.1. ■

4.2 Subharmonic Periodic Solutions

Chapter 5

Analysis Tools: Poincaré Map, Floquet Theory, and GSSA Method

5.1 Model Formulation for Duffing Oscillator

Consider the following buckled beam with one mode of vibration [2]. As depicted in Fig-

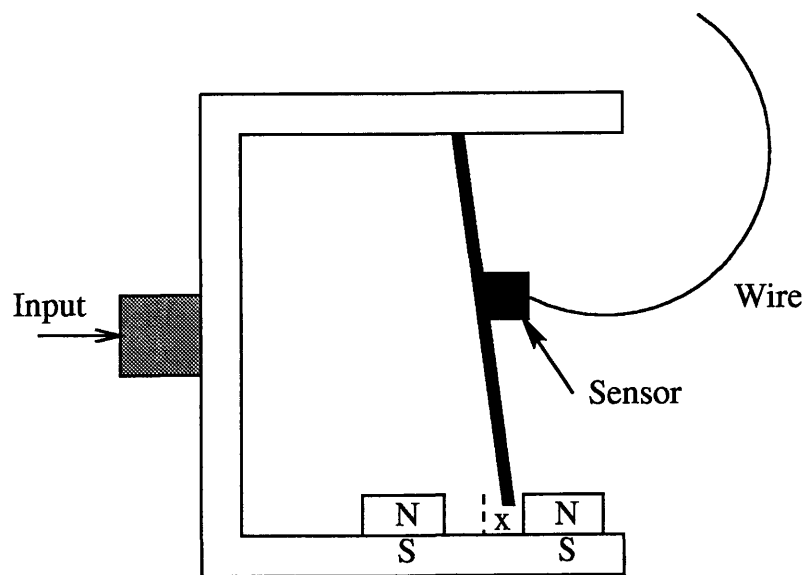


Figure 5.1: Nonlinear interconnected system [2]

ure 5.1, the field force induced by the nonuniform permanent magnet overcomes the elastic force of the beam. Hence the beam bends toward the magnetic poles. Without the influence of the magnetic force, the beam would be straight assuming there is no external force acting on the system. The variable x shown in the picture measures the beam displacement, in particular its tip displacement. The sensor attached to the beam measures the curvature of the tip of the beam as a function of time, assuming the motion of the beam primarily contains first mode dynamics.

There are three steady-state solutions for this system. Two positions are when the beam contacts to either of the magnetic North poles; these equilibria are stable. The third

equilibrium is the midpoint between the two poles; since for small perturbations the beam leaves this fixed point, we can conclude that this equilibrium is unstable.

Using Newton's second law of motion, we can formulate the system dynamics as the following nonlinear differential equation which is Duffing's oscillator [2]:

$$\ddot{x} + \delta\dot{x} - x + x^3 = M \cos(\omega t) \quad (5.1)$$

where δ is the damping of the system which is greater than or equal to zero, and M is the amplitude of the driving signal. In state-space representation, we have

$$\begin{aligned} \frac{d}{dt}x &= y \\ \frac{d}{dt}y &= x - x^3 - \delta y + M \cos(\omega t). \end{aligned} \quad (5.2)$$

Without input, $M = 0$, there are three fixed points for these coupled differential equations, namely, $\{0, 0\}$, $\{-1, 0\}$, and $\{1, 0\}$. With a simple calculation, we can show $\{0, 0\}$ is an unstable fixed point while the other two equilibria are stable.

5.2 Time Simulations for the Duffing Oscillator

To understand the dynamics of the Duffing oscillator, first we simulate the system dynamics for two different initial conditions. For the first case, we choose the following system parameters: $\omega = 1.0$, $M = 0.3$, and $\delta = 0.15$ with an initial condition of $\{1 \ 1.45\}$. Figure 5.2 depicts the steady-state response of the displacement and the velocity of the system.

For given these parameters and the initial condition $\{1 \ 1.45\}$, the system has a large amplitude period-one steady-state response. Figure 5.2 depicts the phase plan plot for the position and the velocity of the response.

For the next case, the system parameters $\omega = 1.0$, $M = 0.3$, and $\delta = 0.22$ with an initial condition of $[1 \ 0.725]^T$ are chosen. The steady-state response of the displacement and the velocity of the system is depicted in Fig. 5.3. In this case, the steady-state of the system has a period of $3T$ where T is the period of the driving signal.

Based on these observations, we will study the system dynamics, particularly the stability of these steady-state responses. First, we employ the generalized state-space averaging (GSSA) method by computing approximated steady-state solutions of the system,

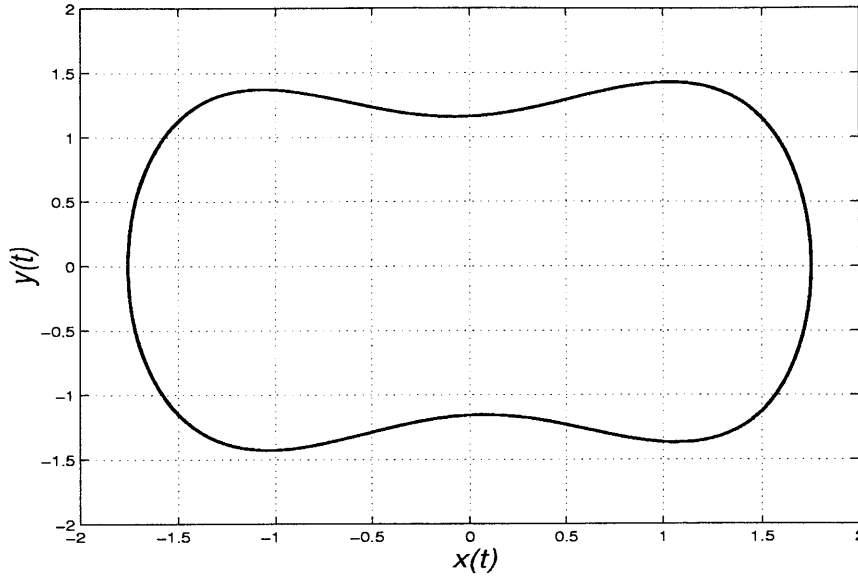


Figure 5.2: Duffing oscillator: Harmonic steady-state response

and then we will examine the stability of the steady-state solution. Next, the methods of Floquet and Poincaré are used to examine the stability of the steady-state solutions.

5.3 Generalized State-Space Averaging Method

Using the GSSA technique, we compute the model of the system and study both harmonic and subharmonic steady-state responses. First, the harmonic steady-state solutions for $\omega = 1$, $M = 0.3$ and $\delta = 0.15$ or $\delta = 0.22$ are computed. Since we know that for $\delta = 0.22$ the system has a period-three steady-state response, we will develop a subharmonic model using the generalized state-space averaging method.

5.3.1 Harmonic Solutions for Duffing Oscillator

Applying the GSSA method to the system (5.2), we obtain the following equations

$$\frac{d}{dt}X_k(t) = -jk\omega X_k(t) + Y_k(t), \quad \text{where } -\infty < k < \infty \quad (5.3a)$$

$$\frac{d}{dt}Y_k(t) = X_k(t) - F_k(X_k) - (\delta + jk\omega)Y_k(t) + G_k \quad (5.3b)$$

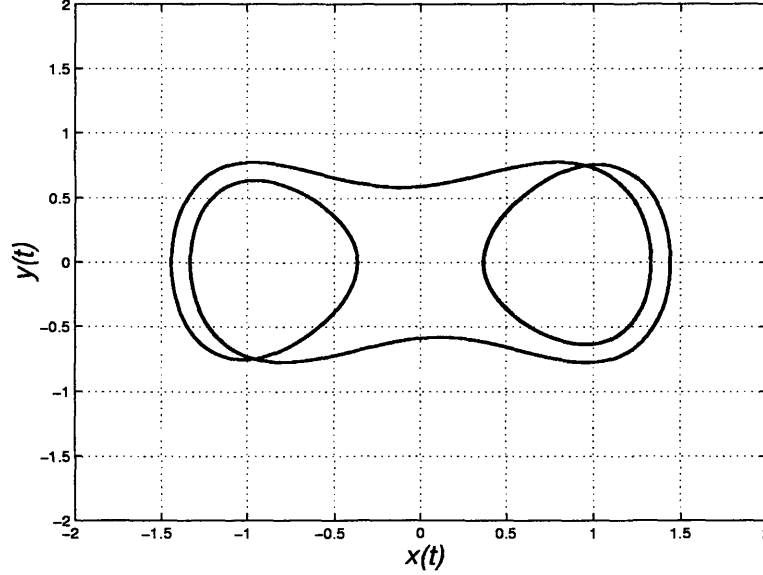


Figure 5.3: Duffing oscillator: Subharmonic steady-state response

where F_k and G_k are defined as

$$\begin{aligned}
 F_k(X_k) &= \sum_{m_1} \sum_{m_2} \sum_{m_3} X_{m_1} X_{m_2} X_{\{k-m_3-m_2-m_3\}} \quad -\infty \leq k \leq \infty \\
 G_k &= \begin{cases} \frac{M}{2} & \text{for } k = \pm 1 \\ 0 & \text{for } k \neq \pm 1 \end{cases} \quad (5.4)
 \end{aligned}$$

For each given ω , δ , and k , there is a corresponding steady-state solution for the system.

For $\omega = 1$, $M = 0.3$ and $\delta = 0.15$, we study the effect of truncation at levels of k equal to 7, 11, 17, and 25. These levels of truncation give us insight into how the approximated solution improves; the higher the truncation level, the higher the refinement of the solution. Figure 5.4 depicts the steady-state solution of the system. Invoking Theorem 4.1, we can compute the stability of the steady-state solution. Figure 5.5 depicts the eigenvalues of the system. The fundamental eigenvalues of the system at this operating point are $\mu_{1,2} = -0.0750 \pm j0.2115$. Since the real parts of the fundamental eigenvalues are negative, this steady-state solution is a stable operating point. Furthermore, since the order of the full system is two, we expect that there are two fundamental eigenvalues. Recall that ideally the other eigenvalues are related to the fundamental eigenvalues by $\pm k\omega$. The dispersed

eigenvalues in the Fig. 5.4 are due to the truncation.

At this truncation level, the steady-state solution of the system (5.2) takes the following form

$$\bar{x}(t) = X_0 + 2 \sum_{k=-7}^{k=7} X_k^R \cos(kt) - X_k^I \sin(kt). \quad (5.5)$$

where X_k^R and X_k^I are the real and the imaginary parties of X_k .

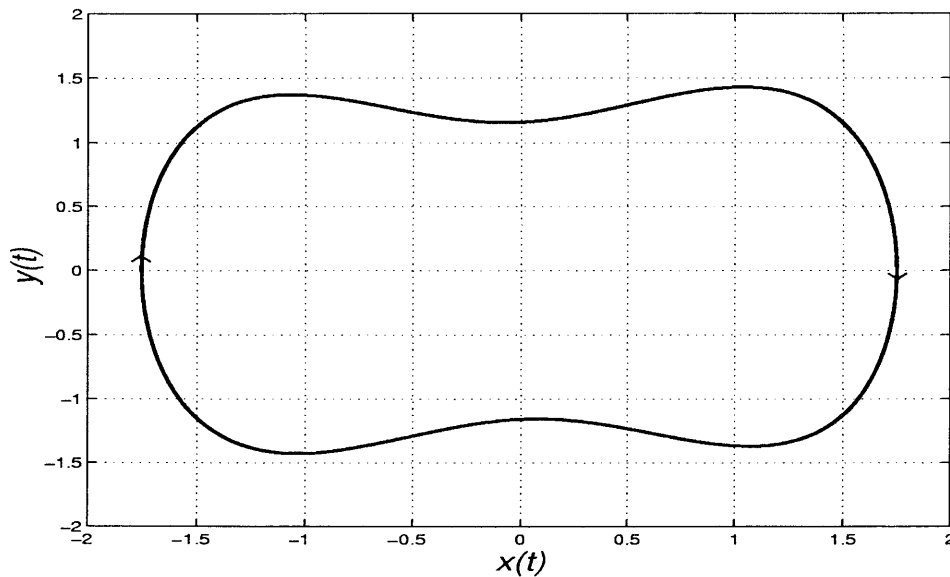


Figure 5.4: Approximated harmonic solutions: $k = \pm 7$ and $\delta = 0.15$

To improve the refinement of the steady-state solution, we need to increase the level of truncation. Figures 5.6 and 5.7 depict the steady-state solution and the corresponding eigenvalues for $k = \pm 11$. Increased refinements are shown in Figs. 5.8 to 5.11 which show the steady-state and corresponding eigenvalues for truncation levels of $k = \pm 17$ and $k = \pm 25$, respectively.

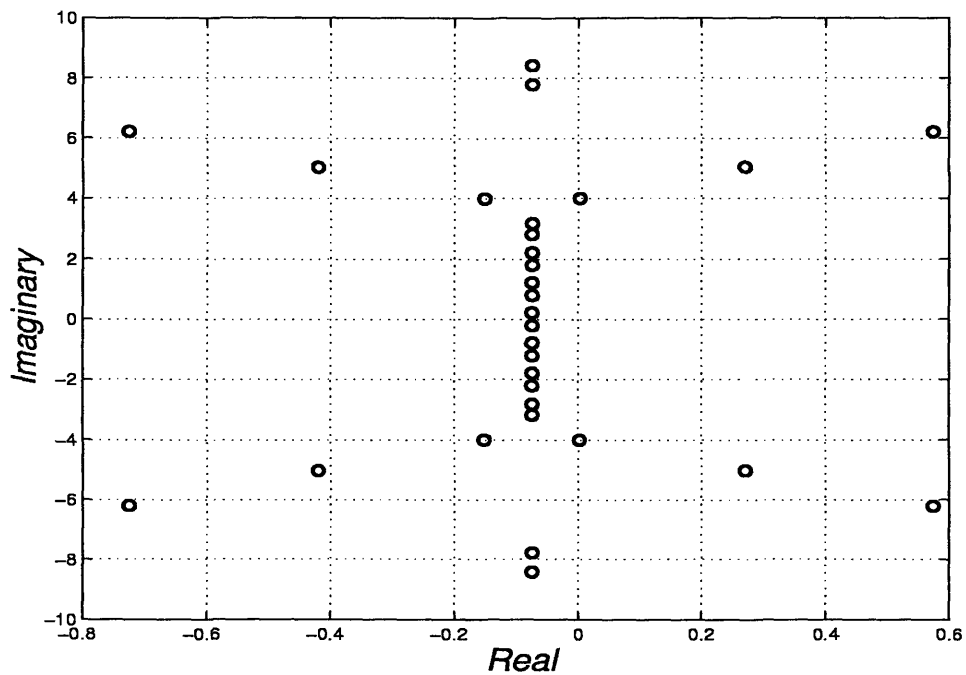


Figure 5.5: Eigenvalues of the approximated harmonic system: $k = \pm 7$ and $\delta = 0.15$

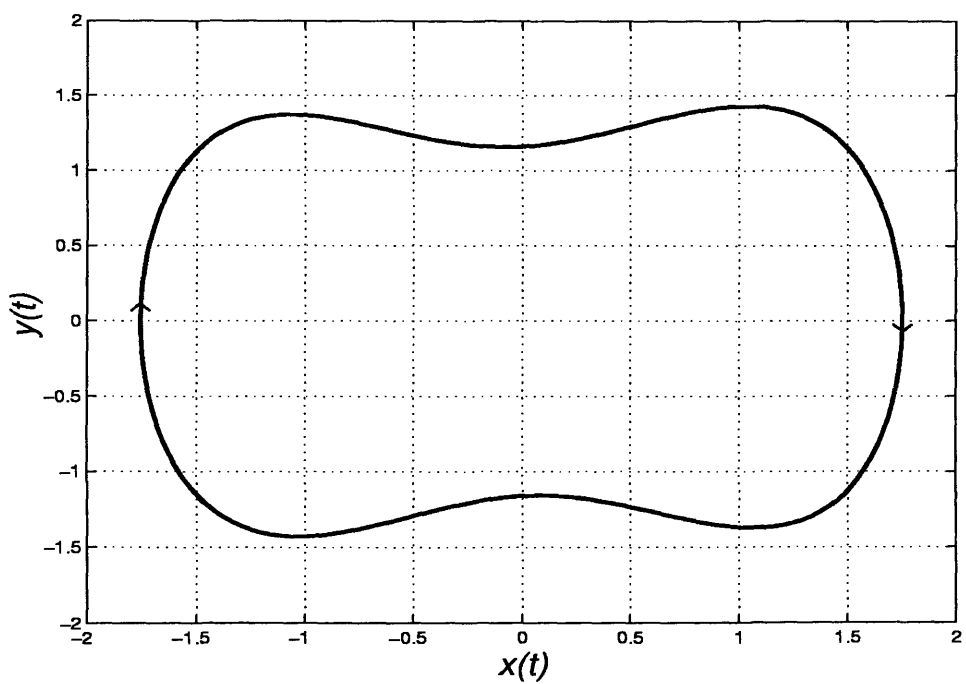


Figure 5.6: Approximated harmonic solutions: $k = \pm 11$ and $\delta = 0.15$

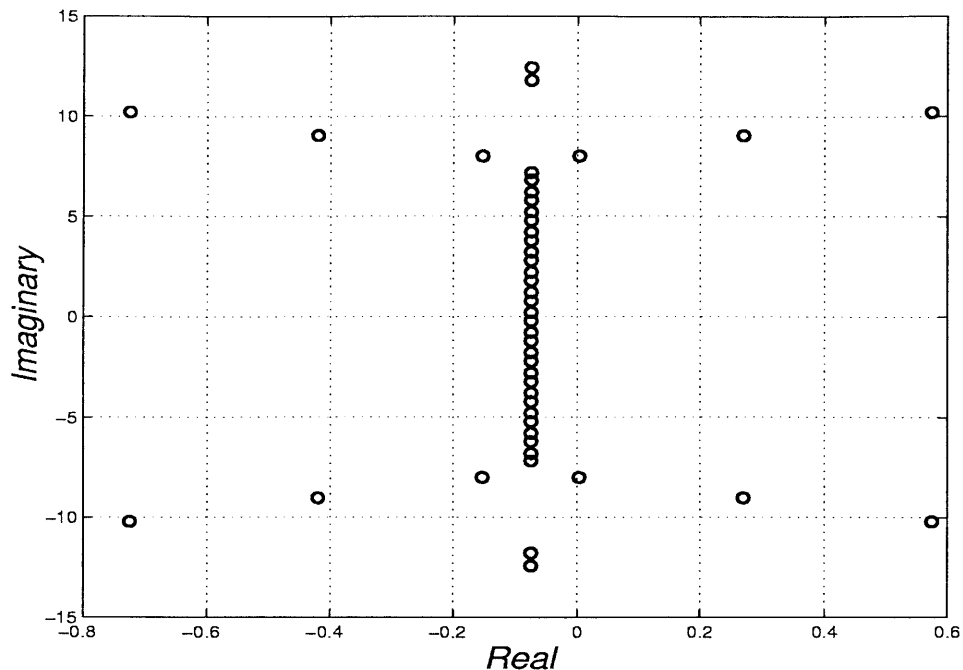


Figure 5.7: Eigenvalues of the approximated harmonic system: $k = \pm 11$ and $\delta = 0.15$

For the second set of simulations, we choose the following parameters: $\delta = 0.22$, $M = 0.3$, and $\omega = 1$. Although the full system simulations show for these parameters a stable subharmonic response, we will here study harmonic responses and their stability. We examine the subharmonic responses in the next section.

Similar steps are taken to approximate the steady-state solutions. Figures 5.12 and 5.13 depict the steady-state harmonic solution and the corresponding eigenvalues for $k = \pm 7$. The fundamental eigenvalues of the system are $\mu_1 = 0.8790$ and $\mu_2 = -1.0990$. Since μ_1 is greater than zero, this operating point is an unstable fixed point. Similarly, Figs. 5.14 to 5.19 show more refined steady-state solutions and the corresponding eigenvalues.

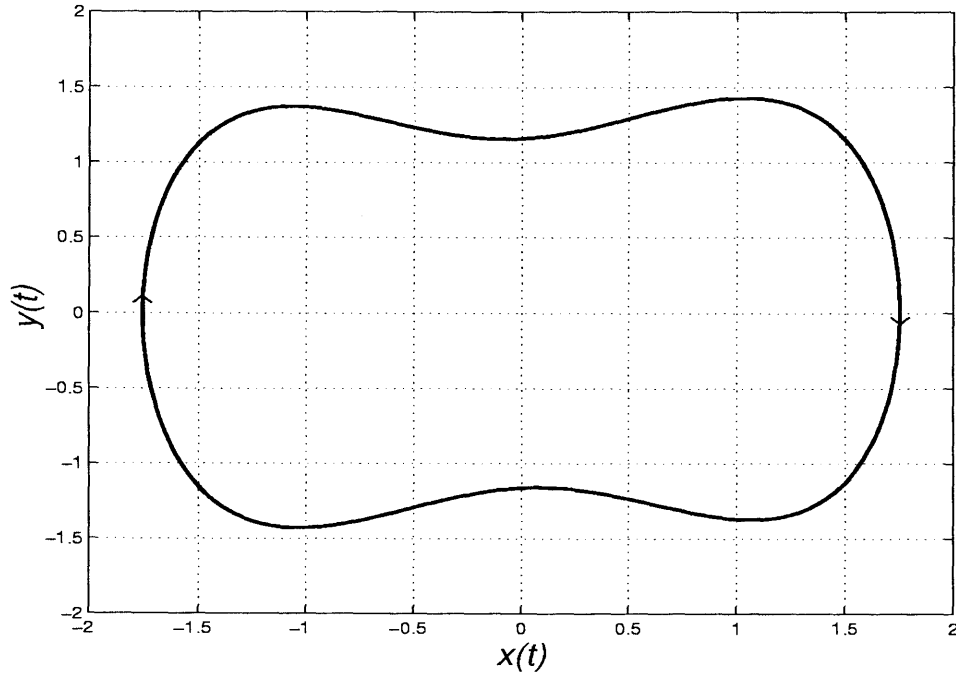


Figure 5.8: Approximated harmonic solutions: $k = \pm 17$ and $\delta = 0.15$

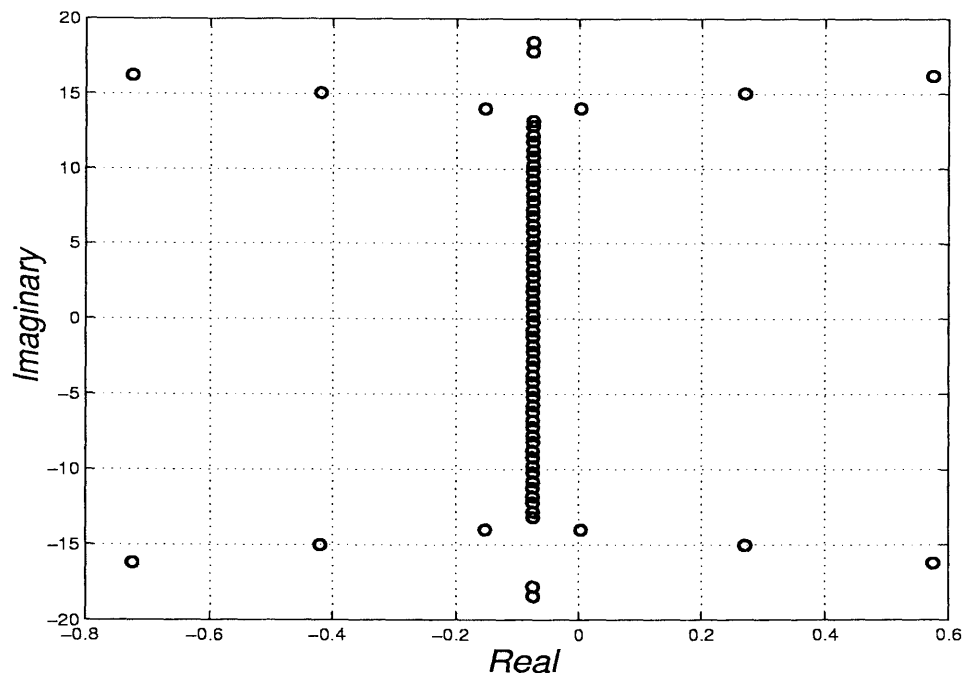


Figure 5.9: Eigenvalues of the approximated harmonic system: $k = \pm 17$ and $\delta = 0.15$

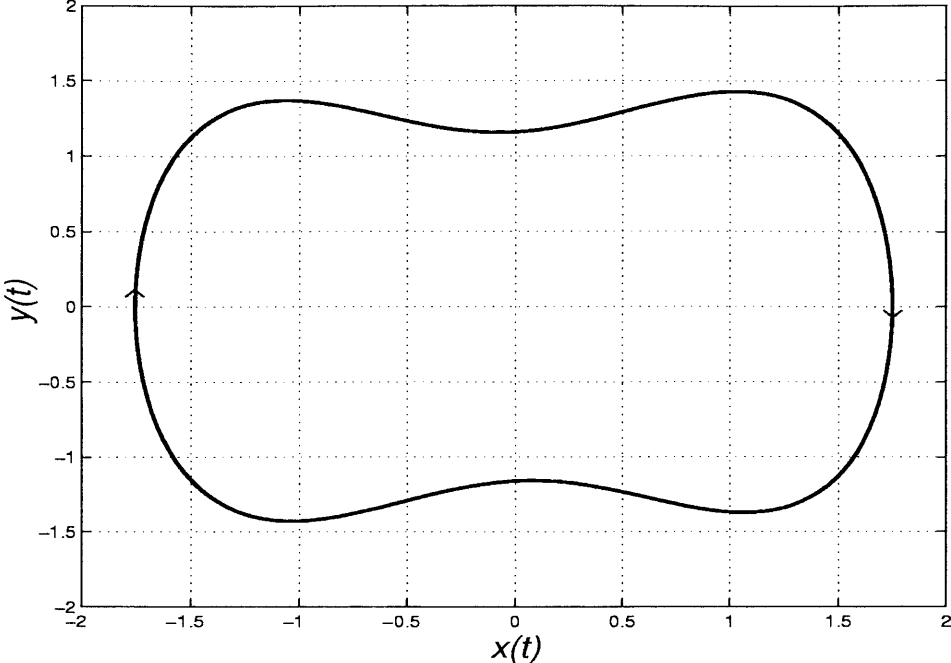


Figure 5.10: Approximated harmonic solutions: $k = \pm 25$ and $\delta = 0.15$

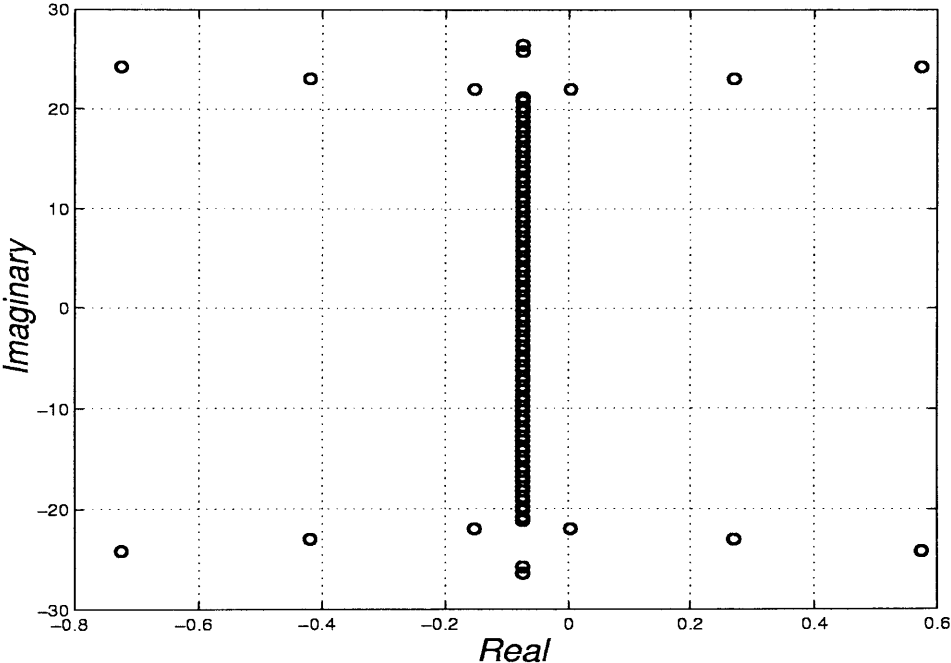
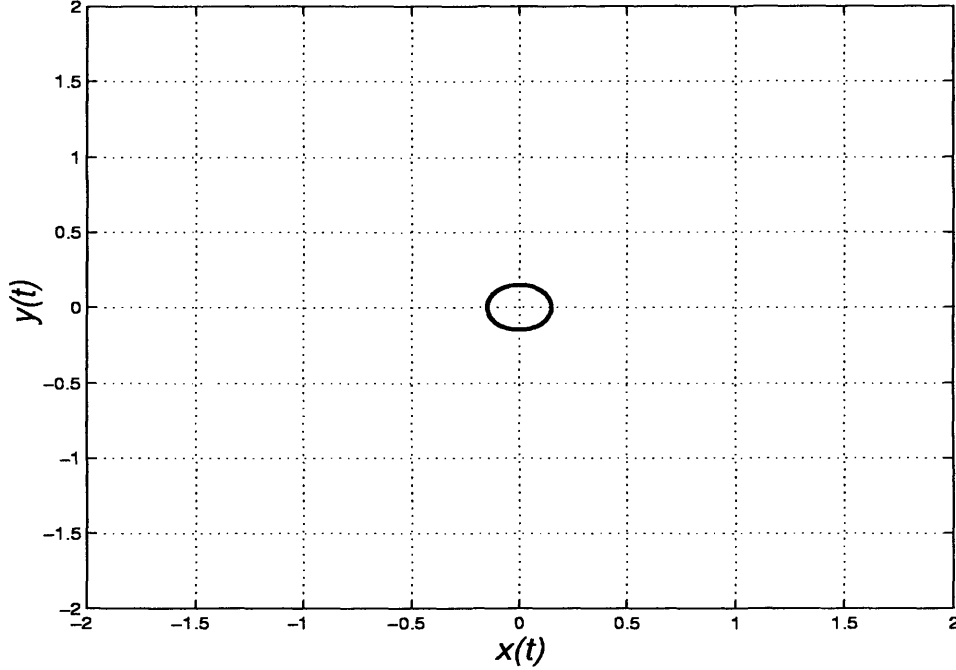


Figure 5.11: Eigenvalues of the approximated harmonic system: $k = \pm 25$ and $\delta = 0.15$

Figure 5.12: Approximated harmonic solutions: $k = \pm 7$ and $\delta = 0.22$

5.3.2 Subharmonic Solutions for Duffing Oscillator

Applying the GSSA method to the system (5.2) to formulate the subharmonic steady-state solution, we have the following

$$\frac{d}{dt}X_{k\frac{\omega}{n}}(t) = -jk\frac{\omega}{n}X_{k\frac{\omega}{n}}(t) + Y_{k\frac{\omega}{n}}(t), \quad \text{where } -\infty < k < \infty \quad (5.6a)$$

$$\frac{d}{dt}Y_{k\frac{\omega}{n}}(t) = X_{k\frac{\omega}{n}}(t) - F_{k\frac{\omega}{n}}(X_{k\frac{\omega}{n}}) - \left(\delta + jk\frac{\omega}{n}\right)Y_{k\frac{\omega}{n}}(t) + G_k. \quad (5.6b)$$

where $F_{k\frac{\omega}{n}}$ and $G_{k\frac{\omega}{n}}$ are defined as

$$F_k(X_{k\frac{\omega}{n}}) = \sum_{m_1} \sum_{m_2} \sum_{m_3} X_{m_1\frac{\omega}{n}} X_{m_2\frac{\omega}{n}} X_{[k-m_3-m_2-m_3]\frac{\omega}{n}} \quad -\infty \leq k \leq \infty$$

$$G_{k\frac{\omega}{n}} = \begin{cases} \frac{M}{2} & \text{for } k\frac{\omega}{n} = \pm 1 \\ 0 & \text{for } k\frac{\omega}{n} \neq \pm 1 \end{cases} \quad (5.7)$$

For each given ω , δ , k and n , there is a corresponding steady-state solution of the

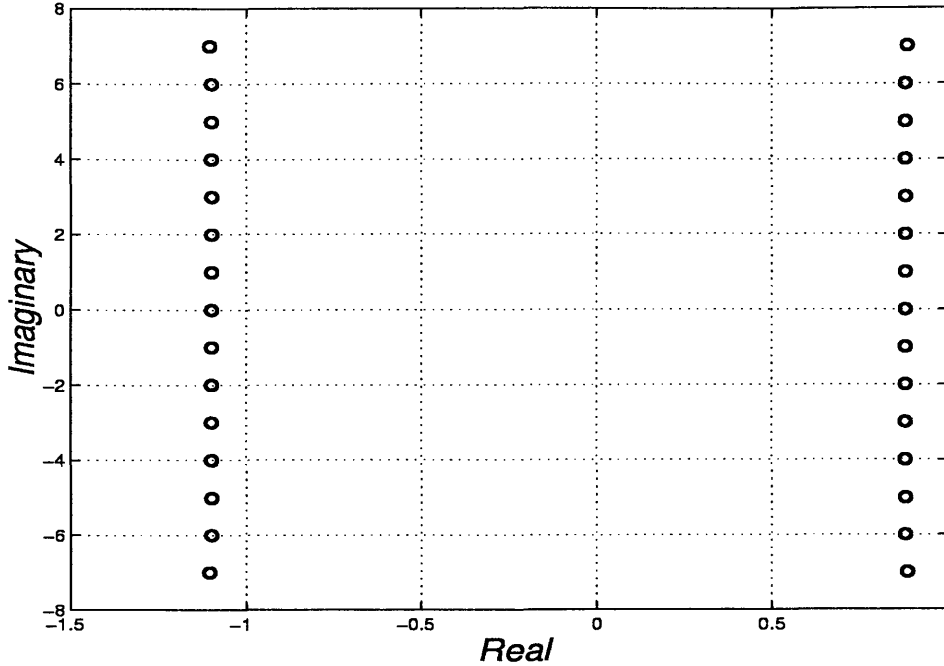


Figure 5.13: Eigenvalues of the approximated harmonic system: $k = \pm 7$ and $\delta = 0.22$

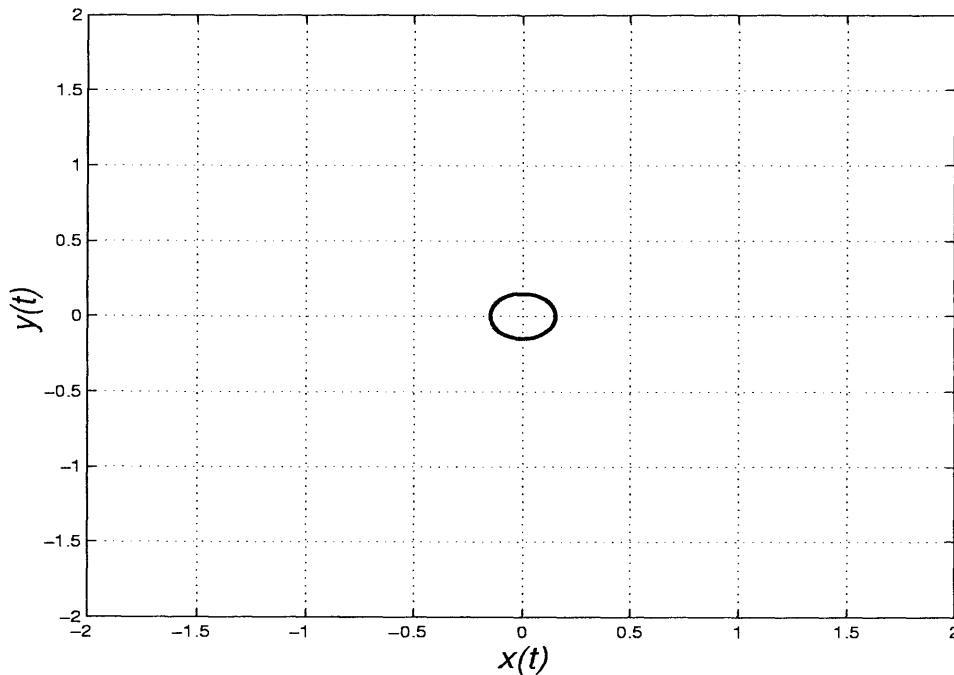
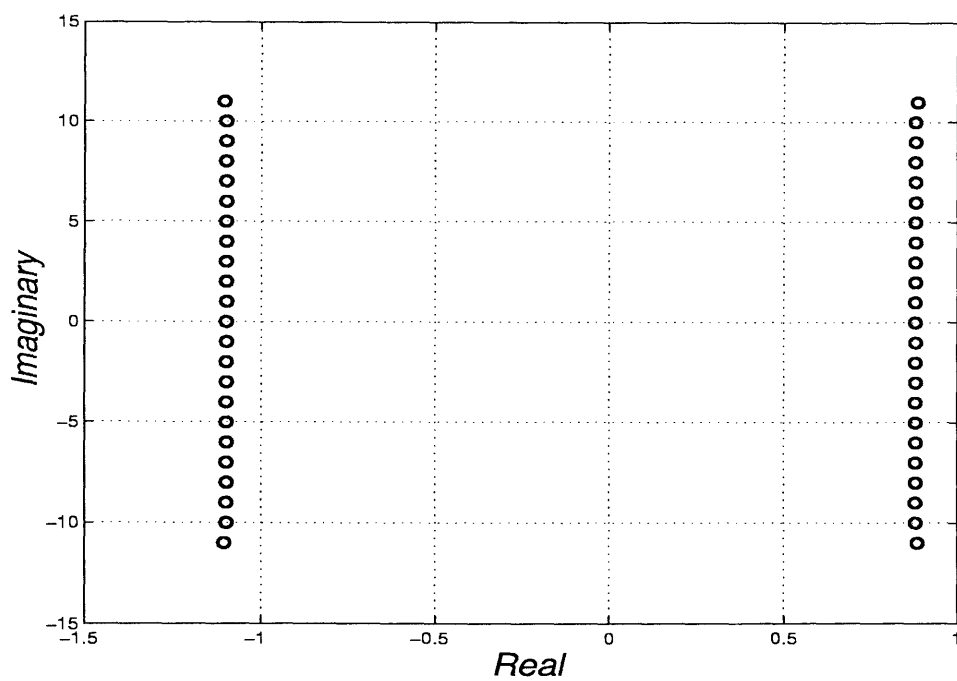
system.

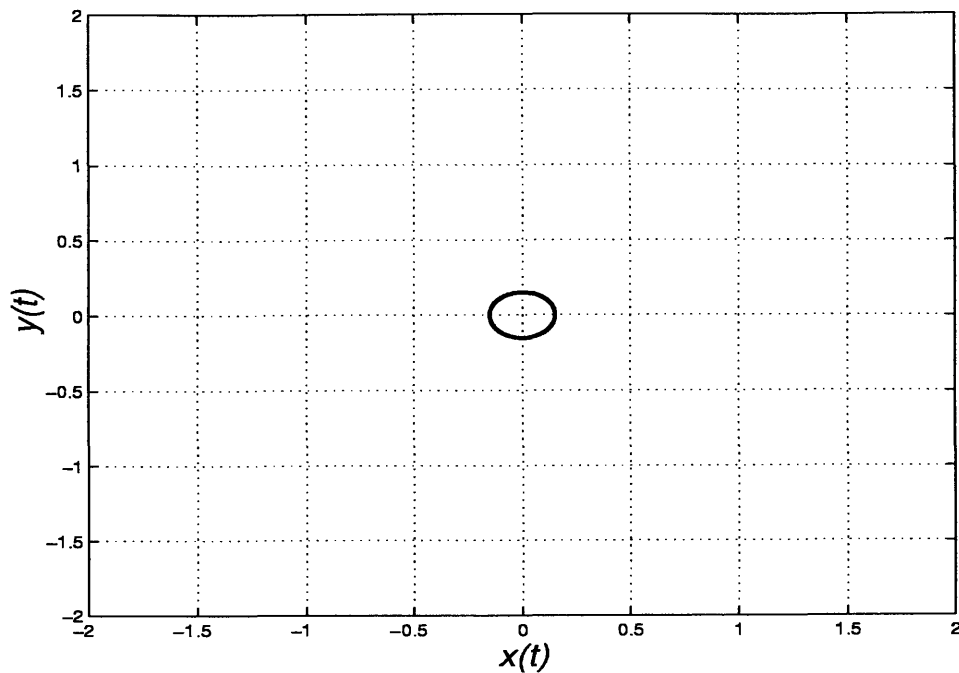
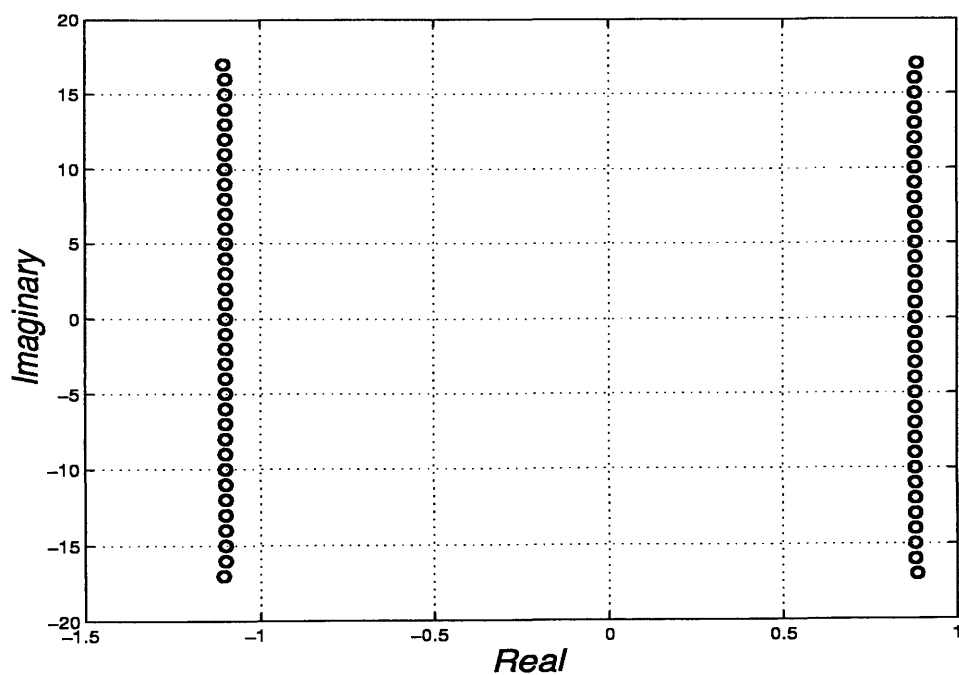
We obtain the same truncation levels as for the harmonic cases. We consider $\frac{1}{3}$ subharmonic responses for $\delta = 0.22$, $M = 0.3$ and $\omega = 1$. Figures 5.20 and 5.21 show the steady-state solution and the corresponding eigenvalues of the system with truncation level of $k = \pm 7$.

The fundamental eigenvalues of this operating point are $\mu_{1,2} = -0.1100 \pm j0.1295$. Since the real parts of the eigenvalues are less than zero, this operating point is a stable fixed point. In this case the approximated steady-state solution takes the following form

$$\bar{x}_{\frac{1}{3}}(t) = X_0 + 2 \sum_{k=-7}^{k=7} X_{\frac{k}{3}}^R \cos\left(\frac{k}{3}t\right) - X_{\frac{k}{3}}^I \sin\left(\frac{k}{3}t\right) \quad (5.8)$$

For further refinements of the approximated solution, Figures 5.22 to 5.27 depict the steady-state subharmonic solutions and the corresponding eigenvalues.

Figure 5.14: Approximated harmonic solutions: $k = \pm 11$ and $\delta = 0.22$ Figure 5.15: Eigenvalues of the approximated harmonic system: $k = \pm 11$ $\delta = 0.22$

Figure 5.16: Approximated harmonic solutions: $k = \pm 17$ and $\delta = 0.22$ Figure 5.17: Eigenvalues of the approximated harmonic system: $k = \pm 17$ $\delta = 0.22$

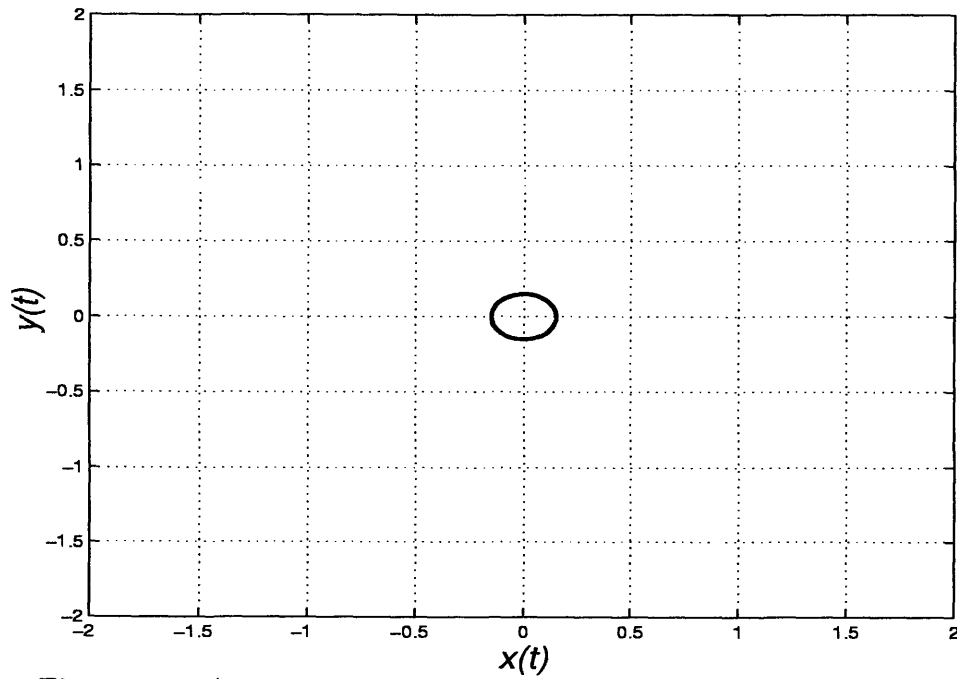


Figure 5.18: Approximated harmonic solutions: $k = \pm 25$ and $\delta = 0.22$

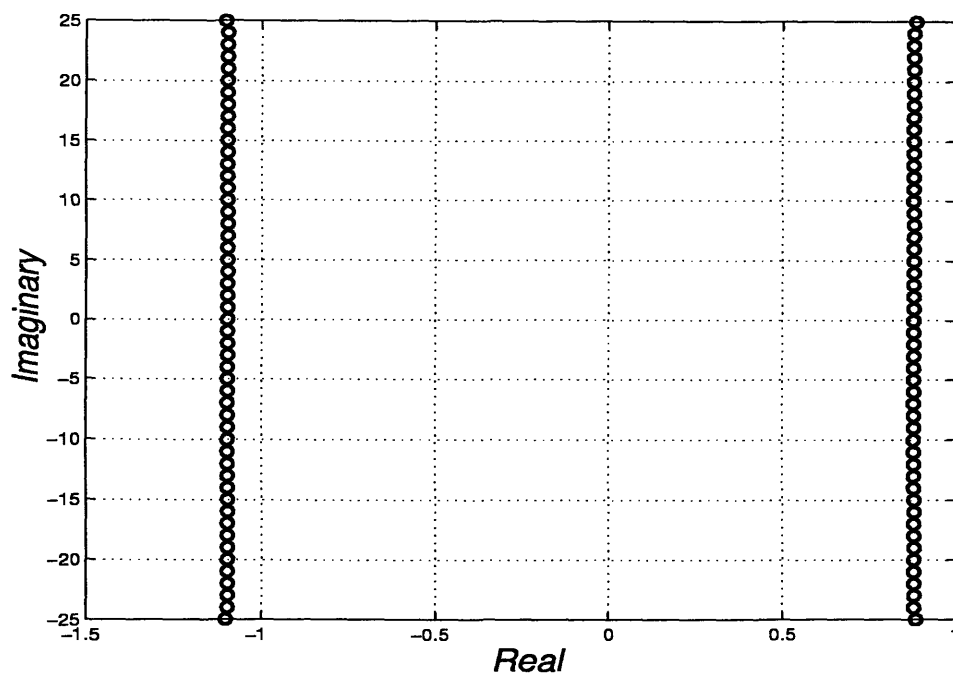
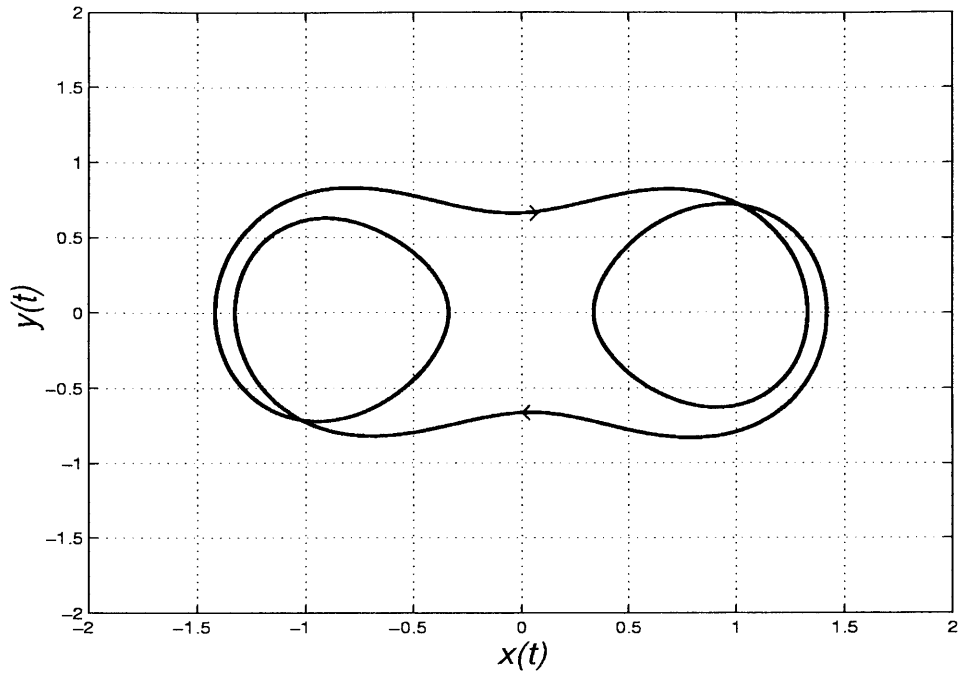
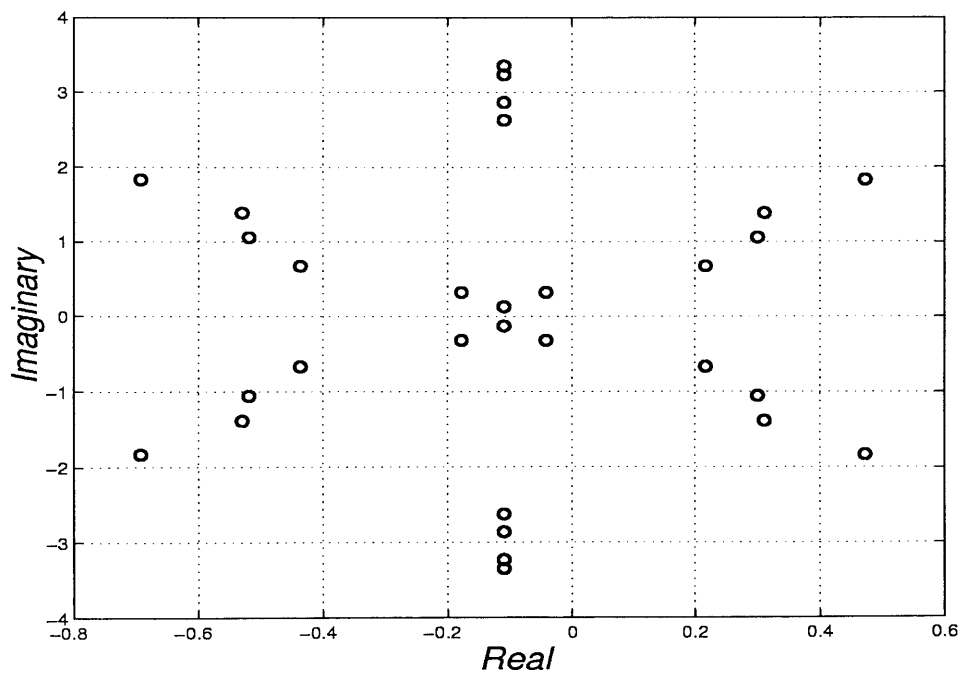
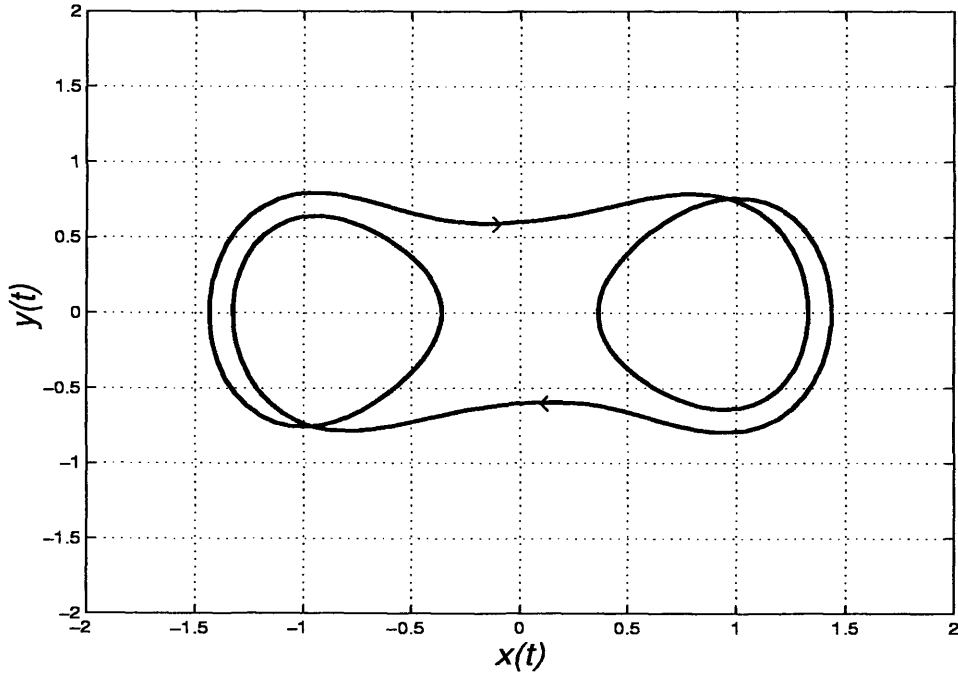
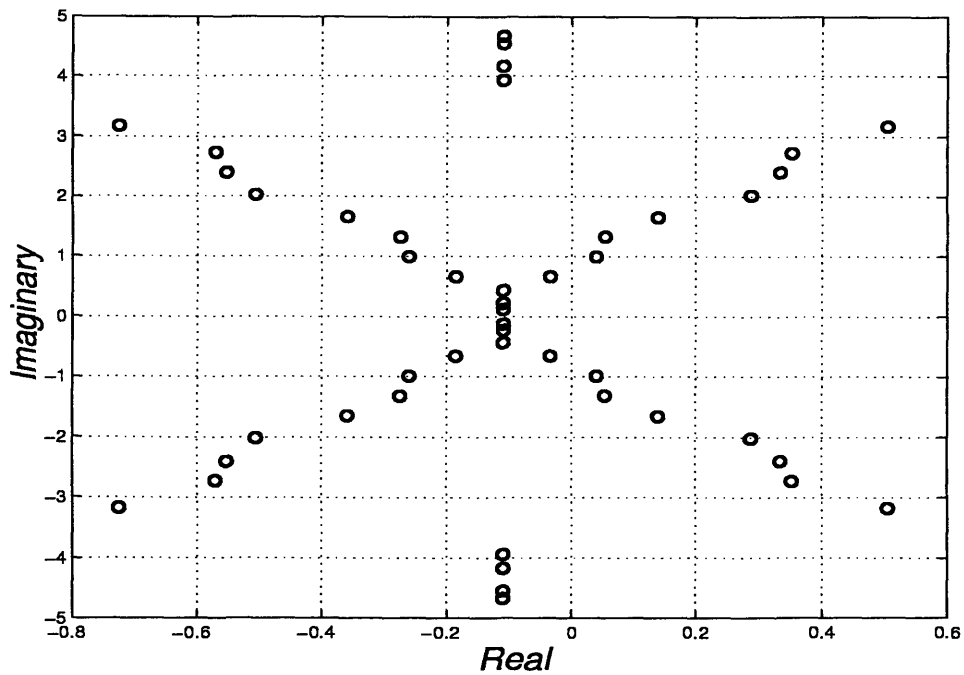


Figure 5.19: Eigenvalues of the approximated harmonic system: $k = \pm 25$ $\delta = 0.22$

Figure 5.20: Approximated Subharmonic solutions: $k = \pm 7$ and $\delta = 0.22$ Figure 5.21: Eigenvalues of the approximated subharmonic system: $k = \pm 7$

Figure 5.22: Approximated Subharmonic solutions: $k = \pm 11$ and $\delta = 0.22$ Figure 5.23: Eigenvalues of the approximated subharmonic system: $k = \pm 11$

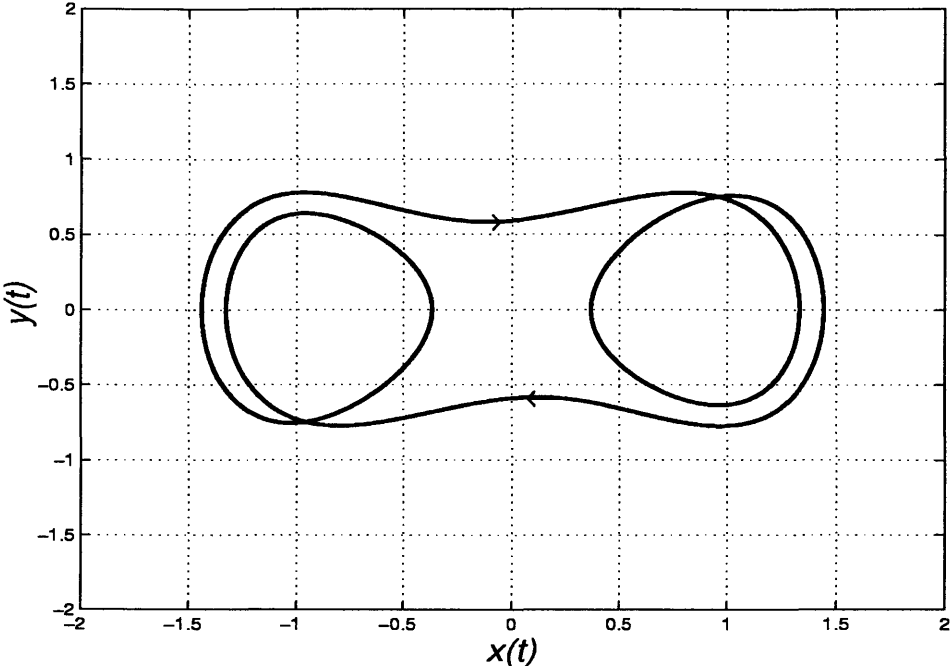


Figure 5.24: Approximated Subharmonic solutions: $k = \pm 17$ and $\delta = 0.22$

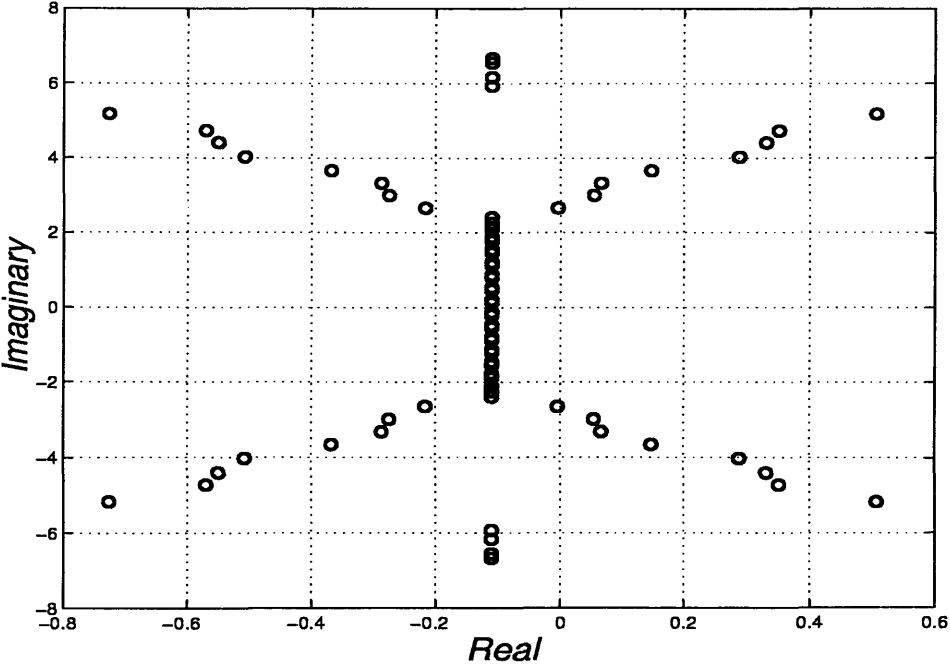
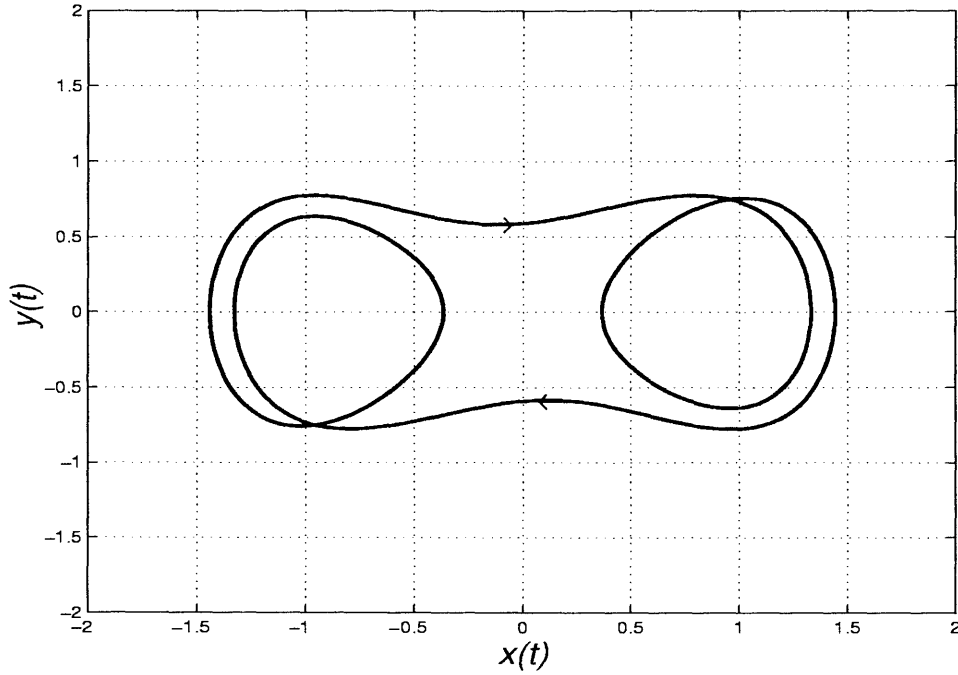
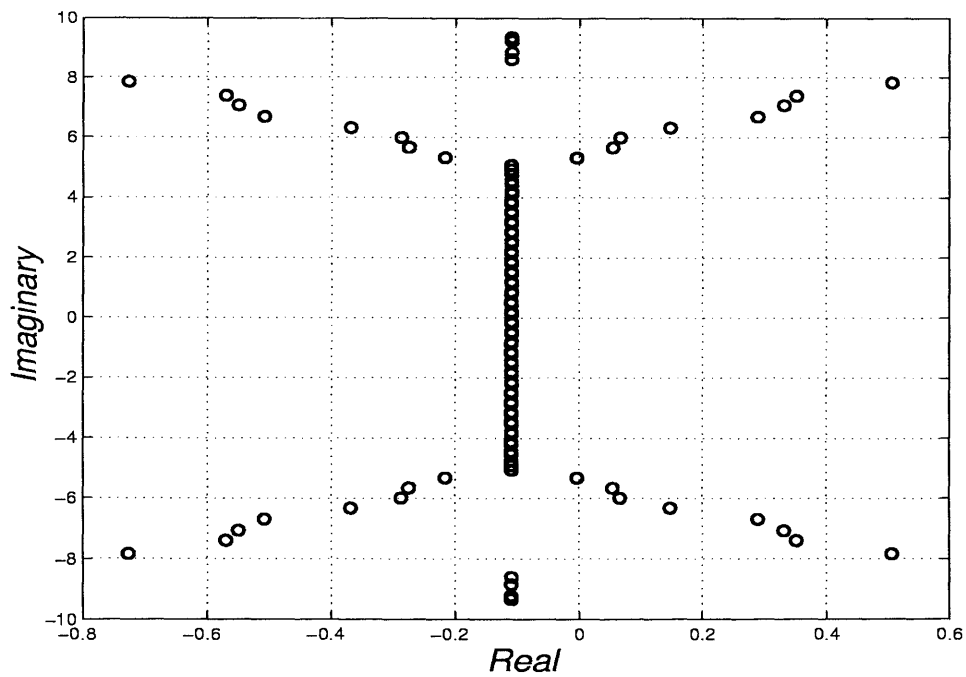


Figure 5.25: Eigenvalues of the approximated subharmonic system: $k = \pm 17$

Figure 5.26: Approximated Subharmonic solutions: $k = \pm 25$ and $\delta = 0.22$ Figure 5.27: Eigenvalues of the approximated subharmonic system: $k = \pm 25$

5.4 Floquet Theory

The Floquet machinery can be used to analyze the stability of linear time-variant systems. The theory will not be proven here, but we give some applications and point out the underlying assumptions. For further reading on Floquet theory see [52,73,74,55,75,69,76].

Given the system

$$\frac{dx}{dt} = A(t, p)x, \quad \text{with} \quad A(t + T, p) = A(t, p) \quad (5.9)$$

where $x \in \mathbb{R}^{n \times 1}$ are state variables, $A(x, p) \in \mathbb{R}^{n \times n}$ is the system matrix, and $p \in \mathbb{R}^{m \times 1}$ are system parameters.

The fundamental solution set of (5.9) is given by the set $\{x_1(t), x_2(t), \dots, x_n(t)\}$. Then the fundamental matrix solution of (5.9) can be formulated as

$$\Phi(t) = \begin{bmatrix} x_1(t) & x_2(t) & \dots & x_n(t) \end{bmatrix} \quad (5.10)$$

where $\Phi \in \mathbb{R}^{n \times n}$ is a matrix. Since $\{x_1(t), x_2(t), \dots, x_n(t)\}$ are fundamental solutions of (5.9), this implies that

$$\frac{d\Phi(t)}{dt} = A(t, p)\Phi(t). \quad (5.11)$$

Using the following transformation $t = \tau + T$, we can write equation (5.9) as

$$\begin{aligned} \frac{dx(\tau + T)}{d\tau} &= A(\tau + T, p)x(\tau + T) \\ &= A(\tau, p)x(\tau + T), \quad \text{since} \quad A(\tau + T, p) = A(\tau, p). \end{aligned} \quad (5.12)$$

The fundamental solution set of (5.12) is given by $\{x_1(t + T), x_2(t + T), \dots, x_n(t + T)\}$. For this fundamental solution set, there exists another fundamental solution matrix of (5.9) which is given by

$$\begin{bmatrix} x_1(t + T) & x_2(t + T) & \dots & x_n(t + T) \end{bmatrix} \quad (5.13)$$

The fundamental matrix satisfies the differential equation (5.9) which yields

$$\frac{d\Phi(t + T)}{dt} = A(t, p)\Phi(t + T). \quad (5.14)$$

Since (5.10) and (5.13) are fundamental matrices of the system, the following equation must hold,

$$\Phi(t + T) = \Phi(t)\Psi. \quad (5.15)$$

Equation (5.15) says that $\Phi(t + T)$ is a linear combination of $\Phi(t)$, where Ψ is an $n \times n$ constant matrix. Since equation (5.15) holds for all time t , then for one cycle

$$\Phi(T) = \Phi(0)\Psi. \quad (5.16)$$

The matrix Ψ is referred to as the *monodromy* matrix. Define

$$\Phi(t) = V(t)P^{-1} \quad (5.17)$$

where P^{-1} is an $n \times n$ constant matrix. Then using a simple transformation of variables, we obtain

$$\Phi(t + T) = V(t + T)P^{-1} \quad (5.18a)$$

$$\Phi(t)\Psi = V(t + T)P^{-1} \quad (5.18b)$$

$$V(t)P^{-1}\Psi = V(t + T)P^{-1} \quad (5.18c)$$

$$V(t + T) = V(t)J, \quad \text{where } J = P^{-1}\Psi P. \quad (5.18d)$$

If Ψ has independent eigenvectors, then J is a diagonal matrix with diagonal elements μ_m , where μ_m are the eigenvalues of Ψ . Since J is a diagonal matrix, (5.18d) can be written element wise

$$v_m(t + T) = \mu_m v_m(t). \quad (5.19)$$

Furthermore,

$$v_m(t + NT) = \mu_m^N v_m(t). \quad (5.20)$$

where the μ_m are known as characteristic multipliers or Floquet multipliers.

From (5.20), it is clear that as $t \rightarrow \infty$ or $N \rightarrow \infty$,

$$\begin{aligned} v_m(t) &\rightarrow 0 && \text{if } |\mu_m| < 1 \\ v_m(t) &\rightarrow \infty && \text{if } |\mu_m| > 1. \end{aligned} \quad (5.21)$$

If the system has a periodic steady-state solution, there is always one eigenvalue that has magnitude equal to one. The Floquet exponent, or characteristic exponent, ρ_m is defined as

$$\mu_m = e^{\rho_m T} \quad \text{or} \quad \rho_m = \frac{1}{T} \ln(\mu_m). \quad (5.22)$$

Hence, if the real part of ρ_m is less than zero, the steady-state solution of the system is stable. If the real part of ρ_m is greater than zero, then the steady-state solution is unstable.

In this analysis, the system is linear with periodic coefficients. Suppose the system is nonlinear, then we need first to find a steady-state solution of the nonlinear system using harmonic balancing or integrating the differential equation using computer simulations. If the nonlinear system is linearized around this periodic steady-state solution, the variational system will take the form as defined in (5.9) to which we can apply Floquet theory to assess the stability of the steady-state solution.

5.4.1 Application of Floquet Theory to Duffing Oscillator

Consider the following nonlinear dynamical system.

$$\frac{dx}{dt} = f(x, p, t) \quad (5.23)$$

where $x(t) \in \mathbb{R}^{n \times 1}$ is a state vector, $f(x, p, t) \in \mathbb{R}^{n \times 1}$ is a nonlinear vector field, and p are system parameters.

Suppose (5.23) has a periodic steady-state solution $\bar{x}(t)$ with period T . Then to examine the stability of this steady-state solution, we employ the Floquet machinery.

Here we outline the steps to invoke the Floquet analysis to assess the stability of a nonlinear system with a periodic steady-state solution.

- Given a nonlinear system with steady-state periodic solutions: compute the steady-state solution $\bar{x}(t)$ by any method, such as harmonic balance, perturbation method, or by simulating the system dynamics.
- Linearize the system around this operating point $\bar{x}(t)$.
- Compute n linearly independent solutions of the linearized system $[x_1(t), x_2(t), \dots, x_n(t)]$ in one cycle where the length of the cycle is equal to T , given that the system matrix

has a period of T .

- Form the fundamental matrix solution of the system $\Phi(T)$, where $\Phi(T) \in \mathbb{R}^{n \times n}$.
- Compute the monodromy matrix Ψ using the relationship defined in (5.16) and $\Phi(0)$, which depend, on the initial conditions of the state variables.
- Compute the eigenvalues of Ψ , i.e., $\{\mu_m\}$.
 1. If for some m , $|\mu_m| > 1$, then the solution $\bar{x}(t)$ is an unstable solution.
 2. If all $|\mu_m| < 1$ except one equal to 1, then $\bar{x}(t)$ is a stable solution.
 3. If more than one eigenvalue is equal to 1, then we need to perform a nonlinear analysis to examine the stability of the system, such as using the center manifold theory.
 4. Compute the Floquet exponents ρ_m using the relationship defined in (5.22) if needed.

Now we use the Floquet theory to ascertain the stability of the steady-state solutions of the Duffing oscillator that were computed earlier using the generalized state-space averaging method. Since we approximated the steady-state solutions at four truncation levels, we will study each case in order to gain insight into the variations of the Floquet multipliers. The Floquet exponents are compared to the fundamental eigenvalues of the generalized state-space averaging method. Since the system response for different parameters can be either harmonic or subharmonic periodic solutions, first we will investigate the stability of the harmonic periodic solutions.

5.4.1.1 Harmonic Solutions of Duffing Oscillator

Choosing the following system parameters $\omega = 1$, $\delta = 0.15$ and $M = 0.3$, the steady-state periodic solution of the system takes the following form

$$\bar{x}(t) = X_0 + 2 \sum_{k=-q}^{k=q} X_k^R \cos(kt) - X_k^I \sin(kt) \quad (5.24)$$

where q is the truncation level which takes the values 7, 11, 17, and 25. X_k^R and X_k^I are the real and the imaginary parts of X_k .

Linearizing the system defined in (5.2) around the operating point $\bar{x}(t)$, the variational system is given by

$$\begin{aligned}\frac{d\tilde{x}_1}{dt} &= \tilde{x}_2 \\ \frac{d\tilde{x}_2}{dt} &= -\delta\tilde{x}_2 + \tilde{x}_1 - 3\bar{x}^2\tilde{x}_1\end{aligned}\quad (5.25)$$

where $\tilde{x}(t)$ is the perturbation around the equilibrium point. Therefore, if the variational system is stable; then the dynamics of $\tilde{x}(t)$ go to zero in the steady-state, and the steady-state periodic solution $\bar{x}(t)$ is a stable operating point. The system matrix of the variational system is given by

$$A = \begin{bmatrix} 0 & 1 \\ 1 - 3\bar{x}^2(t) & -\delta \end{bmatrix}. \quad (5.26)$$

The system matrix is periodic in time with a period of $\frac{T}{2}$, where T is the period of the forcing function. In order to compute Ψ , first, we need to calculate $\tilde{\Psi}$. Then, Ψ yields

$$\Psi = \tilde{\Psi}^2 \quad \text{where} \quad \tilde{\Phi}\left(t + \frac{T}{2}\right) = \tilde{\Phi}(t)\tilde{\Psi}. \quad (5.27)$$

Hence, to compute the eigenvalues of Ψ , we need to compute the eigenvalues of $\tilde{\Psi}$, which are

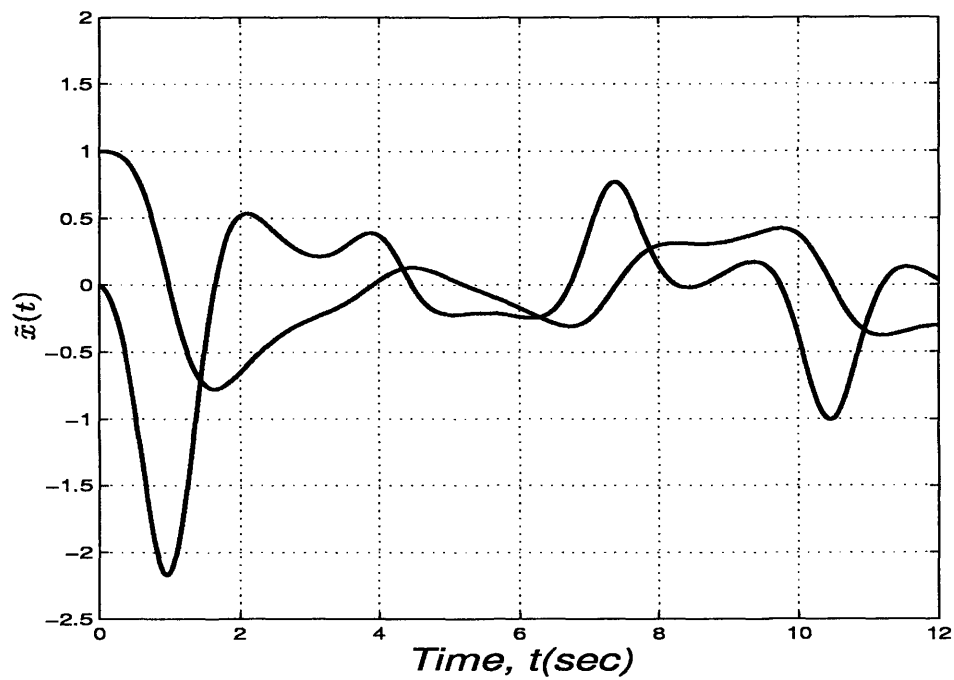
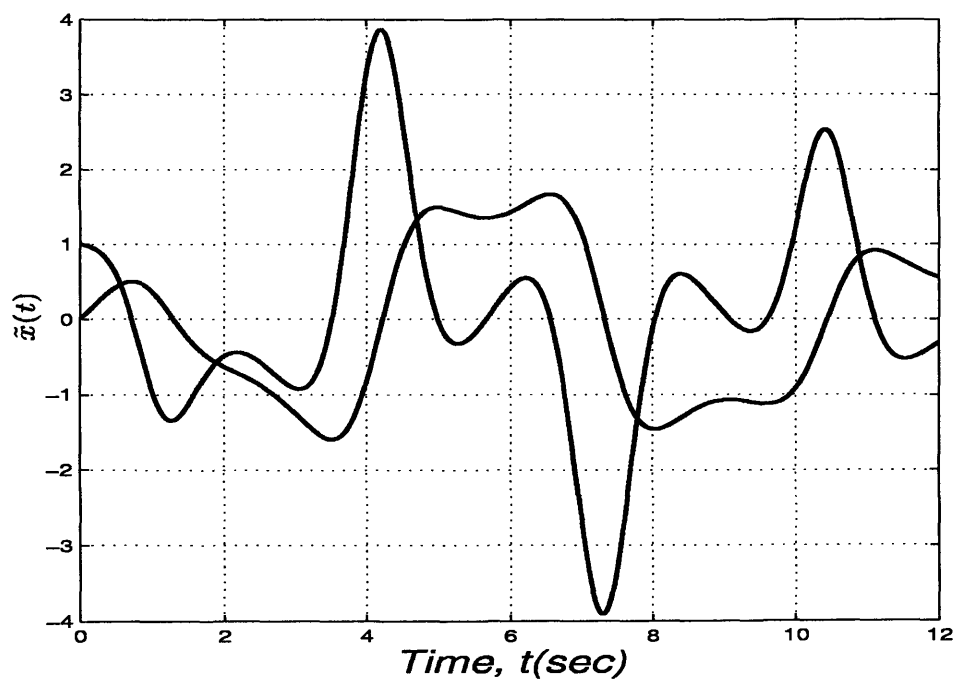
$$\lambda[\Psi] = \lambda\left[\tilde{\Psi}\left(\frac{T}{2}\right)\right]^2 \quad \text{where} \quad \lambda[\cdot] = \text{eigenvalues of } [\cdot]. \quad (5.28)$$

Simulating the variational system (5.25) with two different initial conditions and choosing the system parameters as $\omega = 1$, $M = 0.3$ and $\delta = 0.15$, the monodromy matrix $\tilde{\Psi}$ at the sampling points of 0 and $\frac{T}{2}$ was computed. Figures 5.28 and 5.29 depict the time simulations for these initial conditions with the steady-state solutions that correspond to the truncation level for $k = \pm 7$. Sampling at the times 0 and $\frac{T}{2}$, from Figs. 5.28 and 5.29 the monodromy matrix $\tilde{\Psi}$ yields

$$\tilde{\Psi} = \begin{bmatrix} -0.2294 & -1.3767 \\ 0.2135 & -0.9018 \end{bmatrix}. \quad (5.29)$$

The Floquet characteristic multipliers are given by

$$\mu_{1,2} = -0.5656 \pm j0.4253. \quad (5.30)$$

Figure 5.28: Variational system simulations for $\tilde{x}_0 = [1 \ 0]$ Figure 5.29: Variational system simulations for $\tilde{x}_0 = [0 \ 1]$

Using the relation defined in (5.28), the Floquet characteristic multipliers of Ψ are

$$\mu_{1,2} = 0.1390 \pm j0.4811 \quad (5.31)$$

and the corresponding the Floquet exponentials are

$$\rho_{1,2} = -0.1101 \pm j0.2052. \quad (5.32)$$

Following similar steps and choosing the steady-state solutions that correspond to the truncation levels of $k = \pm 11$, $k = \pm 17$, and $k = \pm 25$ we computed the Floquet characteristics and exponents. Table 5.1 shows those values where $\omega = 1$, $M = 0.3$ and $\delta = 0.15$.

| k | Floquet Multipliers | Floquet Exponents |
|----------|----------------------------|--------------------------|
| 7 | $0.1424 - j0.6079$ | $-0.0750 - j0.2134$ |
| | $0.1424 + j0.6079$ | $-0.0750 + j0.2134$ |
| 11 | $0.1433 - j0.6077$ | $-0.0750 - j0.2131$ |
| | $0.1433 + j0.6077$ | $-0.0750 + j0.2131$ |
| 17 | $0.1433 - j0.6077$ | $-0.0750 - j0.2131$ |
| | $0.1433 + j0.6077$ | $-0.0750 + j0.2131$ |
| 25 | $0.1433 - j0.60777$ | $-0.0750 - j0.2131$ |
| | $0.1433 + j0.6077$ | $-0.0750 + j0.2131$ |

Table 5.1: Approximated harmonic Solutions: $\delta = 0.15$

Similarly, for the second case, in the harmonic steady-state solutions where $\omega = 1$, $M = 0.3$ and $\delta = 0.22$, using similar truncation levels, the corresponding steady-state solutions were used to compute the Floquet characteristics and exponents. Table 5.2 summarizes the results.

| k | Floquet Multipliers | Floquet Exponents |
|----------|----------------------------|--------------------------|
| 7 | 251.7523 | 0.8779 |
| | 0.0010 | -1.1004 |
| 11 | 251.7521 | 0.8799 |
| | 0.0010 | -1.1004 |
| 17 | 251.7521 | 0.8799 |
| | 0.0010 | -1.1004 |
| 25 | 251.7521 | 0.8799 |
| | 0.0010 | -1.1004 |

Table 5.2: Approximated harmonic Solutions: $\delta = 0.22$

5.4.1.2 Subharmonic Solutions of Duffing Oscillator

Finally, for subharmonic solutions the steady-state solutions take the following form

$$\bar{x}_{\frac{1}{3}}(t) = X_0 + 2 \sum_{k=-q}^{k=q} X_{\frac{k}{3}}^R \cos\left(\frac{k}{3}t\right) - X_{\frac{k}{3}}^I \sin\left(\frac{k}{3}t\right). \quad (5.33)$$

In this case, the subharmonic steady-state solutions that correspond to the system parameters $\omega = 1$, $M = 0.3$ and $\delta = 0.22$ were used to compute the Floquet characteristics and exponents. The time simulations for the variational system are shown in Figs. 5.30 and 5.31 with truncation level of $k = \pm 7$.

Sampling at the time instances 0 and $\frac{T}{2}$ from Figs. 5.30, and 5.31 the monodromy matrix $\tilde{\Psi}$ is computed

$$\tilde{\Psi} = \begin{bmatrix} 0.3249 & -0.1255 \\ 0.0368 & 0.3685 \end{bmatrix}. \quad (5.34)$$

The Floquet characteristic multipliers are given by

$$\mu_1 = 0.3467 + j0.0644 \quad \mu_2 = 0.3467 + j0.0644. \quad (5.35)$$

Using the relation defined in (5.28), the Floquet characteristic multipliers of Ψ are

$$\mu_1 = 0.1160 + j0.0446 \quad \mu_2 = 0.1160 - j0.0446 \quad (5.36)$$

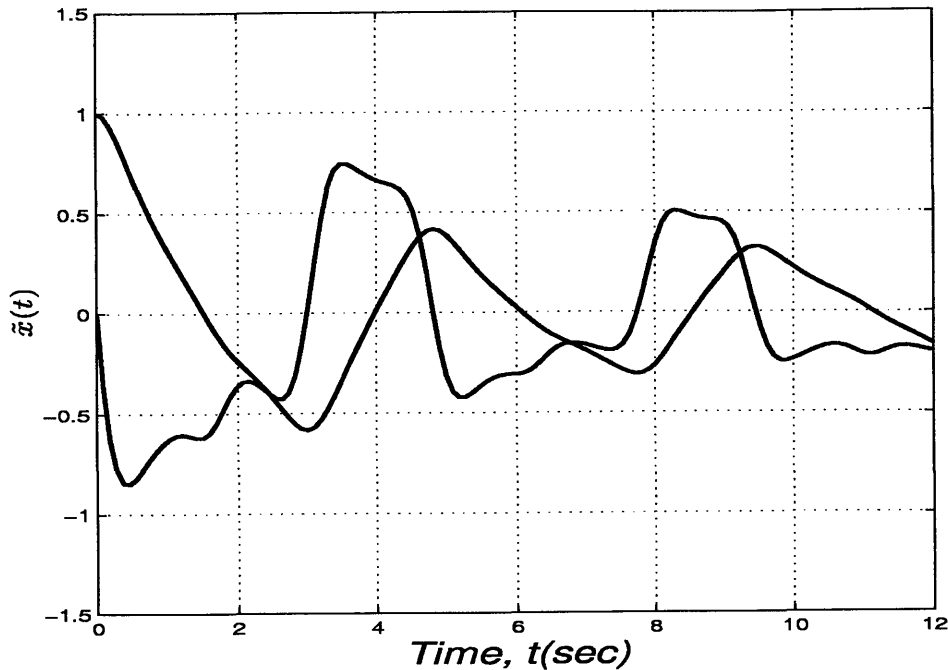
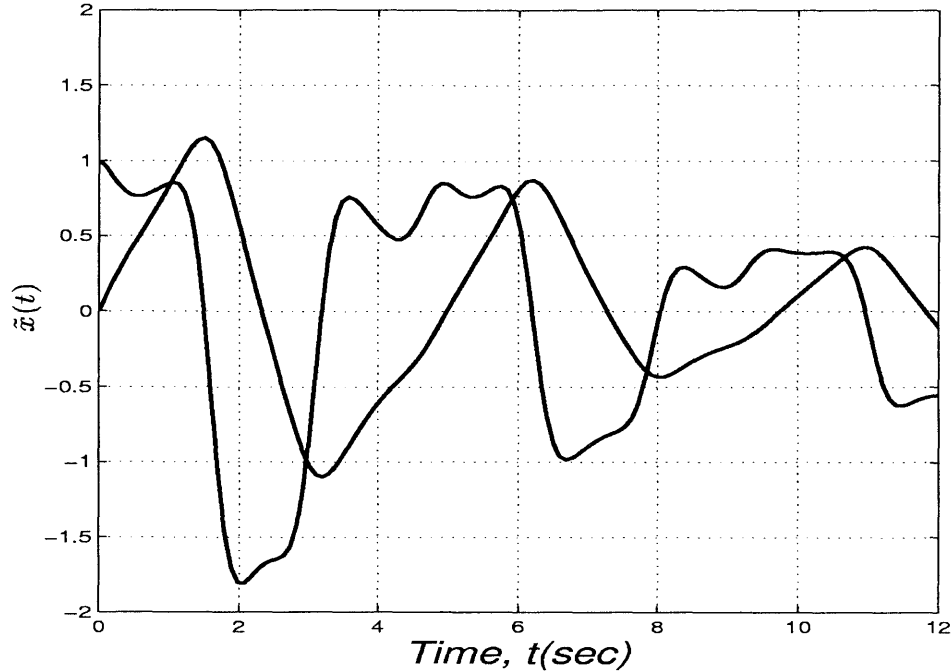


Figure 5.30: Variational system simulations for $\tilde{x}_0 = [1 \ 0]$

and the corresponding Floquet exponents are

$$\rho_1 = -0.1106 + j0.0195 \quad \rho_2 = -0.1106 - j0.0195. \quad (5.37)$$

Using similar procedures and choosing the subharmonic steady-state solutions that correspond to the truncation levels of $k = \pm 11$, $k = \pm 17$, and $k = \pm 25$ we computed the Floquet characteristics and exponents. Table 5.3 shows these results.

Figure 5.31: Variational system simulations for $\tilde{x}_0 = [0 \ 1]$

| k | Floquet Multipliers | Floquet Exponents |
|----------|----------------------------|--------------------------|
| 7 | $0.1160 + j0.04461$ | $-0.1106 + j0.0195$ |
| | $0.1160 - j0.0446$ | $-0.1106 - j0.0195$ |
| 11 | $0.0744 + j0.1004$ | $-0.1103 + j0.0495$ |
| | $0.0744 - j0.1004$ | $-0.1103 - j0.0495$ |
| 17 | $0.0722 + j0.1010$ | $-0.1107 + j0.0504$ |
| | $0.0722 - j0.1010$ | $-0.1107 - j0.0504$ |
| 25 | $0.0711 + j0.1038$ | $-0.1100 + j0.0514$ |
| | $0.0711 - j0.1038$ | $-0.1100 - j0.0514$ |

Table 5.3: Approximated subharmonic Solutions: $\delta = 0.22$

5.5 Poincaré Maps

Before introducing Poincaré map theory, let us first define the Poincaré section [2]. A Poincaré section is a hypersurface in the state-space that is transverse to the flow of a given dynamical system. For instance, in n -dimensional space, a hypersurface is a surface whose

dimension is $(n - 1)$. A flow is transverse to a surface if the normal of the surface $n(x)$ and the flow of the vector field are not orthogonal at points of intersection.

DEFINITION 5.1

A transformation that maps the current intersections of the flow of the vector field and the Poincaré section to the subsequent intersections on the Poincaré section is called the Poincaré map.

One advantage of using a Poincaré map is it reduces the system dimensions by one state since the Poincaré section is an $(n - 1)$ space. Since a discrete map is less complicated than a continuous vector field, a Poincaré map also mitigates the complexity of the analysis of the dynamical system. Furthermore, the stability of a periodic solution of a system can be assessed by studying the evolution of the Poincaré map. One disadvantage of Poincaré maps is one must know first a periodic solution of the system analytically or numerically. Hence, if the system has complicated dynamics, one can integrate the system by using numerical integration, since finding closed form analytical solution is impossible for higher order systems. We are only giving a brief introduction of Poincaré maps, for further reading see [77,78,55,79–81,76].

In this study, we use the Poincaré maps to assess the stability of nonlinear systems. To understand the mechanics involved in computations of the stability of periodic solutions of a dynamical systems, let us consider the following nonlinear dynamical system

$$\frac{dx}{dt} = f(x, t, p) \quad (5.38)$$

where $x \in \mathbb{R}^{n \times 1}$ is a state variable, $f(x, t, p) \in \mathbb{R}^{n \times 1}$ is a nonlinear vector field, and p is a system parameter.

Suppose this system has a periodic steady-state solution with a period T . Let $x_0 = \tau_0$, where τ_0 is a point on the steady-state periodic solution. Then the trajectory initiated from τ_0 at $t = t_0$ is represented by $x(\tau_0, t, t_0)$. To construct the Poincaré map of this trajectory, we collect discrete points of the trajectory at an interval of T . Hence, the stroboscopic points of the trajectory, or the Poincaré map, can be represented as

$$P(\tau) = x(\tau, t_0 + T, t_0). \quad (5.39)$$

If the steady-state solution of the system (5.38) is periodic, then

$$x(\tau_0, t + T, t_0) = \tau_0 \quad \Rightarrow \quad P(\tau_0) = \tau_0. \quad (5.40)$$

It is clear that the fixed point of the Poincaré map is a steady-state periodic solution of the system (5.38). Perturbing the map from the steady-state solution $\tau = \tau_0$, we have the following

$$P(\tau_0 + \zeta) = P(\tau_0) + \frac{\partial P(\tau_0)}{\partial \tau} \zeta + \text{h.o.t.} \quad (5.41)$$

where ζ is the perturbation of the steady-state solution of the map while h.o.t. are the higher order terms of ζ , including the quadratic terms. Since the perturbation is small in amplitude, we can ignore the higher order terms, and the variational system is given by

$$P(\zeta) = \frac{\partial P(\tau_0)}{\partial \tau} \zeta. \quad (5.42)$$

Hence the Poincaré fixed point τ_0 is stable if the magnitude of the eigenvalues of $\left\{ \frac{\partial P(\tau_0)}{\partial \tau} \right\}$ are less than one.

To assess the stability of the steady-state periodic solution of the system (5.38), our objective is to compute the Jacobian matrix of the map and then examine the magnitude of the eigenvalues of the Jacobian matrix. If all eigenvalues are inside a unit disc, then the steady-state periodic solution is stable; otherwise, if some of the eigenvalues have a magnitude which are greater than one, the steady-state solution is unstable. If some of the eigenvalues have a magnitude of less than one and some have a magnitude greater one, and one or more eigenvalues have a magnitude of one, then the linearization of the Poincaré map cannot give information about the stability of the system; therefore, nonlinear analysis is required to assess the stability of the solution. Normal forms and the center manifold theorem are examples of the tools that can be used to analyze such systems.

If we differentiate (5.38) with respect to τ , we have

$$\frac{d}{dt} \left[\frac{\partial x(\tau, t)}{\partial \tau} \right] = \frac{\partial f(x(\tau, t, p))}{\partial x} \frac{\partial x}{\partial \tau} \quad (5.43)$$

Further simplifications yield

$$\frac{d\Gamma(\tau, t)}{dt} = \frac{\partial f(x(\tau, t, p))}{\partial x} \Gamma(\tau, t) \quad \text{where} \quad \Gamma(\tau, t) = \frac{\partial x(\tau, t)}{\partial \tau} \quad (5.44)$$

From (5.39), we have

$$\frac{\partial P(\tau)}{\partial \tau} = \frac{\partial x(\tau, t_0 + T, t_0)}{\partial \tau} = \Gamma(t_0 + T) \quad (5.45)$$

Hence, our problem is reduced to computing a steady-state solution of the system (5.38). However, if the system dynamics are nonlinear, the chances of computing an analytical solution are very small; therefore, we can compute the steady-state solution employing a computer simulation. Furthermore, using the steady-state solution, we need to solve the differential equation defined in (5.44), for a given initial condition $\Gamma(t_0)$. For a given initial condition, we can compute $\Gamma(t_0 + T)$ simply by integrating the differential equation. One easy way to integrate the system is by computer simulation.

5.5.1 Application of the Poincaré Map to the Duffing Oscillator

From the generalized state-space model, we computed steady-state solutions for different truncation levels. Using these steady-state solutions, the variational model of the Poincaré map can be computed as defined in equation (5.44). For a given steady-state solution $\bar{x}(t)$, equation (5.44) takes the following form

$$\frac{d\Gamma}{dt} = \begin{bmatrix} 0 & 1 \\ 1 - 3\bar{x}^2(t) & -\delta \end{bmatrix} \Gamma(\tau, t). \quad (5.46)$$

Hence, to find the Jacobian matrix of the Poincaré map, we need to compute the solutions of the system defined in (5.46) for one cycle with a length of T or simply $\Gamma(t_0 + T)$. If we choose $t_0 = 0$ and $\Gamma(0) = I$, then we compute $\Gamma(T)$ by analytical methods or by simulations. Using $\bar{x}(t)$ which corresponds to a truncation level of $k = \pm 7$, we integrated the system defined in (5.46) through computer simulations in one cycle and computed $\Gamma(T)$, where

$$\Gamma(T) = \begin{bmatrix} -0.2294 & -1.3767 \\ 0.2135 & -0.9018 \end{bmatrix}. \quad (5.47)$$

Hence the eigenvalues of the Jacobian matrix of the Poincaré map are given by

$$\mu_1 = 0.1390 + j0.4811 \quad \mu_2 = 0.1390 - j0.4811. \quad (5.48)$$

Since the magnitudes of μ_1 and μ_2 are less than one, the Poincaré fixed point is stable which implies that the steady-state periodic solution $\bar{x}(t)$ is a stable solution.

Since equation (5.46) is equivalent to (5.26), the eigenvalues of the Poincaré map are equal to the Floquet characteristic multipliers; therefore, we do not need to compute the characteristic multipliers.

5.6 Connections Between Poincaré Map, Floquet Theory, and GSSA

In this thesis, steady-state harmonic and subharmonic periodic solutions and their stability of the Duffing oscillator were investigated. The generalized state-space averaging method was used to compute the steady-state periodic solutions, and the fundamental eigenvalues were examined to assess the stability of the periodic solutions. The stability of these steady-state solutions were also examined by using Floquet theory and Poincaré maps. Tables 5.4, 5.5, and 5.6 show the fundamental eigenvalues of the generalized state-space averaging method, the Floquet exponents, and the Poincaré maps eigenvalues. The eigenvalues of GSSA and Floquet exponents give same measure. However, the GSSA approach is much simpler than Floquet theory.

| M = 0.3 and $\omega = 1$ | | | |
|--|---------------------|--------------------------|---------------------------|
| k | GSSA Eigen | Floquet Exponents | Poincaré Map Eigen |
| 7 | $-0.0750 + j0.2115$ | $-0.0750 + j0.2134$ | $0.1424 + j0.6079$ |
| | $-0.0750 - j0.2115$ | $-0.0750 - j0.2134$ | $0.1424 - j0.6079$ |
| 11 | $-0.0750 + j0.2115$ | $-0.0750 + j0.2131$ | $0.1433 + j0.6077$ |
| | $-0.0750 - j0.2115$ | $-0.0750 - j0.2131$ | $0.1433 - j0.6077$ |
| 17 | $-0.0750 + j0.2115$ | $-0.0750 + j0.2131$ | $0.1433 + j0.6077$ |
| | $-0.0750 - j0.2115$ | $-0.0750 - j0.2131$ | $0.1433 - j0.6077$ |
| 25 | $-0.0750 + j0.2115$ | $-0.0750 + j0.2131$ | $0.1433 + j0.6077$ |
| | $-0.0750 - j0.2115$ | $-0.0750 - j0.2131$ | $0.1433 - j0.6077$ |

Table 5.4: Harmonic Solutions: $\delta = 0.15$

| M = 0.3 and $\omega = 1$ | | | |
|--|-------------------|--------------------------|---------------------------|
| k | GSSA Eigen | Floquet Exponents | Poincaré Map Eigen |
| 7 | 0.8790 | 0.8779 | 251.7523 |
| | -1.0990 | -1.1004 | 0.0010 |
| 11 | 0.8790 | 0.8799 | 251.7521 |
| | -1.0990 | -1.1004 | 0.0010 |
| 17 | 0.8790 | 0.8799 | 251.7521 |
| | -1.0990 | -1.1004 | 0.0010 |
| 25 | 0.8790 | 0.8799 | 251.7521 |
| | -1.0990 | -1.1004 | 0.0010 |

Table 5.5: Harmonic solutions: $\delta = 0.22$

| M = 0.3 and $\omega = 1$ | | | |
|--|----------------------|--------------------------|---------------------------|
| k | GSSA F. Eigen | Floquet Exponents | Poincaré Map Eigen |
| 7 | $-0.110 + j0.1295$ | $-0.1106 + j0.0195$ | $-0.1160 + j0.0446$ |
| | $-0.110 - j0.1295$ | $-0.1106 - j0.0195$ | $-0.110 - j0.0446$ |
| 11 | $-0.110 + j0.1212$ | $-0.1103 + j0.0495$ | $-0.0744 + j0.1004$ |
| | $-0.110 - j0.1212$ | $-0.1103 - j0.0495$ | $-0.0744 - j0.1004$ |
| 17 | $-0.110 + j0.1299$ | $-0.1107 + j0.0514$ | $-0.0722 + j0.1010$ |
| | $-0.110 - j0.1299$ | $-0.1107 - j0.0514$ | $-0.0722 - j0.1010$ |
| 25 | $-0.110 + j0.1300$ | $-0.1100 + j0.0514$ | $-0.0711 + j0.1038$ |
| | $-0.110 - j0.1300$ | $-0.1100 - j0.0514$ | $-0.0711 - j0.1038$ |

Table 5.6: Subharmonic Solutions: $\delta = 0.22$

5.6 Connections Between Poincaré Map, Floquet Theory, and GSSA

Chapter 6

Applications

6.1 Single-phase Ferroresonance

To apply the generalized state-space averaging methodology to the single-phase ferroresonance model defined in Equation (2.3), we write the equations in state space representation

$$\begin{aligned}
 \dot{x} &= y \\
 \dot{y} &= z \\
 \dot{z} &= -a_1 z - a_2 y - a_3 x - a_4 x^4 y - a_5 x^5 + a_6 M \cos(t)
 \end{aligned} \tag{6.1}$$

where x is the flux of the transformer core. The dynamics of the slowly varying model are given by

$$\begin{aligned}
 \dot{X}_k(t) &= -jk\omega X_k(t) + Y_k(t) \quad -\infty \leq k \leq \infty \\
 \dot{Y}_k(t) &= -jk\omega Y_k(t) + Z_k(t) \\
 \dot{Z}_k(t) &= -(a_1 + jk\omega)Z_k(t) - a_2 Y_k(t) - a_3 X_k(t) - a_4 H_k(X_k(t), Y_k(t)) - a_5 F_k(X_k(t)) + a_6 G_k
 \end{aligned} \tag{6.2}$$

where H_k , F_k , and G_k are defined as

$$\begin{aligned}
 H_k(X_k, Y_k) &= \sum_{m_1} \sum_{m_2} \sum_{m_3} \sum_{m_4} X_{m_1} X_{m_2} X_{m_3} X_{m_4} Y_{k-m_1-m_2-m_3-m_4} \quad -\infty \leq k \leq \infty \\
 F_k(X_k) &= \sum_{m_1} \sum_{m_2} \sum_{m_3} \sum_{m_4} X_{m_1} X_{m_2} X_{m_3} X_{m_4} X_{k-m_1-m_2-m_3-m_4} \quad -\infty \leq m_i \leq \infty \\
 G_k &= \begin{cases} \frac{M}{2} & \text{for } k = \pm m \\ 0 & \text{for } k \neq \pm m \end{cases}
 \end{aligned} \tag{6.3}$$

Our task is to examine the existence and stability of steady-state solutions of the slowly varying system defined in (6.2). If such solutions exist, then the full system (6.1) will have periodic steady-state solutions and their stability depends on the evolution of the slowly varying system. Hence, in the following sections we will investigate existence and stability of harmonic periodic steady-state solutions of the system defined in (6.1) by studying the

slowly varying system (6.2).

6.1.1 Harmonic Periodic Solutions

The equations that govern the fixed point solutions of the slowly varying system are given by

$$\begin{aligned}
 -jk\omega X_k + Y_k &= 0 \quad k \geq 0 \\
 -jk\omega Y_k + Z_k &= 0 \\
 -(a_1 + jk\omega)Z_k - a_2 Y_k - a_3 X_k - a_4 H_k - a_5 F_k + G_k &= 0
 \end{aligned} \tag{6.4}$$

The existence of nontrivial solutions of these equations implies existence of periodic solutions of the system defined in (6.1). Since the system dynamics depend on four parameters R , L , C , and M , for each given value of these parameters it is necessary to compute a corresponding steady-state solution for the full system. In general, one fixes some of the parameters and then studies the steady-state solutions of the system based on the variations of other parameters. In the following subsections we will investigate the existence of harmonic periodic steady-state solutions of the system by varying the transmission line inductance L and the magnitude of the input voltage M .

6.1.1.1 Line Inductance Variations

In this analysis for each fixed value of M , we take all the possible values of L and examine if harmonic periodic solution exists. We set the other parameters to $R = 0.002$ pu, $C = 50$ pu, and $M = 0.25$ pu. The line inductance is varied from 0.00001 pu to 0.05 pu. For the range L is less than 0.0264, only one flux amplitude in the steady-state solution exists while for L greater than this value three amplitudes of the flux exist for each given L . The critical value which corresponds to the bifurcation point is $L = 0.0264$ pu for $M = 0.25$ pu. Figure. 6.1 depicts the steady state solution curves for $M = 0.25$ pu and L taking values from 0.0001 pu to 0.05 pu.

6.1.1.2 Input Voltage Magnitude Variations

Similarly, for each fixed value of L , we vary all possible values of M and examine the steady-state solutions of the system. Figure 6.2 depicts the steady-state solutions of the system

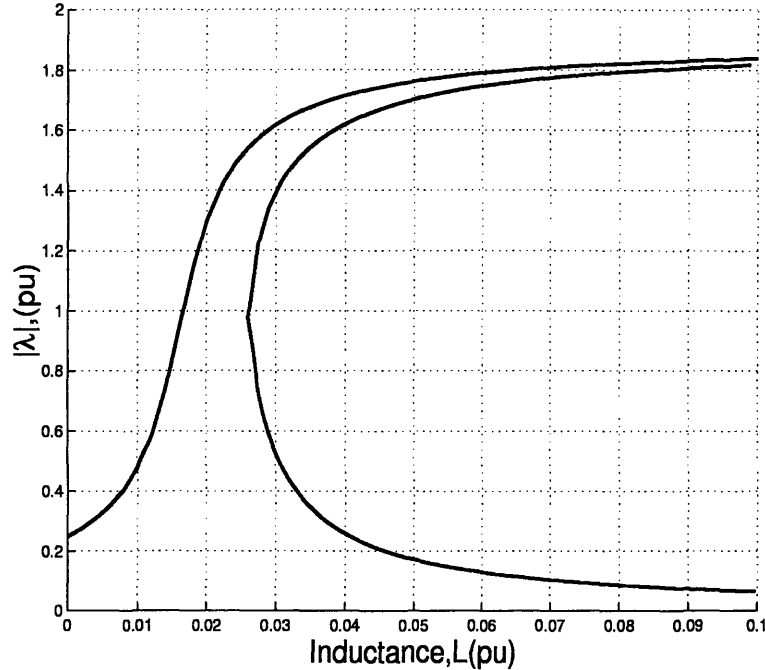


Figure 6.1: Steady-state solutions for $M = 0.25$ pu: Single-phase

with line inductance set to 0.025 pu and the magnitude of the input voltage M varying from 0 to 0.35 pu. At the locations P_1 and P_2 in Fig. 6.2 the steady-state solution of the system can jump from one value to another. In the region between the points P_1 and P_2 in Fig. 6.2, the system has multiple steady-state solutions.

6.1.2 Stability of Harmonic Periodic Solutions

The stability of the three steady-state solution curves C_1 , C_2 , and C_3 were examined by computing the eigenvalues of the slowly varying system. The eigenvalues of the solution curves C_1 and C_3 in Fig. 6.2 indicate stability while the eigenvalues of the solution curve C_2 show instability. Figs. 6.3, 6.4, and 6.5 depict the eigenvalues of the curves C_1 , C_2 , and C_3 respectively. Similarly, Figures 6.6 and 6.7 show the eigenvalues of the points P_1 and P_2 respectively. At these locations, ferroresonance can occur, particularly, the amplitude for the flux can jump for small perturbations of the amplitude of the input voltage.

To verify the jump amplitudes found in the analysis, we simulated the system dynamics in Matlab. For the first simulation, we chose the following parameters: $R = 0.002$ pu, $C = 50$ pu, $L = 0.025$ pu, and $M = 0.173$ pu. For this input, the magnitude of the cor-

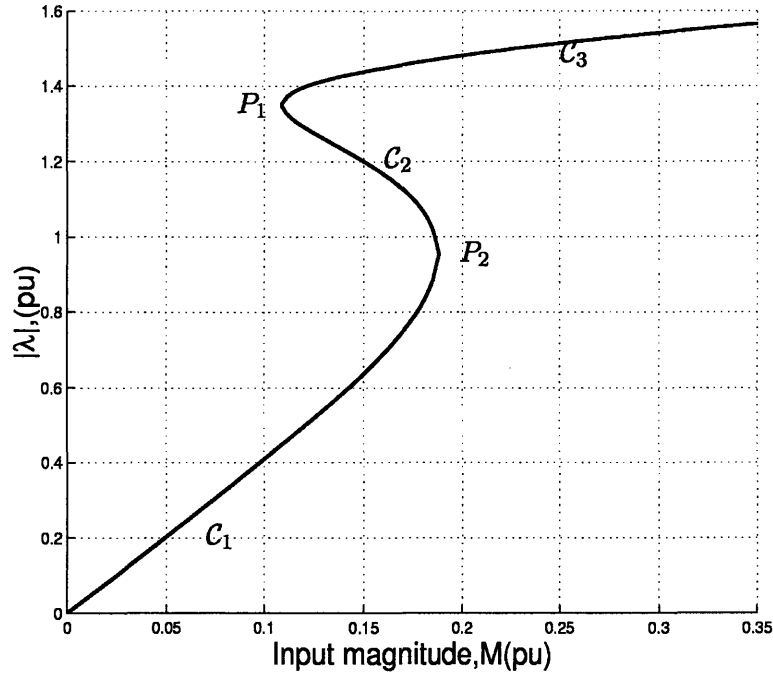


Figure 6.2: Steady-state solutions for $L = 0.025$ pu: Single-phase

responding flux amplitude was 0.7754 pu. After 800 sec, we applied a disturbance signal $\gamma(t)$ with an amplitude of 0.012 pu to the system, and we removed the disturbance signal at $t = 1000$ sec. Due to this disturbance the system response changed slightly, and after the disturbance vanished the response returned to its original value. This indicates that for these given parameters ferroresonance cannot occur. Figure 6.8 shows the simulations of the system for these parameters where $\lambda(t)$ is the flux of the core, $v(t)$ is the input voltage of the transformer, and $\gamma(t)$ is the disturbance signal.

For the second simulation, the input amplitude was changed to $M = 0.1735$ pu. Before the disturbance the amplitude of the flux reached a steady-state value of 0.7754 pu. As above a disturbance signal was applied to the system with an amplitude of 0.012 pu. Due to the disturbance the flux magnitude jumped to 1.5099 pu. After the disturbance signal vanished, the amplitude of the flux persisted at 1.5099 pu. Hence, the system underwent a ferroresonance phenomenon, particularly, jump amplitude. The amplitude of the flux increased by 51.35 percent. Figure 6.9 depicts the time simulations of the system under these conditions.

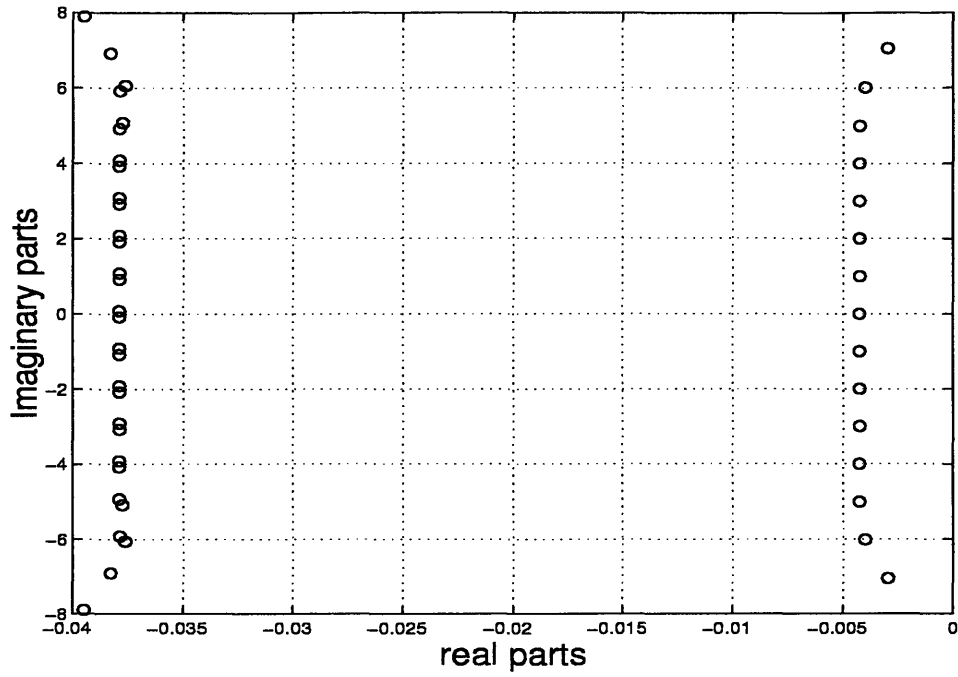


Figure 6.3: Eigenvalues for curve C_1 : Single-phase

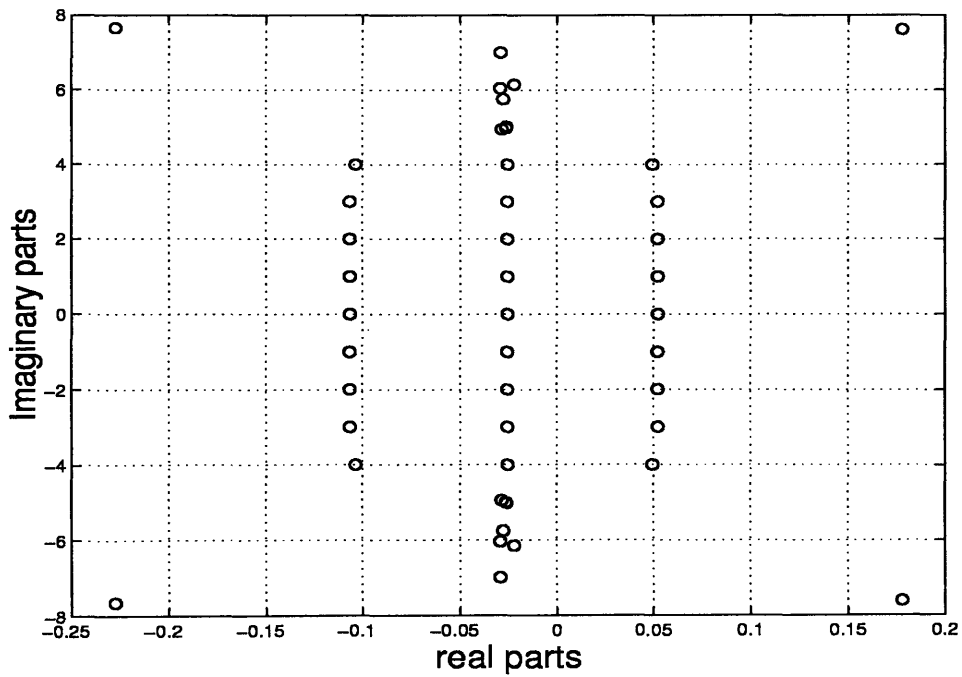
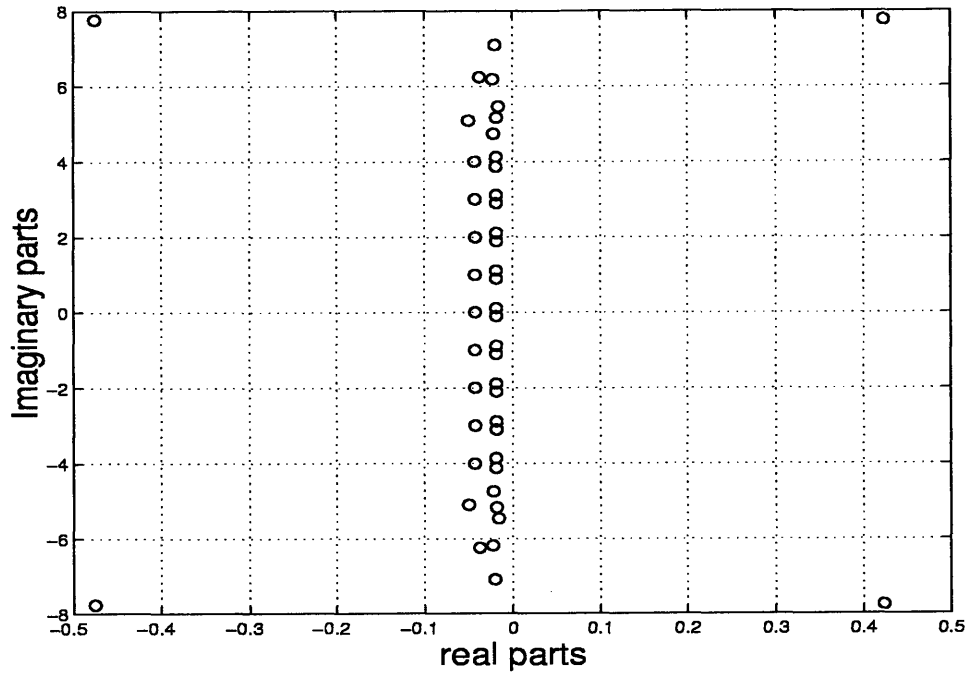
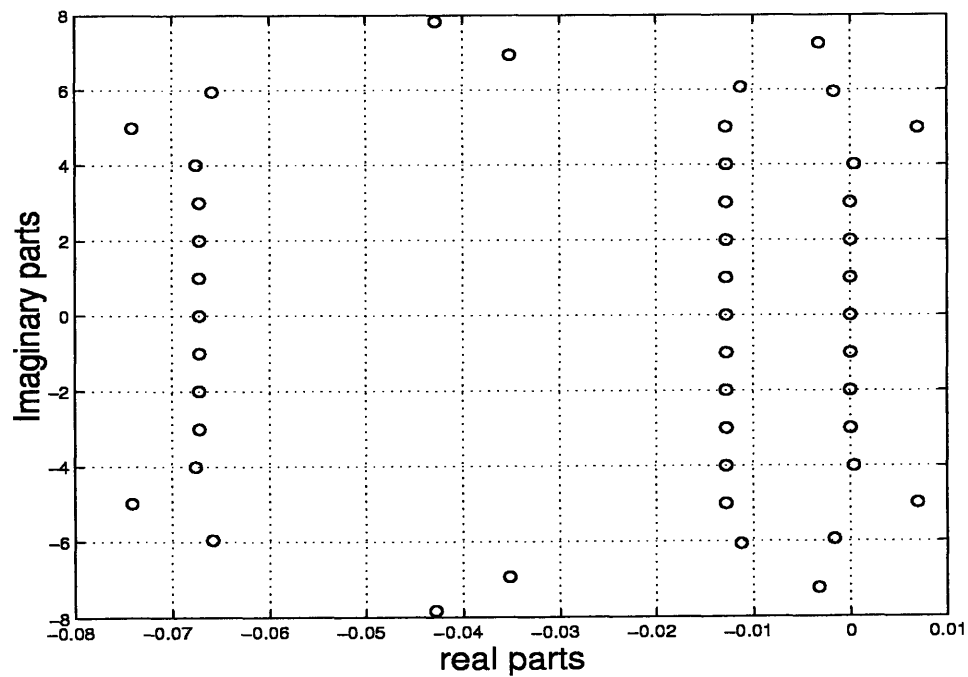


Figure 6.4: Eigenvalues for curve C_2 : Single-phase

Figure 6.5: Eigenvalues for curve C_3 : Single-phaseFigure 6.6: Eigenvalues for point P_1 : Single-phase

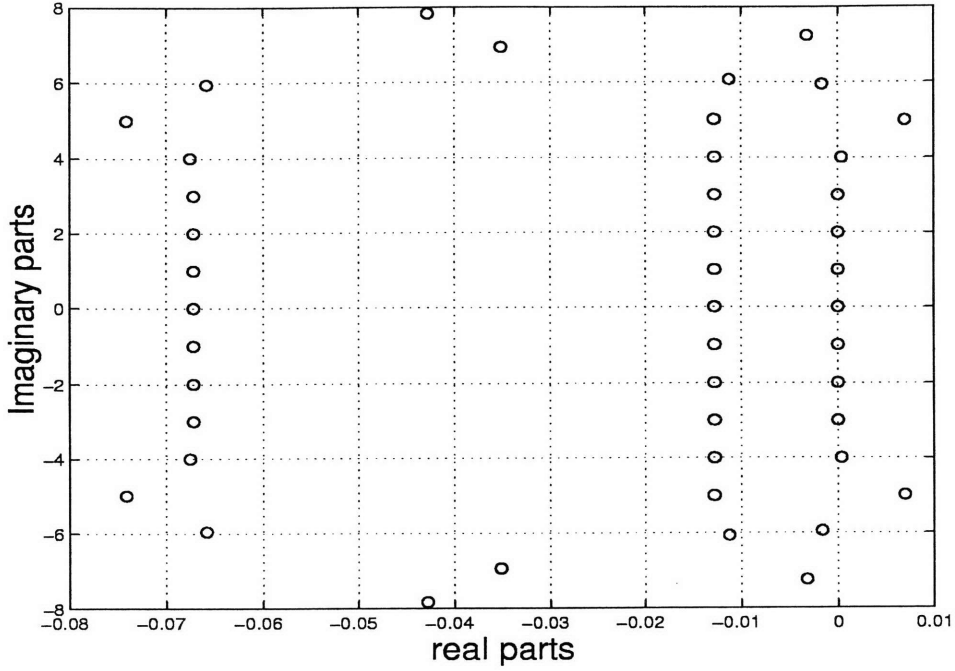


Figure 6.7: Eigenvalues for point P_2 : Single-phase

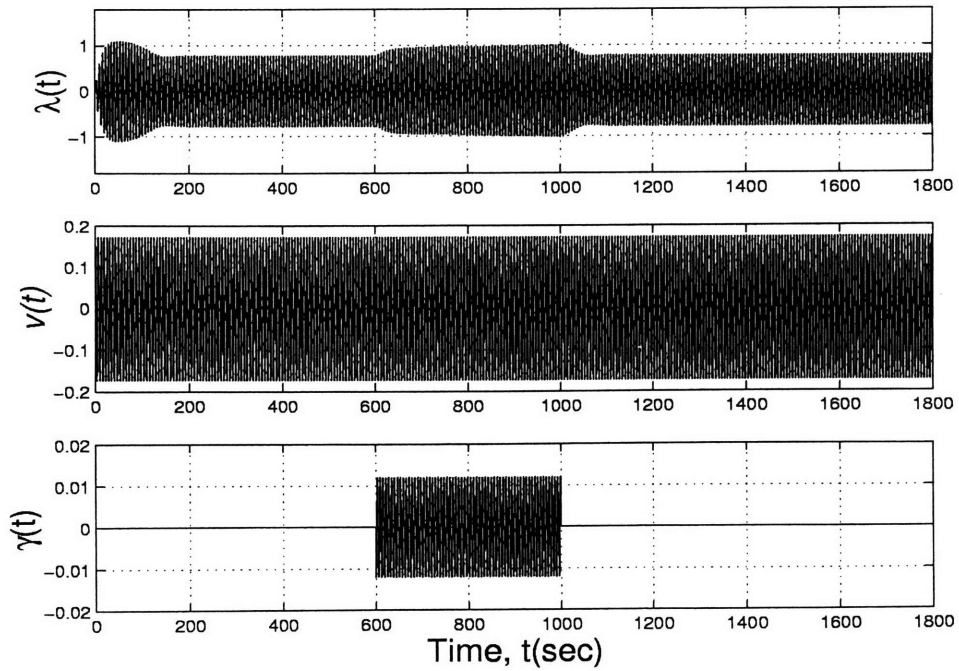


Figure 6.8: Time simulations for $\lambda(t)$ case one: Single-phase

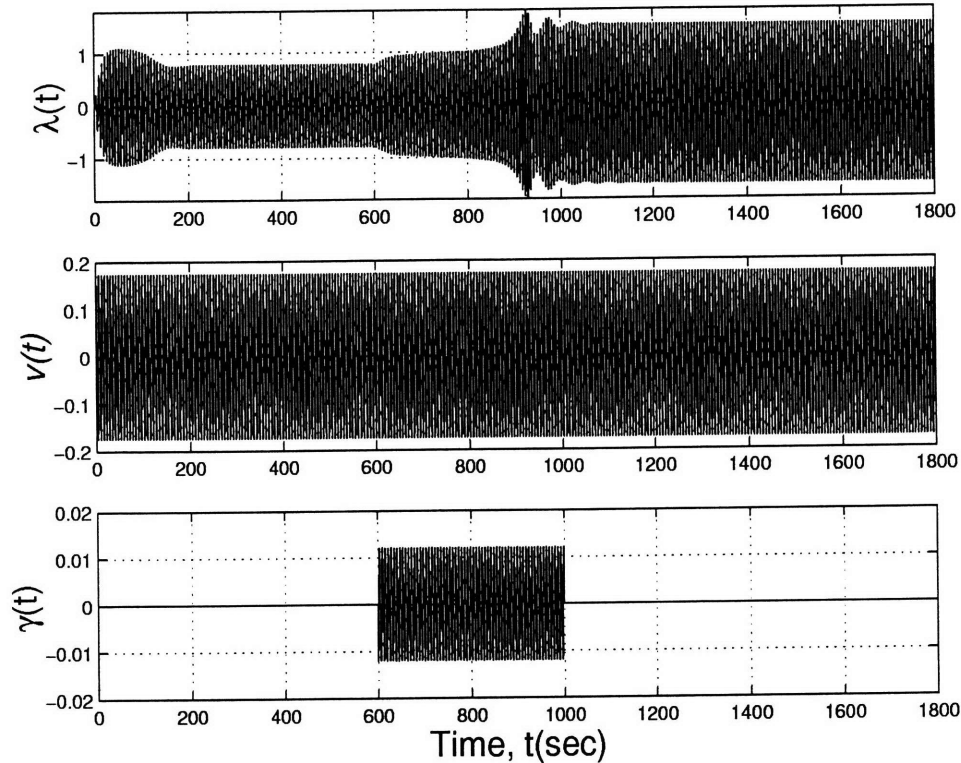


Figure 6.9: Time simulations for $\lambda(t)$ case two: Single-phase

6.1.3 Robustness analysis for the steady-state solutions

In general to model the nonlinear characteristics of transformer cores, we run an experiment and collect the root mean square values of current $i_L(t)$ and voltage $v(t)$ of the transformer primary side. Then, we compute the flux $\lambda(t)$ and fit this data to a curve using the least squares technique. One general model is

$$i_L = K_1\lambda + K_2\lambda^5. \quad (6.5)$$

In this model we ignore any other terms since the coefficients of these terms are very small.

We may still ask how the response of the above model is different than the response of the following model

$$i_L = K_1\lambda + K_2\lambda^5 + \sum_{n=1}^m \alpha_n x_2^{2n+5} \quad \text{where } \alpha_n < 1. \quad (6.6)$$

To examine this issue, we consider the following nonlinear differential equation:

$$\begin{aligned} \dot{x}_1 &= -a_1x_1 - a_2x_2 + a_3 \cos(t) \\ \dot{x}_2 &= x_3 \\ \dot{x}_3 &= a_4 \left[x_1 - K_1x_2 - K_2x_2^5 - \sum_{n=1}^m \alpha_n x_2^{2n+5} \right] \quad \text{where } \alpha_n < 1 \end{aligned} \quad (6.7)$$

The equilibrium state of the system can be computed by finding the roots of the following equation.

$$\begin{aligned} a_1x_1 + a_2x_2 - a_3 \cos(t) &= 0 \\ x_3 &= 0 \\ a_4 \left[x_1 - K_1x_2 - K_2x_2^5 - \sum_{n=1}^m \alpha_n x_2^{2n+5} \right] &= 0 \end{aligned} \quad (6.8)$$

Suppose for $\alpha_n = 0$ that a steady-state solution $\{\bar{x}_1, \bar{x}_2, \bar{x}_3\}$ exists. This steady-state solution is a periodic steady-state solution.

Now we are asking the question: does a steady-state solution exist for small increment of α_n ?

To answer this question, we apply the implicit function theorem to the system of equations defined in (6.8). Hence, the incremental relationship between the variables of Δx_1 , Δx_2 , Δx_3 , and $\Delta \alpha_n$ is given by

$$\begin{bmatrix} \Delta x_1 \\ \Delta x_2 \end{bmatrix} = \begin{bmatrix} a_1 & a_2 \\ 1 & -(1 + 5\bar{x}_2^4 + \sum_{n=1}^m (2n+5)\alpha_n \bar{x}_2^{2n+4}) \end{bmatrix}^{-1} \begin{bmatrix} 0 \\ \sum_{n=1}^m \bar{x}_2^{2n+5} \Delta \alpha_n \end{bmatrix} \quad (6.9)$$

The matrix

$$\begin{bmatrix} a_1 & a_2 \\ 1 & -(1 + 5\bar{x}_2^4 + \sum_{n=1}^m (2n+5)\alpha_n \bar{x}_2^{2n+4}) \end{bmatrix} \quad (6.10)$$

is the Jacobian matrix of the system at each given steady-state solution. Since this matrix is periodic, we apply Floquet theory to incremental system and compute the monodromy matrix. If the magnitudes of the eigenvalues of the monodromy matrix are not equal to one,

then the Jacobian matrix is invertible. As we showed earlier, the Floquet exponents are equivalent to the fundamental eigenvalues of the generalized state-space averaging model. As shown in Fig. 6.2, at the locations P_1 and P_2 there exist zero eigenvalues for the generalized state-space averaging model. Hence, at these locations there are some Floquet multipliers that have magnitude equal to one. Therefore, the Jacobian matrix is not invertible at these locations. However, for all other steady-state solutions, the Jacobian matrix is invertible.

Hence, as long as the Jacobian matrix is invertible there exists a steady-state solution for small values of α_n . This implies that if we compute multiple steady-state solutions of the system for $\alpha_n = 0$, then there still exist multiple solutions of the system for small α_n .

6.2 Three-phase Ferroresonance: All Switches Closed

Applying the generalized state-space averaging technique to the model defined in (2.9), we have the following infinite set of nonlinear differential algebraic equations

$$\dot{X}_{1,k} = -jk\omega X_{1,k} - a_1 X_{7,k} - a_2 F_{1,k} + a_3 X_{4,k} \quad (6.11a)$$

$$\dot{X}_{2,k} = -jk\omega X_{2,k} - a_1 X_{8,k} - a_2 F_{2,k} + a_3 X_{5,k} \quad (6.11b)$$

$$\dot{X}_{3,k} = -jk\omega X_{3,k} - a_1 X_{9,k} - a_2 F_{3,k} + a_3 X_{6,k} \quad (6.11c)$$

$$\dot{X}_{4,k} = -(jk\omega + a_5)X_{4,k} + a_4 G_{1,k} - a_4 X_{1,k} \quad (6.11d)$$

$$\dot{X}_{5,k} = -(jk\omega + a_5)X_{5,k} + a_4 G_{2,k} - a_4 X_{2,k} \quad (6.11e)$$

$$\dot{X}_{6,k} = -(jk\omega + a_5)X_{6,k} + a_4 G_{3,k} - a_4 X_{3,k} \quad (6.11f)$$

$$\dot{X}_{7,k} - \dot{X}_{9,k} = -jk\omega X_{7,k} + jk\omega X_{9,k} + X_{1,k} - X_{3,k} \quad (6.11g)$$

$$\dot{X}_{8,k} - \dot{X}_{9,k} = -jk\omega X_{8,k} + jk\omega X_{9,k} + X_{2,k} - X_{3,k} \quad (6.11h)$$

$$0 = K_1(X_{7,k} + X_{8,k} + X_{9,k}) + K_5(F_{1,k} + F_{2,k} + F_{3,k}) \quad (6.11i)$$

where $F_{1,k}$, $F_{2,k}$ and $F_{3,k}$ are defined as

$$F_{1,k}(X_{7,k}) = \sum_{m_1} \sum_{m_2} \sum_{m_3} \sum_{m_4} X_{7,m_1} X_{7,m_2} X_{7,m_3} X_{7,m_4} X_{7,k-m_1-m_2-m_3-m_4} \quad (6.12a)$$

$$F_{2,k}(X_{8,k}) = \sum_{m_1} \sum_{m_2} \sum_{m_3} \sum_{m_4} X_{8,m_1} X_{8,m_2} X_{8,m_3} X_{8,m_4} X_{8,k-m_1-m_2-m_3-m_4} \quad (6.12b)$$

$$F_{3,k}(X_{9,k}) = \sum_{m_1} \sum_{m_2} \sum_{m_3} \sum_{m_4} X_{9,m_1} X_{9,m_2} X_{9,m_3} X_{9,m_4} X_{9,k-m_1-m_2-m_3-m_4} \quad (6.12c)$$

$$-\infty \leq k \leq \infty \quad \text{and} \quad -\infty \leq m_i \leq \infty$$

and $G_{1,k}$, $G_{2,k}$ and $G_{3,k}$ are defined as

$$G_{1,k} = \begin{cases} \frac{M}{2} & \text{for } k = \pm 1 \\ 0 & \text{otherwise} \end{cases} \quad (6.13a)$$

$$G_{2,k} = \begin{cases} -\frac{M}{4} (1 \pm j\sqrt{3}) & \text{for } k = \pm 1 \\ 0 & \text{otherwise} \end{cases} \quad (6.13b)$$

$$G_{3,k} = \begin{cases} -\frac{M}{4} (1 \mp j\sqrt{3}) & \text{for } k = \pm 1 \\ 0 & \text{otherwise} \end{cases} \quad (6.13c)$$

$$-\infty \leq k \leq \infty \quad \text{and} \quad -\infty \leq m_i \leq \infty$$

and

$$X_k = \left[V_{1,k} \quad V_{2,k} \quad V_{3,k} \quad I_{1,k} \quad I_{2,k} \quad I_{3,k} \quad \Lambda_{1,k} \quad \Lambda_{2,k} \quad \Lambda_{3,k} \right]^T. \quad (6.14)$$

The steady-state response of the system can be computed from the following nonlinear algebraic equations.

$$-jk\omega X_{1,k} - a_1 X_{7,k} - a_2 F_{1,k} + a_3 X_{4,k} = 0 \quad (6.15a)$$

$$-jk\omega X_{2,k} - a_1 X_{8,k} - a_2 F_{2,k} + a_3 X_{5,k} = 0 \quad (6.15b)$$

$$-jk\omega X_{3,k} - a_1 X_{9,k} - a_2 F_{3,k} + a_3 X_{6,k} = 0 \quad (6.15c)$$

$$-(jk\omega + a_5)X_{4,k} + a_4 G_{1,k} - a_4 X_{1,k} = 0 \quad (6.15d)$$

$$-(jk\omega + a_5)X_{5,k} + a_4 G_{2,k} - a_4 X_{2,k} = 0 \quad (6.15e)$$

$$-(jk\omega + a_5)X_{6,k} + a_4 G_{3,k} - a_4 X_{3,k} = 0 \quad (6.15f)$$

$$-jk\omega X_{7,k} + jk\omega X_{9,k} + X_{1,k} - X_{3,k} = 0 \quad (6.15g)$$

$$-jk\omega X_{8,k} + jk\omega X_{9,k} + X_{2,k} - X_{3,k} = 0 \quad (6.15h)$$

$$K_1(X_{7,k} + X_{8,k} + X_{9,k}) + K_5(F_{1,k} + F_{2,k} + F_{3,k}) = 0 \quad (6.15i)$$

In order to examine the existence of periodic solutions of the system defined in (2.9), we need to investigate the steady-state solutions of the transformed system. In this thesis we are investigating the existence of periodic solutions and the stability of the full system.

6.2.1 Harmonic Periodic Solutions

To study the harmonic solutions of the system (2.9), we vary two parameters of the transformed system, the length of the transmission line and the magnitude of the input voltage M .

Fixing the magnitude of the input voltage M to 1.0 pu, we vary the transmission line length from 0 to 120 miles. Figure 6.10 shows the magnitude of the flux of phase one versus the transmission line length. From this figure, it is clear that ferroresonance cannot occur since there are no multiple steady-state solutions. Initially the system is inductive and as the transmission line length increases it becomes capacitive which increases the magnitude of the flux.

Similarly fixing the length of the transmission line to 40, 60, and 120 miles respectively, we vary the magnitude of the input voltage from 0 to 3.0 pu. Figure 6.11 depicts the magnitude of the flux of phase one versus the magnitude of the input voltage for different values of transmission line length.

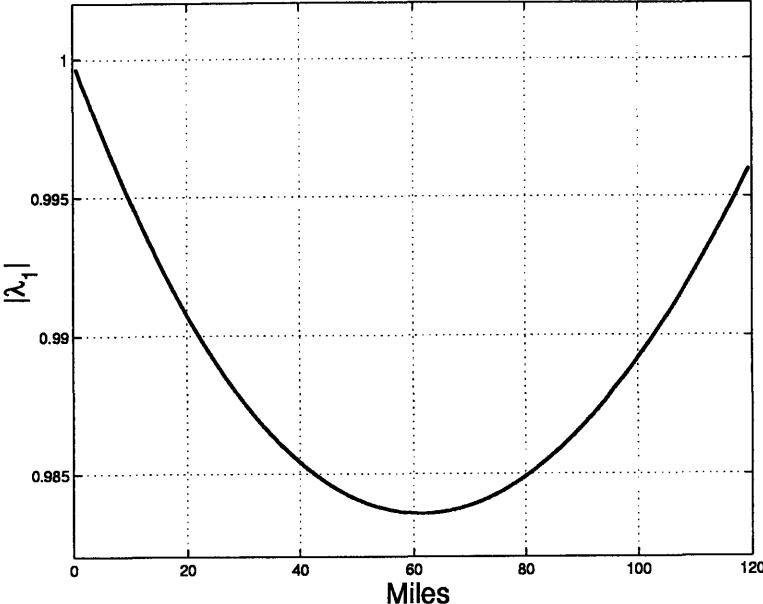


Figure 6.10: Steady-state solutions for $M = 1.0$ pu: All switches closed

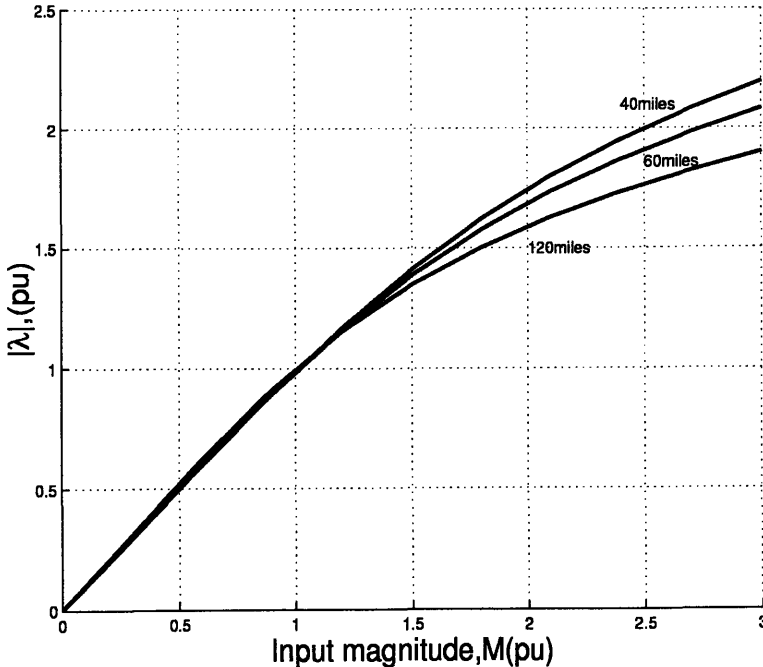


Figure 6.11: Steady-state solutions for 40, 60, and 120 mile transmission line lengths

6.2.2 Stability of Harmonic Periodic Solutions

For each given steady-state solution of the system (6.11), we need to compute the corresponding linearized Jacobian matrix of the system to assess the stability of the system defined in (2.9). Since the system defined in (6.11) is a differential-algebraic system, we need to simplify the system dynamics in order to compute the eigenvalues of the system or use the generalized eigenanalysis method. In this thesis we simplified system dynamics.

To compute the eigenvalues of the system defined in (6.11), we propose the following: Eliminate $X_{9,k}$ and $G_{3,k}$ from equation (6.11c) using equation (6.11i). Then the simplified system takes the following form

$$\dot{X}_{1,k} = -jk\omega X_{1,k} - a_1 X_{7,k} - a_2 F_{1,k} + a_3 X_{4,k} \quad (6.16a)$$

$$\dot{X}_{2,k} = -jk\omega X_{2,k} - a_1 X_{8,k} - a_2 F_{2,k} + a_3 X_{5,k} \quad (6.16b)$$

$$\dot{X}_{3,k} = -jk\omega X_{3,k} + a_1(X_{7,k} + X_{8,k}) + a_2(F_{1,k} + F_{2,k}) + a_3 X_{6,k} \quad (6.16c)$$

$$\dot{X}_{4,k} = -(jk\omega + a_5)X_{4,k} + a_4 G_{1,k} - a_4 X_{1,k} \quad (6.16d)$$

$$\dot{X}_{5,k} = -(jk\omega + a_5)X_{5,k} + a_4 G_{2,k} - a_4 X_{2,k} \quad (6.16e)$$

$$\dot{X}_{6,k} = -(jk\omega + a_5)X_{6,k} + a_4 G_{3,k} - a_4 X_{3,k} \quad (6.16f)$$

$$\dot{X}_{7,k} - \dot{X}_{9,k} = -jk\omega X_{7,k} + jk\omega X_{9,k} + X_{1,k} - X_{3,k} \quad (6.16g)$$

$$\dot{X}_{8,k} - \dot{X}_{9,k} = -jk\omega X_{8,k} + jk\omega X_{9,k} + X_{2,k} - X_{3,k} \quad (6.16h)$$

Then, the variational system takes the form

$$\mathcal{Q}\dot{\hat{X}}_{i,k} = J\hat{X}_{i,k} \quad \text{where} \quad \mathcal{Q} = I - \mathcal{M} \quad \text{and} \quad J = J_1 + \mathcal{P} \quad (6.17)$$

where $I \in \mathbb{R}^{n \times n}$ is the identity matrix, $J \in \mathbb{C}^{n \times n}$ is a complex matrix, and $\mathcal{Q} \in \mathbb{R}^{n \times n}$ is a real matrix. Hence the eigenvalues of the system can be computed by finding the roots of the following algebraic equation

$$\det(J - \mathcal{Q}\lambda) = 0 \quad (6.18)$$

where λ 's are the eigenvalues of the system. To compute the matrices J_1 , \mathcal{M} , and \mathcal{P} , we perform the following steps. Define

$$\dot{X}_{i,k} = U(X_{i,k}) \Big|_{X_{9,k}=0} \quad i = 1, 2, \dots, 8 \quad (6.19a)$$

$$Z_k = K_1(X_{7,k} + X_{8,k} + X_{9,k}) + K_2(F_{1,k} + F_{2,k} + F_{3,k}) \quad (6.19b)$$

$$\mathcal{F} = \begin{bmatrix} X_{1,k} & X_{2,k} & \dots & X_{8,k} \end{bmatrix} \quad (6.19c)$$

$$\mathcal{V} = \begin{bmatrix} X_{7,k} & X_{8,k} & X_{9,k} \end{bmatrix} \quad (6.19d)$$

Then, let

$$J_1 = \text{Jacobian}(U, \mathcal{F}) \quad \text{and} \quad J_2 = \text{Jacobian}(Z, \mathcal{V}) \quad (6.20)$$

where $J_1 \in \mathbb{C}^{n \times n}$ is a complex matrix and $J_2 \in \mathbb{R}^{m \times m}$. The dimension of the reduced system, n and m can be computed from the following equation

$$n = \text{deg} * (2k + 1) \quad \text{and} \quad m = 3 * (2k + 1) \quad (6.21)$$

where deg is the order of the system defined in (6.11) and k is the number of harmonics used for the approximation of the solution. For example, if the system contains 8 first order differential equations and one algebraic equation, then the degree of the system will be 8 and n and m will be 24 and 9 respectively, if only the first harmonic considered. If we take up to the seventh harmonics, then n and m will be 120 45.

Now, define

$$A_1 = \begin{bmatrix} J_2(:, 1) & J_2(:, 4) & \dots & J_2(:, n-2) \end{bmatrix} \quad (6.22a)$$

$$A_2 = \begin{bmatrix} J_2(:, 2) & J_2(:, 5) & \dots & J_2(:, n-1) \end{bmatrix} \quad (6.22b)$$

$$A_3 = \begin{bmatrix} J_2(:, 3) & J_2(:, 6) & \dots & J_2(:, n) \end{bmatrix} \quad (6.22c)$$

The notation $J_2(:, i)$ stands for the i^{th} column of the matrix J_2 . Then,

$$\begin{aligned} X_{9,k} &= -A_3^{-1} A_1 X_{7,k} - A_3^{-1} A_2 X_{8,k} \\ \dot{X}_{9,k} &= -A_3^{-1} A_1 \dot{X}_{7,k} - A_3^{-1} A_2 \dot{X}_{8,k} \end{aligned} \quad (6.23)$$

Since K_1 , the coefficient of the linear term, is not equal to zero, the matrix A_3 is always invertible. Hence, the left side of the differential equation that represents the reduced system is given by

$$\begin{bmatrix} 1 & & & 0 \\ & 1 & & \\ & & \ddots & \\ & & & 1 \\ 0 & & & 1 \end{bmatrix} \begin{bmatrix} \dot{X}_{1,k} \\ \dot{X}_{2,k} \\ \vdots \\ \dot{X}_{8,k} \end{bmatrix} - \begin{bmatrix} 0 & & & 0 \\ 0 & & & \\ & 0 & & \\ & & \ddots & \\ & & & -A_3^{-1}A_1 \\ 0 & & & -A_3^{-1}A_2 \end{bmatrix} \begin{bmatrix} \dot{X}_{1,k} \\ \dot{X}_{2,k} \\ \vdots \\ \dot{X}_{8,k} \end{bmatrix} \quad (6.24)$$

Similarly, the right side is

$$J_1 \begin{bmatrix} X_{1,k} \\ X_{2,k} \\ \vdots \\ \dot{X}_{8,k} \end{bmatrix} + \begin{bmatrix} 0 & & & \\ & 0 & & \\ & & \ddots & \\ & & & 0 \\ & & & -jk\omega A_3^{-1}A_1 \\ & & & -jk\omega A_3^{-1}A_2 \end{bmatrix} \begin{bmatrix} X_{1,k} \\ X_{2,k} \\ \vdots \\ \dot{X}_{8,k} \end{bmatrix} \quad (6.25)$$

then, we have

$$\mathcal{M} = \begin{bmatrix} 0 & & & & 0 \\ & 0 & & & \\ & & 0 & & \\ & & & \ddots & \\ & & & & -A_3^{-1}A_1 \\ 0 & & & & -A_3^{-1}A_2 \end{bmatrix} \text{ and } \mathcal{P} = \begin{bmatrix} 0 & & & & \\ & 0 & & & \\ & & \ddots & & \\ & & & 0 & \\ & & & & -jk\omega A_3^{-1}A_1 \\ & & & & -jk\omega A_3^{-1}A_2 \end{bmatrix} \quad (6.26)$$

Figure 6.12 shows the eigenvalues of the system for $M = 1.0$ pu with a 60 mile transmission line length. The steady-state solution of the system is stable since the real parts of the eigenvalues of the linearized system are strictly less than zero as shown in the figure. Hence, if all switches are closed, the system is not vulnerable to ferroresonance for any bounded external disturbance.

To verify these results, time simulations were performed. Figure 6.12 shows a Simulink block diagram. Similarly, Figures 6.13, 6.14, and 6.15 depict the flux linkages $\lambda_1(t)$, $\lambda_2(t)$, and $\lambda_3(t)$ of the transformer core. In these simulations, the transmission line length is 60 miles and the magnitude of the input voltage M is 1.0 pu. These simulations agree with the analytical results found earlier.

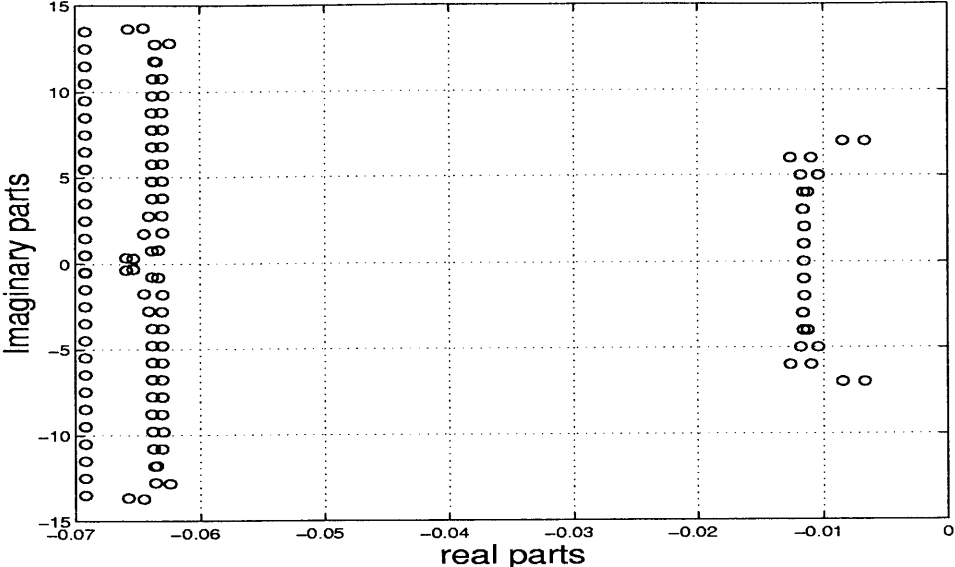


Figure 6.12: Eigenvalues of the linearized system: All switches closed

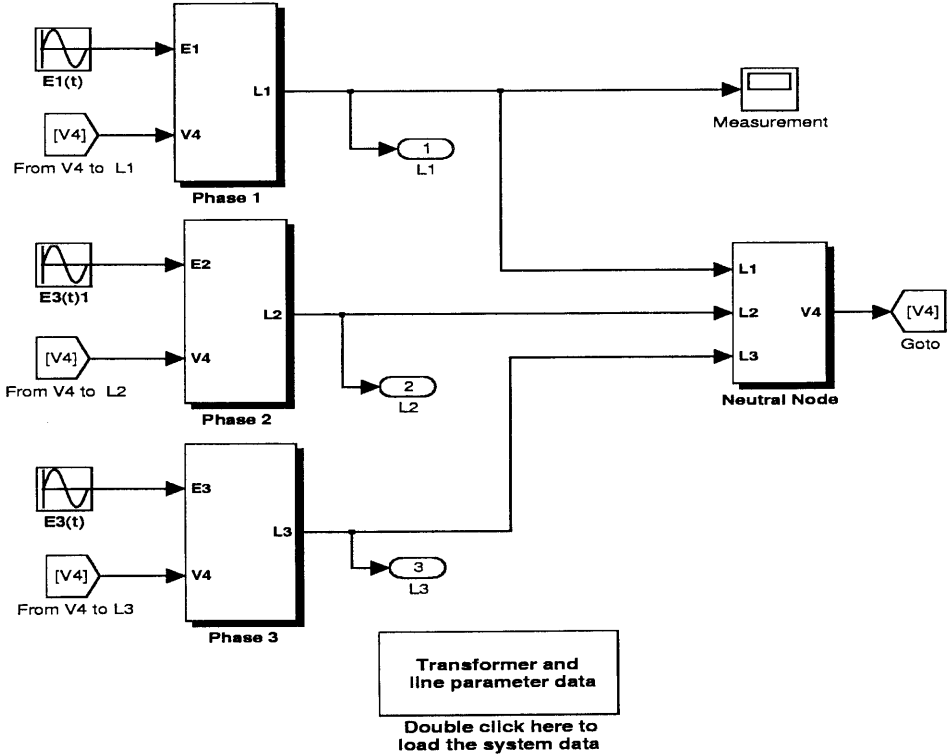


Figure 6.13: Simulink block diagram for the system: All switches closed

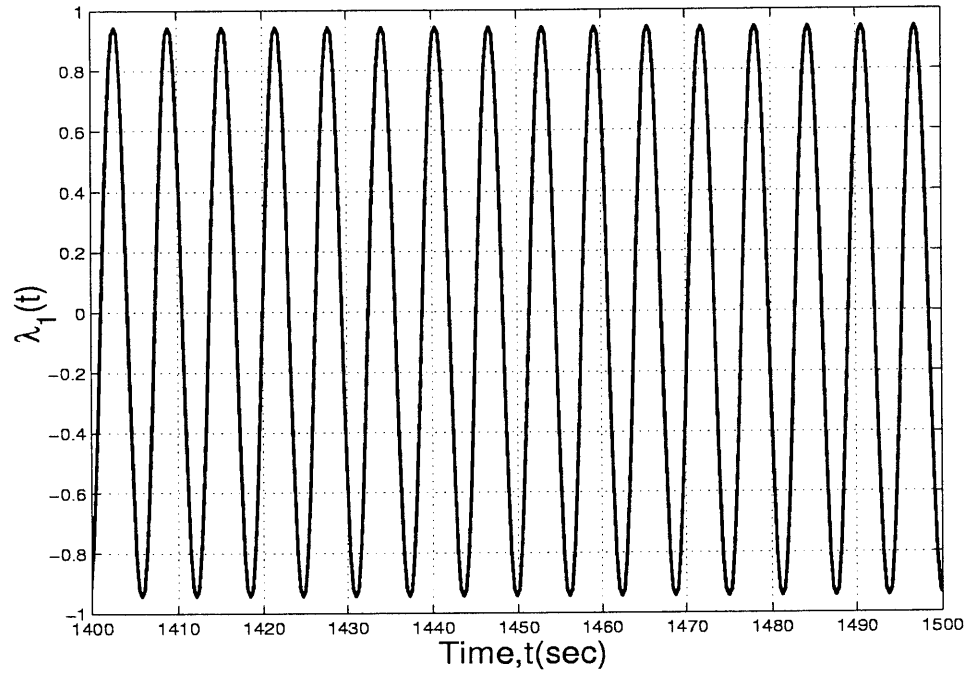


Figure 6.14: Time simulations for $\lambda_1(t)$: All switches closed

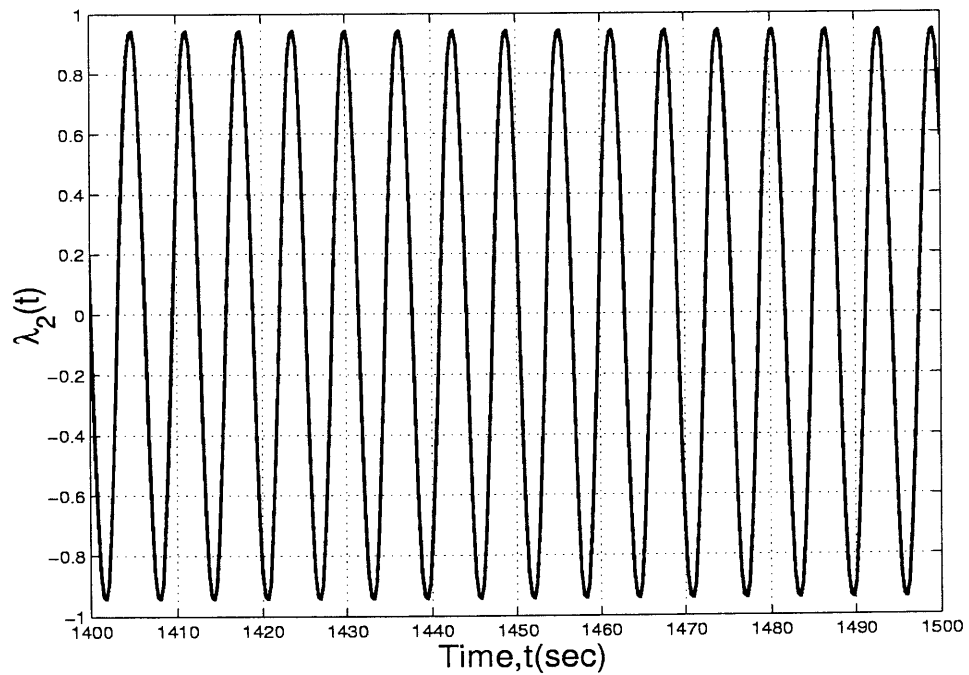
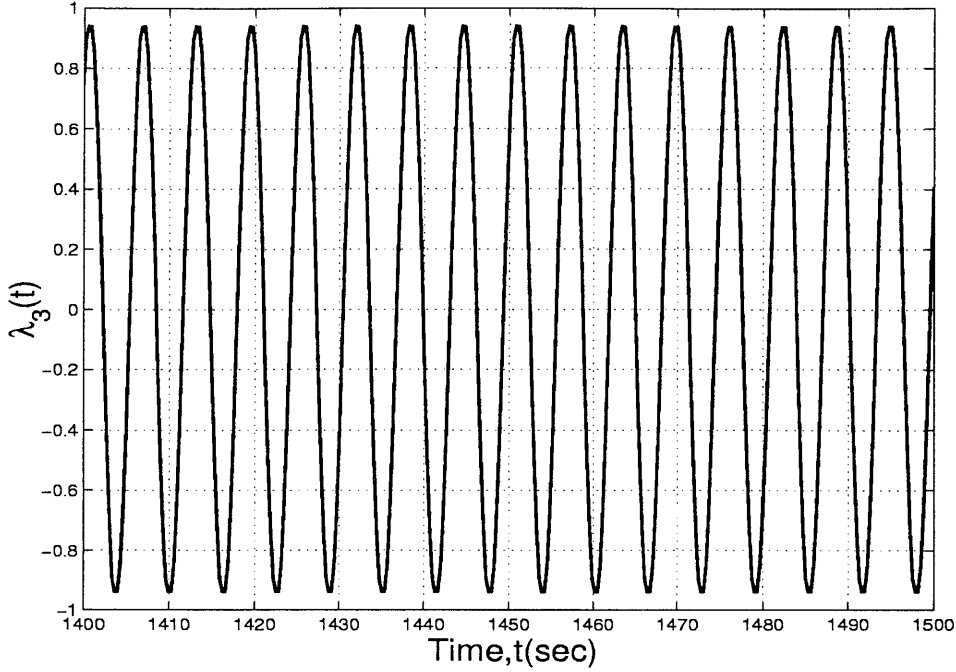


Figure 6.15: Time simulations for $\lambda_2(t)$: All switches closed

Figure 6.16: Time simulations for $\lambda_3(t)$: All switches closed

6.3 Three-phase Ferroresonance: One Switch Opened

Applying the generalized state space averaging methodology to the model defined in (2.16), we have the following infinite dimensional nonlinear differential algebraic equation

$$\dot{X}_{1,k} = -jk\omega X_{1,k} + a_1 X_{10,k} + a_2 F_{3,k} - a_3 X_{5,k} \quad (6.27a)$$

$$\dot{X}_{2,k} = -jk\omega X_{2,k} - a_1 X_{8,k} - a_2 F_{1,k} + a_3 X_{6,k} \quad (6.27b)$$

$$\dot{X}_{3,k} = -jk\omega X_{3,k} - a_1 X_{9,k} - a_2 F_{2,k} + a_3 X_{7,k} \quad (6.27c)$$

$$\dot{X}_{4,k} = -jk\omega X_{4,k} + a_6 X_{5,k} \quad (6.27d)$$

$$\dot{X}_{5,k} = -(jk\omega + a_5) X_{5,k} + a_4 X_{1,k} - a_4 X_{4,k} \quad (6.27e)$$

$$\dot{X}_{6,k} = -(jk\omega + a_5) X_{6,k} + a_4 G_{2,k} - a_4 X_{2,k} \quad (6.27f)$$

$$\dot{X}_{7,k} = -(jk\omega + a_5) X_{7,k} + a_4 G_{3,k} - a_4 X_{3,k} \quad (6.27g)$$

$$\dot{X}_{8,k} + \dot{X}_{10,k} = -jk\omega X_{8,k} + jk\omega X_{10,k} + X_{2,k} - X_{1,k} \quad (6.27h)$$

$$\dot{X}_{9,k} + \dot{X}_{10,k} = -jk\omega X_{9,k} + jk\omega X_{10,k} + X_{3,k} - X_{1,k} \quad (6.27i)$$

$$0 = K_1(X_{8,k} + X_{9,k} - X_{10,k}) + K_5(F_{1,k} + F_{2,k} - F_{3,k}) \quad (6.27j)$$

where $F_{1,k}$, $F_{2,k}$ and $F_{3,k}$ are defined as

$$F_{1,k}(X_{8,k}) = \sum_{m_1} \sum_{m_2} \sum_{m_3} \sum_{m_4} X_{8,m_1} X_{8,m_2} X_{8,m_3} X_{8,m_4} X_{8,k-m_1-m_2-m_3-m_4} \quad (6.28a)$$

$$F_{2,k}(X_{9,k}) = \sum_{m_1} \sum_{m_2} \sum_{m_3} \sum_{m_4} X_{9,m_1} X_{9,m_2} X_{9,m_3} X_{9,m_4} X_{9,k-m_1-m_2-m_3-m_4} \quad (6.28b)$$

$$F_{3,k}(X_{10,k}) = \sum_{m_1} \sum_{m_2} \sum_{m_3} \sum_{m_4} X_{10,m_1} X_{10,m_2} X_{10,m_3} X_{10,m_4} X_{10,k-m_1-m_2-m_3-m_4} \quad (6.28c)$$

$$-\infty \leq k \leq \infty \quad \text{and} \quad -\infty \leq m_i \leq \infty$$

$G_{2,k}$ and $G_{3,k}$ are defined as

$$G_{2,k} = \begin{cases} -\frac{M}{4} (1 \pm j\sqrt{3}) & \text{for } k = \pm 1 \\ 0 & \text{otherwise} \end{cases} \quad (6.29a)$$

$$G_{3,k} = \begin{cases} -\frac{M}{4} (1 \mp j\sqrt{3}) & \text{for } k = \pm 1 \\ 0 & \text{otherwise} \end{cases} \quad (6.29b)$$

and

$$X_k = \left[V_1 \quad V_2 \quad V_3 \quad V_4 \quad I_1 \quad I_2 \quad I_3 \quad \Lambda_2 \quad \Lambda_3 \right]^T. \quad (6.30)$$

We set the time derivatives in (6.27) to zero in order to compute the steady-state solution of the system which gives the following nonlinear algebraic equations

$$-jk\omega X_{1,k} + a_1 X_{10,k} + a_2 F_{3,k} - a_3 X_{5,k} = 0 \quad (6.31a)$$

$$-jk\omega X_{2,k} - a_1 X_{8,k} - a_2 F_{1,k} + a_3 X_{6,k} = 0 \quad (6.31b)$$

$$-jk\omega X_{3,k} - a_1 X_{9,k} - a_2 F_{2,k} + a_3 X_{7,k} = 0 \quad (6.31c)$$

$$-jk\omega X_{4,k} + a_6 X_{5,k} = 0 \quad (6.31d)$$

$$-(jk\omega + a_5) X_{5,k} + a_4 v_1 - a_4 X_{1,k} = 0 \quad (6.31e)$$

$$-(jk\omega + a_5) X_{6,k} + a_4 G_{2,k} - a_4 X_{2,k} = 0 \quad (6.31f)$$

$$-(jk\omega + a_5) X_{7,k} + a_4 G_{3,k} - a_4 X_{3,k} = 0 \quad (6.31g)$$

$$-jk\omega (X_{8,k} + X_{10,k}) + X_{2,k} - X_{1,k} = 0 \quad (6.31h)$$

$$-jk\omega (X_{9,k} + X_{10,k}) + X_{3,k} - X_{1,k} = 0 \quad (6.31i)$$

$$K_1 (X_{8,k} + X_{9,k} - X_{10,k}) + K_5 (F_{1,k} + F_{2,k} - F_{3,k}) = 0 \quad (6.31j)$$

In order to examine the existence of periodic solutions of the system defined (2.15), we investigate the steady-state solutions of the transformed system. Here we are only investigating existence of periodic solutions of the system (6.27).

6.3.1 Harmonic Periodic Solutions

To investigate periodic harmonic steady-state solutions of the system defined in (2.15), we vary two system parameters, the length of transmission lines and the magnitude of the input voltage M . Varying the length of the transmission will changes the line impedance. Fixing

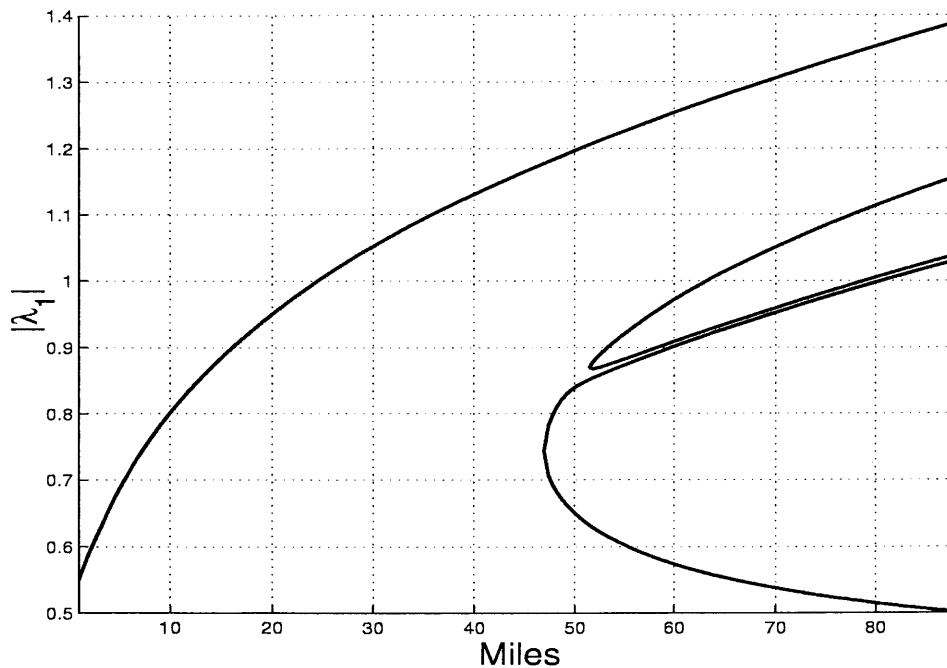


Figure 6.17: Steady-state solutions for $M = 1.0$ pu: One switch opened

the magnitude of the input voltage to 1.0 pu, we vary the transmission line length from 0 to 90 miles. Figure 6.17 shows the magnitude of the flux of phase one versus the length of the transmission line. From this figure, when the transmission line length is less than 46.5 miles, one steady-state solution exists, and three steady-state solutions exist when the transmission line length is between 46.5 and 51.5 miles. When the transmission line length is greater than 51.5 miles five steady-state solutions exist. In the regions where the system has multiple solutions, the system is vulnerable to ferroresonance for small disturbances or changes of the magnitude of the input voltage.

Furthermore, fixing the length of the transmission lines to 60 miles, we vary the magnitude of the input voltage M from 0 to 1.3 pu. Figure 6.18 depicts the magnitude of the flux of phase one versus the magnitude of the input voltage M while Fig. 6.19 shows the middle region of Fig. 6.18.

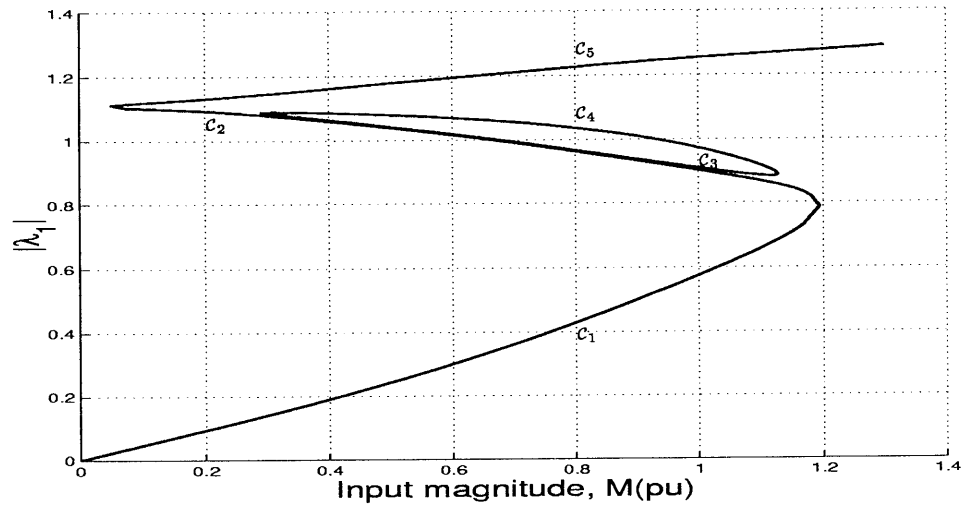


Figure 6.18: Steady-state solutions for 60 mile transmission line length: One switch opened

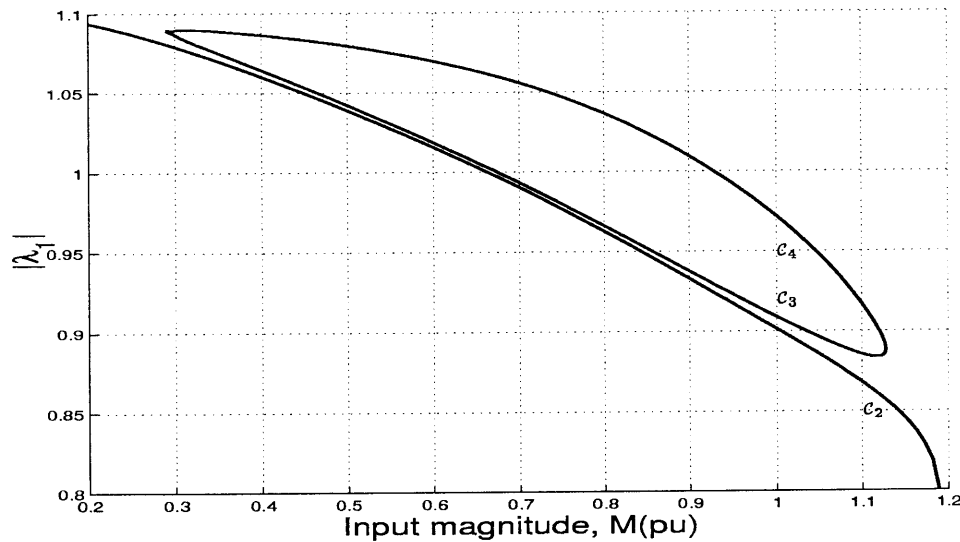


Figure 6.19: Steady-state solutions for 60 mile transmission line length: One switch opened

6.3.2 Stability of Harmonic Periodic Solutions

To assess the stability of each steady-state solution of the system (6.27), we need to formulate the variational system which will give the stability criterion of the system around that operating point. Since the system defined in (6.27) is an differential-algebraic system, we need to simplify the system dynamics in order to compute the eigenvalues of the system.

Since the derivations for the reduced model is similar to the one we showed in Section 6.2, we put all the results in Appendix A.1.

Ascertaining the stability of the system, we computed the steady-state harmonic solutions of the system and then examined the corresponding eigenvalues of the system. Figures 6.20, 6.21, 6.22, 6.23, and 6.24 show the eigenvalues of the system for $M = 1.0$ pu with a 60 mile transmission line length. In the figures, curves \mathcal{C}_1 , \mathcal{C}_4 , and \mathcal{C}_5 correspond to stable steady-state solutions while curves \mathcal{C}_2 and \mathcal{C}_3 are unstable steady-state solutions.

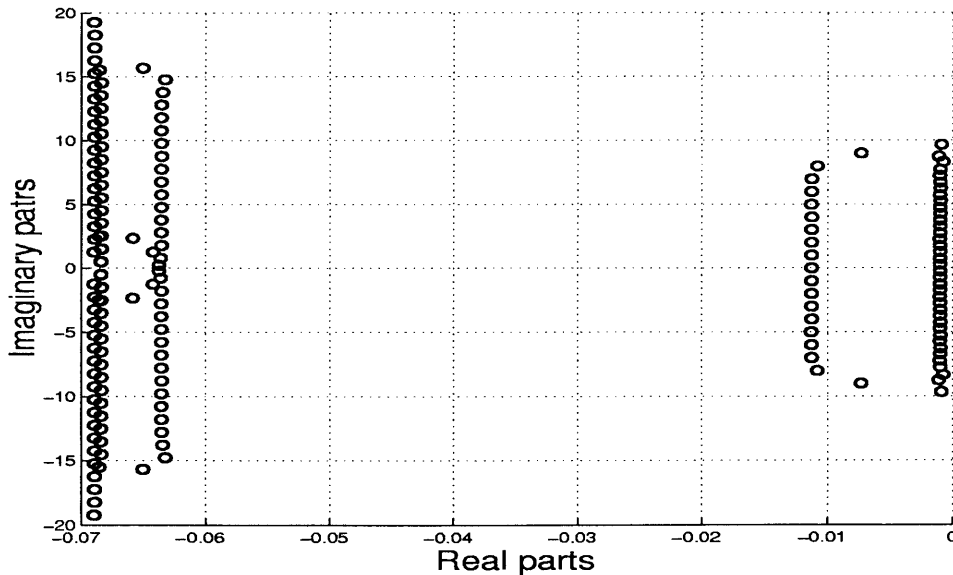
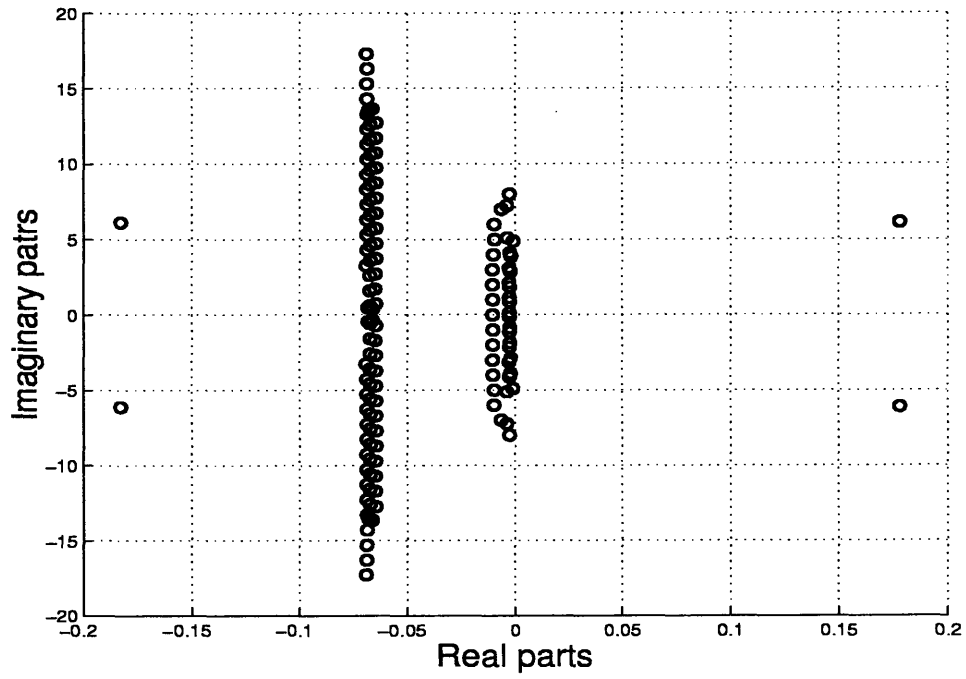
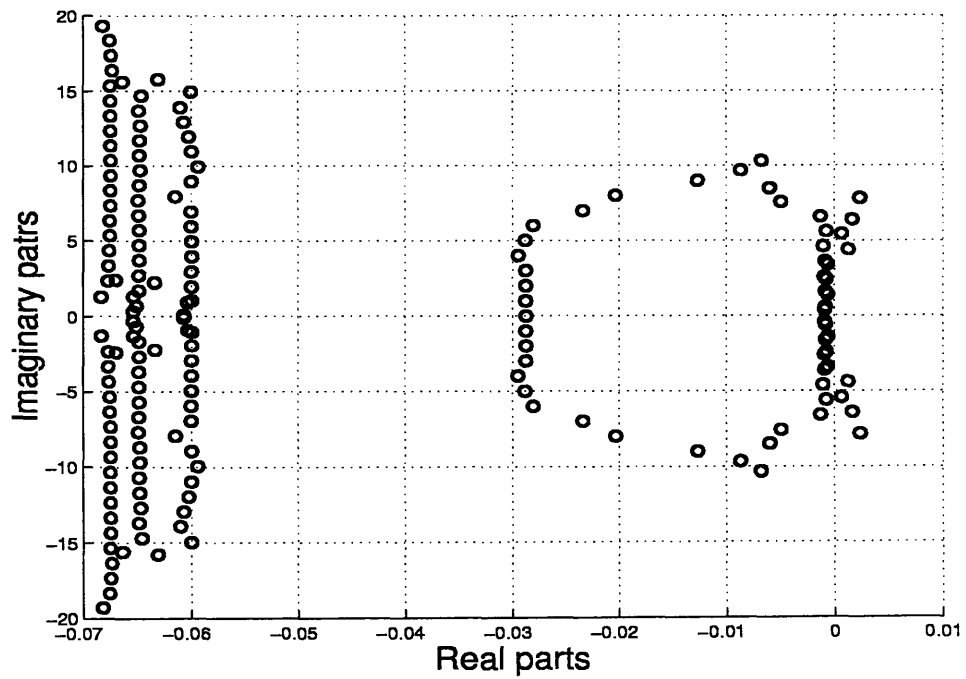


Figure 6.20: Eigenvalues for curve \mathcal{C}_1 : One switch opened

For further verification, a time simulations were performed using Matlab. Figure 6.25 shows Simulink input file block diagram. Figures 6.26, 6.27, and 6.28 depict the flux linkages $\lambda_1(t)$, $\lambda_2(t)$, and $\lambda_3(t)$ of the transformer core. In these simulations, the transmission line length is 60 miles and the magnitude of the input voltage M is 1.0 pu.

Figure 6.21: Eigenvalues for curve C_4 : One switch openedFigure 6.22: Eigenvalues for curve C_5 : One switch opened

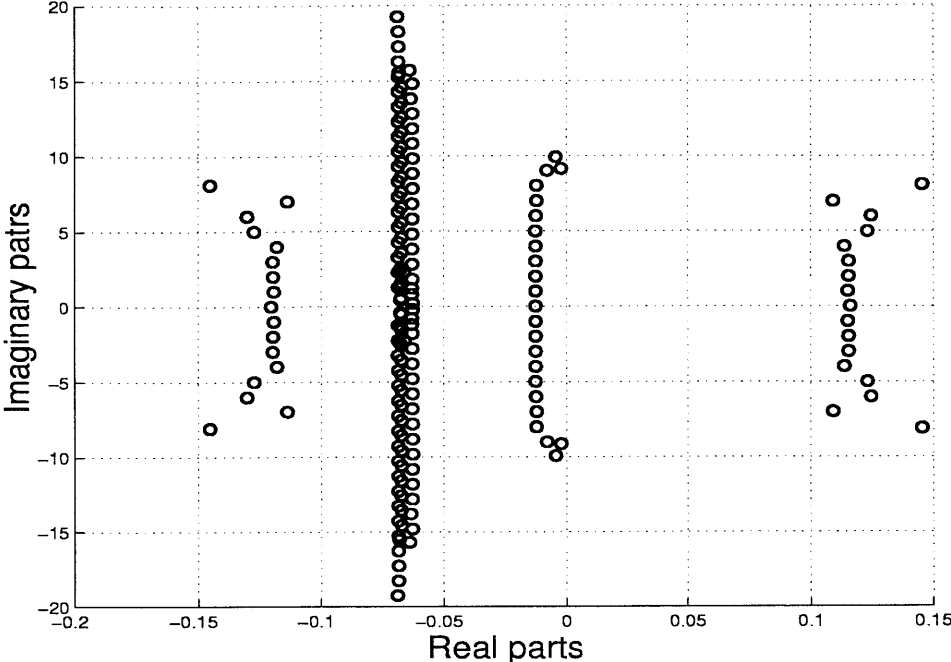


Figure 6.23: Eigenvalues for curve C_2 : One switch opened

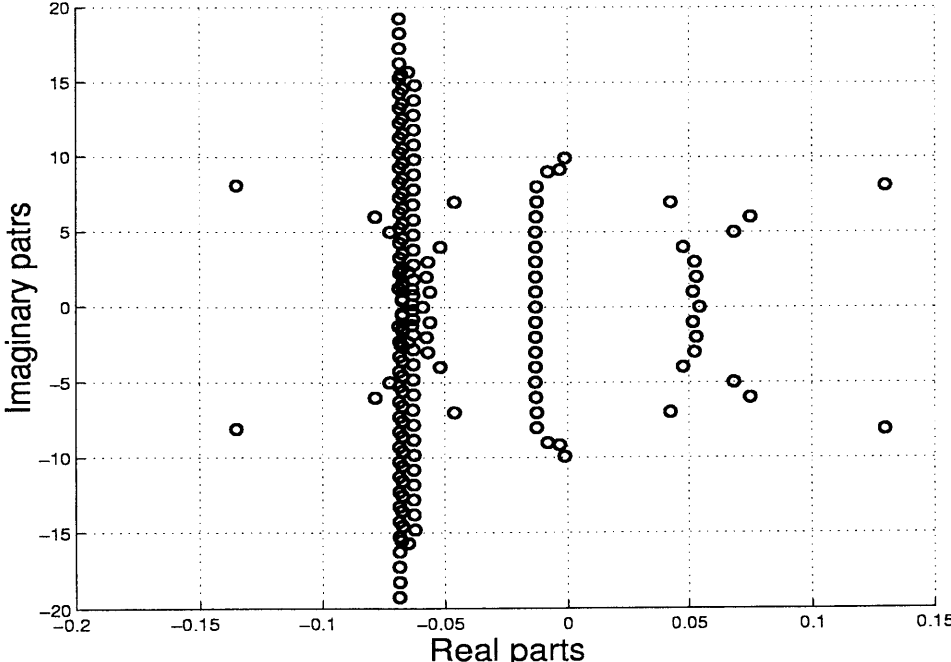


Figure 6.24: Eigenvalues for curve C_3 : One switch opened

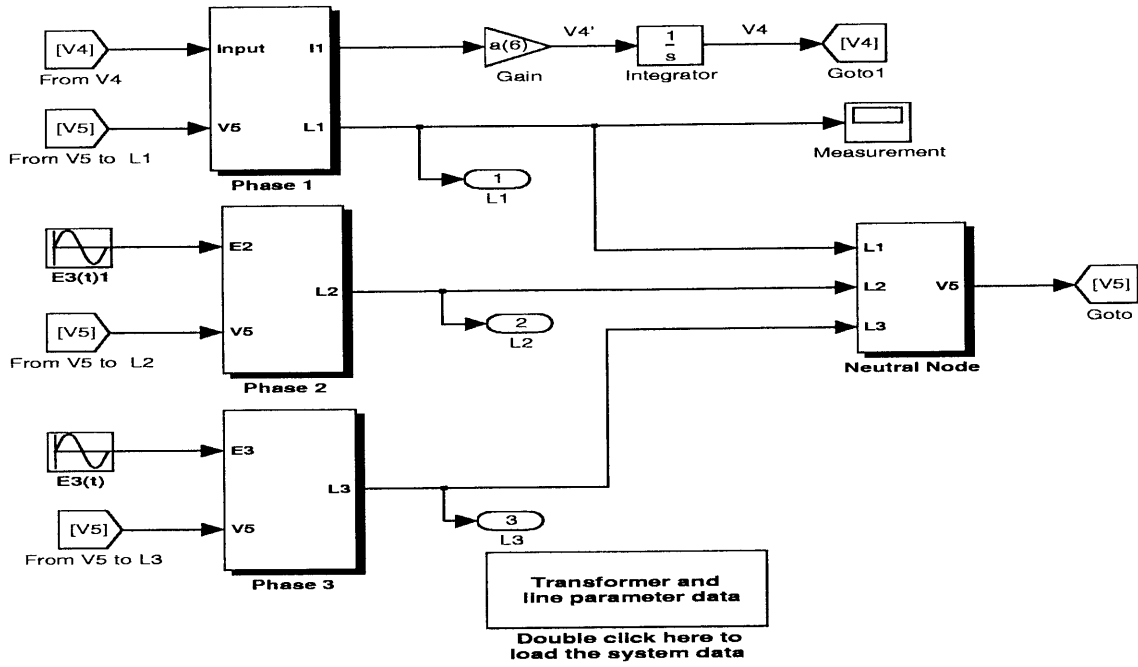


Figure 6.25: Simulink block diagram for the system: One switch opened

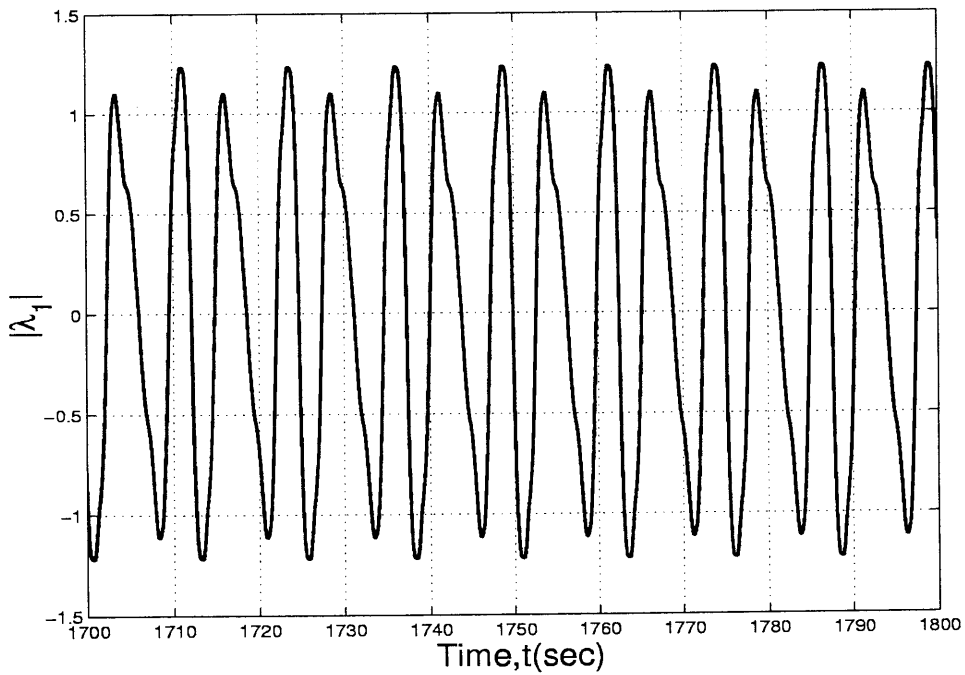
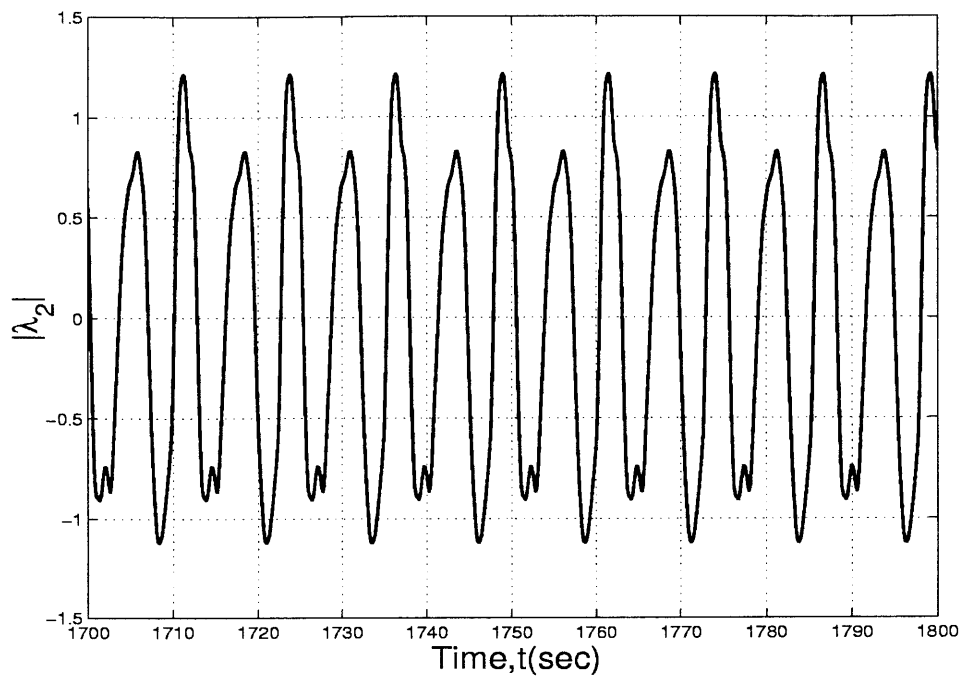
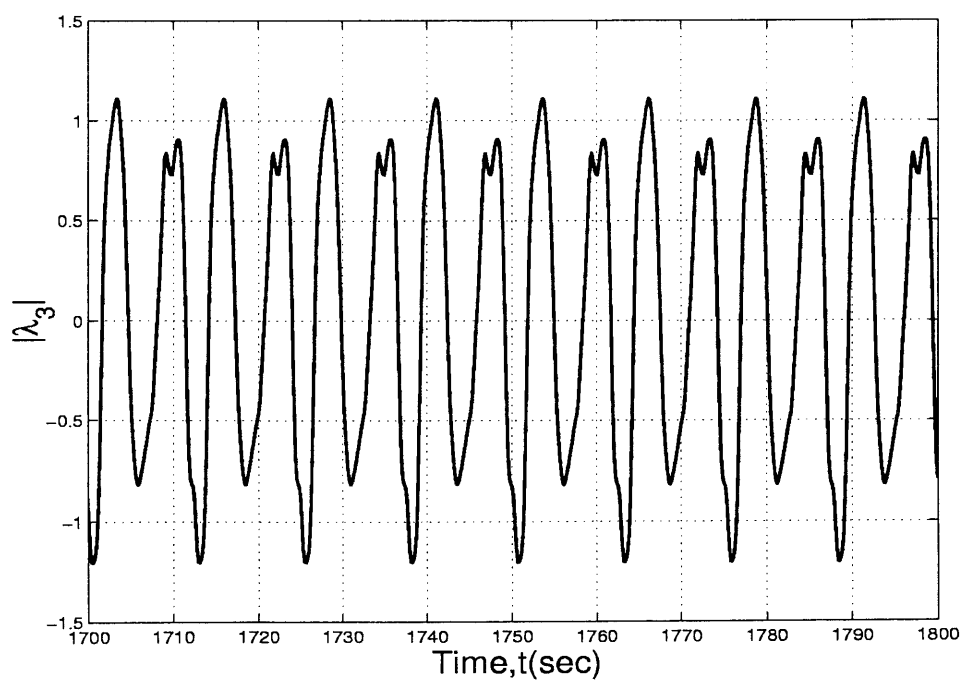


Figure 6.26: Time simulations for $\lambda_1(t)$: One switch opened

Figure 6.27: Time simulations for $\lambda_2(t)$: One switch openedFigure 6.28: Time simulations for $\lambda_3(t)$: One switch opened

6.4 Three-phase Ferroresonance: Two Switches Opened

Formulating the slowly varying system, we apply the generalized state space averaging methodology to the model defined in (2.20). The transformed system takes the following form

$$\dot{X}_{1,k} = -jk\omega X_{1,k} + a_1 X_{9,k} + a_2 F_{1,k} - a_3 X_{6,k} \quad (6.32a)$$

$$\dot{X}_{2,k} = -jk\omega X_{2,k} - a_1 X_{10,k} - a_2 F_{2,k} + a_3 X_{7,k} \quad (6.32b)$$

$$\dot{X}_{3,k} = -jk\omega X_{3,k} - a_1 X_{11,k} - a_2 F_{3,k} + a_3 X_{8,k} \quad (6.32c)$$

$$\dot{X}_{4,k} = -jk\omega X_{4,k} + a_6 X_{6,k} \quad (6.32d)$$

$$\dot{X}_{5,k} = -jk\omega X_{5,k} + a_6 X_{7,k} \quad (6.32e)$$

$$\dot{X}_{6,k} = -(jk\omega + a_5) X_{6,k} + a_4 X_{1,k} - a_4 X_{4,k} \quad (6.32f)$$

$$\dot{X}_{7,k} = -(jk\omega + a_5) X_{7,k} + a_4 X_{2,k} - a_4 X_{5,k} \quad (6.32g)$$

$$\dot{X}_{8,k} = -(jk\omega + a_5) X_{8,k} + a_4 G_{3,k} - a_4 X_{3,k} \quad (6.32h)$$

$$\dot{X}_{9,k} + \dot{X}_{11,k} = -jk\omega X_{9,k} - jk\omega X_{11,k} + X_{3,k} - X_{1,k} \quad (6.32i)$$

$$\dot{X}_{10,k} + \dot{X}_{11,k} = -jk\omega X_{10,k} - jk\omega X_{11,k} + X_{3,k} - X_{2,k} \quad (6.32j)$$

$$0 = K_1(X_{9,k} + X_{10,k} - X_{11,k}) + K_5(F_{1,k} + F_{2,k} - F_{3,k}) \quad (6.32k)$$

where $F_{1,k}$, $F_{2,k}$ and $F_{3,k}$ are defined as

$$F_{1,k}(X_{9,k}) = \sum_{m_1} \sum_{m_2} \sum_{m_3} \sum_{m_4} X_{9,m_1} X_{9,m_2} X_{9,m_3} X_{9,m_4} X_{9,k-m_1-m_2-m_3-m_4} \quad (6.33a)$$

$$F_{2,k}(X_{10,k}) = \sum_{m_1} \sum_{m_2} \sum_{m_3} \sum_{m_4} X_{10,m_1} X_{10,m_2} X_{10,m_3} X_{10,m_4} X_{10,k-m_1-m_2-m_3-m_4} \quad (6.33b)$$

$$F_{3,k}(X_{11,k}) = \sum_{m_1} \sum_{m_2} \sum_{m_3} \sum_{m_4} X_{11,m_1} X_{11,m_2} X_{11,m_3} X_{11,m_4} X_{11,k-m_1-m_2-m_3-m_4} \quad (6.33c)$$

$$G_{3,k} = \begin{cases} -\frac{M}{4} (1 \mp j\sqrt{3}) & \text{for } k = \pm 1 \\ 0 & \text{otherwise} \end{cases} \quad (6.33d)$$

$$-\infty \leq k \leq \infty \quad \text{and} \quad -\infty \leq m_i \leq \infty$$

and

$$X_{i,k} = \left[V_{1,k} \quad V_{2,k} \quad V_{3,k} \quad V_{4,k} \quad I_{1,k} \quad I_{2,k} \quad I_{3,k} \quad \Lambda_{1,k} \quad \Lambda_{2,k} \quad \Lambda_{3,k} \right]^T \quad i = 1, \dots, 10. \quad (6.34)$$

To compute the steady-state solutions of the system, we set the time derivatives in (6.32) to zero which gives the following nonlinear algebraic equations

$$-jk\omega X_{1,k} + a_1 X_{9,k} + a_2 F_{1,k} - a_3 X_{6,k} = 0 \quad (6.35a)$$

$$-jk\omega X_{2,k} - a_1 X_{10,k} - a_2 F_{2,k} + a_3 X_{7,k} = 0 \quad (6.35b)$$

$$-jk\omega X_{3,k} - a_1 X_{11,k} - a_2 F_{3,k} + a_3 X_{8,k} = 0 \quad (6.35c)$$

$$-jk\omega X_{4,k} + a_6 X_{6,k} = 0 \quad (6.35d)$$

$$-jk\omega X_{5,k} + a_6 X_{7,k} = 0 \quad (6.35e)$$

$$-(jk\omega + a_5) X_{6,k} + a_4 X_{1,k} - a_4 X_{4,k} = 0 \quad (6.35f)$$

$$-(jk\omega + a_5) X_{7,k} + a_4 X_{2,k} - a_4 X_{5,k} = 0 \quad (6.35g)$$

$$-(jk\omega + a_5) X_{8,k} + a_4 G_{3,k} - a_4 X_{3,k} = 0 \quad (6.35h)$$

$$-jk\omega X_{9,k} - jk\omega X_{11,k} + X_{3,k} - X_{1,k} = 0 \quad (6.35i)$$

$$-jk\omega X_{10,k} - jk\omega X_{11,k} + X_{3,k} - X_{2,k} = 0 \quad (6.35j)$$

$$K_1(X_{9,k} + X_{10,k} - X_{11,k}) + K_5(F_{1,k} + F_{2,k} - F_{3,k}) = 0 \quad (6.35k)$$

In order to examine the existence of periodic solutions of the system defined (2.20), we investigate the steady-state solutions of the transformed system. Here we are only investigating existence of periodic solutions of the system (6.15).

6.4.1 Harmonic Periodic Solutions

To investigate periodic harmonic steady-state solutions of the system (2.20), we vary two system parameters, the length of transmission line and the magnitude of the input voltage M . Fixing the magnitude of the input voltage to 1.0 pu, we vary the transmission line length from 0 to 80 miles. Figure 6.29 shows the magnitude of the flux of phase one versus the length of the transmission line. From this Figure, when the transmission line length approaches 41 miles, the system is vulnerable to ferroresonance for small disturbances or changes of the magnitude of the input voltage.

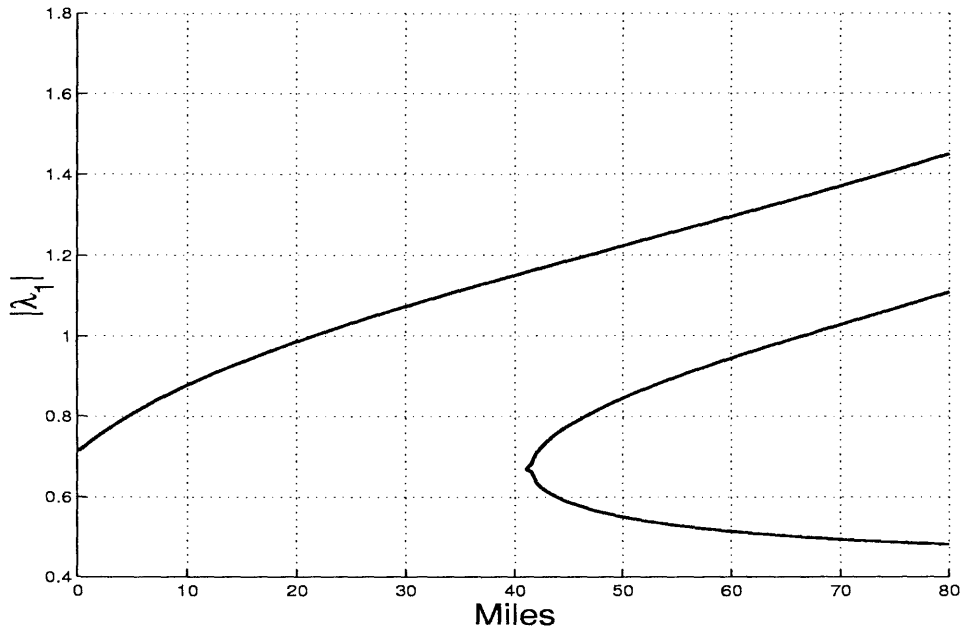


Figure 6.29: Steady-state harmonic solutions for $M = 1.0$ pu: Two switches opened

Fixing the length of the transmission line to 60 miles, we vary the magnitude of the input voltage of the generation from 0 to 1.7 pu. Figure 6.30 depicts the magnitude of the flux of phase one versus the magnitude of the input voltage.

6.4.2 Stability of Harmonic Periodic Solutions

To ascertain the stability of each steady-state solution of the system (6.32), we need to formulate the variational system which will give the stability criterion of the system around that operating point. Since the system defined in (6.32) is a differential algebraic system, we need to simplify the system dynamics in order to compute the eigenvalues of the system.

Since the derivations for the reduced model is similar to the one we showed in Section 6.2, we put all the results in Appendix A.2.

Hence, the steady-state harmonic solutions of the system were computed and the corresponding eigenvalues of the system were examined. Figures 6.31, 6.32, and 6.33 show the eigenvalues of the system for $M = 1.0$ pu with a 60 mile of transmission line length. In the figure, curves \mathcal{C}_1 and \mathcal{C}_3 correspond to stable steady-state solutions while curve \mathcal{C}_2 is an

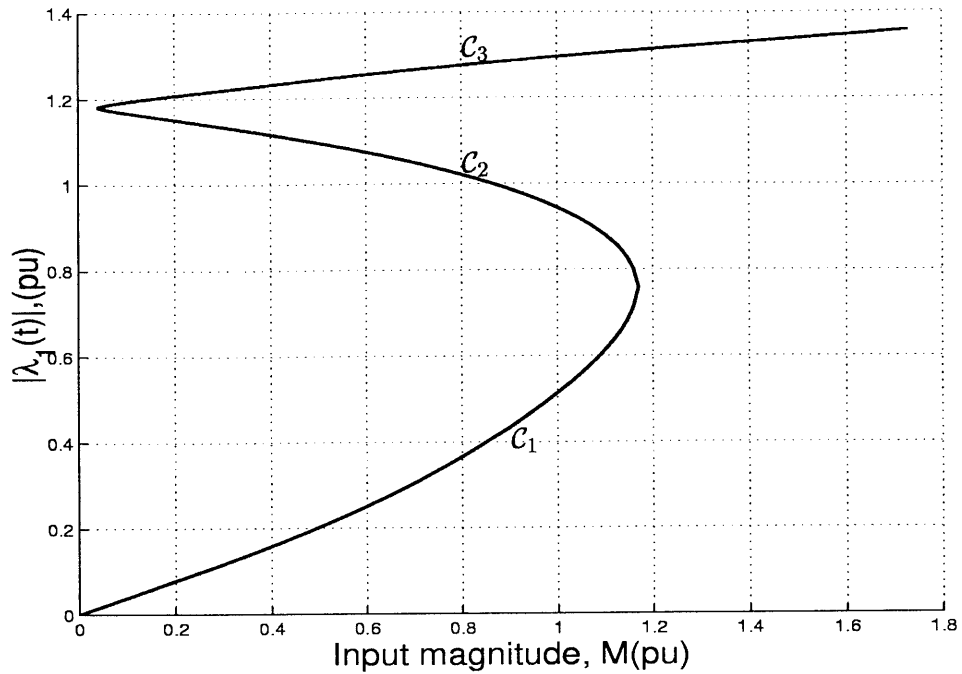
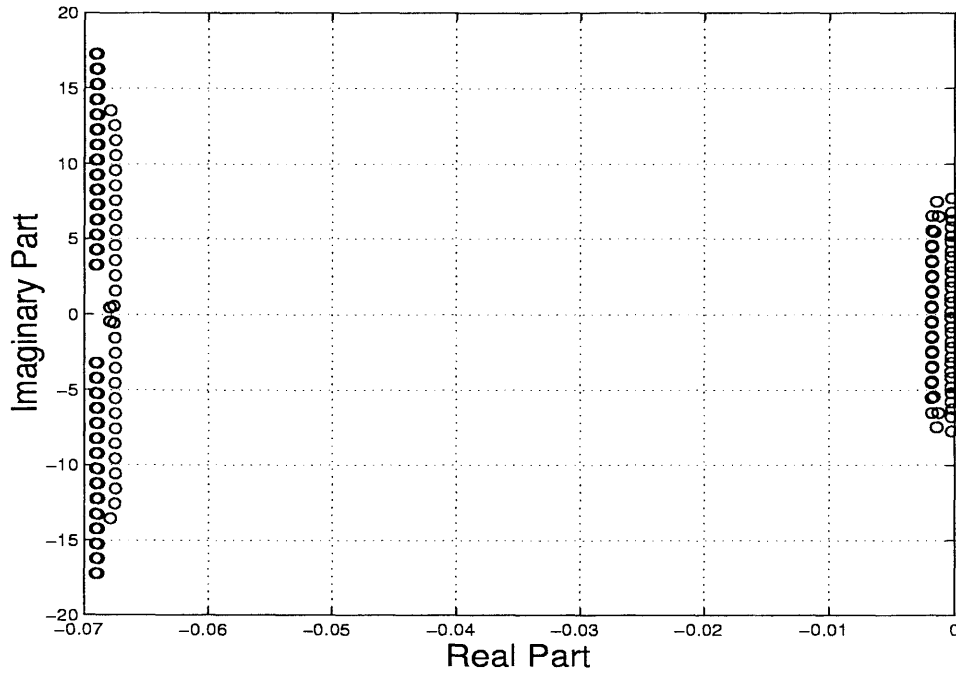
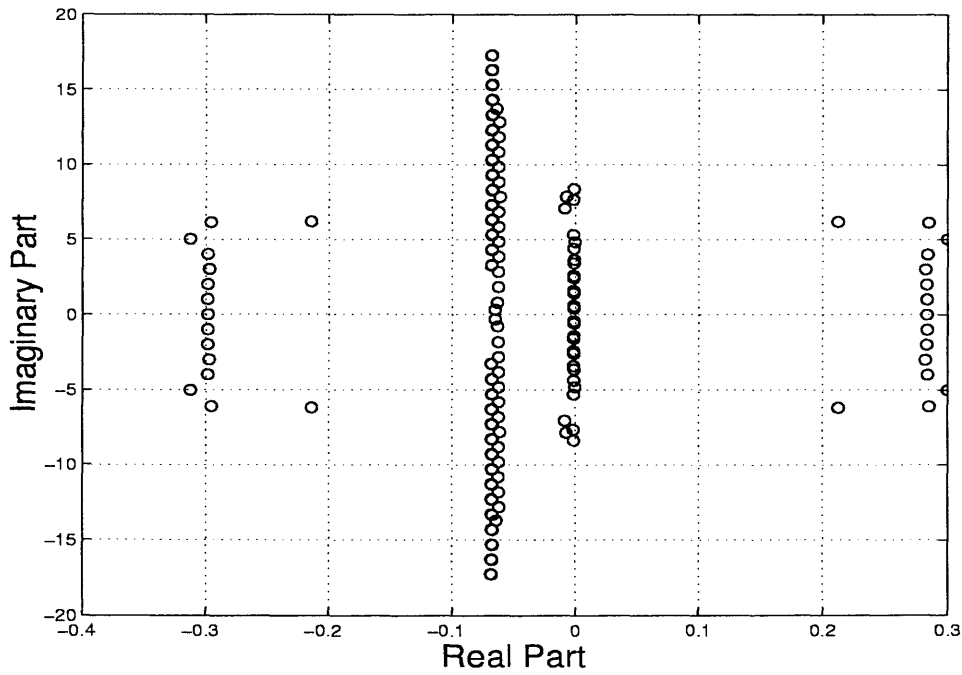


Figure 6.30: Steady-state solutions for 60 mile transmission line length: Two switches opened

unstable steady-state solution.

For further verification, a time simulation were performed using Matlab. Figure 6.34 shows Simulink input file. Figures 6.35, 6.36, and 6.37 depict the flux linkages $\lambda_1(t)$, $\lambda_2(t)$, and $\lambda_3(t)$ of the transformer core. In these simulations, the transmission line length is 60 miles and the magnitude of the input voltage M is 1.0 pu.

Figure 6.31: Eigenvalues for curve C_1 : Two switches openedFigure 6.32: Eigenvalues for curve C_2 : Two switches opened

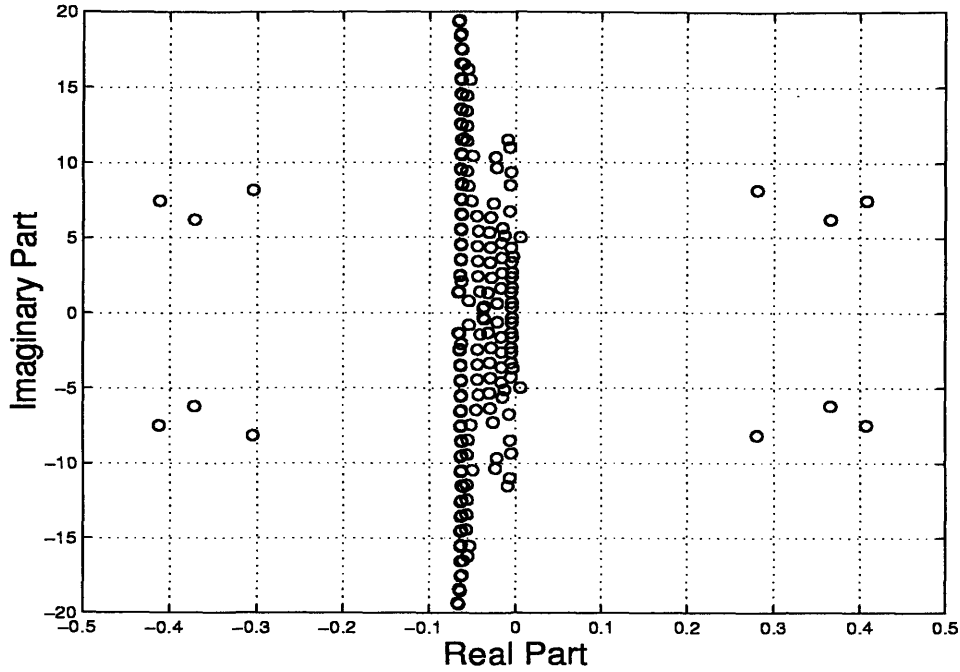


Figure 6.33: Eigenvalues for curve C_3 : Two switches opened

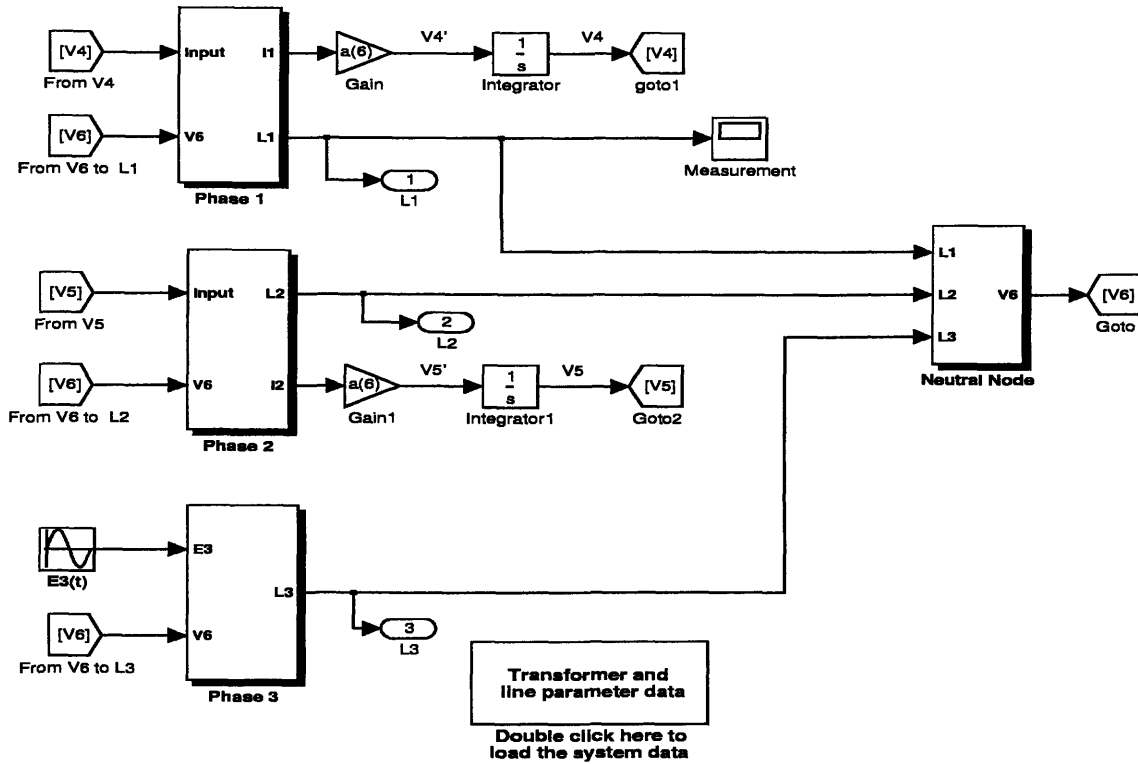


Figure 6.34: System time simulations: Two switches opened

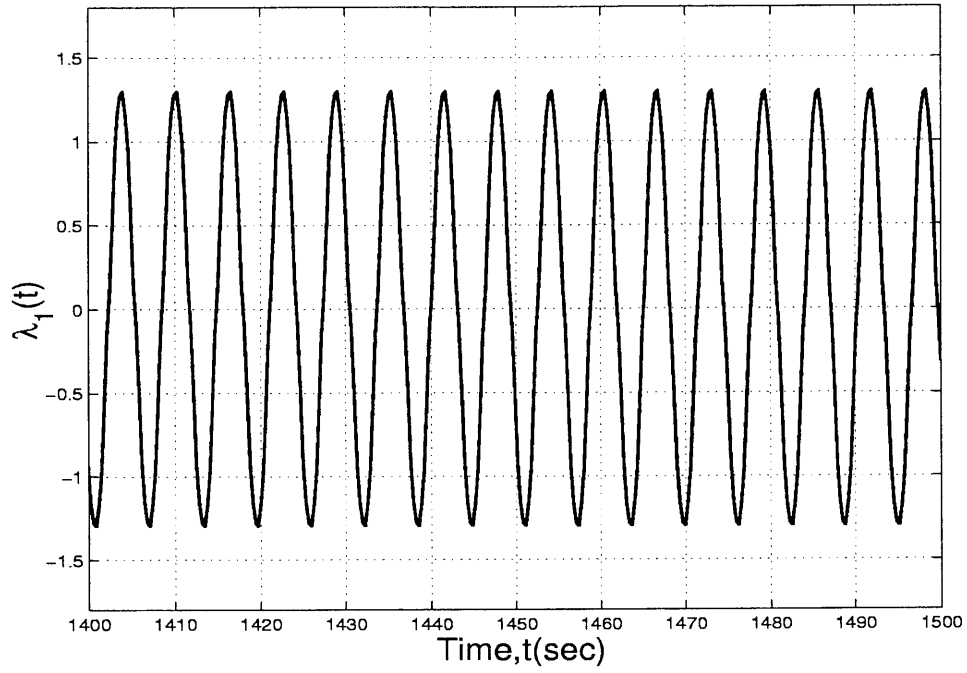


Figure 6.35: Time simulations for $\lambda_1(t)$: Two switches opened

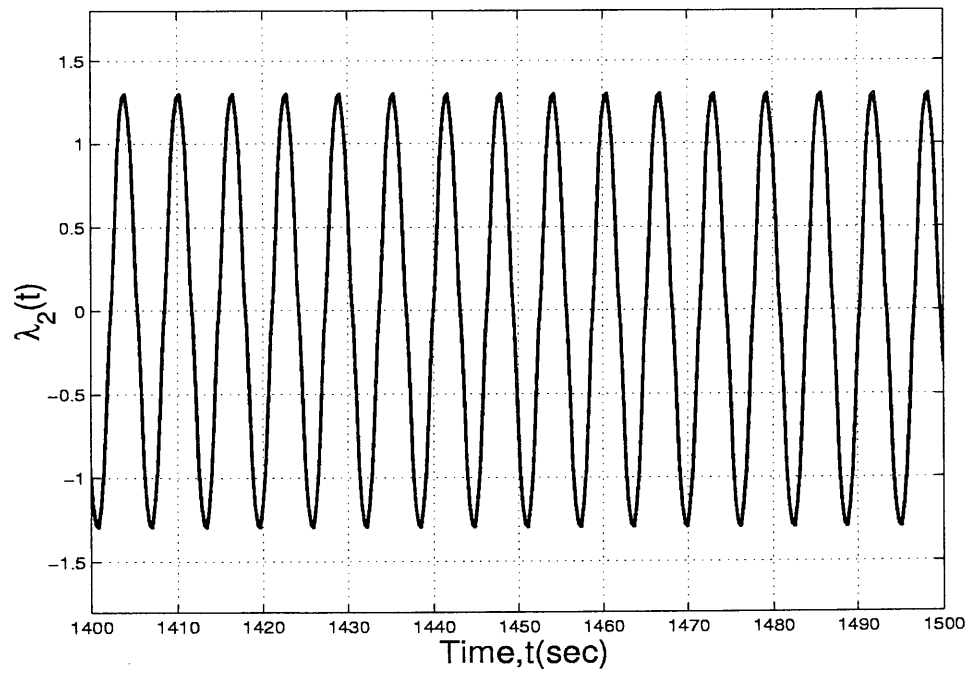


Figure 6.36: Time simulations for $\lambda_2(t)$: Two switches opened

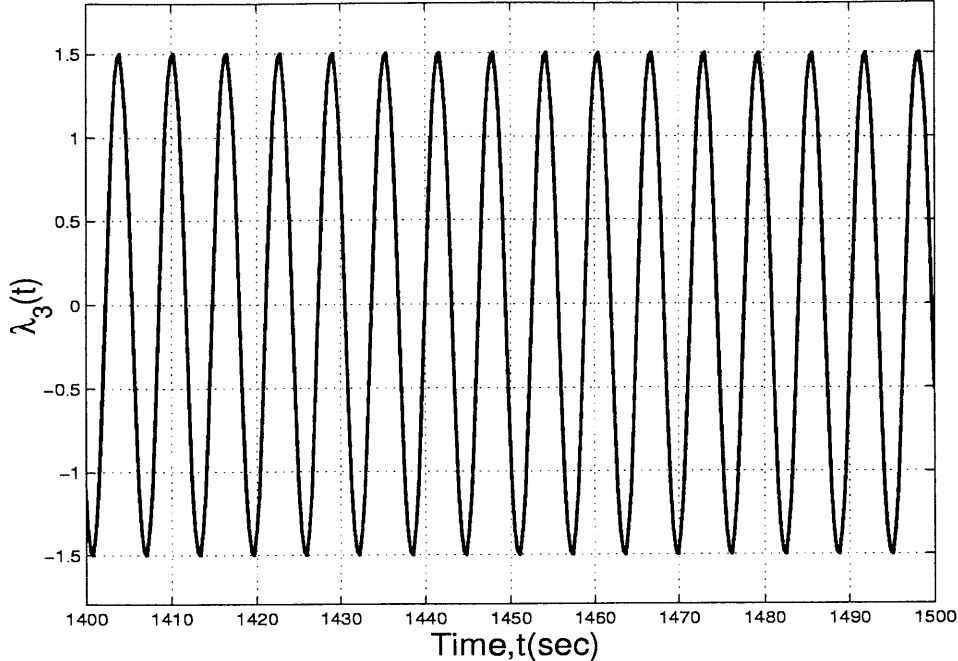


Figure 6.37: Time simulations for $\lambda_3(t)$: Two switches opened

6.5 Switching Simulations

To further understand the effect of switching, we simulated the system incorporating the switching effects. In order to simulate the switching characteristics, we model the switching devices with timers and switches using Simulink library parts. Figure 6.38 shows the Simulink model. To capture the three stable steady-state solutions \mathcal{C}_1 , \mathcal{C}_4 , and \mathcal{C}_5 , we open the switch S_1 , at different times, particularly at $t = 800$ sec, $t = 801$ sec, and $t = 805$ sec.

For the first case, we start the system simulation at $t = 0$ sec, and after 800 sec we turn the first switch S_1 off. Figures 6.39, 6.40, and 6.41 depict the time simulations of $\lambda_1(t)$, $\lambda_2(t)$, and $\lambda_3(t)$, respectively. This solution is on the solution curve \mathcal{C}_4 for $M = 1.0$ with a 60 mile transmission line length. However, the amplitudes of the time simulations and steady-state solution curve \mathcal{C}_4 do not agree since the amplitude of the time simulation is 1.07 pu and the solution on curve \mathcal{C}_4 at $M = 1.0$ pu is 0.97 pu. The solution curve \mathcal{C}_4 was computed by considering harmonics only up to fifth harmonic. When the number of harmonics was increased to nine the two solutions agreed.

Next, we turn S_1 off at $t = 801$ sec. Figures 6.42, 6.43, and 6.44 show the time

responses of $\lambda_1(t)$, $\lambda_2(t)$, and $\lambda_3(t)$ respectively. In this case the solution is on solution curve C_1 . Finally, we turn S_1 off at $t = 805$ sec. The time simulations of the system due to this switching are shown in Figs 6.45, 6.46, and 6.47. From the figures it is clear that this solution is on curve C_5 . Hence, the three time simulations agree with the solutions derived from the analysis in Section 6.3.

Similarly, to simulate two switching conditions, we open S_1 at $t = 800$ sec and then open S_2 at $t = 1500$ sec. Figures 6.48, 6.49, and 6.50 show the time simulations of $\lambda_1(t)$, $\lambda_2(t)$, and $\lambda_3(t)$. For the final case, we open simultaneously both S_1 and S_2 at $t = 800$ sec. Figures 6.51, 6.52, and 6.53 show the time simulation responses of $\lambda_1(t)$, $\lambda_2(t)$, and $\lambda_3(t)$. The results found in these two simulations agree with the solutions derived from the analysis in Section 6.4.

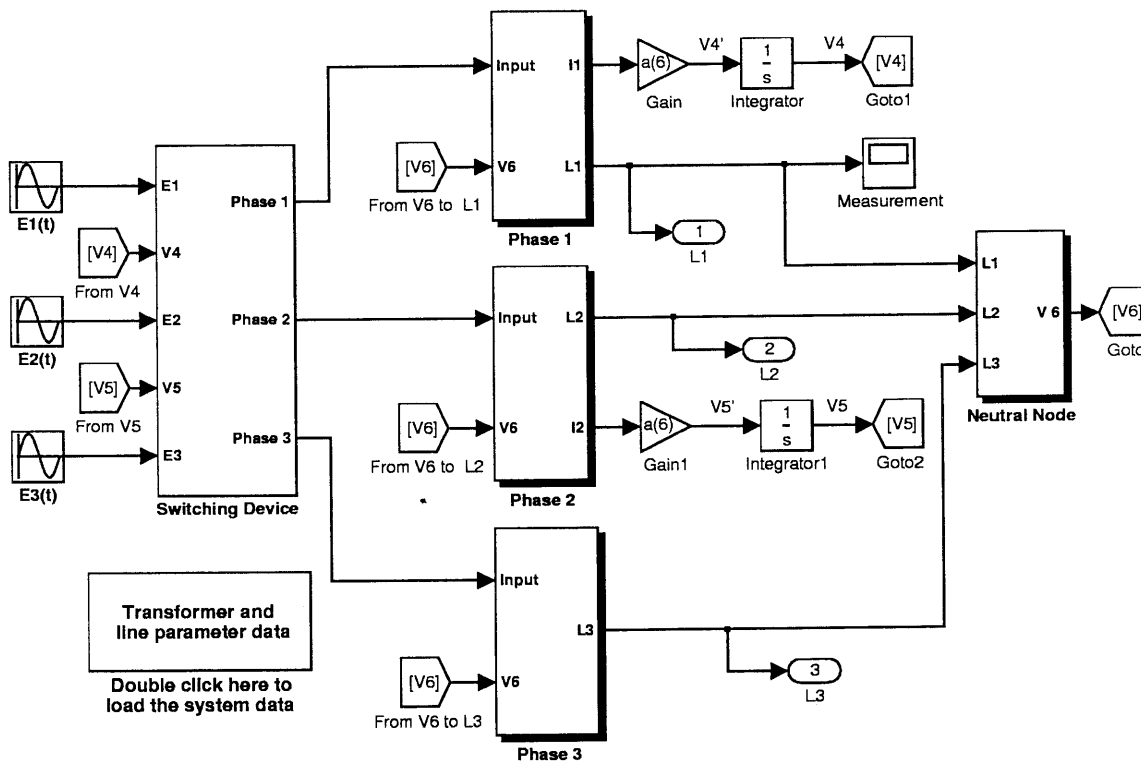
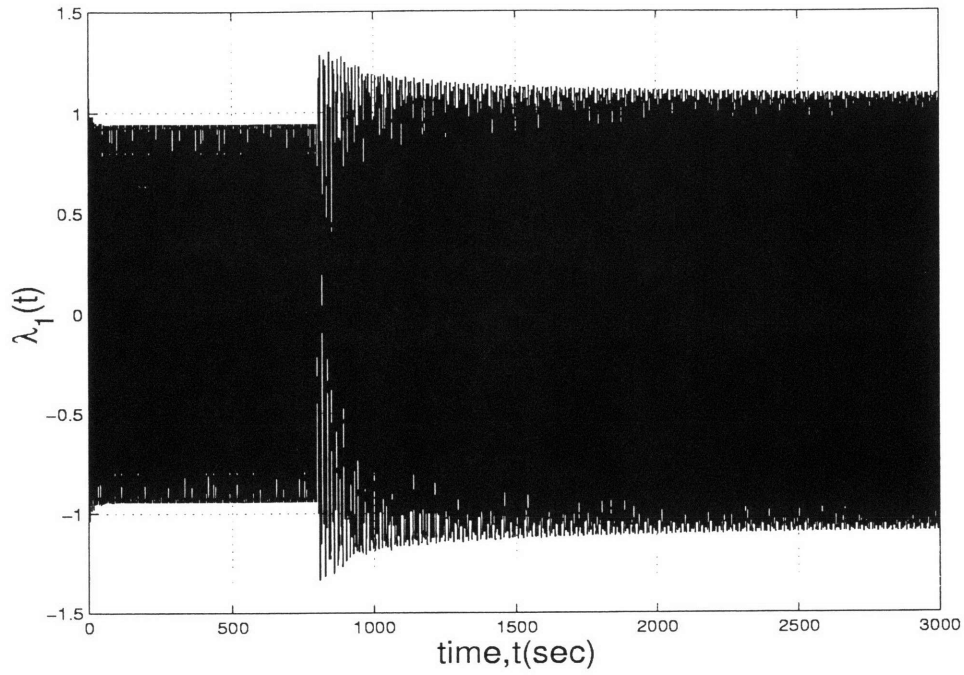
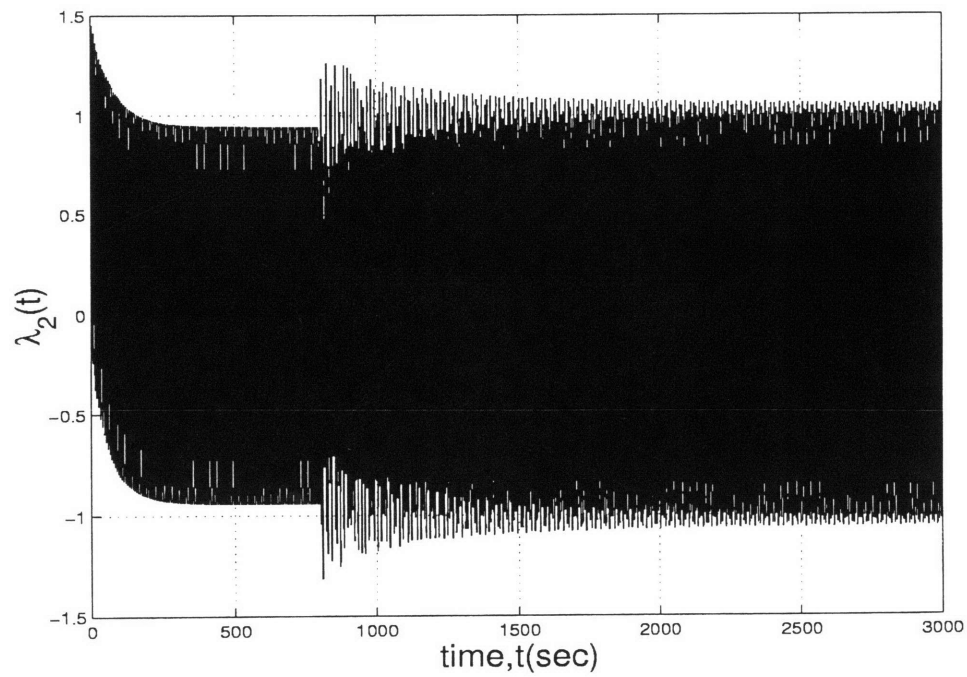


Figure 6.38: Simulink block diagram for the system: Switching simulations

Figure 6.39: Time simulations for $\lambda_1(t)$: S_1 opened solution oneFigure 6.40: Time simulations for $\lambda_2(t)$: S_1 opened solution one

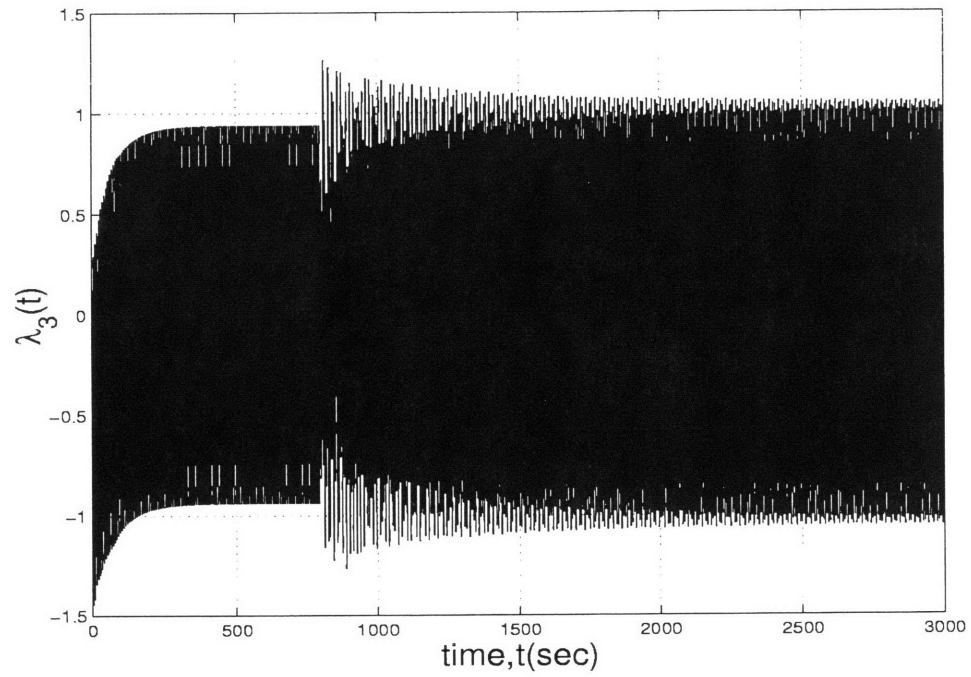


Figure 6.41: Time simulations for $\lambda_3(t)$: S_1 opened solution one

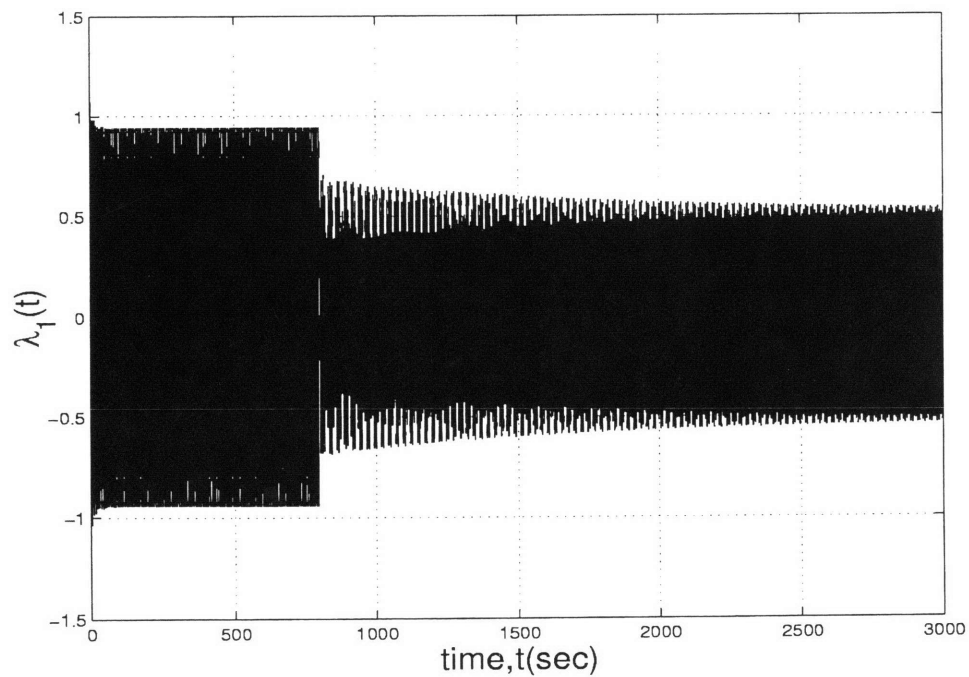
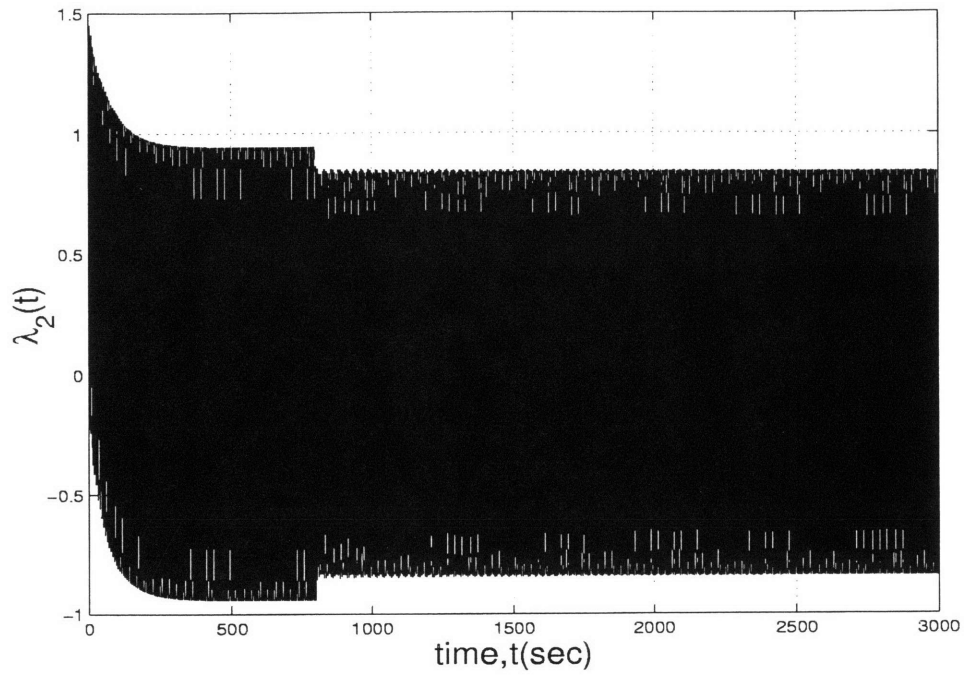
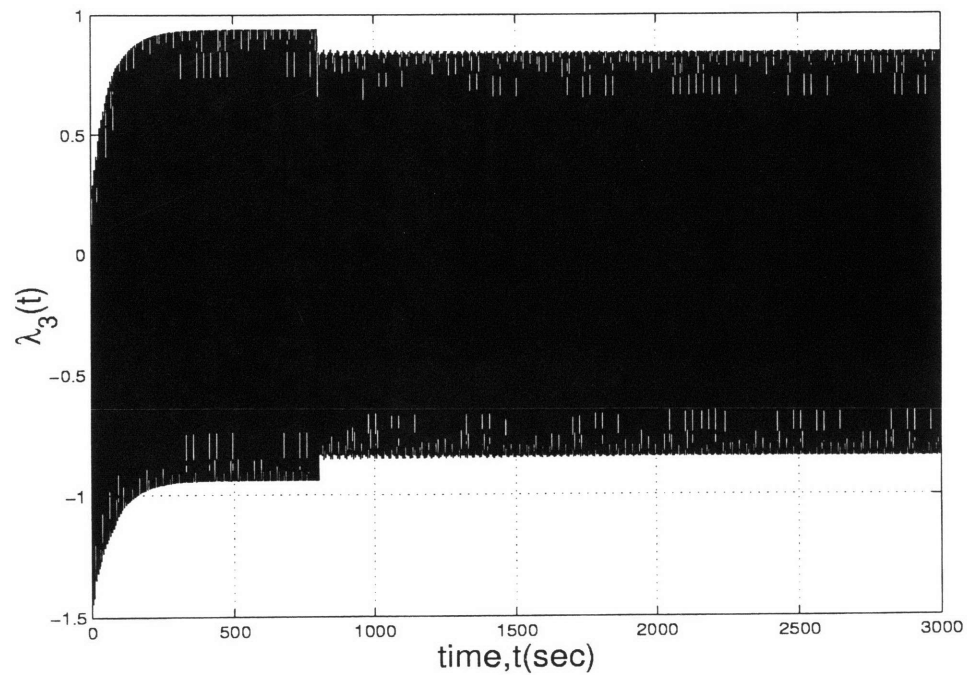


Figure 6.42: Time simulations for $\lambda_1(t)$: S_1 opened solution Two

Figure 6.43: Time simulations for $\lambda_2(t)$: S_1 opened solution TwoFigure 6.44: Time simulations for $\lambda_3(t)$: S_1 opened solution Two

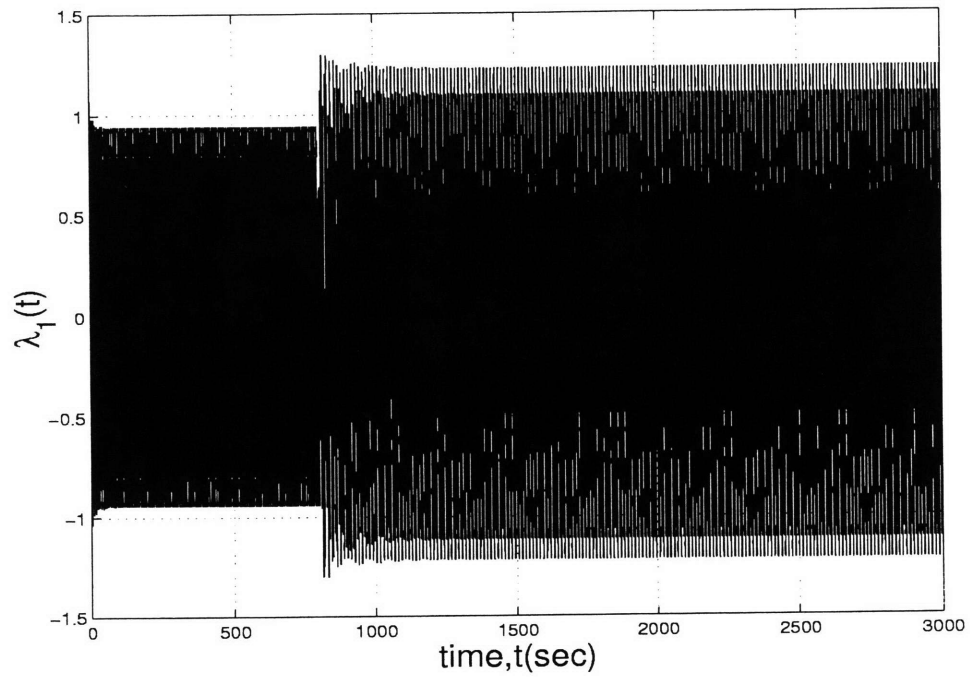


Figure 6.45: Time simulations for $\lambda_1(t)$: S_1 opened solution Three

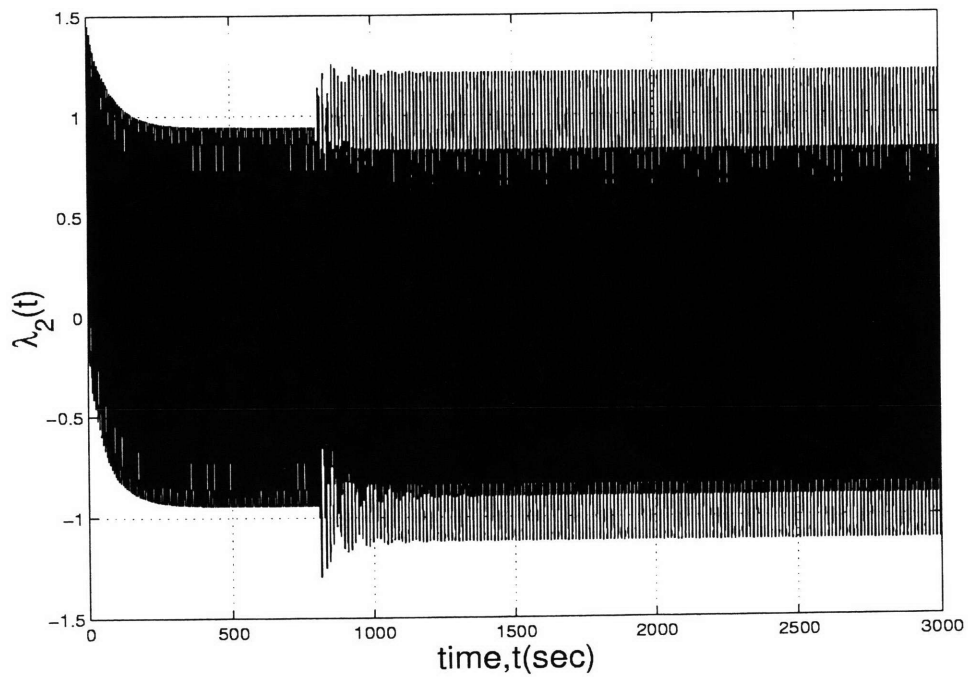


Figure 6.46: Time simulations for $\lambda_2(t)$: S_1 opened solution Three

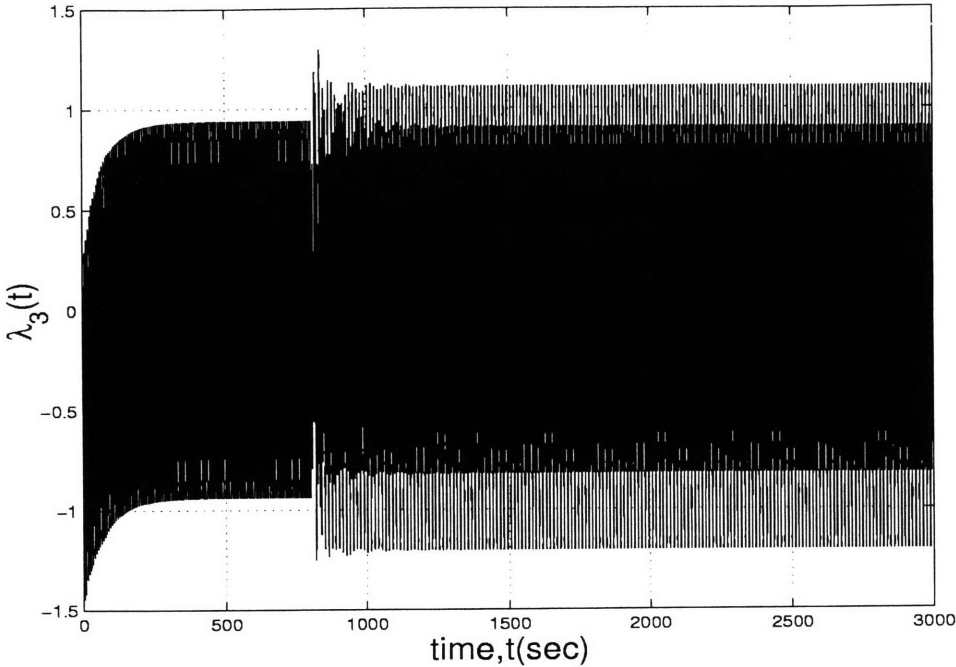


Figure 6.47: Time simulations for $\lambda_3(t)$: S_1 opened solution three

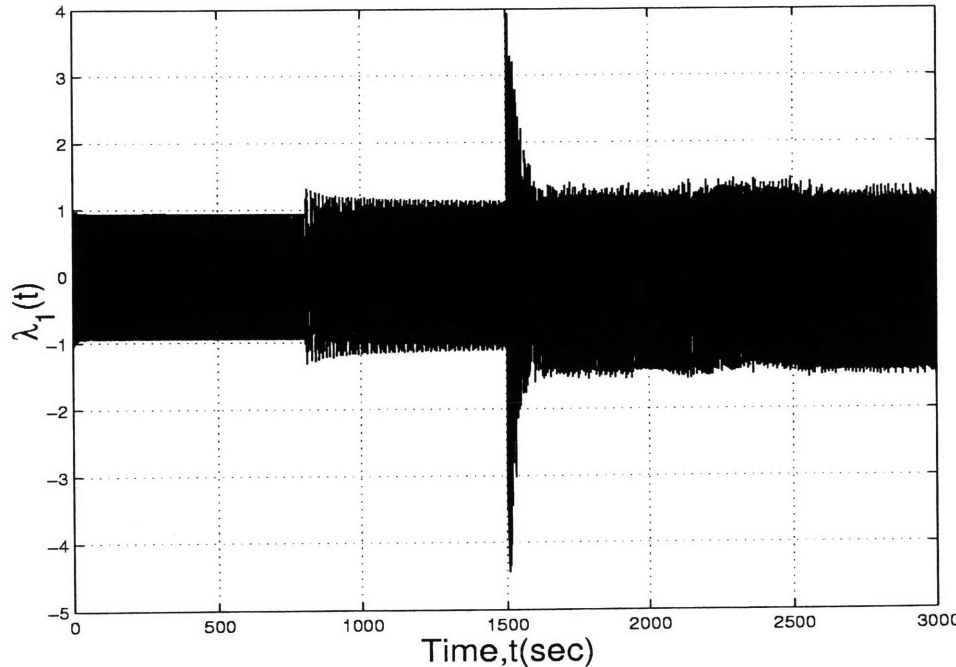


Figure 6.48: Time simulations for $\lambda_1(t)$: S_1 and S_2 opened solution case one

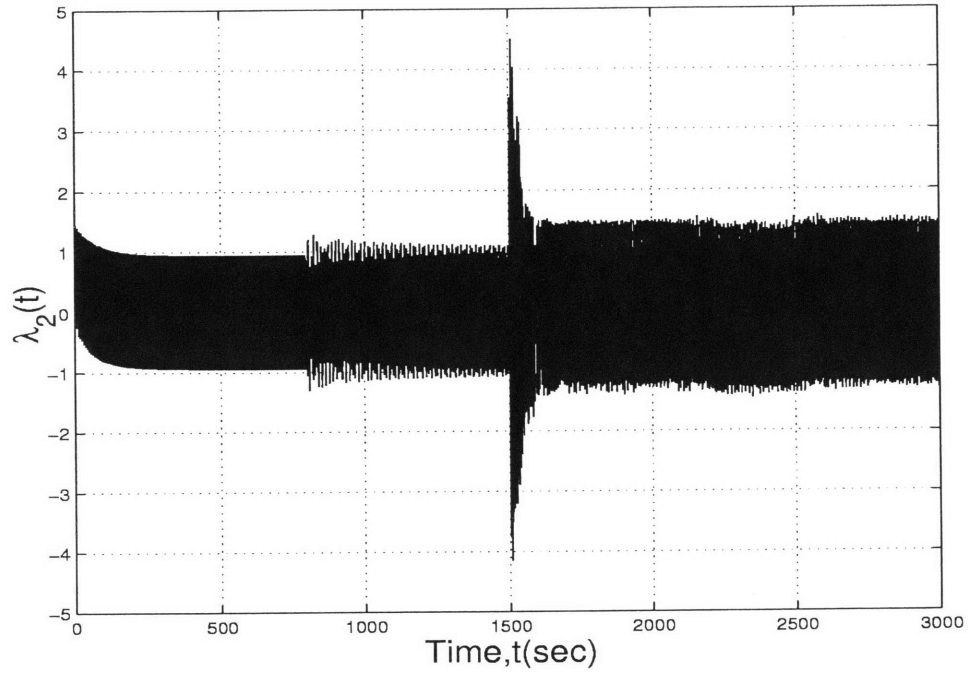


Figure 6.49: Time simulations for $\lambda_2(t)$: S_1 and S_2 opened solution case one

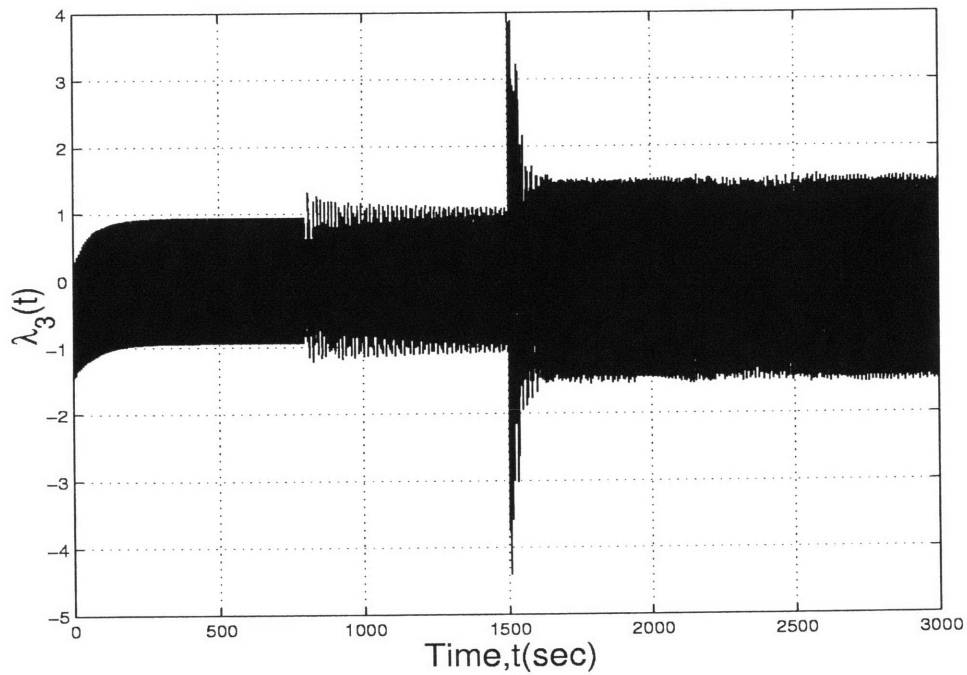
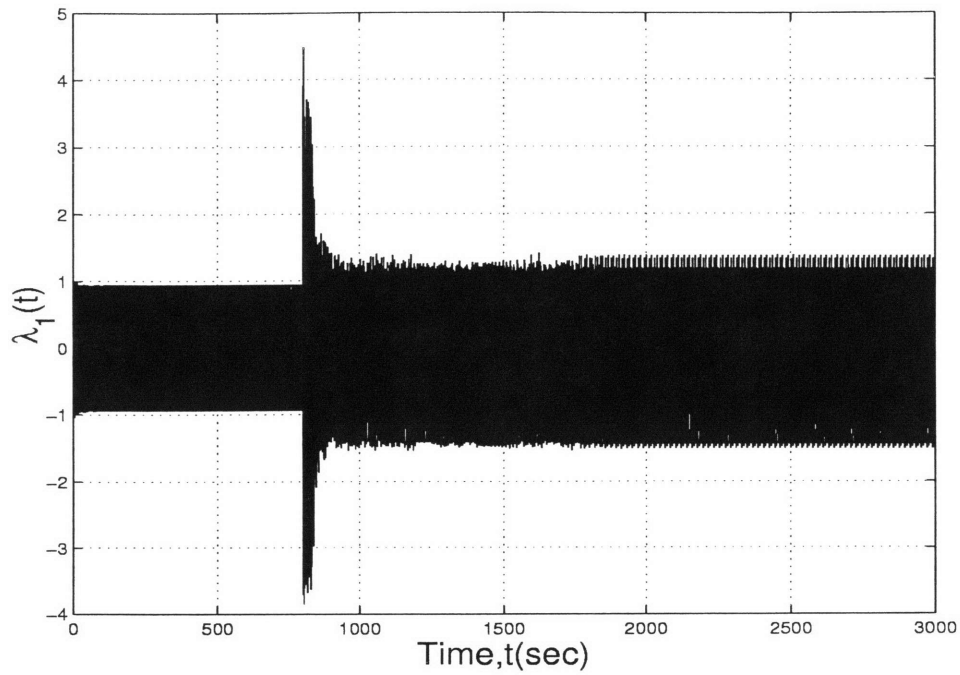
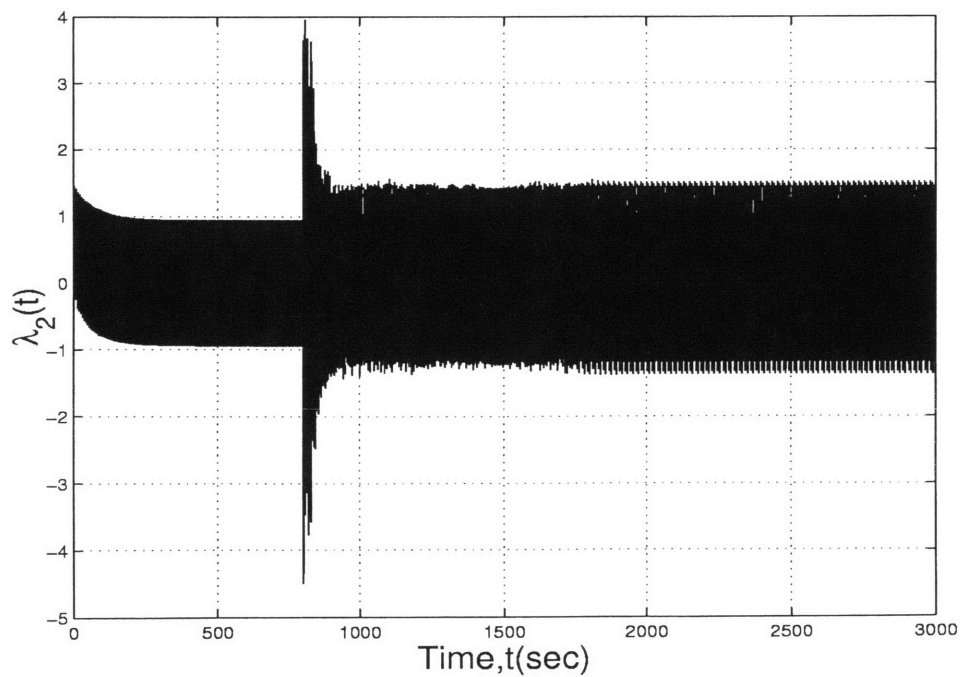


Figure 6.50: Time simulations for $\lambda_3(t)$: S_1 and S_2 solution case one

Figure 6.51: Time simulations for $\lambda_1(t)$: S_1 and S_2 opened solution case twoFigure 6.52: Time simulations for $\lambda_2(t)$: S_1 and S_2 opened solution case two

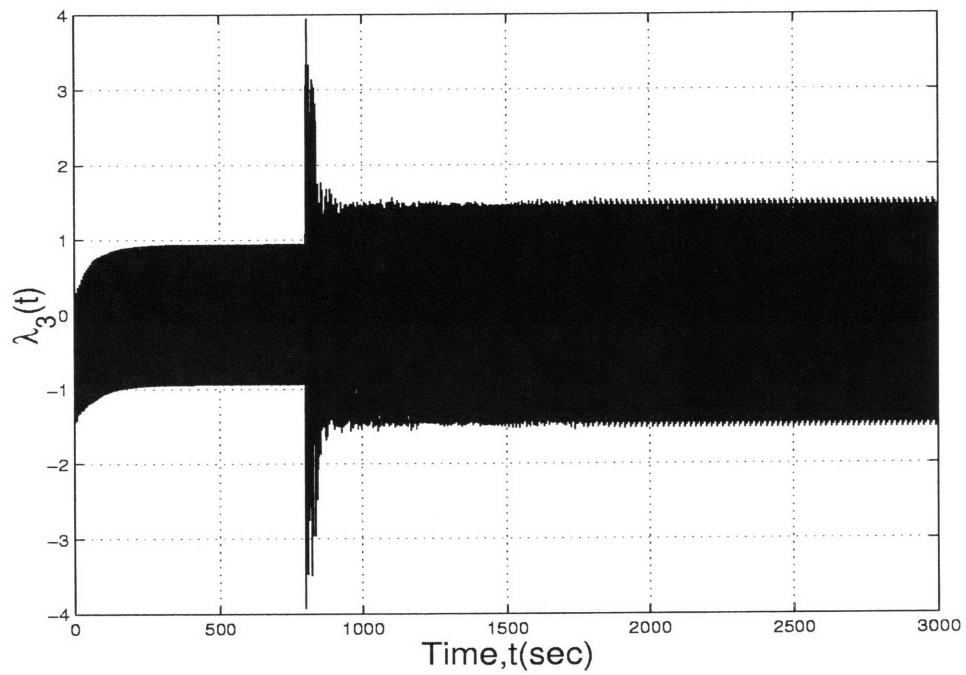


Figure 6.53: Time simulations for $\lambda_3(t)$: S_1 and S_2 opened solution case two

Chapter 7

Concluding Remarks

7.1 Summary

In Chapter 1, the historical background of ferroresonance was introduced. In that chapter we also highlighted the two approaches used to solve the ferroresonance problem: experimental investigations and theoretical investigations. The two general models related to ferroresonance, single-phase and three-phase ferroresonance models, were introduced in Chapter 2. For the single-phase model, we developed a full model of the single-phase transformer including the generation and the transmission line parameters. For the three-phase models, we developed three models: all circuit breakers closed, one conductor opened and two conductors opened. The models of these systems were differential-algebraic equations (DAE).

The theory for the synchronous incremental-input describing function was presented in Chapter 3. An example was used to prove the theory. This theory was also applied to a single-phase transformer. This example shows that for different input magnitudes and line parameters the system can have one solution or multiple solutions. However, a flaw existed in this theory as previously developed.

To fix the flaw in the theory, we first reviewed the Nyquist criterion. In that chapter we showed that the necessary and sufficient condition for stability of a loop-gain is that no intersections between the $(-1, 0)$ point and the frequency response loci of the loop-gain exist for all values of ω and for all non-negative values of σ . An example was introduced to illustrate the flaw and show how the modified incremental-input describing function can determine the stability of general systems. Time simulations were performed to verify these results.

In Chapter 4, the theory of the generalized state-space averaging (GSSA) methodology was introduced. Harmonic and subharmonic models were presented using the GSSA method. An example was illustrated to show the mechanics of GSSA for both harmonic and subharmonic solutions. Furthermore, existence and stability of harmonic and subharmonic solutions were addressed. In the chapter, we proposed theorems which guarantee the stability of harmonic and subharmonic solutions of the system. The relation between the

stability of GSSA model and the full model was also shown.

The Duffing's oscillator was used as benchmark test for GSSA. In Chapter 5 Floquet theory and the Poincaré maps in particular were used to investigate the stability issues. Both harmonic and subharmonic steady-state solutions were considered. In the Chapter, We showed that the fundamental eigenvalues of GSSA and Floquet exponents are equal. We also pointed out the relationship between Floquet multipliers and the eigenvalues of the Poincaré maps.

In Chapter 6, the generalized state-space averaging method was applied to ferroresonance models: single-phase models and three-phase models. In the single-phase models, we computed the harmonic solutions of the system by fixing all parameters and varying the inductance L of the transmission lines. Similarly, we fixed all parameters and varied the magnitude of the input voltage M . The stability of these steady-state solutions was examined. The solution bifurcations were also discussed in the chapter particularly, saddle-node bifurcations. Furthermore, issues of robustness of the steady-state solution of the system to a model possible error were addressed. In the chapter, we also point out how the theoretical results agreed with the time simulations of the systems.

We also showed existence of five harmonic steady-state solutions for the three-phase opened one conductor model: three stable and two unstable solutions. These stable solutions were also verified by simulating the full system using Matlab.

Finally, this theory can be applied to different power system network topologies. In the design process for a new power system network, one can use this theory to study the conditions under which the system could experience a ferroresonance problem depending on system parameters, such as, transmission line length or the amplitude of the input voltage.

In existing power system networks, one can also use this theory to study the ferroresonance problem, compute critical system parameter values and propose ways to mitigate the problem. To eliminate one or two opened conductors during a system switching, one can use circuit breakers that can open the three-phases simultaneously. This approach eliminates the path through which the energy flows back and forth, i.e., between the transmission line capacitance and the nonlinear inductance of the transformer core. The choice of the power transformers can also play an important role. The transformer losses such as eddy current loss and hysteresis losses can damp the energy that oscillating between the capacitor and nonlinear inductor. By modifying the transformer core and adding tertiary windings, one can also mitigate the problem. Furthermore, one can control the loading of the transformer

using an automatic monitoring system. If the load drops to some critical value, a local loading can be initiated which will damp the oscillations. Remotely controlled flexible alternating current transmission systems (FACTS) can be used to regulate the transmission line impedance which in turn can reduce the transmission line capacitance from the critical value since the critical capacitance is known.

7.2 Suggestions for Future Work

The purpose of this thesis was to solve the ferroresonance problem both single-phase and three-phase models using the generalized state-space averaging method. Although the objectives of the thesis were accomplished, there are more tasks that need to be completed: improvement of the transformer core models, simplification of the DAE model, modification of the truncation scheme to improve the approximation of the matrix A , computation of subharmonic steady-state solutions, and improvements to the numerical solutions.

In the frequency domain approach, the synchronous incremental-input describing function needs improvement particularly, for multi-input multi-output systems.

7.2.1 Other Models for the Transformer Core

Although, in general, there are three model representations for the nonlinearity of the transformer cores, odd polynomial representations, pseudo-nonlinear core model with hysteresis, and true-nonlinear core model with hysteresis, in this thesis, we only investigated the odd polynomial model. To gain more insight into the characteristics of the ferroresonance problem, investigations of dynamic models of the transformer core are required; the model we used in this thesis was a static model.

7.2.2 Simplification of the System Model (DAE)

In Chapter 2, we used ABC coordinates to compute the model of the network. The nonlinear differential-algebraic equations were coupled which increases the complexity of the model. Other coordinates may reduce this complexity. The positive, negative, and zero sequence coordinates may simplify this problem [82,83]. This approach gives three separate uncoupled models which in turn may simplify the analysis of the system.

7.2.3 MIMO Synchronous Incremental-Input Describing Function

In Chapter 3, we showed how the synchronous incremental-input describing function is easy to apply to single-phase systems to assess the stability of a steady-state solution. A large number of practicing engineers use this method due to its simplicity. One way to increase the potential of this graphical method is to derive the multi-input multi-output synchronous incremental-input describing function using the Nyquist multi-input multi-output (MIMO) stability criterion. It could then be used to investigate the stability of steady-state solutions for three-phase ferroresonance models. Furthermore, to improve the approximation of the steady-state solutions, application of the describing function matrix is required.

7.2.4 Methods to Approximate Matrix A

If the matrix A defined in (4.27) is truncated, the eigenvalues of the transformed system spread out at the end points as shown in Fig. 7.1 where the truncation level is $k = \pm 35$. Decoupled harmonics induce these spreading eigenvalues. If we take all the harmonics, the eigenvalues will line up along the fundamental eigenvalues of the system.

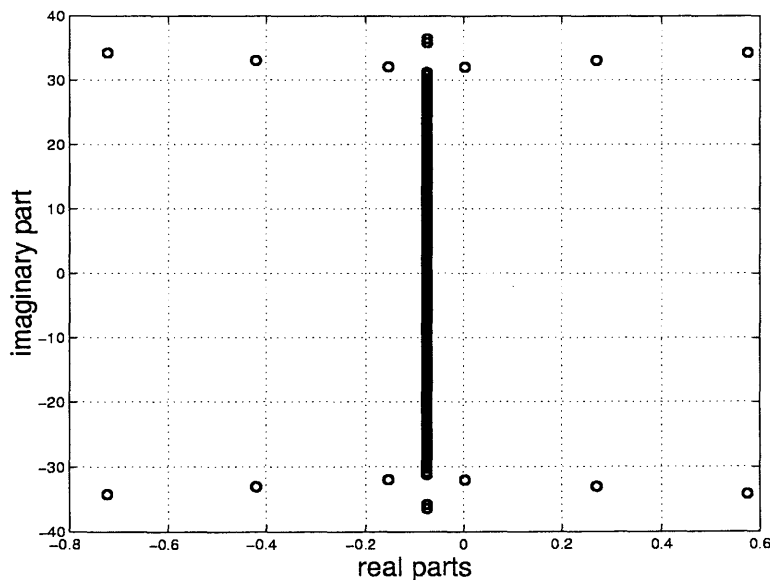


Figure 7.1: Eigenvalues of approximated system: $k = \pm 35$

If the boundaries of the matrix A are smoothed using smoothing filters, such as

moving average filters, the incorrect eigenvalues will vanish, and the eigenvalues of A_0 , the approximated matrix, will be a proper subset of the eigenvalues of A . These results were investigated by experimental trials. A rigorous mathematical justification is required. This approximation will allow us to simulate the generalized state-space averaging model. At the present time one cannot simulate this system since the eigenvalues of the end points spread out which in turn can cause some of them to be unstable as shown in Fig. 7.1.

7.2.5 Investigations of Subharmonic Steady-state Solutions

To complete the other portion of the ferroresonance problem, computations of subharmonic steady-state solutions are required. Here, in this thesis, we only focused on the harmonic solutions which in general are of the most interest.

7.2.6 Improvement of Numerical Computations

To implement the numerical formulations for the steady-state solutions and eigenvalues of the system, all symbolic mathematical operations were performed in Maple. After the equations were generated, the Matlab Optimization Toolbox was used to search numerical solutions of the system equations. This two-fold method was very slow; for instance, some simulations took 24 hours or more. A one step method coded in C could improve the simulation time.

7.2 Suggestions for Future Work

Appendix A

Appendices

A.1 Three-Phase Ferroresonance: Opened One Conductor

To assess the stability of each steady-state solution of the system (6.27), we need to formulate the variational system which will give the stability criterion of the system around that operating point. Since the system defined in (6.27) is an differential algebraic system, we need to simplify the system dynamics in order to compute the eigenvalues of the system.

To compute the eigenvalues of the system defined in (6.27), we propose the following simplification procedures. First, eliminate $X_{10,k}$ and $F_{3,k}$ from equation (6.27c) using equation (6.27j). Then the reduced system takes the following form

$$\dot{X}_{1,k} = -jk\omega X_{1,k} + a_1 X_{8,k} + a_1 X_{9,k} + a_2 F_{1,k} + a_2 F_{2,k} - a_3 X_{5,k} \quad (\text{A.1a})$$

$$\dot{X}_{2,k} = -jk\omega X_{2,k} - a_1 X_{8,k} - a_2 F_{2,k} + a_3 X_{6,k} \quad (\text{A.1b})$$

$$\dot{X}_{3,k} = -jk\omega X_{3,k} - a_1 X_{9,k} - a_2 F_{3,k} + a_3 X_{7,k} \quad (\text{A.1c})$$

$$\dot{X}_{4,k} = -jk\omega X_{4,k} + a_6 X_{5,k} \quad (\text{A.1d})$$

$$\dot{X}_{5,k} = -(jk\omega + a_5) X_{4,k} + a_4 X_{1,k} - a_4 X_{4,k} \quad (\text{A.1e})$$

$$\dot{X}_{6,k} = -(jk\omega + a_5) X_{5,k} + a_4 G_{2,k} - a_4 X_{2,k} \quad (\text{A.1f})$$

$$\dot{X}_{7,k} = -(jk\omega + a_5) X_{6,k} + a_4 G_{3,k} - a_4 X_{3,k} \quad (\text{A.1g})$$

$$\dot{X}_{8,k} + \dot{X}_{10,k} = -jk\omega X_{8,k} - jk\omega X_{10,k} + X_{2,k} - X_{1,k} \quad (\text{A.1h})$$

$$\dot{X}_{9,k} + \dot{X}_{10,k} = -jk\omega X_{9,k} - jk\omega X_{10,k} + X_{3,k} - X_{1,k} \quad (\text{A.1i})$$

Then, the simplified variational system takes the form

$$Q \hat{X}_{i,k} = J \hat{X}_{i,k} \quad \text{where} \quad Q = I + M \quad \text{and} \quad J = J_1 - P \quad (\text{A.2})$$

where $I \in \mathbb{R}^{n \times n}$ is the identity matrix, $J \in \mathbb{C}^{n \times n}$ is a complex matrix, and $Q \in \mathbb{R}^{n \times n}$ is a real matrix. Hence the eigenvalues of the system can be derived from the following algebraic

equation

$$\det(J - Q\mu) = 0 \quad (\text{A.3})$$

where the μ 's are the eigenvalues of the system. similarly, to compute the matrices J_1 , \mathcal{M} , and \mathcal{P} , we take the following steps. Define

$$\dot{X}_{i,k} = U(X_{i,k}) \Big|_{X_{10,k}=0} \quad i = 1, 2, \dots, 9 \quad (\text{A.4a})$$

$$Z_k = K_1(X_{8,k} + X_{9,k} - X_{10,k}) + K_5(F_{1,k} + F_{2,k} - F_{3,k}) \quad (\text{A.4b})$$

$$\mathcal{F} = \begin{bmatrix} X_{1,k} & X_{2,k} & \cdots & X_{9,k} \end{bmatrix} \quad (\text{A.4c})$$

$$\mathcal{V} = \begin{bmatrix} X_{8,k} & X_{9,k} & X_{10,k} \end{bmatrix} \quad (\text{A.4d})$$

Then, let

$$J_1 = \text{Jacobian}(U, \mathcal{F}) \quad \text{and} \quad J_2 = \text{Jacobian}(Z, \mathcal{V}) \quad (\text{A.5})$$

where $J_1 \in \mathbb{C}^{n \times n}$ is a complex matrix and $J_2 \in \mathbb{R}^{m \times m}$. The dimension of the reduced system, n and m can be computed from the following equation

$$n = \text{deg} * (2k + 1) \quad \text{and} \quad m = 3 * (2k + 1) \quad (\text{A.6})$$

where deg is the order of the system defined in (A.1) and k is the number of harmonics used for the approximation of the solution. For example, if the system contains 9 first order differential equations and one algebraic equation, then the degree of the system will be 9 and n and m will be 27 and 9 respectively, if only the first harmonic considered. If we take up to the seventh harmonics, then n and m will be 135 and 45 respectively.

Now, define

$$A_1 = \begin{bmatrix} J_2(:, 1) & J_2(:, 4) & \cdots & J_2(:, n-2) \end{bmatrix} \quad (\text{A.7a})$$

$$A_2 = \begin{bmatrix} J_2(:, 2) & J_2(:, 5) & \cdots & J_2(:, n-1) \end{bmatrix} \quad (\text{A.7b})$$

$$A_3 = \begin{bmatrix} J_2(:, 3) & J_2(:, 6) & \cdots & J_2(:, n) \end{bmatrix} \quad (\text{A.7c})$$

The notation $J_2(:, i)$ stands for the i^{th} column of the matrix J_2 . Then,

$$\begin{aligned} X_{10,k} &= -A_3^{-1}A_1X_{8,k} - A_3^{-1}A_2X_{9,k} \\ \dot{X}_{10,k} &= -A_3^{-1}A_1\dot{X}_{8,k} - A_3^{-1}A_2\dot{X}_{9,k} \end{aligned} \quad (\text{A.8})$$

Since K_1 is not zero, the matrix A_3 is always invertible. Hence, the left side of the differential equation that represent the reduced system is given by

$$\begin{bmatrix} 1 & & & & 0 \\ & 1 & & & \\ & & \ddots & & \\ & & & 1 & \\ 0 & & & & 1 \end{bmatrix} \begin{bmatrix} \dot{X}_{1,k} \\ \dot{X}_{2,k} \\ \vdots \\ \dot{X}_{9,k} \end{bmatrix} + \begin{bmatrix} 0 & & & & 0 \\ & 0 & & & \\ & & 0 & & \\ & & & \ddots & \\ 0 & & & & -A_3^{-1}A_1 \\ & & & & & -A_3^{-1}A_2 \end{bmatrix} \begin{bmatrix} \dot{X}_{1,k} \\ \dot{X}_{2,k} \\ \vdots \\ \dot{X}_{9,k} \end{bmatrix} \quad (\text{A.9})$$

Similarly, the right side yields

$$J_1 \begin{bmatrix} X_{1,k} \\ X_{2,k} \\ \vdots \\ \dot{X}_{9,k} \end{bmatrix} - \begin{bmatrix} 0 & & & & \\ & 0 & & & \\ & & \ddots & & \\ & & & 0 & \\ & & & & -jk\omega A_3^{-1}A_1 \\ & & & & & -jk\omega A_3^{-1}A_2 \end{bmatrix} \begin{bmatrix} X_{1,k} \\ X_{2,k} \\ \vdots \\ \dot{X}_{9,k} \end{bmatrix} \quad (\text{A.10})$$

Then, we have

$$\mathcal{M} = \begin{bmatrix} 0 & & & & 0 \\ & 0 & & & \\ & & 0 & & \\ & & & \ddots & \\ & & & & -A_3^{-1}A_1 \\ 0 & & & & & -A_3^{-1}A_2 \end{bmatrix} \text{ and } \mathcal{P} = \begin{bmatrix} 0 & & & & \\ & 0 & & & \\ & & \ddots & & \\ & & & 0 & \\ & & & & -jk\omega A_3^{-1}A_1 \\ & & & & & -jk\omega A_3^{-1}A_2 \end{bmatrix} \quad (\text{A.11})$$

A.2 Three-Phase Ferroresonance: Opened Two conductors

To ascertain the stability of each steady-state solution of the system (6.32), we need to formulate the variational system which will give the stability criterion of the system around that operating point. Since the system defined in (6.32) is a differential-algebraic system, we need to simplify the system dynamics in order to compute the eigenvalues of the system.

To compute the eigenvalues of the system defined in (6.32), we propose the following simplification procedure. Eliminate $X_{11,k}$ and $F_{3,k}$ from equation (6.32c) using equation (6.32k). Then the reduced system takes the following form

$$\dot{X}_{1,k} = -jk\omega X_{1,k} + a_1 X_{9,k} + a_2 F_{1,k} - a_3 X_{6,k} \quad (\text{A.12a})$$

$$\dot{X}_{2,k} = -jk\omega X_{2,k} + a_1 X_{10,k} + a_2 F_{2,k} + a_3 X_{7,k} \quad (\text{A.12b})$$

$$\dot{X}_{3,k} = -jk\omega X_{3,k} - a_1 X_{9,k} - a_1 X_{10,k} - a_2 F_{1,k} - a_2 F_{2,k} + a_3 X_{8,k} \quad (\text{A.12c})$$

$$\dot{X}_{4,k} = -jk\omega X_{4,k} + a_6 X_{6,k} \quad (\text{A.12d})$$

$$\dot{X}_{5,k} = -jk\omega X_{5,k} + a_6 X_{7,k} \quad (\text{A.12e})$$

$$\dot{X}_{6,k} = -(jk\omega + a_5) X_{6,k} + a_4 X_{1,k} - a_4 X_{4,k} \quad (\text{A.12f})$$

$$\dot{X}_{7,k} = -(jk\omega + a_5) X_{7,k} + a_4 X_{2,k} - a_4 X_{5,k} \quad (\text{A.12g})$$

$$\dot{X}_{8,k} = -(jk\omega + a_5) X_{8,k} + a_4 E_3 - a_4 X_{3,k} \quad (\text{A.12h})$$

$$\dot{X}_{9,k} + \dot{X}_{11,k} = -jk\omega X_{9,k} - jk\omega X_{11,k} + X_{3,k} - X_{1,k} \quad (\text{A.12i})$$

$$\dot{X}_{10,k} + \dot{X}_{11,k} = -jk\omega X_{10,k} - jk\omega X_{11,k} + X_{3,k} - X_{2,k} \quad (\text{A.12j})$$

Then, the simplified variational system takes the form

$$Q \hat{X}_{i,k} = J \hat{X}_{i,k} \quad \text{where} \quad Q = I + M \quad \text{and} \quad J = J_1 - P \quad (\text{A.13})$$

where $I \in \mathbb{R}^{n \times n}$ is the identity matrix, $J \in \mathbb{C}^{n \times n}$ is a complex matrix, and $Q \in \mathbb{R}^{n \times n}$ is a real matrix. Hence the eigenvalues of the system can be derived from the following algebraic equation

$$\det(J - Q\mu) = 0 \quad (\text{A.14})$$

where the μ 's are the eigenvalues of the system. To compute the matrices J_1 , M , and P ,

we take the following steps. Define

$$\dot{X}_{i,k} = U(X_{i,k}) \Big|_{X_{11,k}=0} \quad i = 1, 2, \dots, 10 \quad (\text{A.15a})$$

$$Z_k = K_1(X_{9,k} + X_{10,k} - X_{11,k}) + K_2(G_{1,k} + G_{2,k} - G_{3,k}) \quad (\text{A.15b})$$

$$\mathcal{F} = \begin{bmatrix} X_{1,k} & X_{2,k} & \dots & X_{10,k} \end{bmatrix} \quad (\text{A.15c})$$

$$V = \begin{bmatrix} X_{9,k} & X_{10,k} & X_{11,k} \end{bmatrix} \quad (\text{A.15d})$$

Then, let

$$J_1 = \text{Jacobian}(U, \mathcal{F}) \quad \text{and} \quad J_2 = \text{Jacobian}(Z, V) \quad (\text{A.16})$$

where $J_1 \in \mathbb{C}^{n \times n}$ is a complex matrix and $J_2 \in \mathbb{R}^{m \times m}$. The dimension of the reduced system, n and m can be computed from the following equation

$$n = \text{deg} * (2k + 1) \quad \text{and} \quad m = 3 * (2k + 1) \quad (\text{A.17})$$

where deg is the order of the system defined in (A.12) and k is the number of harmonics used for the approximation of the solution. For example, if the system contains 10 first order differential equations and one algebraic equation, then the degree of the system will be 10 and n and m will be 30 and 9 respectively, if only the first harmonic considered. If we take up to the seventh harmonics, then n and m will be 150 and 45 respectively.

Now, define

$$A_1 = \begin{bmatrix} J_2(:, 1) & J_2(:, 4) & \dots & J_2(:, n-2) \end{bmatrix} \quad (\text{A.18a})$$

$$A_2 = \begin{bmatrix} J_2(:, 2) & J_2(:, 5) & \dots & J_2(:, n-1) \end{bmatrix} \quad (\text{A.18b})$$

$$A_3 = \begin{bmatrix} J_2(:, 3) & J_2(:, 6) & \dots & J_2(:, n) \end{bmatrix} \quad (\text{A.18c})$$

The notation $J_2(:, i)$ stands for the i^{th} column of the matrix J_2 . Then,

$$\begin{aligned} X_{11,k} &= -A_3^{-1} A_1 X_{9,k} - A_3^{-1} A_2 X_{10,k} \\ \dot{X}_{11,k} &= -A_3^{-1} A_1 \dot{X}_{9,k} - A_3^{-1} A_2 \dot{X}_{10,k} \end{aligned} \quad (\text{A.19})$$

Since K_1 is not zero, the matrix A_3 is always invertible. Hence, the left side of the differential

equation that represents the reduced system is given by

$$\begin{bmatrix} 1 & & & 0 \\ & 1 & & \\ & & \ddots & \\ & & & 1 \\ 0 & & & 1 \end{bmatrix} \begin{bmatrix} \dot{X}_{1,k} \\ \dot{X}_{2,k} \\ \vdots \\ \dot{X}_{9,k} \end{bmatrix} + \begin{bmatrix} 0 & & & 0 \\ & 0 & & \\ & & \ddots & \\ & & & -A_3^{-1}A_1 \\ 0 & & & -A_3^{-1}A_2 \end{bmatrix} \begin{bmatrix} \dot{X}_{1,k} \\ \dot{X}_{2,k} \\ \vdots \\ \dot{X}_{9,k} \end{bmatrix} \quad (\text{A.20})$$

Similarly, the right side yields

$$J_1 \begin{bmatrix} X_{1,k} \\ X_{2,k} \\ \vdots \\ \dot{X}_{9,k} \end{bmatrix} - \begin{bmatrix} 0 & & & \\ & 0 & & \\ & & \ddots & \\ & & & 0 \\ & & & -jk\omega A_3^{-1}A_1 \\ & & & -jk\omega A_3^{-1}A_2 \end{bmatrix} \begin{bmatrix} X_{1,k} \\ X_{2,k} \\ \vdots \\ \dot{X}_{9,k} \end{bmatrix} \quad (\text{A.21})$$

Then, we have

$$\mathcal{M} = \begin{bmatrix} 0 & & & 0 \\ & 0 & & \\ & & \ddots & \\ & & & -A_3^{-1}A_1 \\ 0 & & & -A_3^{-1}A_2 \end{bmatrix} \text{ and } \mathcal{P} = \begin{bmatrix} 0 & & & \\ & 0 & & \\ & & \ddots & \\ & & & 0 \\ & & & -jk\omega A_3^{-1}A_1 \\ & & & -jk\omega A_3^{-1}A_2 \end{bmatrix} \quad (\text{A.22})$$

A.3 Synchronous Incremental-Input Describing Function

In Chapter 3, we discussed the theory of the synchronous incremental-input describing function. In that chapter we only concentrated on stable minimum-phase systems. Recall that the objective of the synchronous incremental-input describing function is to examine existence of jump amplitudes. First we compute the stable steady-state solution and then examine if we perturb the input amplitude or internal system parameters whether the system will operate at the same steady-state solution or if it will jump to another steady-

state solution which is also stable.

The theory can be applied to larger classes of systems. Here we apply the theory to unstable open-loop non-minimum-phase systems. To ascertain the stability of the system, we perform two tasks. First, we examine the stability of the steady-state solution. If the steady-state solution is stable then we further examine if the ferroresonance phenomenon exists when the input voltage or internal system parameters are disturbed. Otherwise, if the steady-state solution is unstable, then there is no need to investigate the ferroresonance problem.

To examine the stability of the steady-state solution of the system, first we compute the describing function gain $N(\mathcal{A})$, where \mathcal{A} is the amplitude of the periodic steady-state solution. Then, we compute the loop-gain of the system and apply the Nyquist criterion as outlined in Section 3.2.1. If the system is unstable in closed-loop for a given A , then we do not need to examine further the existence of jump amplitudes. However, if the system is stable in closed-loop, then we analyze further the steady-state solution for existence of jump amplitudes, subharmonic solutions, or amplitude-modulated periodic responses.

Investigating the ferroresonance problem, we need first to compute the gain of the synchronous incremental-input describing function $N(\mathcal{A}, \phi)$ of the nonlinear element. Second, we compute the incremental loop-gain of the system and invoke the modified synchronous incremental-input function theory to assess existence of jump amplitudes, subharmonic solutions, or amplitude-modulated periodic responses, as outlined in Chapter 3.

To understand the mechanics of the theory, let us apply it to an example.

EXAMPLE A.1

Suppose we have the following transfer function.

$$G(s) = \frac{N(s)}{D(s)}, \quad \text{where} \tag{A.23}$$

$$N(s) = 9000s^4 + 3100s^3 + 107300s^2 + 305800s + 2173500$$

$$D(s) = s^6 + 11s^5 + 198s^4 + 1459s^3 + 10019s^2 + 39476s + 23567$$

Two poles of $G(s)$ lie in the right-half plane, namely, $s = 0.0179 \pm 9.9744i$. Hence, $G(s)$ is an unstable nonminimum-phase open-loop transfer function. Figure A.1 depicts the frequency response of the system. Note that P is equal to 2, where P is the number of open-loop unstable poles as discussed in Chapter 3. Furthermore, suppose $N(\mathcal{A})$ is the

describing function gain of the system for a given \mathcal{A} . The characteristic equation of the system yields

$$1 + N(\mathcal{A})G(s) = 0 \quad (\text{A.24})$$

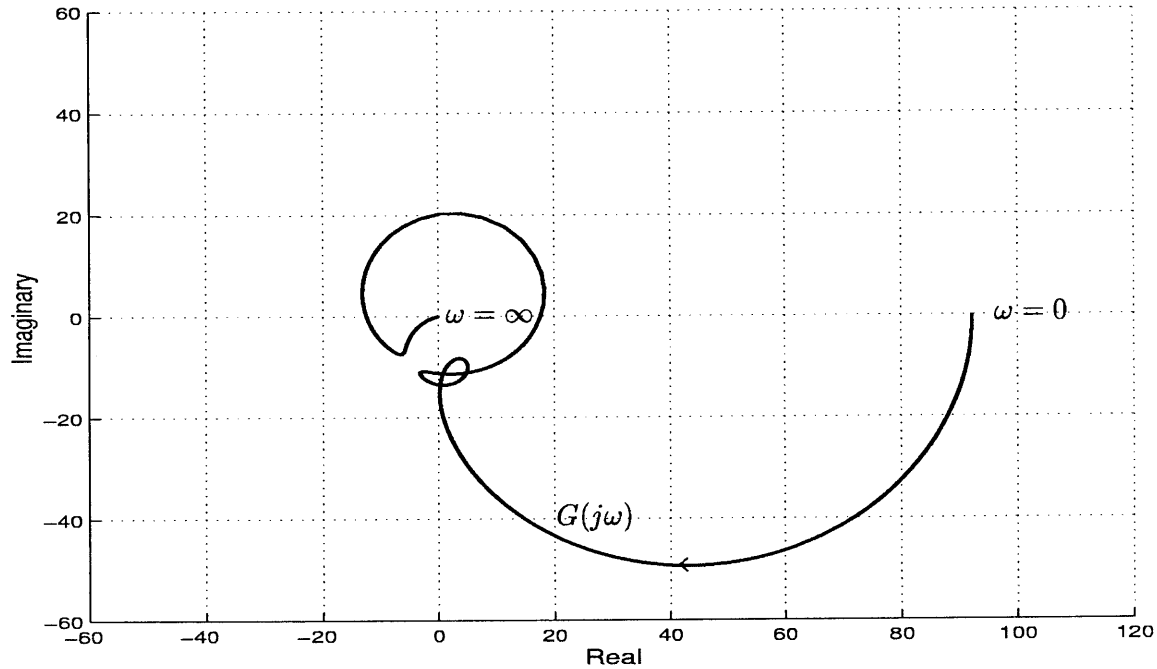


Figure A.1: Open-loop frequency response of the system: $\omega \geq 0$

To examine the stability of the system in closed-loop, we write Equation (A.24) as

$$G(j\omega) = -\frac{1}{N(\mathcal{A})}, \quad \text{where } -\infty \leq \omega \leq \infty. \quad (\text{A.25})$$

and then plot the left and the right side of the equation. If the two loci intersect, then we conclude that the system is unstable in closed-loop. Since \mathcal{A} is a positive real number, $-\frac{1}{N(\mathcal{A})}$ will always lie in the left-half plane. Therefore, the critical points are $-\frac{1}{N(\mathcal{A})}$ for each given \mathcal{A} .

To apply the Nyquist criterion to this loop-gain with the critical points $-\frac{1}{N(\mathcal{A})}$, we plot the frequency response of $G(j\omega)$ for both negative and positive frequencies. Figure A.2

shows the frequency response of the system for both negative and positive frequencies. The thicker lines are the positive frequencies while the thinner lines are the negative frequencies. From the figure, there are three possible critical regions, namely, A , B , and C . Next we

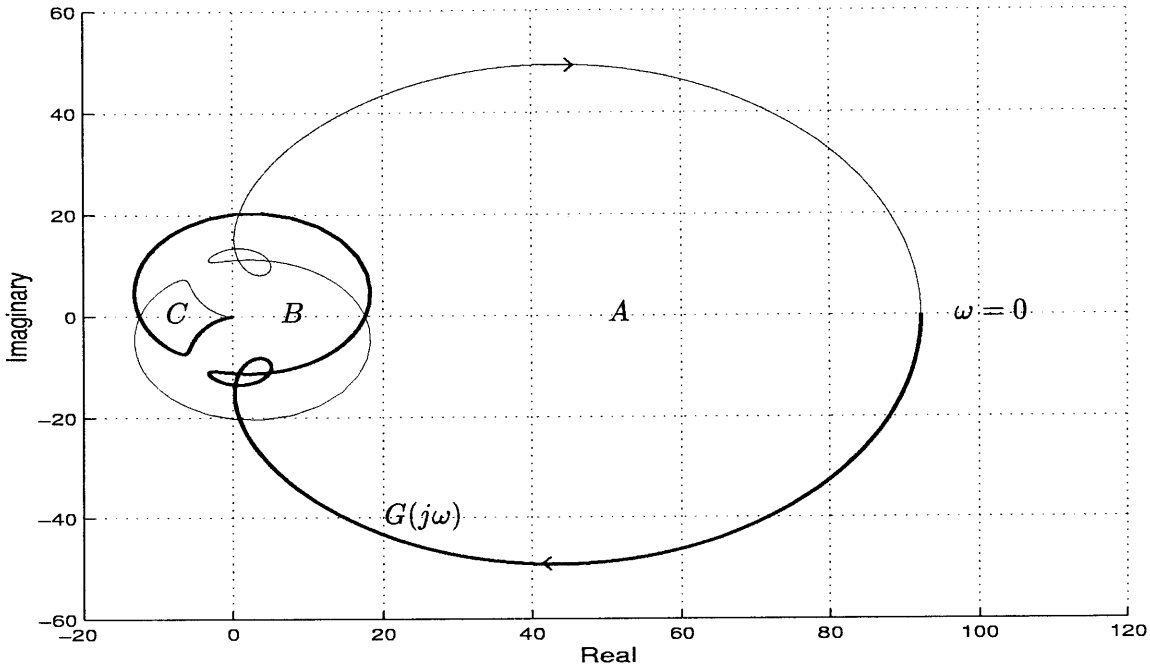


Figure A.2: Open-loop frequency response of the system: $-\infty \leq \omega \leq \infty$

need to compute \mathcal{N} , the number of encirclements of the critical points for each given range of \mathcal{A} .

In region A , \mathcal{N} is equal to 1. Hence, the number of zeros Z that lie in the right-half plane are equal to 3. The system is unstable in closed-loop for some range of amplitudes \mathcal{A} .

Next, in region B , \mathcal{N} is equal to -1 . There is one pole in the right-half plane of the closed-loop system. Hence, in this region the closed-loop system is unstable for some range of \mathcal{A} .

Finally, in C , \mathcal{N} is equal to -2 . In this region there are no poles in the right-half plane of the closed-loop system. Hence, there are some ranges of \mathcal{A} for which the system is stable in closed-loop. Furthermore, \mathcal{N} is equal to zero for regions outside of A , B , and C . Therefore, these regions the closed-loop system is unstable for some range of \mathcal{A} .

Since region C is the only region in which the system can operate, we need to examine if the system is susceptible to ferroresonance phenomenon in this region. To investigate this, we compute the synchronous incremental-input gain of the nonlinear element $N(\mathcal{A}, \phi)$ and then examine the incremental loop-gain of the system. The characteristic equation of the incremental system is given by

$$1 + N(\mathcal{A}, \phi)G(s) = 0, \quad \text{where } s \in C. \quad (\text{A.26})$$

Furthermore, we can write this as

$$G(\sigma + j\omega_s) = -\frac{1}{N(\mathcal{A}, \phi)}, \quad \sigma \geq 0 \quad (\text{A.27})$$

where ω_s is the frequency of the input signal.

Hence, if there is an intersection between $G(\sigma + \omega_s)$ and $-\frac{1}{N(\mathcal{A}, \phi)}$ in region C , we conclude that the system is susceptible to ferroresonance phenomenon, i.e., jump amplitudes, subharmonic responses, or amplitude-modulated periodic responses. Figure A.3 depicts $G(\omega)$ and the negative inverse of $N(\mathcal{A}, \phi)$. From the figure, it is clear that there are some input frequencies ω_s and input amplitudes for which the system can operate under ferroresonance condition. To find these ranges one can use the modified synchronous incremental-input describing function that we formulated in Chapter 3.

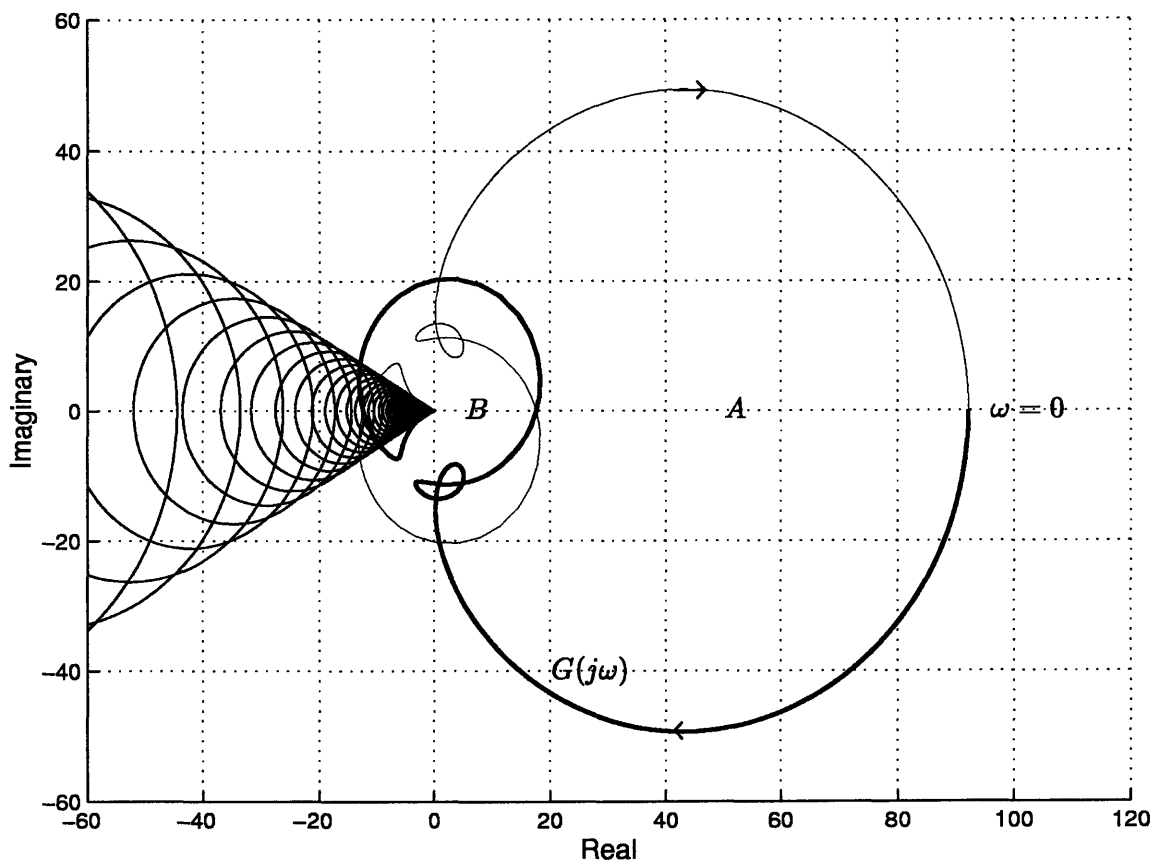


Figure A.3: $G(j\omega)$ and $-\frac{1}{N(A,\phi)}$ loci

A.3 Synchronous Incremental-Input Describing Function

Bibliography

- [1] P. Odessey and E. Weber, "Critical conditions in ferroresonance," *AIEE Transactions on Basic Sciences*, vol. 57, pp. 444–452, August 1938.
- [2] J. Guckenheimer and P. Holmes, *Nonlinear Oscillations, Dynamical Systems and Bifurcations of Vector Fields*. Springer-Verlag, 1983.
- [3] E. Clarke, H. A. Peterson, and P. H. Light, "Abnormal voltage conditions in three-phase systems produced by single-phase switching," *AIEE Transactions*, vol. 60, pp. 329–339, 1941.
- [4] B. A. Kumar and S. Ertem, "Capacitor voltage transformer induced ferroresonance-causes, effects and design considerations," *Electric Power Systems Research*, vol. 21, pp. 23–31, July 1991.
- [5] P. Boucherot, "Existence de deux régimes en ferro-résonance," *R.G.E*, pp. 827–828, December, 10 1920.
- [6] C. T. Weller, "Experience with grounded-neutral, y-connected potential transformer on ungrounded system," *AIE Trans*, p. 299, March 1931.
- [7] L. Crann and R. Flickinger, "Overvoltage on 14.4/24.9-kv rural distribution systems," *AIEE Transmission and Distribution*, pp. 1208–1212, October 1954.
- [8] G. G. Auer and A. J. Schultz, "An analysis of 14.4/24.9-kv grounded-wye distribution system overvoltages," *AIEE Transmission and Distribution*, pp. 1027–1032, August 1954.
- [9] P. E. Hendrickson, I. B. Johnson, and N. R. Schultz, "Abnormal voltage conditions produced by open conductors on 3-phase circuit using shunt capacitors," *AIEE Transmission and Distribution*, pp. 1183–1193, December 1953.
- [10] R. H. Hopkinson, "Ferroresonant overvoltage control based on tna test on three-phase delta-wye transformer banks," *IEEE Transactions on Power Apparatus and Systems*, vol. 86, no. 10, pp. 1258–1265, October 1967.
- [11] R. H. Hopkinson, "Ferroresonant overvoltage control based on tna test on three-phase wye-delta transformer banks," *IEEE Transactions on Power Apparatus and Systems*, vol. 87, no. 2, pp. 352–361, October 1968.
- [12] D. R. Smith, S. R. Swanson, and J. D. Borst, "Overvoltage with remotely-switched cable-fed grounded wye-wye transformers," *IEEE Transactions on Power Apparatus and Systems*, vol. 94, no. 5, pp. 1843–1851, September/October 1975.

-
- [13] D. D. Mairs, D. L. Stuehm, and B. A. Mork, "Overvoltage on five-legged core transformers on rural electric systems," *IEEE Transactions on Industry Applications*, vol. 25, no. 2, pp. 366–370, March/April 1989.
- [14] B. A. Mork and D. L. Stueham, "Application of nonlinear dynamic and chaos to ferroresonance in distribution systems," *Transactions on Power Delivery*, vol. 9, no. 2, pp. 1009–1017, 1994.
- [15] R. Rüdtenberg, *Transient Performance of Electric Power Systems*. McGraw-hill Book Company, 1950.
- [16] W. Thomson, "Resonant nonlinear control circuits," *AIEE Transactions on Basic Sciences*, vol. 57, pp. 469–476, August 1938.
- [17] W. T. Thomson, "Similitude of critical conditions in ferroresonance circuits," *AIEE Transactions on Basic Sciences*, vol. 58, pp. 127–130, March 1939.
- [18] C. Hayashi, *Forced Oscillations in Non-linear Systems*. Nippon Printing and Publishing Company, Ltd., 1953.
- [19] C. Hayashi, *Nonlinear Oscillations in Physical Systems*. McGraw-Hill Book Company, 1964.
- [20] C. Kieny, "Application of bifurcation theory in studying and understanding the global behavior of a ferroresonant electric power circuit," *IEEE Transactions on Power Delivery*, vol. 6, no. 2, pp. 866–872, April 1991.
- [21] IEE Proc. C, *Ferroresonance in Power Systems: Fundamental Solutions*, July 1991.
- [22] A. Araujo, A. Soudack, and J. Marti, eds., *Ferroresonance in Power Systems: Chaotic Behaviour*, IEE Proc., May 3 1993.
- [23] C. Kieny and G. L. Roy, "Ferroresonance study using galerkin method with pseudo-arclength continuation method," *IEEE Transactions on Power Delivery*, vol. 6, pp. 1841–1847, October 1991.
- [24] N. Janssens, T. Craenenbroeck, D. Dommelen, and F. Meulebroeke, "Direct calculations of the stability domains of three-phase ferroresonance in isolated neutral networks with grounded-neutral voltage transformers," *IEEE Trans. Power Delivery*, vol. 11, pp. 1546–1553, July 1996.
- [25] S. Naidu and B. Souza, "Analysis of ferroresonant circuits using a newton-raphson scheme," *IEEE Transactions on Power Delivery*, vol. 12, pp. 1793–1798, October 1997.

- [26] A. Semlyen and A. Medina, "Computation of the periodic steady state in systems with nonlinear components using a hybrid time and frequency domain methodology," *IEEE Transactions on Power Systems*, vol. 10, pp. 1498–1504, August 1995.
- [27] T. Craenenbroeck, W. Michiels, W. Michiels, D. Dommelen, and K. Lust, "Bifurcation analysis of three-phase ferroresonant oscillations in ungrounded power systems," *IEEE Transactions on Power Delivery*, vol. 14, pp. 531–536, April 1999.
- [28] G. Franklin, J. Powell, and A. Emami-naeini, *Feedback Control of Dynamic Systems*. Addison-wesley, 1994.
- [29] M. Green and D. J. N. Limebeer, *Linear Robust Control*. Prince Hall, 1995.
- [30] B. Kuo, *Automatic Control Systems*. Prentice-Hall, Inc., six ed., 1991.
- [31] K. Ogata, *Modern Control Engineering*. Prentice-Hall, second ed., 1990.
- [32] A. Gelb and V. Velde, *Multiple-Input Describing Functions and Nonlinear System Design*. McGraw-Hill Book Company, New York, 1968.
- [33] J. Hockenberry, "The describing function method," ph.d area exam report, Massachusetts Institute of Technology, March 1999.
- [34] A. Mees, "Describing functions: Ten years on,," *IMA Journal of Applied Mathematics*, vol. 32, pp. 221–233, 1984.
- [35] P. A. Cook, *Nonlinear Dynamical Systems*. Prentice-Hall International, UK, 1986.
- [36] J. C. West, J. L. Douce, and R. K. Livesley, "The dual-input describing function and its use in the analysis of nonlinear feedback systems," *Proceedings IEE (London)*, vol. 103B, pp. 463–472, 1956.
- [37] G. W. Swift, "An analytical approach to ferroresonance," *IEEE Trans on Power Apparatus and Systems*, vol. PAS-88, pp. 42–46, January 1969.
- [38] X. Chen and S. S. Venkata, "A three-phase three-winding core-type transformer model for low-frequency transient studies," *IEEE Transactions on Power Delivery*, vol. 12, pp. 775–782, April 1997.
- [39] R. Iravani, A. Chandhury, I. Hassan, J. Martinez, B. M. A. Morched, M. Parniani, D. Shirmohammadi, and R. Walling, "Modeling guidelines for low frequency transients," tech. rep., IEEE.
- [40] D. Jacobson, L. Marti, and W. Menzies, "Modeling ferroresonance in a 230KV transformer-terminated double-circuit transmission line," IPST'99 International Conference on Power Systems Transients, June 20-24 1999.

-
- [41] K. Karsai, D. Kerenyi, and L. Kiss, *Large Power Transformers*. Elsevier, Amsterdam, 1987.
- [42] M. of the Staff of the Department of Electrical Engineering MIT, *Magnetic Circuits and Transformers*. John Wiley & Sons, Inc. New York, 1943.
- [43] T. Tran-Quoc and L. Pierrat, "An efficient nonlinear transformer model and its application to ferroresonance study," *IEEE Trans. on Magnetics*, vol. 31, pp. 2060–2063, May 1995.
- [44] S. Prusty and M. V. S. Rao, "New method for predetermination of true saturation characteristics of transformers and nonlinear reactors," *IEEE Proc*, vol. 127, no. 2, pp. 106–110, 1980.
- [45] N. Gernay, S. Mastero, and Vroman, "Review of ferroresonance phenomena in high voltage power systems and presentation of a voltage transformer model for predetermining them," *CIGRE*, pp. 33–18, 1974.
- [46] J. Mohamed and B. Lesieutre, "Analysis of ferroresonance using the generalized state-space averaging technique," pp. 359–364, 31st North American Power Symposium, San Luis Obispo, CA, October 1999.
- [47] V. Caliskan, G. Verghese, and A. Stanković, "Multi-frequency averaging of DC/DC converters," *IEEE Transactions on Power Electronics*, vol. 14, pp. 124–133, January 1999.
- [48] J. Kassakian, M. Schlecht, and G. Verghese, *Principle of Power Electronics*. Addison-Wesley Publishing Company, 1991.
- [49] P. Mattavelli, G. Verghese, and A. Stanković, "Phasor dynamics of thyristor-controlled series capacitor systems," IEEE Power Engineering Society Summer Power Meeting, 1996.
- [50] J. Noworolski and S. Sanders, "Generalized in-place circuit averaging," pp. 445–451, IEEE Power Electronics Specialists Conference 1991, June 1991.
- [51] S. Sanders, J. Noworolski, X. Liu, and G. Verghese, "Generalized averaging method for power conversion circuits," *IEEE Power Electronics Specialist Conference*, pp. 333–340, June 1990.
- [52] P. Drazin, *Nonlinear Systems*. Cambridge University Press, 1992.
- [53] D. Jordan and P. Smith, *Nonlinear Ordinary Differential Equations*. Clarendon Press, Oxford, second ed., 1987.

-
- [54] A. Nayfeh, *Introduction to Perturbation Techniques*. John Wiley & Sons, Ltd., 1981.
- [55] A. Nayfeh and B. Balachandran, *Applied Nonlinear Dynamics*. John Wiley & Sons, Inc., 1995.
- [56] I. Sokolnikoff and E. Sokolnikoff, *Higher Mathematics for Engineering and Physicists*. McGraw-Hill Book Company, Inc., 1941.
- [57] H. Turnbull, *Theory of Equations*. Oliver and Boyd, 1942.
- [58] The MathWorks, Inc., *Matlab User's Guide*.
- [59] D. P. Atherton, *Nonlinear Control Engineering*. Van Nostrand Reinhold Company, London, 1975.
- [60] J. C. Doyle, B. A. Francis, and A. R. Trappenbaum, *Feedback Control Theory*. New York: Macmillan Publishing Company, 1992.
- [61] C. R. Wylie and L. C. Barrett, *Advanced Engineering Mathematics*. McGraw-Hill, 1982.
- [62] H. W. Bode, *Network Analysis and Feedback Amplifier Design*. D. Van Nostrand Company, Inc., 1945.
- [63] A. I. Mees, "The describing function matrix," *J. Inst. Maths Applics*, vol. 10, pp. 49–67, August 1972.
- [64] H. Khalil, *Nonlinear Systems*. Prentice-Hall, Inc, second ed., 1996.
- [65] J. Slotine and W. Li, *Applied Nonlinear Control*. Prentice-Hall, 1991.
- [66] M. Vidyasagar, *Nonlinear Systems Analysis*. Prentice-Hall, 1993.
- [67] U. Grenander and S. G., *Toeplitz Forms and Their Applications*. Berkeley, CA, 1958.
- [68] A. I. Mees, "Limit cycle stability," *J. Inst. Maths Applics*, vol. 11, pp. 281–295, August 1973.
- [69] T. Sobczyk, "A reinterpretation of the floquet solution of the ordinary differential equation system with periodic coefficients as a problem of an infinite matrix," *The International Journal of Computation and Mathematics in Electrical and Electronic Engineering*, vol. 5, no. 1, pp. 1–22, 1986.
- [70] J. Padovan and I. Zeid, "Sub/supperharmonics oscillations and perturbation procedure," *Int. J. Nonlinear Mechanics*, vol. 16, no. 16, pp. 465–478, 1981.

- [71] T. Burton, "Non-linear oscillator limit cycle analysis using a time transformation approach," *Int. J. Nonlinear Mechanics*, vol. 17, no. 1, pp. 7–19, 1982.
- [72] F. Ling and X. Wu, "Fast galerkin method and its applications to determine periodic solutions of nonlinear oscillators," *Int. J. Nonlinear Mechanics*, vol. 22, no. 2, pp. 89–98, 1987.
- [73] R. Grimshaw, *Nonlinear Ordinary Differential Equations*. CRC Press, 1993.
- [74] R. Miller and A. Michel, *Ordinary Differential Equations*. Academic Press, 1982.
- [75] H. Reinhard, *Differential Equations*. Mcmillan Publishing Company, 1987.
- [76] D. Zwillinger, *Hand Book of Differential Equations*. Academic Press, Inc., 1992.
- [77] H. Fujisaka and C. Sato, "Computing the number, location, and stability for fixed points of Poincaré maps," *IEEE Transactions on Circuits and Systems-I: Fundamental Theory and Applications*, vol. 44, pp. 303–311, April 1997.
- [78] S. Wiggins, *Introductions to Applied Nonlinear Dynamical Systems and Chaos*. Springer-Verlag, 1990.
- [79] S. H. Strogatz, *Nonlinear Dynamics and Chaos*. Addison-Wesley, 1994.
- [80] P. Bergé, Y. Pomeau, and C. Vidal, *Order Within Chaos*. John Wiley & Sons, 1984.
- [81] T. Parker and L. Chua, *Practical Numerical Algorithms for Chaotic Systems*. Springer-Verlag, 1989.
- [82] A. Stanković, "Dynamic phasors in modeling of arcing faults on overhead lines," pp. 510–514, International Conference on Power System Transients, June 1999.
- [83] A. Stanković, S. Sanders, and T. Aydin, "Analysis of unbalanced AC machines with dynamic phasors," pp. 219–224, Naval Symposium on Electric Machines, October 1998.